UNIVERSITAT POLITÈCNICA DE VALÈNCIA

INSTITUTO INTERUNIVERSITARIO DE INVESTIGACIÓN DE RECONOCIMIENTO MOLECULAR Y DESARROLLO TECNOLÓGICO

Gated nanomaterials as delivery platform for the treatment of inflammatory disorders

PhD. THESIS

Submitted by

Alba García Fernández

PhD. Supervisors:

Prof. Ramón Martínez Máñez
Dr. Félix Sancenón Galarza
Dra. María del Mar Orzáez Calatayud

València, September 2019

RAMÓN MARTÍNEZ MÁÑEZ, PhD in Chemistry and Professor at the *Universitat Politècnica de València*, FÉLIX SANCENÓN GALARZA, PhD in Chemistry and Lecturer at the *Universitat Politècnica de València* and MARÍA DEL MAR ORZÁEZ CALATAYUD, PhD in Biology

CERTIFY:

That the work *"**Gated nanomaterials as delivery platform for the treatment of inflammatory disorders**"* has been developed by Alba García Fernández under their supervision in the Instituto Interuniversitario de Investigación de Reconocimiento Molecular y Desarrollo Tecnológico (IDM) of the *Universitat Politècnica de València*, forming part of the Unidad Mixta UPV-CIPF de Investigación en Mecanismos de Enfermedades y Nanomedicina, as a Thesis Project in order to obtain the degree of PhD in Biotechnology at the *Universitat Politècnica de València.*

Valencia, September 2nd 2019

Dr. Félix Sancenón Galarza

Dra. María del Mar Orzáez Calatayud

Prof. Ramón Martínez Máñez

A mi familia

"Perquè hi haurà un dia que no podrem més i llavors ho podrem tot."

Vicent Andrés Estellés

Acknowledgements

Agradecimientos

No me gustaría poner punto y final a esta etapa sin dedicarles unas pequeñas líneas a todas aquellas personas que directa o indirectamente me han ayudado y apoyado para poder llegar al final de este largo camino y han hecho que el recorrido sea mucho más fácil.

En primer lugar me gustaría dar las gracias a mis directores de tesis Ramón, Félix y Mar. A Ramón por darme la oportunidad de unirme a su grupo de investigación y realizar la tesis doctoral, por la confianza depósitada durante estos años y que a día de hoy sigue depositando en mí. Gracias por darnos la libertad de poder desarrollar nuestras propias ideas, cosa que no suele pasar en muchos grupos, así como la oportunidad de colaborar en diferentes proyectos de nuestro propio grupo como de otros grupos, resultando en experiencias muy enriquecedoras tanto a nivel personal como profesional. A Félix, que siempre está ahí, dispuesto a ayudar cuando se le necesita y haciendo las cosas mucho más fáciles en el día a día. Gracias por tu gran apoyo y dedicación así como por los buenos momentos tanto dentro como fuera del laboratorio. En general gracias por preocuparte tanto por nosotros. A Mar, muchas gracias por abrirme las puertas de tu laboratorio desde el principio, incluso antes de que formaramos la unidad mixta, y darme la oportunidad de formarme en el mundo bio. Para mí ha sido una de las mejores experiencias, y con la que más he disfrutado durante esta tesis. Gracias por tu disposición y constante ayuda, por tu positividad, por preocuparte por nosotras, tus consejos y sobre todo gracias por tus ánimos.

Por una parte, quiero dar las gracias a todos mis compañeros del grupo del IDM con los que he compartido todo este tiempo. Desde los que estaban desde el principio cuando llegué a este grupo… Elena, Carmen, Andrea y Mari Carmen muchas gracias por ayudarnos y guiarnos a los predocs. Y a los que se fueron haciendo doctores durante el camino…gracias Edgar, Cris T, Núria, Luís Enrique, Carol, Cris M, María Moragues, Lluís, Mar, María Ruíz y Cris G por vuestros consejos, ayuda y buenos mmomentos. Por último agradecer a todos mis compañeros, que empezamos o casi empezamos esta etapa a la vez en el

laboratorio y hemos compartido tantas penas y alegrías, así como a las nuevas incorporaciónes. Gracias a Adrián, Lorena, Xente, Àngela, Marta, Amelia, Santi, Elisa, Tania, Eva, María, Borja, Andy, Paula, Andrea Escudero, Serena, Angy y Juanfran. Gracicas a Bea, con la que también comparto penas y alegrías en casa y siempre está ahí para escucharme y ayudarme. Gracias también a Toni, mi compañero de fatigas (nunca mejor dicho cuando conseguía que fuera a spinning con él jeje) con el que he formado tan buen equipo en estos últimos años sacando tantos proyectos adelante entre los que se encuentra poner en formato esta tesis! En especial gracias a Luís, Bea, Irene e Iris que se han convertido en grandes amigos durante todos estos años. Irene, mi compañera de fatigas en el CIPF, gracias por tu apoyo y ayuda en esta última etapa que tanto hemos sufrido! Luís, desde aquella noche en el pódium de Mya lo nuestro fue un descubrimiento, gracias por tu apoyo y todas los momentos tan divertidos. Gracias a Bea, que es ya casi mi segunda madre, gracias por tu ayuda, por tus consejos, por tus riñas y por aguantarme y apoyarme tanto dentro como fuera del laboratorio. También muchas gracias por todos los buenos momentos, que no son pocos, y los que aún quedan por llegar. Por último, gracias a Iris, que un poco de casualidad pasó a formar parte de mi vida y a día de hoy se ha convertido también en una persona muy importante. Muchas gracias a ti también por estar siempre ahí, por escucharme, apoyarme y también aguantarme dentro y fuera del laboratorio.

Por otra parte, quiero también agradecer a mi otra familia del laboratorio del CIPF. Gracias a Mónica por toda su ayuda y orientación así como todo el conocimiento bio que me ha transmitido. Gracias a Carmen, que aunque estuviste poco tiempo dejaste mucha huella en mí con tu energía, positividad y consejos. Gracias a Alberto, por su buen rollo y por esas sesiones tan maravillosas de confocal, en las que tan bien me lo paso y que se han convertido en mi parte experimental favorita. Gracias a Estefania, Ally, Paula, Paula Carrascosa y las principesas! Alejandra, Gema, Mónica, Elena y Araceli por todo el apoyo incondicional durante todo este tiempo, y sobre todo esos buenos momentos y risas tanto en el laboratorio como fuera de él. Con unas compañeras como vosotras da gusto ir a trabajar ya que el ambiente tan bueno que hemos creado es

una gran fuente de energía que hasta en los peores momentos te saca una sonrisa.

Moltes gràcies també als meus amics Sonia, Paula, Àlex, Marc i Carles per estar ahí i ajudar-me a desconectar. Gràcies pel vostre suport, per escoltar-me encara que vos sonara a locura tot el que feia, i per preocupar-vos tant per mi quan pensaveu que està tesi anava a acabar en mí, cosa que jo també pensava! Però ací continue, i espere continuar fent comboi en vosaltres per molt de temps.

Quiero agradecer también a mi otra gran familia de amigos. La familia Biotec, que siempre está a pesar del tiempo y de la distancia. Muchas gracias por todos los buenos momentos vividos siempre y por vuestro incondicional apoyo siempre que se os necesita. En especial gracias a Bea la Balle por estar ahí, por nuestras quedadas para despejarnos y ayudar en todo lo que puedes. A Anna, que a día de hoy seguimos siendo las que eramos hace 5 años, gracias por todos estos años de amsitad en las buenas y en las maduras. Gracias a Carles, gracias también por todos estos años de amsitad, por estar siempre ahí y por preocuparte tanto por mí. Y sobre todo, gracias a Alba por tu amistad que no conoce horas ni impedimientos, porque me apoyas, aconsejas y ayudas en todo…y mira que en este último año me ha pasado de todo…y ahí has estado siempre, día a día aguantando mis momentos de desperación e intentando hacer que las cosas fueran más fáciles.

Y como no, gracias a Carlos. Sin esperarlo, en este último año y medio te has convertido en una persona fundamental en mi vida. Y a pesar de los efectos colaterales de tu tesis y la mía, entre momentos tan difíciles también sale lo mejor. Gracias por transmitirme tu alegría y positividad, por apoyarme y por animarme, por aguantarme, por entenderme, por tratar de hacerme desconectar y por intentar sacarme siempre una sonrisa. Gracias por estar siempre ahí.

Por último, quiero dar las gracias a las personas más importantes de mi vida, mi familia. Gracias mamá, papá y Joel por vuestro apoyo incondicional ya que sin vosotros nada de esto habría sido posible. Gracias por darme la fuerza que necesitaba en los peores momentos y ayudarme a levantarme. Gracias por respaldar y apoyar mis decisiones a pesar de que no entendaís muchas de las cosas que hago. Y sobre todo, muchas gracias por estar en el día a día animándome a ser mejor y darme todo lo que soy.

Resumen

La presente tesis doctoral titulada “Nanomateriales con puertas moleculares como plataforma de liberación controlada de fármacos para el tratamiento de desórdenes inflamatorios” se centra en el diseño, preparación, caracterización y evaluación de nanomateriales híbridos orgánico-inorgánicos, basados en nanopartículas mesoporosas de sílice, funcionalizadas con biomoléculas que actúan como puertas moleculares para la liberación controlada de fármacos en aplicaciones biomédicas, en concreto en el campo de la inflamación.

En el primer capítulo se introducen, a nivel general, los diferentes conceptos relacionados con la nanotecnología, nanomedicina, los materiales mesoporosos y las puertas moleculares, así como la interacción de las nanopartículas a nivel biológico con el organismo y las células. Finalmente se introducen conceptos básicos de inflamación, respuesta inflamatoria, su papel en los desórdenes inflamatorios así como la aplicación de los nanomateriales como terapia.

A continuación, en el segundo capítulo, se exponen los objetivos generales de la presente tesis doctoral así como los objetivos concretos que son abordados en los diferentes capítulos experimentales.

En el tercer capítulo se describe un nanomaterial para la liberación controlada del inhibidor de caspasa-1, VX-765, aprovechando que las nanopartículas se acumulan preferencialmente en las zonas inflamadas. En concreto, se han preparado nanopartículas mesoporosas de sílice, cargadas con el fármaco VX-765 y funcionalizadas covalentemente con ε-poli-L-lisina que actúa como puerta molecular. El correcto funcionamiento de la puerta molecular se ha comprobado a través de estudios de liberación controlada en presencia de proteasas, produciéndose la liberación del cargo sólo en presencia de la enzima. Se ha comprobado la ausencia de toxicidad del nanodispositivo así como su internalización en el modelo celular de monocitos humanos THP-1. La actividad anti-inflamatoria del material se ha comprobado tanto *in vitro*, en el modelo celular de THP-1, como *in vivo* en ratones en un modelo de inflamación de bolsa de aire. Los resultados muestran la acumulación preferente de las nanopartículas en las zonas inflamadas así como un aumento del efecto terapéutico del fármaco

que se atribuye a las ventajas que ofrece la encapsulación. Se concluye que las nanopartículas mesoporosos de sílice con puertas moleculares podrían ser una herramienta importante para el desarrollo de nuevas estrategias terapéuticas en el campo de la inflamación.

Basándonos en los resultados obtenidos en el capítulo tres, en el capítulo cuatro se describe un sistema de liberación controlada para el tratamiento de la inflamación pulmonar aguda. Debido a la falta de efectividad de los tratamientos actuales en pacientes de inflamación pulmonar aguda, la búsqueda de terapias alternativas que permitan la administración directa de fármacos a los pulmones se ha convertido en un área de investigación de interés. Aprovechando la acumulación preferente de las nanopartículas en las zonas inflamadas, así como en los pulmones, en este capítulo se presenta un nanosistema para la liberación dirigida de fármacos en inflamación pulmonar. Se ha preparado un nanosistema basado en nanopartículas mesoporosas de sílice cargadas con el glucocorticoide dexametasona y funcionalizadas covalentemente con una puerta molecular peptídica que reconoce el receptor del factor de necrosis tumoral 1 (TNFR1), que a su vez actúa como agente diana para la acumulación preferente en macrófagos pro-inflamatorios. El funcionamiento de la puerta molecular se ha comprobado en ensayos de liberación en presencia de extracto lisosomal, así como su internalización selectiva en ensayos celulares empleando macrófagos pro-inflamatorios. Finalmente la actividad terapéutica del sistema diseñado se ha corroborado en ensayos *in vitro* en macrófagos pro-inflamatorios, e *in vivo* en un modelo de ratón de inflamación pulmonar aguda. Se ha comprobado la acumulación preferente de las nanopartículas en los pulmones inflamados a través de ensayos de biodistribución, así como la mejora del efecto terapéutico de la dexametasona en la reducción del daño pulmonar, minimizando los efectos adversos asociados a la administración del fármaco libre. Con todo ello se concluye que las nanopartículas mesoporosas de sílice pueden ser utilizadas para el tratamiento de la inflamación pulmonar aguda pudiendo ser una herramienta útil para superar las limitaciones de los tratamientos actuales.

En el quinto capítulo se describe otro sistema de liberación controlada de fármacos para inflamación pulmonar aguda. En este caso, se aborda el uso de un

nuevo inhibidor del inflamasoma, QM-378, como terapia farmacológica alternativa. Teniendo en cuenta la baja o nula efectividad de las terapias farmacológicas en la inflamación pulmonar aguda, el QM-378 se encapsula en nanopartículas mesoporosas de sílice funcionalizadas con la puerta molecular péptidica que reconoce TNFR1, con el objetivo de potenciar la administración directa en los pulmones inflamados tal y como se describía en el capítulo anterior. En primer lugar se ha comporbado el funcionamiento de la puerta molecular así como la internalización selectiva en macrófagos pro-inflamatorios. En los ensayos *in vitro* en modelos celulares de inflamaciónse ha demostrado el efecto terapéutico del QM-378 tras su encapsulación. Finalmente se ha comprobado el efecto terapéutico del QM-378 y del fármaco encapsulado en las nanopartículas en un modelo *in vivo* de inflamación pulmonar aguda. La acumulación preferente de las nanopartículas en los pulmones inflamados queda demostrada a través de los ensayos de biodistribución, así como la mejora del efecto terapéutico del QM-378 en la reducción del daño pulmonar, debido a las ventajas de la encapsulación en un nanosistema dirigido. Con todo ello se concluye que el QM-378 es un buen candidato para el tratamiento de la inflamación pulmonar aguda, y que su encapsulación en las nanopartículas mesoporosas de sílice ofrece una administración pulmonar directa y controlada, consiguiendose así una mejora en el perfil terapéutico del fármaco.

Por último, en el capítulo seis, se presentan las conclusiones principales extraídas de los estudios con los diferentes nanosistemas preparados para su aplicación biomédica así como las conclusiones generales extraídas del desarrollo de esta tesis doctoral. La conclusión principal es que el desarrollo de nanomateriales mesoporosos de sílice para la liberación controlada de fármacos se presenta como una nueva estrategia con gran potencial en el campo de las enfermedades inflamatorias. Se espera que los resultados obtenidos sirvan de base para el diseño de nuevos nanomateriales inteligentes con aplicación en distintas áreas de la nanomedicina.

Resum

La present tesi doctoral titulada “Nanomaterials amb portes moleculars com a plataforma d'alliberament controlat de fàrmacs per al tractament de desordres inflamatoris” se centra en el disseny, preparació, caracterització i avaluació de nanomaterials híbrids orgànic-inorgànics, basats en nanopartícules mesoporoses de sílice, funcionalitzades amb biomolècules que actuen com a portes moleculars per a l'alliberament controlat de fàrmacs en aplicacions biomèdiques, en concret en el camp de la inflamació.

En el primer capítol s'introdueix, a nivell general, els diferents conceptes relacionats amb la nanotecnologia, nanomedicina, els materials mesoporosos i les portes moleculars, així com la interacció de les nanopartícules a nivell biològic amb l’organisme i les cèl·lules. Finalment s'introdueixen conceptes bàsics d'inflamació, resposta inflamatòria, el seu paper en els desordres inflamatoris així com l'aplicació dels nanomaterials com a teràpia.

A continuació, en el segon capítol, s’exposen els objectius generals de la present tesi doctoral així com els objectius concrets que són abordats en els següents capítols experimentals.

En el tercer capítol es presenta un nanomaterial per a l'alliberament controlat de l'inhibidor de caspasa-1, VX-765, aprofitant que les nanopartícules s'acumulen preferencialment en les zones inflamades. En concret, s'han preparat nanopartícules mesoporoses de sílice, carregades amb el fàrmac VX-765 i funcionalitzades covalentment amb ε-poli-L-lisina com a porta molecular. El funcionament correcte de la porta molecular s'ha comprovat a través d'estudis d'alliberament controlat en presència de proteases, produint-se l'alliberament del fàrmac sol en presència de l'enzim. La no toxicitat del nanosistema, així com la capacitat d'internalització, s'ha comprovat en el model cel·lular de monòcits humans THP-1. L'activitat anti-inflamatòria del material s'ha comprovat tant *in vitro*, en el model cel·lular de THP-1, com *in vivo* en ratolins en un model d'inflamació de bossa d'aire. Els resultats mostren la acumulació preferent de les nanopartícules en les zones inflamades així com un augment de l'efecte terapèutic del fàrmac, atribuÏt als avantatges que ofereix l'encapsulació. Es conclou que les

nanopartícules mesoporoses de sílice amb porta molecular podrien ser una eina important per al desenvolupament de noves estratègies terapèutiques en el camp de la inflamació.

Basant-nos en els resultats obtinguts en el capítol tres, en el capítol quatre es presenta un sistema d'alliberament controlat per al tractament de la inflamació pulmonar aguda. Degut a la falta d'efectivitat dels tractaments actuals en pacients d'inflamació pulmonar aguda, la recerca de teràpies alternatives que permeten l'administració directa de fàrmacs als pulmons s'ha convertit en una àrea d'investigació d'interés. Aprofitant la acumulació preferent de nanopartícules en les zones inflamades, així com en els pulmons, en aquest capítol es presenta un nanosistema per a l'alliberament dirigit de fàrmacs en inflamació pulmonar. S'ha preparat un nanosistema basat en nanopartícules mesoporoses de sílice carregades amb el glucocorticoide dexametasona i funcionalitzades amb la unió covalent de una porta molecular peptídica que reconeix el receptor del factor de necrosi tumoral 1 (TNFR1), que al seu torn actua com a agent diana per a la acumulació preferent en macròfags pro-inflamatoris. El correcte funcionament de la porta molecular s'ha comprovat en assajos d'alliberament en presència d'extracte lisosomal, així com la internalització selectiva en assajos cel·lulars en macròfags pro-inflamatoris. Finalment l'activitat terapèutica del sistema dissenyat s'ha corroborat en assajos *in vitro* en macròfags pro-inflamatoris, i *in vivo* en un model de ratolí d'inflamació pulmonar aguda. S'ha comprovat la acumulació preferent de les nanopartícules en els pulmons inflamats a través d'assajos de biodistribució, així com la millora de l'efecte terapèutic de la dexametasona en la reducció de la lesió pulmonar minimitzant els efectes adversos associats a l'administració del fàrmac lliure. Amb tot això es conclou que les nanopartícules mesoporoses de sílice poden ser utilitzades per al tractament de la inflamació pulmonar aguda ja que poden ajudar a superar les limitacions dels tractaments actuals.

En el cinqué capítol es mostra també un sistema d'alliberament controlat de fàrmacs per a inflamació pulmonar aguda. En aquest cas, es descriu l'ús d'un nou inhibidor de l'inflamasoma, QM-378, com a teràpia farmacològica alternativa al tractament de la inflamació descontrolada en la inflamació pulmonar aguda.

Tenint en compte la poca efectivitat de les teràpies farmacològiques en la inflamació pulmonar aguda, el QM-378 s'encapsula en les nanopartícules mesoporoses de sílice funcionalitzades amb la porta molecular péptidica que reconeix TNFR1, amb l'objectiu de potenciar l'administració directa en els pulmons inflamats tal com es descrivia en el capítol quart. Així doncs, es comprova el correcte funcionament de la porta molecular així com la internalització selectiva en macròfags pro-inflamatoris. A més es demostra el efecte terapèutic del QM-378 després de la seua encapsulació en models celulars de inflamació. Finalment es comprova l'efecte terapèutic del QM-378 en el model *in vivo* d'inflamació pulmonar aguda, així com el seu efecte després de l'encapsulació en les nanopartícules. La acumulació preferent de les nanopartícules en els pulmons inflamats queda demostrada a través dels assajos de biodistribució, així com la millora de l'efecte terapèutic del QM-378 en la reducció de la inflamació pulmonar, atribuït als avantatges de l'encapsulació en un nanosistema dirigit. Amb tot això es conclou que el QM-378 és un bon candidat per al tractament de la inflamació pulmonar aguda, i que la seua encapsulació en les nanopartícules mesoporoses de sílice ofereix una administració pulmonar directa i controlada aconseguint-se així una millora en el perfil terapèutic del fàrmac.

Finalment, es presenten les conclusions principals extretes dels estudis amb els diferents nanosistemes preparats per a la seua aplicació biomèdica així com les conclusions generals extretes del desenvolupament d'està tesi doctoral. La conclusió principal és que el desenvolupament de nanomaterials mesoporosos de sílice per a l'alliberament controlat de fàrmacs es presenta com una estratègia amb molt potencial en el camp de les malalties inflamatòries. S'espera que els resultats obtinguts servisquen de base per al disseny de nous nanomaterials intel·ligents amb aplicació en diferents àrees de la nanomedicina.

Abstract

This PhD thesis entitled "*Gated nanomaterials as delivery platform to manage inflammatory disorders"* is focused on the design, synthesis, characterization and evaluation of hybrid organic-inorganic nanomaterials using mesoporous silica nanoparticles, functionalized with biomolecules acting as molecular gates for controlled drug release in biomedical applications, specifically in the field of inflammation.

The first chapter includes an overview of the different concepts related to nanotechonology, nanomedicine, mesoporous silica materials and molecular gates, as well as the interactions of nanoparticles with biological systems. Finally, basics concepts of inflammation, inflammatory response and its role in inflammatory disorders are included, as well as the role of nanomedicine in inflammatory therapy.

Next, in the second chapter, the general objectives of this PhD thesis and the specific objectives that are addressed in the following experimental chapters are presented.

In the third chapter, we present a new nanodevice for the controlled delivery of VX-765, a caspase 1 inhibitor, which takes advantage of the intrinsic passive targeintg effect of the nanoparticles to inflamed tissues. In particular, mesoporous silica nanoparticles loaded with the drug VX-765 and functionalized with ε-poly-L-lysine (acting as gatekeeper) have been prepared. The proper gating mechanisms of the nanodevice have been tested in the presence of proteases, thus corroborating the cargo is relased only in the presence of the enzymatic stimulus. The non-toxicity of the nanosystem, as well as, the celluar uptakte capacity has been demonstrated in the human monocyte cell line THP-1. The anti-inflammatory activity of the prepared nanodevice has been evaluated both *in vitro*, in the cellular model of THP-1, and *in vivo* using air pouch mouse as model of inflammation. The results showed the preferential accumulation of the nanoparticles in the inflamed tissue, as well as an increase in the therapeutic effect of the entrapped drug. As conclusion, gated mesoporous silica

nanoparticles constitute an important tool for the development of new therapeutic strategies in the inflammatory field.

Based on the previous results presented in chapter three, a drug delivery system for the treatment of acute lung injury is described in chapter four. Attending to the lack of effectiveness of current treatments in acute lung injury patients, the development of new alternative therapies that allow the direct delivery of drugs into the lung has become and attractive research area. In this chapter, we present a nanodevice for the targeted-lung delivery of drugs in acute lung injury, taking advantage of the preferential accumulation of the nanoparticles to the inflamed areas, as well as to the lungs. Mesoporous silica nanoparticles has been prepared, loaded with the glucocorticioid dexamethasone and capped wih a peptide gatekeeper that recognizes the receptor of tumour necrosis factor 1 (TNFR1), which also targets the pro-inflammatory macrophages. The gating properties have been evaluated in drug delivery studies in the presence of lysosomal extract, as well as the preferential nanoparticles' uptake by pro-inflammatory macrophages. Finally, the therapeutic activity of the designed nanoparticles has been studied *in vitro* in pro-inflammatory macrophages, and *in vivo* in an acute lung injury mouse model. The preferential accumulation of the nanoparticles in the inflamed lungs has been corroborated through biodistribution assays, as well as the ability to enhance the dexamethasone therapeutic effect by the reduction of lung injury and minimizing the undesired side effects associated of the free drug administration. As conclusion, gated mesoporous silica nanoparticles can be used for the treatment of acute lung injury and represent a potential tool to overcome the limitations of current treatments.

The fifth chapter also presents a drug delivery system for acute lung injury. In this case, we use the novel inflammasome inhibitor QM-378 as pharmacological alternative therapy to the treatment of uncontrolled inflammation in acute lung injury. Taking into account the inffectiveness of pharmacological therapies to reach inflamed lungs, QM-378 is encapsulated in mesoporous silica nanoparticles capped with a peptidic gate that recognizes TNFR1, with the aim of enhancing the direct drug delivery in lungs. In a first step, the proper working of the gating

ensemble in the final nanodevice was tested and the active targeting effect to pro-inflammatory macrophages is corroborated. Furthermore, the proper anti-inflammatory activity of QM-378 after its encapsulation is demonstrated in inflammatory cellular models. Finally, the therapeutic effect of QM-378 has been tested in an acute lung injury mouse model, as well as its effect after encapsulation in nanoparticles. The preferential accumulation of nanoparticles to inflamed lungs has been also corroborated through biodistribution assays. An enhancement of the therapeutic effect of QM-378 by reducing lung inflammation is demonstrated, due to the advantages of drug encapsulation in a targeted-lung nanosystem. As conclusion, the QM-378 is a suitable candidate for acute lung injury treatment, and its encapsulation in mesoporous silica nanoparticles offers a direct lung drug delivery thus improving the therapeutic profile of the drug.

Finally, the principal conclusions from the studies with the different prepared nanosystems and the general conclusions from this PhD thesis are presented in chapter six. The preparation of mesoporous silica nanoaprticles for drug delivery is presented as potential strategy in the field of inflammatory disorders. It is expected that the results obtained will serve as basis for the design of new nanomaterials for biomedical applications.

Publications

Results of this PhD Thesis and other contributions have resulted in the following scientific publications.

- **A. García-Fernández**, M. Sancho, V. Bisbal-Velasco, R. Martínez-Máñez, M. Orzáez; F. Sancenón; Targeted-lung delivery of glucocorticoids using gated mesoporous silica nanoparticles. A new therapeutic approach for acute lung injury treatment; submitted, **2019**.

- **A. García-Fernández**; B. Lozano-Torres; J. Monreal-Trigo; J. F. Blandez; J. Soto; J. E. Collazos-Castro; M. Alcañiz; M. D. Marcos; M. Orzáez; F. Sancenon**;** Electro-responsive films based on voltage-gated mesoporous silica nanoparticles grafted onto PEDOT-based conducting polymer; *Journal of Controlled Release,* under revision*,* **2019**.

- **A. García-Fernández**, E. Aznar, R. Martínez-Máñez, F. Sancenón**,** Gating techniques in drug delivery systems; *Small,* under revision, **2019*.***

- A. Llopis-Lorente, **A. García-Fernández**, E. Lucena, P. Díez, R. Villalonga, D. Wilson, R. Martínez-Máñez, Nanobots Based on Gated Enzyme-Powered Janus Au-Mesoporous Silica Nanoparticles Capable of Autonomous Motion and Controlled Cargo Delivery**;** Submitted, **2019.**

- S. Jimenez-Falcao, B. de Luís, **A. García-Fernández**, A. Llopis-Lorente, P- Díez, A. Sánchez, F. Sancenón, P. Martínez-Ruíz, R. Martínez-Máñez, R. Villalonga; Glucose-responsive enzyme-controlled mesoporous nanomachine with a layer-by-layer supramolecular architecture**,** *ACS Applied Bio Materials,* **2019**, DOI:10.1021/acsabm.9b00338.

- A. Llopis-Lorente, **A. García-Fernández**, N. Murillo-Cremaes, A. C. Hortelão, T. Patiño, R. Villalonga, F. Sancenón, R. Martínez-Mañez, S. Sánchez; Enzyme-

Powered Gated Mesoporous Silica Nanomotors for On-Command Intracellular Payload Delivery, ACS Nano, under revision, **2019**.

- S. Jimenez-Falcao, N. Joga, **A. García-Fernández**, A. Llopis Lorente, D. Torres, B. de Luis, F. Sancenón, P. Martínez-Ruiz, R. Martínez-Máñez, R. Villalonga, Janus nanocarrier powered by bi-enzymatic cascade system for smart delivery, *Journal of Materials Chemistry B*, **2019**, *7*, 4669-4676.

- T. M. Godoy-Reyes; A. Llopis-Lorente**; A. García-Fernández**; P. Gaviña; A. M. Costero; R. Martínez-Máñez; F. Sancenón. Acetylcholine-responsive cargo release using acetylcholinesterase-capped *nanomaterials, Chemical Communications*, **2019**, *55*, 5785-5788.

- Tania M. Godoy-Reyes; Antoni Llopis-Lorente; **A. García-Fernández**; Pablo Gaviña; Ana M. Costero; Reynaldo Villalonga; Félix Sancenón; Ramón Martínez-Máñez. L-Glutamate-Responsive Delivery System Based on Enzyme-Controlled Self-Immolative Arylboronate-Gated Nanoparticles, *Organic Chemistry Frontiers*, **2019**, *6*, 1058-1063.

- Yolanda Salinas; Carolin Hoerhager; **Alba García Fernández**; Marina Resmini; Félix Sancenón; Ramón MartínezMáñez; Oliver Bruggemann. Biocompatible ZnS-based Quantum dots designed as perfect caps in hybrid materialsfor on-demand pH-triggered release in cancer cells, *ACS Applied Materials & Interfaces*, **2018**, *40*, 34029 -34038.

- L. Polo; N. Gómez Cerezo; **A. García Fernández**; E. Aznar; J.L. Vivancos; D. Arcos; M. Vallet Regí; R. Martínez Máñez.Mesoporous bioactive glasses equipped with stimuli-responsive molecular gates for the controlled delivery of levofloxacin against bacteria, *Journal of Materials Chemistry B*, **2018**,
- A. Llopis-Lorente, B. de Luis, **A. García-Férnandez**, S. Jimenez-Falcao, M. Orzáez, F. Sancenón, R. Villalonga, R. Martínez-Máñez. “Hybrid Nanocarriers

Act by Processing Logic Tasks: Toward the Design of Nanobots Capable of Reading Information from the Environment". *ACS Applied Materials & Interfaces,* **2018**, *10*, 26494-26500.

L. Pascual; C. Cerqueira-Coutinho; **A. García-Fernández**; B. de Luis; E. Soares Bernardos; M. Souza Albernaz; S. Missailidis; R. Martínez-Máñez; R. Santos-Oliveira; M. Orzáez; F. Sancenón. MUC1 aptamer-capped mesoporous silica nanoparticles for controlled drug delivery and radio-imaging applications. *Nanomedicine*, **2017**, *13*, 2495-2505.

- A. Llopis-Lorente, B. de Luis**, A. García-Férnandez, P**. Díez, A. Sánchez, M. D. Marcos, F. Sancenón, R. Villalonga, R. Martínez-Máñez, F. Sancenón. "Au-Mesoporous Silica Nanoparticles Gated with Disulfide-Linked Oligo(Ethylene Glycol) Chains for Tunable Cargo Delivery Mediated by an Integrated Enzym*atic Control* U**nit"**. *Journal of Materials Chemistry B*, **2017**, *5*, 6734-6739.

- **A. García Fernández**; G. García Laínez; M.L. Ferrándiz; E. Aznar; F. Sancenón; M.J. Alcaraz; J.R. Murguía; M.D. Marcos; R. Martínez Máñez; A. M. Costero; M. Orzáez. Targeting the inflammasome by the inhibition of caspase-1 activity using capped mesoporous silica nanoparticles, *Journal of Control Release*, **2017**, *248*, 60- 70.

- C. De la Torre Paredes; L. Mondragón Martínez; C. Coll Merino; **A. García Fernández**; F. Sancenón Galarza; R. Martínez Máñez; P. José Amorós del Toro; E. Pérez Payá; M. Orzáez Calatayud, Caspase 3 Targeted Cargo Delivery in Apoptotic Cells Using Capped Mesoporous Silica Nanoparticles, *Chemistry A European Journa*l, **2015**, *44*, 15506 – 15510.

Abbreviations and Acronyms

ADR	Acquired drug resistance
AIM2	Absent in melanoma 2
ALI	Acute lung injury
ALR	AIM2-like receptor
AMF	Alternating magnetic field
APTES	3-aminopropyltriethoxysilane
ARDS	Acute respiratory distress syndrome
ASC	Apoptosis-associated speck-like protein containing a caspase-recruitment domain
ATP	Adenosine 5'-triphosphate
AuNRs	Gold Nanorods
BAL	Bronchoalveolar lavage
BALF	Bronchoalveolar lavage fluid
BCA	Bicinchoninic acid
BET	Brunauer-Emmet-Teller
BJH	Barret-Joyner-Halenda
C1	Caspase 1
CARD	Caspase-recruitment domain
Casp1	Caspase 1
CET	Cetuximab
CD	Cluster of differentiation
Cdna	Complementariy DNA
CdTe	Cadmium Telluride
CCL	Chemokine C-C motif ligand
CCR	Chemokine C-C motif receptor
COX	Cycloxygenase
CTABr	Cetyltrimethyalmonium bromide
CXCL	Chemokine C-X-C motif ligand
DAMPs	Danger-associated molecular patterns

Dex	Dexamethasone
DLS	Dynamic light scattering
DMSO	Dimethyl sulfoxide
DNA	Deoxryribonucleic acid
Dox/Doxo	Doxorubicin
DR	Drug resistance
DPPC	1,2-dipalmitoyl-sn-glycero-3-phosphocholine
DPPE	1,2-dipalmitoyl-*sn*-glycero-3-phosphoethanolamine
DSPE	1,2-Distearoylphosphatidylethanolamine
DDT	Dithiothreitol
EA	Elemental analysis
ECL	Enhanced chemiluminescence
EDTA	*Ethylenediaminetetraacetic acid*
EDX	Energy dispersive x-ray spectroscopy
EGFR	Epidermal growth factor receptor
EGTA	Ethylene glycol-bis(β-aminoethyl ether)-N,N,N',N'-tetraacetic acid/egtazic acid
ELISA	Enzyme-Linked ImmunoSorbent Assay
ELVIS	Extravasation through leaky vasculature and inflammatory cell-mediated sequestration
EPR	Enhanced Permeability and Retention
FBS	Fetal Bovine Serum
FDA	Food and Drug Administration
FITC	Fluorescein isothiocyanate
FR	Folate receptors
FT-IR	Fourier-transform infrared specstrocospy
GAPDH	Glyceraldehyde-3-phosphate dehydrogenase
GCs	Glucocorticosteroids/Glucocorticoids
GEF	Geftinib
GRAS	Generally recognized as safe
GSDMD	Gasdermin D

GSH	Glutathione
HA	Hyaluronic acid
HAase	Hyaluronidase
HPLC	High-performance liquid chromatography
H&E	Hematoxylin and eosin
IC_{50}	Half maximal inhibitory concentration
ICAM	Intracellular adhesion molecule
IFN-ϒ	Interferon-gamma
ILs	Interleukins
IUPAC	Union of Pure and Applied Chemistry
I.V.	Intravenous
LCST	Low critical solution temperature
LD_{50}	Lethal dose for 50% of the population
LDH	Lactate dehydrogenase
LPS	Lipopolysaccharide
MAPK	Mitogen-activated protein kinases
MCM	Mobil Composition of Matter
MDP	Muramyl dipeptide
MIR	Magnetic resonance imaging
MMPs	Metalloproteinases
MPO	Myeloperoxidase
mRNA	Messenger RNA
MSNs	Mesoporous silica nanoparticles
NCO	(3-isocyanatopropyl)triethoxysilane
NK-κB	Nuclear factor kappa B
NG	Nigericin
NIR	Near-infrared
NLRs	NOD like receptors
NLRP	NOD like receptor pyridine domain containing
NMR	Nuclear magnetic resonance
NPs	Nanoparticles

NSAIDs	Nonsteroidal anti-inflammatory drugs
SBA	Santa Barbara Amorphous
SEM	Scanning electron microscopy
STEM	Scanning transmission electron microscopy
PAS	Periodi Acid Schiff
PAGE	Polyacrylamide gel electrophoresis
PAMPs	Pathogen-associated molecular patterns
PBS	Phosphate buffer saline
PCR	Polymer chain reaction
PDA	Polydopamine
PEI	Polyethyelenimine
PEG	Polyethyelenglycol
PMA	Phorbol 12-myristate 13-acetate
PPRs	Pattern-recognition receptors
PTFE	Polytetrafluoroethylene
PXRD	Powder x-ray diffraction
QDs	Quantum dots
QM-378	1,3-dihydro-2H-indol-2-one derivative
QRT-PCR	Quantitative real time-polymerase chain reaction
qPCR	Quantitative polymerase chain reaction
RGD	Arginylglycylaspartic acid
RhB	Rhodamine B
RIG I	Retinoic acid-inducible gene I
RLR	RIG-I-like receptor
RNA	Ribonucleic acid
ROS	Reactive oxygen species
RP-HPLC	Reversal Phase-High-performance liquid chromatography
RPMI	Roswell Park Memorial Institute
RT	Reverse transcribed
RT-PCR	Reverse transcription polymerase chain reaction
SEM	Standard error of the mean

SDS	Sodium dodecyl sulphate
SP-A	Pulmonary surfactant protein
TAT	Transactivator of transcription
TEM	Transmission electron microscopy
TEOS	Tetraethyl orthosilicate
TFA	Trifuloroacetic acid
TGA	Thermogravmetric analysis
TKI	Tyrosine kinase inhibitor
TLRs	Toll-like receptors
TMAH	Tetramethylammonium hydroxide
TNF-α	Tumour Necrosis Factor-alpha
TNFR/TNF-R	Tumour Necrosis Factor Receptor
TOS	Tocopheryl succinate
Tris	Tris-hydroxymethyl-aminomethane
US	Ultrasouhds
UV-Vis	Ultraviolet-Visible
VEGF	Vascular endothelial growth factor
WST-1	Water soluble tetrazolium-1

Table of Contents

Chapter 1 | General introduction 5

1.1 Nanotechnology and nanomedicine 7

1.2 Mesoporous silica materials in advanced applications 9

1.2.1 Synthesis of mesoporous silica nanoparticles 11

1.2.2 Functionalization of mesoporous silica materials 13

1.2.3 Characterization of mesoporous silica materials 16

1.2.4 Stimuli-responsive gated materials 20

1.3 Gated mesoporous silica nanoparticles as drug delivery systems in biomedical applications 22

1.3.1 Biocompatibility and biodistribution of mesoporous silica nanoparticles 25

1.3.2 Targeting and cellular uptake of mesoporous silica nanoparticles 30

1.3.3 Stimuli responsive gated mesoporous silica nanoparticles 35

1.3.4 Clinical relevance of gated mesoporous silica nanoparticles 63

1.4 Gated mesoporous silica nanoparticles as drug delivery systems in inflammatory disorders 67

1.4.1 Inflammation and inflammatory response 67

1.4.2 Inflammasomes 70

1.4.3 Drug delivery systems as therapeutic approaches in inflammatory disorders 76

Chapter 2 | Objectives 85

Chapter 3 | Targeting inflammasome using mesoporous silica nanoparticles 89

3.1 Abstract 93

3.2 Introduction 93

3.3 Materials and methods 96

3.4 Results and discussion 105

3.5 Conclusions 124

3.6 References 125

3.7 Supporting Information 130

Chapter 4 | Targeted-lung delivery of glucocorticoids for acute lung injury 135
4.1 Abstract 139
4.2 Introduction 140
4.3 Results and discussion 143
4.4 Conclusions 162
4.5 Materials and methods 163
4.6 References 174
4.7 Supporting Information 180

Chapter 5 | Targeted-lung delivery of QM-378 for acute lung injury treatment. 193
5.1 Abstract 197
5.2 Introduction 198
5.3 Materials and methods 201
5.4 Results and discussion 210
5.5 Conclusions 225
5.6 References 225
5.7 Supporting Information 229

Chapter 6 | Conclusions and Perspectives 241

Chapter 1 | General introduction

1.1 Nanotechnology and nanomedicine

Nanotechnology is a multidisciplinary field in which the matter is manipulated at atomic and molecular scale into smaller structures. This field includes from the study of matter with dimensions ranging from one to a few hundred nanometers, to the investigation of practical applications (see Figure 1). Since Richard Feynman[1] introduced the concept in 1959 and Norio Taniguchi[2] defines the new and developing field of nanotechnology in 1974 considerably advances in the nanotechnology area has been achieved. Nanomaterials take advantage of their small sized and acquire new properties that are not observed in their bulk counterparts.[3] These new properties have resulted on the growing

[1] R. P. Feynman, *Caltech Eng. Sci.* **1960**, *23*, 22-36.

[2] N. Taniguchi, *Proc. Intl. Conf. Prod. Eng. Tokyo, Part II, Japan Society of Precision Engineering*, **1974**

[3] A. Alagarasi, *Introduction to Nanomaterials*, in B. Viswanathan, Nanomaterials, **2009**, Ed. Narosa Publishing House.

development of nanosystems and nanodevices with have found applications in areas such as chemistry, biotechnology and medicine.[4,5]

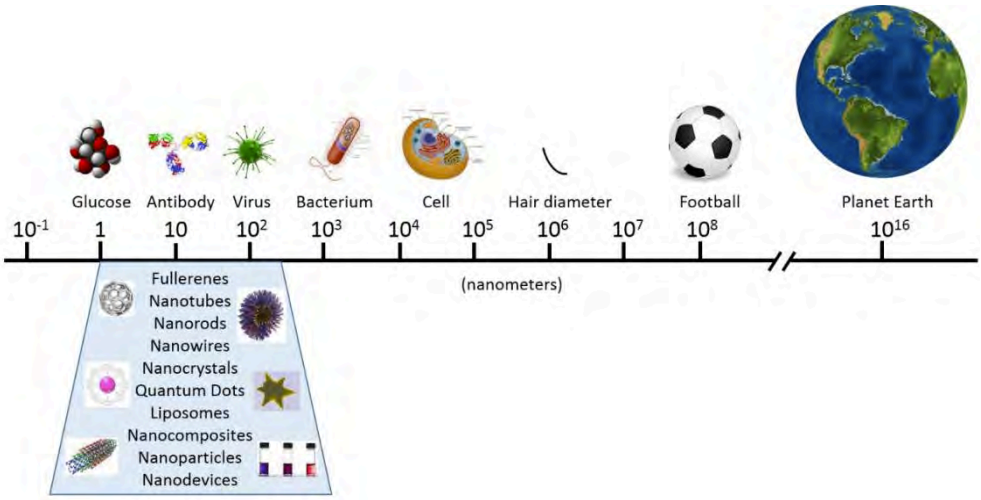

Figure 1. Scheme of nanomaterials scale compared to biomolecules, cells and other items.

One appealing field in nanotechnology is nanomedicine. Nanomedicine results of the combination of nanotechnology with the interaction of biomolecules at the extracellular level and inside the human cells. The main areas of research in nanomedicine are diagnostic applications (in which synthesised nanoparticles allow the recognition of specific biomolecules), regenerative medicine (in which biocompatible nanodevices are designed to allow cell growth), and the development of drug delivery nanosystems (for targeted drug release at specific site). Of the three areas cited above, the development of drug delivery nanosystems is perhaps the most widely developed. These nanocarriers are capable to release drugs at specific regions or cells, improving the drug biodistribution and the therapeutic effect of treatments reducing undesired side effects. In this context, diverse nanoparticles and nanomaterials have been

[4] G. Kagur, T. Singh, A. Kumar, *IJEAR* **2012**, *2*, 50.
[5] B. Szefler, *Int. J. Nanomedicine* **2018**, *13*, 6143.

developed as drug delivery systems based on both organic supports (such as liposomes and polymers) and inorganic supports (including quantum dots, gold, metal oxides and silica-based materials).[6,7]

Nanomedicine is in constant growth and remarkable advancements have been achieved in the last decades, being more than 50 nanomedicines approved by the Food and Drug Administration (FDA).[8] However, there are still many unsolved clinical problems and more research efforts are needed to reach more clinical applications of nanomedicines. In this scenario, several new advances in this area are anticipated in the near future.[9]

1.2 Mesoporous silica materials in advanced applications

Over the last decades, interest in porous materials has drastically increased, due to their large specific surface area and attending their potential applications in different fields such as catalysis,[10] adsorption,[11] sensing,[12] and drug delivery.[13] Porous materials are classified by the International Union of Pure and Applied Chemistry (IUPAC) according to the pore size as microporous (pore size < 2 nm), mesoporous (2-50 nm) and macroporous (>50 nm) materials.[14]

In this context, mesoporous silica materials have attracted great attention since in 1992 researchers from Mobil Oil Company reported the synthesis of these

[6] W. E. Bawarski, E. Chidlowsky, D. J. Bharali, S. A. Mouse, *Nanomedicine*, **2008**, *4*, 273.
[7] Y. H. Choi, H. -K. Han, *J.Pharm. Investig.* **2018**, *48*, 43.
[8] D. Bobo, K. J. Robinson, J. Islam, K. Thurecht, S. R. Corrie, *Pharm. Res.* **2016**, *33*, 2373.
[9] G. G. Genchi, A. Marino, A. Grillone, I. Pezzini, G. Ciofani, *Adv Healthc Mater*, **2017**, *6*, 1700002.
[10] C. Perego, R. Millini, *Chem. Soc. Rev.* **2013**, *42*, 3956.
[11] K. M. Thomas, *Catal. Today* **2007**, *120*, 389.
[12] D. J. Wales, J. Grand, V. P. Ting, R. D. Burke, K. J. Edler, C. R. Bowen, S. Mintova, A. D. Burrows, *Chem. Soc. Rev.* **2015**, *44,* 4290.
[13] I. Slowing, B. G. Trewyn, S. Giri, V. S. -Y. Lin, *Adv. Funct. Mater*. **2007**,*17*, 1225.
[14] a) IUPAC, *Pure appl. Chem.* **1972**, *31*, 578; b) X. S. Zhao, *J. Mater. Chem.* **2006**, *16*, 623.

solids known as M41S phases.[15] The family of M41S were encoded as Mobile Composition of Matter (MCM) and include the MCM-41 with a hexagonal arrangement of the mesopores, MCM-48 with a cubic arrangement of mesopores and MCM-50 with a lamellar structure (Figure 2).[16] These materials are characterized by large surface areas (with values around 500 and 1000 m^2/g), ordered pore systems (with pore size in the 2-10 nm range), and high pore volumes (in the order of 1 cm^3/g). In addition, in 1998 researchers from Santa Barbara University reported the SBA-15 material which is characterized by a hexagonal arrangement of pores with sizes in the 5-30 nm intervals.[17]

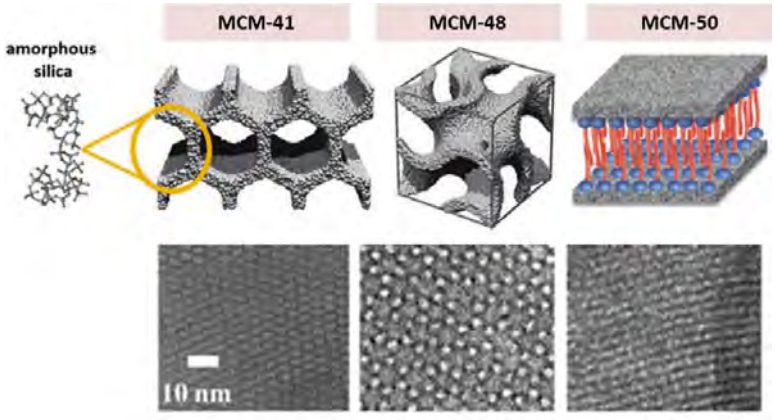

Figure 2. The M41S family of mesoporous silica materials. Schematic 3-D structures on top and corresponding TEM images of the pore network at the bottom. Adapted from *Chem. Soc. Rev.* **2013**, *42*, 3663. Copyright © 2013 The Royal Society of Chemistry and from Handbook of Ecomaterials Springer Cham, **2017**, 978-3-319-48281-1, Copyright © 2017, Springer International Publishing AG.

[15] a) C. T. Kresge, M. E. Leonowicz, W. J. Roth, J. C. Vartuli, J. S. Beck, *Nature* **1992**, *359*, 710; b) J. S. Beck, J. C. Vartuli, W. J. Roth, M. E. Leonowicz, C. T. Kresge, K. D. Schmitt, C. T. W. Chu, D. H. Olson, E. W. Sheppard, *J. Am. Chem. Soc.* **1992**, *114*, 10834.

[16] C. T. Kresge, W. J. Roth, *Chem. Soc. Rev.* **2013**, *42*, 3663.

[17] D. Zhao, J. Feng, Q. Huo, N. Melosh, G. H. Fredrickson, B. F. Chmelka, G. D. Stucky, *Science* **1998**, *279*, 548.

Among these materials, the MCM-41 phase has attracted considerable attention and is the most studied. Its synthesis is well described requiring inexpensive and non-hazardous chemicals, and their size is easily tuneable from micrometric particles to nanoparticles. In addition, this material is featured by high chemical inertness and thermal stability, is biocompatible and its surface can be easily functionalized (using alkoxysilane derivatives) which confers the final materials improved features and advanced functionalities.[18]

1.2.1 Synthesis of mesoporous silica nanoparticles

The synthetic procedure for M41S materials is based on the Stöber method to obtain colloidal mesoporous silica, using a template, acting as structure directing agent, and a silica precursor which polymerizes around the template yielding the final solid mesoporous structure.[19] For this purpose, surfactant molecules are dissolved into polar solvents to obtain liquid crystals, which aggregate themselves forming micelles. These individual micelles self-assembled themselves into supermicellar structures. The features of these supermicellar structures are determined by the used surfactant and the synthesis conditions (such temperature, pH, ionic force among others). In fact, the resulting mesoporous frameworks, such as hexagonal, cubic and laminar, are determined by the structure of these supermicelles. In the final step, silica precursor molecules (such as tetraethyl orthosilicate, sodium silicate or tetramethylammonium silicate) are added and are hydrolysed to form silanol groups (Si-OH), which condensate over the supermicelles, yielding the final network of siloxane bonds (Si-O-Si) with characteristic porous structure. The

[18] J. G. Croissant, Y. Fatieiev, A. Almalik, N. M. Khashab, *Adv. Healthcare Mater.* **2018**, *7*, 1700831.
[19] W. Stöber, A. Fink, E. J. Bohn, *J. Colloid Interf. Sci.* **1968**, *26*, 62.

porous structure and the morphology of the final mesoporous silica material are controlled by the nature of silica precursor, the conditions of pH, ionic force, temperature, time, conformation of the supermicellar structures, the silica-surfactant interactions and the degree of silica polymerization onto the supermicelles. [20]

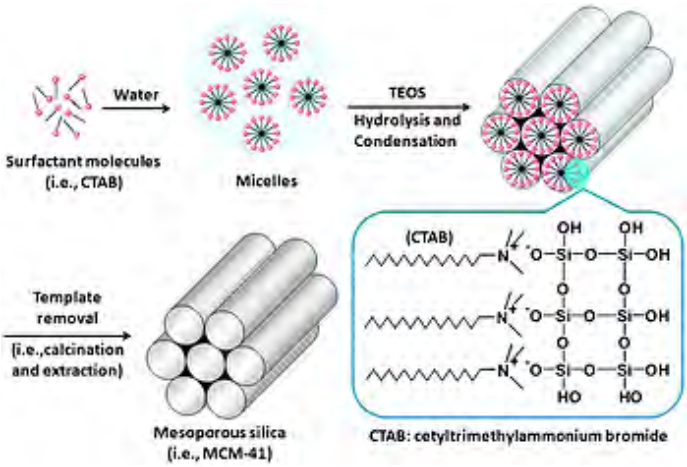

Figure 3. Schematic representation of the synthetic route of mesoporous silica MCM-41 type. Reprinted with permission from *Chem. Soc. Rev.* **2012**, *9*, 3679. Copyright © 2012 The Royal Society of Chemistry.

As described above, within the M41S family, the MCM-41 material is the most widely studied. The synthesis procedure consists in the polymerization of the silica precursor tetraethyl orthosilicate (TEOS) over the supermicelles formed by the surfactant hexadecyltrimethylammonium bromide (CTAB) at 80 °C in basic conditions (adjusted with NaOH) (Figure 3). This mixture is stirred for 2 h and, afterwards, the white solid is collected by centrifugation or filtration. Finally, the surfactant template is removed by calcination of the solid at high temperatures or by extraction process in acidic media. In this case, the final silica scaffold presents

[20] N. K. Raman, M. T. Anderson, C. J. Brinker, *Chem. Mater*. **1996**, *8*, 1682.

a spherical shape of ca. 80-100 nm of diameter with cylindrical unidirectional empty channels of approximately 2.5 nm of diameter, arranged in a hexagonal distribution. In any case, the features of the resulting particles could be easily modified adjusting synthesis parameters such as temperature, time, stirring and used reagents.[21] Moreover, the pore size could also be modified using other type and concentration of surfactant[22], suitable swelling organic molecules[23] or by post-synthesis treatment. In addition, one of the most interesting properties of the MCM-41 based mesoporous materials is that its surface could be modified by introducing small changes in the synthesis route or with a post-synthesis treatment.

1.2.2 Functionalization of mesoporous silica materials

The term functionalization refers to the incorporation of organic groups onto the external or internal surface of mesoporous silica supports, leading to hybrid organic-inorganic materials. These hybrid materials are very attractive in a wide range of applications due to the combination of the properties of the inorganic scaffold with the functional organic moieties anchored onto its surface. The incorporation of these organic molecules allows the modification of surface properties such as; alteration of its reactivity, hydrophilicity, hydrophobicity, binding to guest molecules, stabilization of the final solids towards hydrolysis and chemical attack, etc. In general, two main protocols are used to functionalize

[21] a) H. B. S. Chan, P. M. Budd, T. D. V. Naylor, *J. Mater. Chem.* **2001**, *11*, 951; b) J. Kobler, K. Moller, T. Bein, *ACS Nano* **2008**, *2*, 791.
[22] A. Corma, Q. Kan, M. T. Navarro, J. Perez-Pariente, F. Rey, *Chem. Mater.* **1997**, *9*, 2123.
[23] K. Zhang, L. -L. Xu, J. -G. Jiang, N. Calin, K. -F. Lam, S. -J. Zhang, H. -H. Wu, G. -D. Wu, B. Albela, L. Bonneviot, P. Wu, *J. Am. Chem. Soc*. **2013**, *135*, 2427.

mesoporous silica materials: (i) the grafting procedure and (ii) the co-condensation method.[24]

In the ***grafting procedure***, the inorganic mesoporous silica scaffold is prepared and then, in a post-synthesis step, functionalized with selected organic groups. The surface of silica materials can be easily modified due to the high concentration of silanol groups (Si-OH) present. These groups act as reactive points to covalently anchor organosilanes containing the desired organic groups. Inside the organosilanes the most used are trialkosyxilanes derivatives with $(R'O)_3$-Si-R structure (being R an organic group). The nucleophilic substitution reaction between the silanols and trialkosyxilanes yields multifunctional organic–inorganic hybrid materials in which the organic groups are mainly located on the external surface of the inorganic scaffold (see Figure 4).[25]

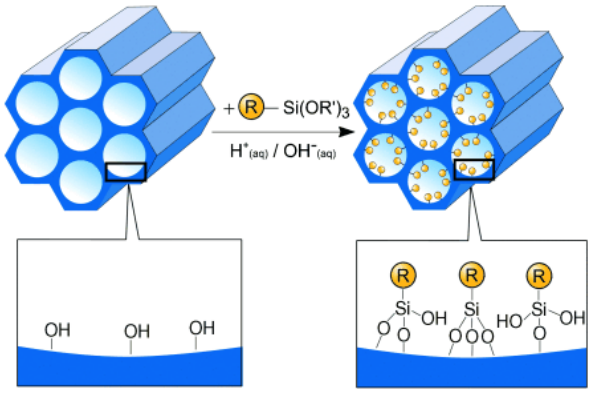

Figure 4. Grafting procedure in a postsynthetic step for functionalization with organic groups upon terminal organosilanes of the type (R'O)3SiR. R=organic functional group. Reprinted with permission from *Angew. Chem. Int. Ed.* **2006**, *45*, 3216. Copyright © 2006 Wiley-VCH.

[24] F. Hoffmann, M. Cornelius, J. Morell, M. Fröba, *Angew. Chem. Int. Ed.* **2006**, *45,* 3216.
[25] A. Stein, B. J. Melde, R. C. Schroden, *Adv. Mater.* **2000**, *12*, 1403.

Using the grafting procedure the original structure of the mesoporous silica is maintained after the functionalization process and therefore allows the synthesis of large amounts of the final hybrid material. In addition, it is possible to achieve a dual functionalization of the material with the modification of the internal surface. For this purpose, when the synthesised mesoporous silica material with the pores filled with the surfactant template, are treated with selected alkoxysilane and the organic moieties are grafted onto the outer surface. Then, the surfactant is removed by the extraction and the scaffold is functionalized with another alkoxysilane. In this second functionalization the organic groups are located in the internal surface of the mesopores.[26]

The ***co-condensation method*** is an alternative process to obtain hybrid materials in which the silica precursor and the selected organosilane are simultaneously introduced in the synthesis procedure and condensate around the surfactant template (see Figure 5). In this case surfactant removal is only suitable by the extraction process. This results in mesoprous silica material with high rate of organic groups homogenously distributed in its surface. However, this procedure presents some drawbacks as the introduction of functional groups can affect the interactions with the surfactant that can result in changes in structure stability and particle morphology. For the above mentioned reasons this method is less commonly used.[27]

[26] A. Casula, A. Llopis-Lorente, A. Garau, F. Isaia, M. Kubicki, V. Lippolis, F. Sancenón, R. Martínez-Máñez, A. Owzarzak, C. Santi, M. A. Scorciapino, C. Caltagirone, *Chem. Commun.* **2017**, *53*, 3729.
[27] R. Anwander, C. Palm, J. Stelzer, O. Groeger, G. Engelhardt, *Stud. Surf. Sci. Catal.* **1998**, *117*, 135.

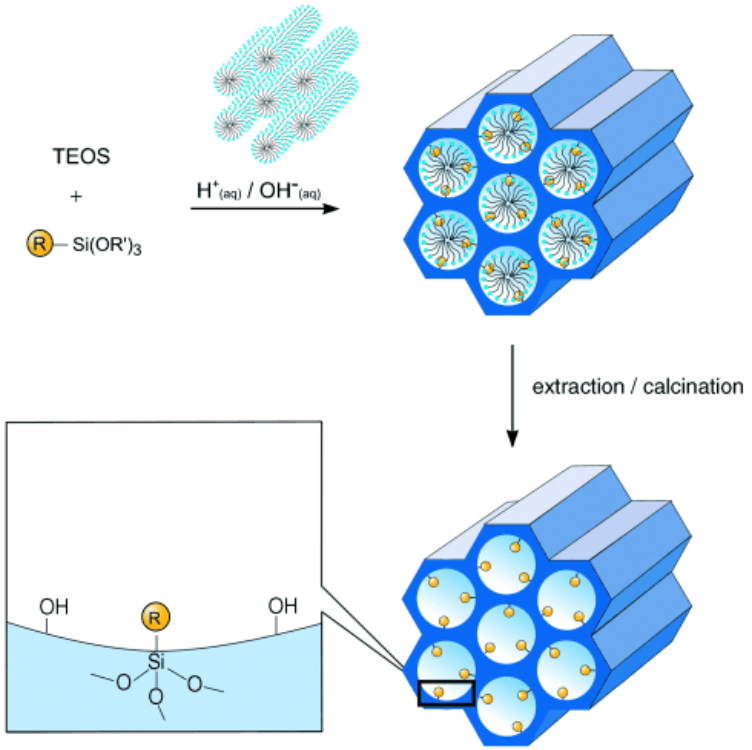

Figure 5. Co-condensation grafting procedure for functionalization with organic groups upon R=organic functional group. Reprinted with permission from *Angew. Chem. Int. Ed.* **2006**, *45*, 3216. Copyright © 2006 Wiley-VCH.

1.2.3 Characterization of mesoporous silica materials

Several standard techniques are employed to characterize the properties of the mesoporous scaffold, its preservation along the different functionalization steps, and to analyse the proper anchoring of the functional groups. The structural properties and porous characteristics are mainly studied by power X-ray diffraction (PXRD), transmission electron microscopy (TEM) and N_2 adsorption-desorption analysis. Besides, dynamic light scattering (DLS) measurements offers information about the hydrodynamic size of the particles. The organic content in

the prepared materials are commonly determined by elemental analysis (AE) and thermogravimetric measurements (TG).

The power X-ray diffraction is used to analyse periodically ordered structure at atomic scales. The source of X-ray emits radiation at different incident angle over the sample, and the diffracted light is collected by the detector to obtain the PXRD patterns. These patterns show the intensity of diffracted light as function of the angle of incident radiation. The intensity peaks or reflections related for each angle are determined by the distance between the atomic planes in the ordered structure in accordance to Brag's law. In the case of MCM-41 based mesoporous silica nanoparticles, the silica phase is an amorphous material but the technique is applicable to characterize the ordered arrangement of the pores. The typical pattern for these materials is characterized by four peaks appearing at low angles being the main peak indexed as the (100) Bragg peak and secondary peaks indexed as (110), (200) and (210) Bragg peaks (see Figure 6).

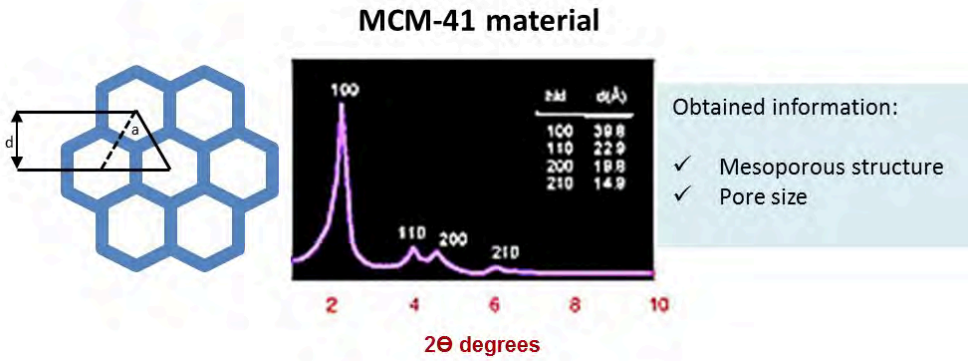

Figure 6. Scheme of the 2D hexagonally lattice with d_{100} spacing and unit cell parameter of MCM-41 material and their characteristic PXRD patterns. Adapted from *Chem. Soc. Rev.* **2013**, *42*, 3663. Copyright © 2013 The Royal Society of Chemistry.

In order to confirm the presence of the mesoporous structure and to visualize the size and morphology of the prepared materials with high resolution, images produced by the detection of primary electrons transmitted through the

sample, transmission electron microscopy (TEM) is used (see Figure 7). In addition, scanning electron microscopy (SEM), which produces images detecting secondary electrons from the surface of material, can be also used to characterize the morphology of mesoporous silica material.

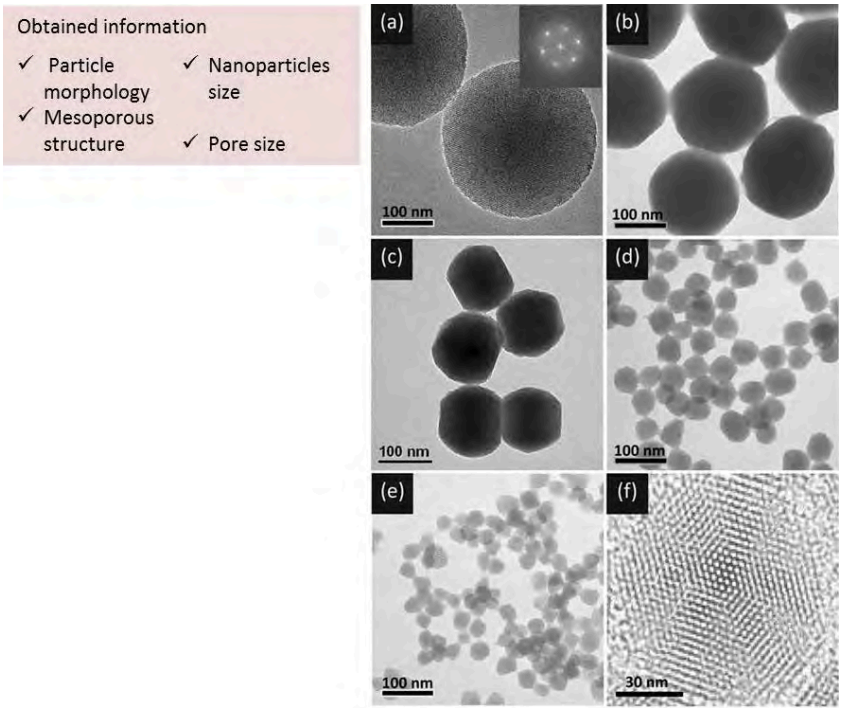

Figure 7. TEM images of mesoporous silica with different average sizes: (a) 280 nm; inset: FFT analysis of the TEM image; (b) 170, (c) 110, (d) 50, (e) 30 nm. (f) High resolution TEM image of a single particle in (c). Reproduced with permission from *Small* **2009**, *5*, 1408. Copyright © 2009 Wiley-VCH.

The textural properties of the mesoporous silica materials are determined by the analysis of the N_2 adsorption-desorption isotherms. These curves give information of the amount of N_2 adsorbed onto the porous material as function of the relative pressure. These isotherms are classified into six types, attending to the structure of the material, being the isotherms IV and V typical of porous

scaffolds (see Figure 8).[28] Moreover, the surface area is usually determined by applying the Brunauer-Emmet-Teller (BET) method on the adsorption section of the isotherm[29] and pore size and pore volume could be calculated using the Barret-Joyner-Halenda (BJH) model.[30]

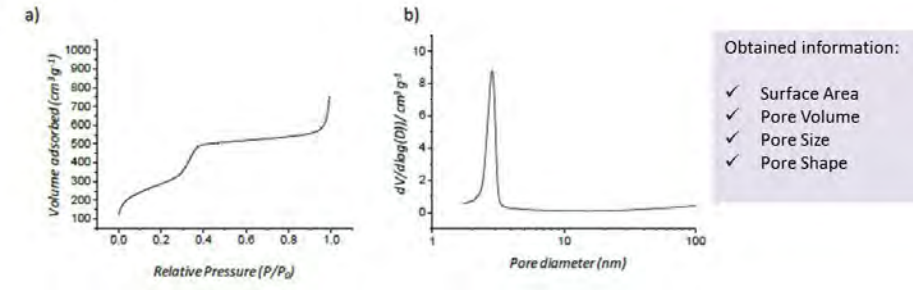

Figure 8. a) N_2 adsorption-desorption isotherm characteristic of mesoporous silica materials and b) pore size- volume distribution**.**

The dynamic light scattering (DLS) measure the fluctuation in scattered light attending the Brownian motion of the particles in a solution upon laser irradiation. The movement of the particles are related with this fluctuation and used to determine the particle size and size distribution. Besides, the DLS allows the determination of the charge on the surface material by the zeta potential function. In this case, the movement of the particles upon an alternating electric field between two electrodes is used to determinate the zeta potential value.

Finally, in order to determine the content of functional organic molecules in the hybrid mesoporous silica materials, several techniques can be employed. The most used is the thermogravimetric analysis (TG), which provides the percentage of loss weight in organic matter as a function of the temperature from

[28] K. S .W. Sing, D. H. Everett, R. A. W. Haul, L. Moscou, R. A. Pierotti, J. Rouquerol, T. Siemieniewska, *Pure Appl. Chem.* **1985**, *57*, 603.
[29] S. Brunauer, P. H. Emmett, T. Teller, *J. Am. Chem. Soc.* **1938**, *60*, 309.
[30] E. P. Barrett, L. G. Joyner, P. P. Halenda, *J. Am. Chem. Soc.* **1951**, *73*, 373.

the hybrid material. Besides, the elemental analysis (EA) consists in the combustion of the sample and gives information about the content of carbon, hydrogen, nitrogen and sulphur. All these results can be correlated and used to calculate the total amount of each organic functional group present in the prepared materials. In addition, Fourier-transform infrared spectroscopy (FT-IR) could be used to elucidate the presence of the functional organic molecules from the specific IR absorption peaks of the different organic groups. This technique is sometimes difficult to study in mesoporous materials because depends on the amount of functionalization and the absence of overlapping signals. Solid-state nuclear magnetic resonance (NMR) could also be used to evaluate the proper anchoring of the organic moieties onto the surface of the inorganic scaffold. However, this technique requires large amount of sample and time to finally obtain patterns with less resolution than conventional NMR. One appealing approach employed in last years is the combination of scanning transmission electron microscopy with energy dispersive X-ray spectroscopy (STEM-EDX) used to map the presence of certain elements.

1.2.4 Stimuli-responsive gated materials

The functionalization of the inorganic materials with organic (bio)molecules or supramolecules improved the properties of the materials leading to the development of novel advanced systems.[31] In this scenario, the design of stimuli-responsive gated materials is an appealing approach with applications in several scientific areas such as controlled delivery of chemical species, (bio)chemical sensors among others.

[31] a) M. Faustini, L. Nicole, E. Ruiz-Hitzky, C. Sanchez, *Adv. Funct. Mater*. **2018**, 28, 1704158; b) T. Wagner, S. Haffer, C. Weinberger, D. Klaus, M. Tiemann, *Chem. Soc. Rev*. **2013**, *42*, 4036.

Gated materials are predesigned to deliver molecules from a porous support in response to selected stimuli.[32] These materials are composed by two subunits: (i) an inorganic porous scaffold in which a cargo (ca. drugs, dyes, fluorophores, small biomolecules, etc) is loaded; (ii) (bio)molecules or supramolecular ensembles onto the external surface acting as gatekeepers.[33] The role of gatekeepers is to confine the cargo in the inner of the porous support. Supramolecular structures, bulky organic molecules, polymers, peptides, DNA, enzymes, and inorganic nanoparticles have been used as gatekeepers.[34] In the presence of external stimuli, the gatekeepers change their size/shape/conformation or are simply displaced allowing cargo release in a controlled fashion (see Figure 9). Different stimuli, such as pH,[35] redox potential,[36] target molecules,[37] light,[38] temperature[39] and magnetic fields have been applied as stimuli to trigger the release of guest molecules from gated materials.[33]

[32] a) C. -H. Lu, I. Willner, *Angew. Chem. Int. Ed.* **2015**, *54*, 12212; b) Y. Zhang, J. Yu, H. N. Bomba, Y. Zhu, Z. Gu, *Chem. Rev.* **2016**, *116*, 12536; c) M. Manzano, M. Vallet-Regí, *Chem. Commun.* **2019**, *55*, 2731; d) T. Zhao, L. Chen, Q. Li, X. Li, *J. Mater. Chem. B* **2018**, *6*, 7112.

[33] a) E. Aznar, M. Oroval, Ll. Pascual, J. R. Murguía, R. Martínez-Máñez, F. Sancenón, *Chem. Rev.* **2016**, *116*, 561; b) A. García-Fernámdez, E. Aznar, R. Martínez-Máñez, F. Sancenón, *Small* **2019**,

[34] a) J. Wen , K. Yang, F. Liu , H. Li, Y. Xu, S. Sun, *Chem. Soc. Rev.* **2017**, *12*, 6024; b) A. Llopis-Lorente, B. Lozano-Torres, A. Bernardos, R. Martínez-Máñez, F. Sancenón, *J. Mater. Chem. B* **2017**, *5*, 3069; c) C. Coll, L. Mondragón, R. Martínez-Máñez, F. Sancenón, M. D. Marcos, J. Soto, P. Amorós, E. Pérez-Payá, Angew. *Chem. Int. Ed.* **2011,** *50,* 2138; d) E. Aznar, M. D. Marcos, R. Martinez-Manez, F. Sancenon, J. Soto, P. Amoros, P. Guillem, J. *Am. Chem. Soc.* **2009**, *131*, 6833.

[35] a) A. Bernardos, E. Aznar, C. Coll, R. Martínez-Máñez, J. M. Barat, M. D. Marcos, F. Sancenón, J. Soto, *J. Control. Release* **2008**, *131*, 181; b) V. Cauda, C. Argyo, A. Schlossbauer, T. J. Bein, *J. Mater. Chem.* **2010**, *20*, 4305.

[36] a) C. Giménez, C. de la Torre, M. Gorbe, E. Aznar, F. Sancenón, JR. Murguía, R. Martínez-Máñez, M. D. Marcos, P. Amorós, *Langmuir* **2015**, *31*, 3753; b) R. Liu, X. Zhao, T. Wu, P. Feng, *J. Am. Chem. Soc.* **2008**, *130*, 14418.

[37] a) Y. Zhao, B. G. Trewyn, I. I. Slowing, V. S.-Y. Lin, *J. Am. Chem. Soc.* **2009**, *131*, 8398; b) Y. L. Choi, J. Jaworsky, M. L. Seo, S. J. Lee, J. H. Jung, *J. Mater. Chem.* **2011**, *21*, 7882.

[38] Q. Lin, Q. Huang, C. Li, C. Bao, Z. Liu, F. Li, L. Zhu, L. *J. Am. Chem. Soc.* **2010**, *132*, 10645.

[39] C. Chen, J. Geng, F. Pu, X. Yang, J. Ren, X. Qu, *Angew. Chem. Int. Ed.* **2011**, *50*, 882.

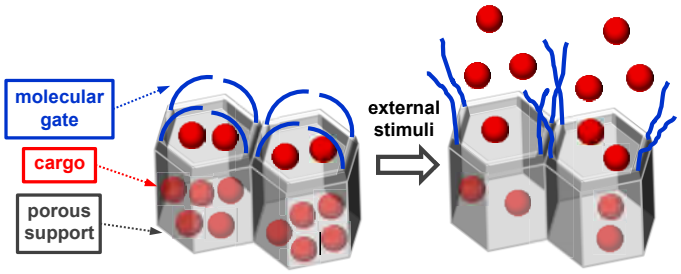

Figure 9. Scheme of the principal components and operation of a molecular gate.

The first example in this field was reported by Fujiwara and co-workers in 2003,[40] and since this pioneering development numerous gated systems have been described. Among possible porous supports, MSNs are perhaps the most widely used. MSNs present unique characteristics as high loading capacity, biocompatibility, chemical inertness and high surface area which can be easily functionalised to develop gated materials.[41] These features make MSNs a suitable candidate for its application in controlled release in the field of nanomedicine as drug delivery systems.[42]

1.3 Gated mesoporous silica nanoparticles as drug delivery systems in biomedical applications

The development of novel drug delivery systems is an important part of nanomedicine. In the last years, a myriad of drug delivery systems have been described as an alternative to conventional therapeutic approaches, due to the potential of nanoformulations to improve the therapeutic effect of some current

[40] N. K. Mal, M. Fujiwara, Y. Tanaka, *Nature* **2003**, *421*, 350.
[41] P. Yang, S. Gai, J. Lin, *Chem. Soc. Rev.* **2012**, *41*, 3679.
[42] a) Y. Zhao, B. G. Trewyn, I. I. Slowing, V. S.-Y. Lin, *J. Am. Chem. Soc.* **2009**, *131*, 8398; b) C. Argyo, V. Weiss, C. Brauchle, T. Bein, *Chem. Mater.* **2013**, 26, 435.

drugs. Among the systems developed those based on the use of lyposomes,[43] polymers,[44] and nanoparticles[45] have been widely used to encapsulate or conjugated selected drugs and/or imaging agents.

As an alternative to these traditional drug delivery systems, stimuli-responsive gated mesoporous silica nanoparticles are suitable candidates as vehicles for the controlled release of certain molecules in biomedical applications. The mesoporous scaffolds are able to enclose and protect hydrophobic and hydrophilic drugs during their transport, overcoming common issues such as poor solubility and stability of drugs or undesired side effects. In addition, surface functionalization with specific targeting moieties allows these nanodevices to gain selectivity towards specific cells types while sparing normal tissues. In order to do that, specific biomolecules whose receptors are overexpressed in the target cells can be anchored to the nanoparticles' surface. Besides, the combination of diverse functionalities in the same scaffold is possible, yielding multifunctional nanosystems which are able to combine, for instance, targeted drug delivery with molecular imaging and diagnosis.[46]

[43] T. M. Allen, P. R. Cullis, *Adv. Drug Deliv. Rev*. **2013**, *65*, 36.
[44] L. Jaimes-Aguirre, B. V. Gibbens-Bandala, E. Morales-Avila, B. E. Ocampo-García, M. Seyedeh-Fatemeh, M. A. Amirhosein, *Curr. Pharm. Des*. **2016**, *22*, 2886.
[45] a) P. Yang, S. Gai, J. Lin, *Chem. Soc. Rev.* **2012,** *41*,3679; b) S. Chen, X. Hao, X. Liang, Q. Zhang, C. Zhang, G. Zhou, S. Shen, G. Jia, J. Zhang, *J. Biomed. Nanotechnol.* **2016**, *12,* 1.
[46] J. Xie , S. Lee , X. Chen, *Adv. Drug. Deliv. Rev.* **2010,** *62*, 1064.

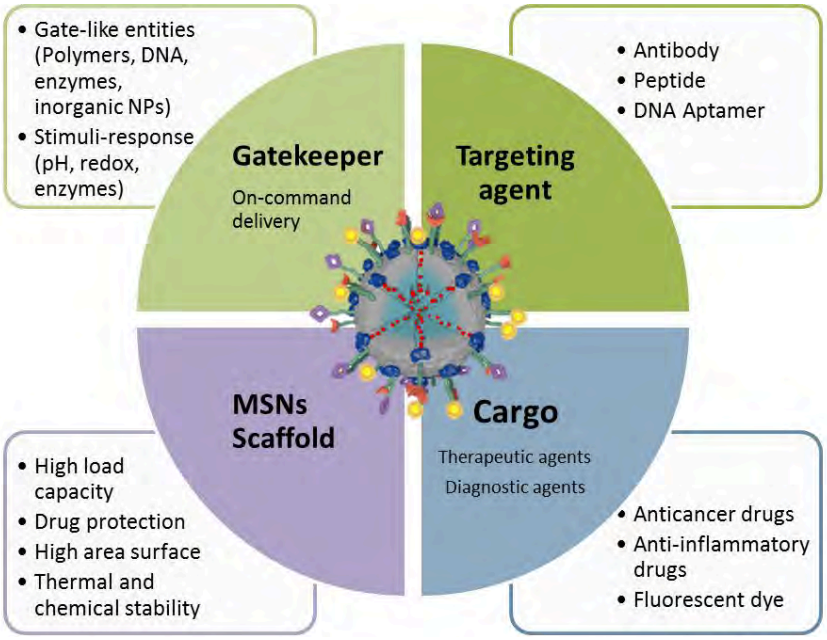

Figure 10. Schematic representation of multifunctional gated mesoporous silica nanoparticles as drug delivery systems. Adapted from *Chem. Mater.* **2014**, *26*, 435. Copyright © 2013 American Chemical Society.

To exploit gated mesoporous silica nanoparticles in biomedical applications, especially as drug delivery systems, it is necessary to understand the interactions of the nanoparticles with the cellular environment. Moreover, the transit of the nanoparticles through the organism prior to their interactions with the targeted or diseased cells and tissues is crucial to understand the biodistribution and thus possible toxicity of these nanomaterials. Besides, the understanding of these interactions is a key clue to design efficient gated mesoporous silica nanoparticles to target cellular uptake and subsequent drug delivery.

1.3.1 Biocompatibility and biodistribution of mesoporous silica nanoparticles

The biological applicability of MSNs in drug delivery processes has been reported in numerous *in vivo* studies. Several of these studies demonstrated the biodistribution, accumulation, retention and clearance effects derived from using these nanomaterials.[47] When nanoparticles are administered a systemic distribution is observed in the bloodstream with preferential accumulation on major target organs. These include liver, lung, kidneys, spleen, brain and gastrointestinal tract, being liver, kidney and lungs the potential organs of accumulation regardless of the nanoparticles administration route. This preferential accumulation is attributed to the high capacity to retain foreign substances of these organs.[48]

Regarding the safety and biocompatibility of the mesoporous silica nanoparticles, the toxicity, degradability and clearance of silicon-based materials has been recently studied.[49] Several studies elucidate that MSNs circulate and accumulate in major organs with no significant toxicity when exposed to animals, despite certain toxic effects (oxidative stress, inflammation and damage) have been observed in some cases. However, severity and toxicity of nanoparticles is controlled by several factors in which the dose and administration exposure played a crucial role.[46]

Another key factor in nanoparticle safety is the biodegradability of silica based materials. The MSNs scaffold is constituted by -Si-O- bonds which are susceptible to hydrolytic breakdown of the siloxane (Si-O-Si) group, thus generating orthosilicic acid ($Si(OH)_4$), which is well-tolerated by the organism and

[47] Y. Chen, H. Chen, J. Shi, *Adv. Mate.r,* **2013**, *25*, 3144.
[48] T. Wu, M. Tang, *J. Appl. Toxical.* **2018**, *38,* 25.
[49] a) J. G. Croissant, Y. Fatieiev, N. M. Khasab, *Adv. Mater*. **2017**, *29*, 1604634; b) M. Linden, *The Enzymes*, **2018**, *43*, 155.

excreted by urine.[50] This fact corroborate the evidence that renal clearance is the main excretion way for MSNs. Moreover, some studies showed that MSNs can also be excreted by hepatobiliary way in a lower proportion (Figure 12).[51]

An interesting research carried out by Liu and co-workers[52] showed all the aspects explained above. *In vivo* studies with mice were carried out by intravenous administration of MSNs in order to determine the systematic single and repeated dose toxicity, biodistribution and clearance of this material. The authors determined a lethal dose 50 (LD_{50}) for a single MSNs dose at 1000 mg/kg. Besides, for a continuous administration during 14 days nanoparticles at 20, 40 and 80 mg/kg were well-tolerated by the animals. Moreover, the toxicity over the organs was analysed and liver injury was only observed at high doses of nanoparticles (>500 mg/kg in single dose), thus corroborating the low toxic profile of the MSNs after intravenous injections. The authors finally conclude that a period of 4 weeks was sufficient for the clearance of 50% of nanoparticles administered from the body analysing the content of silica in the different tissues.

However, it has to be taken into account that the synthetic protocol used for the preparation of each different nanomaterial determines their pharmacokinetic profile, mechanical stability, development of protein corona around the particles in bloodstream and possible changes in the particles during their circulation over time and thus the compatibility and safety.[53] The understanding of these issues is essential to optimise the design of the nanoparticles and therefore their therapeutic effect. In fact, an appropriate surface functionalization is crucial to avoid undesired interactions during the

[50] a) B. C. Bunker, *J. Non-Cryst. Solids* **1994**, *179*, 300; b) J. F. Popplewell, S. J. King, J. P. Day, P. Ackrill, L. K. Fifield, R. G. Cresswell, M. L. D. Tada, K. Liu, *J. Inorg. Biochem.* **1998**, *69*, 177; c) N. Hao, H. Liu, L. Li, D. Chen, L. Li, F. Tang, *J. Nanosci. Nanotechnol.* **2012**, *12*, 6346.

[51] M. Vallet-Regí, M. Colilla, I. Izquierdo-Barba, M. Manzano, *Molecules* **2017**, *23*, 47.

[52] T. Liu, L. Li, X. Teng, X. Huang, H. Liu, D. Chen, J. Ren, J. He, F. Tang, *Biomaterials* **2011**, *32*, 1657.

[53] F. Tang, L. Li, D. Chen, *Adv. Mater*. **2012**, *24*, 1504.

transit into the organism and can enhance half-life time circulation in the blood of the drug delivery systems to finally reach the specific or diseased tissue.[54]

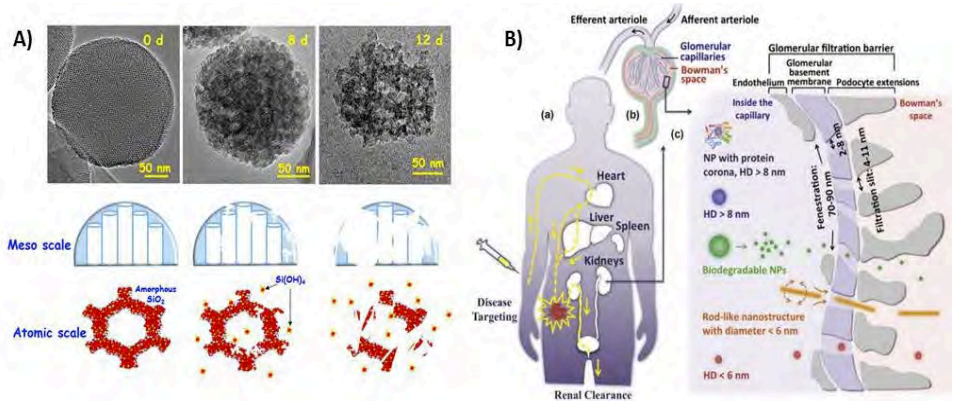

Figure 12. A) Illustration of *in vitro* degradation process of MSNs scaffold; B) Schematic representation of renal clearance excretion way for nanoparticles: a) NPs circulation in the body, targeting the diseased tissue and untargeted ones which are rapidly cleared out of the body through the urinary system. (b) Kidney corpuscle structure scheme. (c) Representation of the glomerular filtration process. The glomerular capillary wall is made of three specialized layers: fenestrated endothelium, glomerular basement membrane, and podocyte extensions of glomerular epithelial cells, allowing a nano scale filtration phenomenon. Adaption of the figures from Molecules **2018**, *23*, 47 and *Mater. Today* **2013**, *16*, 477.

Besides the accumulation in major organs, nanoparticles have the ability to accumulate in areas of diseased organs and tissues. This phenomenon is known as passive targeting and is mostly associated to the enhanced permeability and retention effect (EPR). MSNs present this kind of passive targeting to tumours tissues, showing a preferential and large accumulation in the tumours compared

[54] M. Manzano, M. Vallet-Regí, *J. Mater. Sci. Mater. Med.* **2018**, *29,* 65.

to major organs.[55] The characteristic tumour vasculature, which increase permeability, leaky tumour vessels and ineffective lymphatic drainage, allows the extravasation of macromolecules and nanoparticles such as MSNs to these solid tumours.[56] On the other hand, recent studies demonstrated a similar effect with the leaky vasculature of inflamed tissues.[57] The nanoparticles are internalized by inflammatory cells (characterized by enhanced endocytic activity) and transported to the inflamed site of action which is present in inflammatory disorders and in tumour microenvironments. This phenomenon, called ELVIS mechanism (extravasation through leaky vasculature and inflammatory cell-mediated sequestration), also justifies the accumulation and penetration of nanoparticles in some diseased organs or tissues.[58] This effect has an important role for the development of nanocarrier-based therapies targeting inflammation or inflammatory diseases. In this case, nanoparticles could be used as a kind of "Trojan horse" to lead with inflammation processes using nanoparticles loaded with anti-inflammatory drugs.

Regarding functionalization, strategies of surface modification are also applied to enhance the stability of the nanoparticles in the bloodstream. One of the most used strategies is the modification of nanoparticle surface with polyethyelenglycol (PEG). Different studies demonstrated that these PEGylated nanoparticles systematically reduce toxicity and regulate the rate of nanoparticles clearance.[59] Moreover, molecules with target moieties are attached to nanoparticles surface to promote an active targeting, also known as ligand-

[55] a) R. Ngoune, A. Peters, D. von Elverfeldt, K. Winkler, G. Pütz, *J Control Release*., **2016**, *238*, 58; b) A. Baeza, M. Vallet-Regí, *Curr Top Med Chem*., **2015**, *15*, 2306.
[56] H. Maeda, H. Nakamura, J. Fang, *Adv. Drug. Deliv. Rev*. **2013**, *65*, 71.
[57] K.-H. Chen, D. J. Lundy, E. K.-W. Toh, C.-H. Chen, C. Shih, P. Chen, H.-C. Chang, J. J. Lai, P. S. Stayton, A. S. Hoffmand, P. C.-H. Hsieh, *Nanoscale*, **2015**, *7*, 15863.
[58] a) E. Koziolová, K. Venclíková, T. Etrych, *Physiol. Res*. **2018**, *30*, S281; b) F. Yuan, L. D. Quan, L. Cui, S. R. Goldring, D. Wang, *Adv. Drug. Deliv. Rev*. **2012**, *64*, 1205.
[59] a) S. R. Blumen, K. Cheng, M. E. Ramos-Nino, D. J. Taatjes, D. J. Weiss, C. C. Landry B. T. Mossman, *Am. J. Respir. Cell. Mol. Biol.* **2007**, *36*, 333; b) Q. He, Z. Zhang, F. Gao, Y. Li, J. Shi, *Small* **2011**, 7, 271.

mediated targeting, thus enhancing the passive targeting effect and making the nanoparticles more specific to a target site (see Figure 11).[60] In this case ligand molecules are selected to bind surface molecules or receptors overexpressed in the diseased organs, tissues or cells. Among the different targeting molecules, antibodies, aptamers, peptides and proteins are the most commonly used to functionalize the surface of the nanoparticles.[61] Attending to these effects, gated mesoporous silica nanoparticles are ideal nanocarriers for drug delivery therapies, being cancer therapy approaches the most exploited application.

An in depth comprehension and intensive research is necessary to ensure the biocompatibility, biodistribution and therapeutic efficacy of these drug delivery systems in order to bring these novel nanomedicines to the clinic. Despite contradictory results are found in the literature, mainly ascribed to the fact that each prepared material presents unique features, many studies are contributing to elucidate the biosafety of MSNs. In fact, some nanomedicines based on silica materials, which will be explained in more detail below, are already in the early stages of clinical trials.[62]

[60] S. Salmaso, P. Caliceti, *J. Drug Deliv.* **2013**, 374252.
[61] A. Baeza, M Colilla, M. Vallet-Regí, *Expert Opin. Drug Del.*, **2015**, *12*, 319.
[62] NIH, U.S. National Library of Medicine, ClinicalTrials.gov, retrived from https://clinicaltrials.gov/.

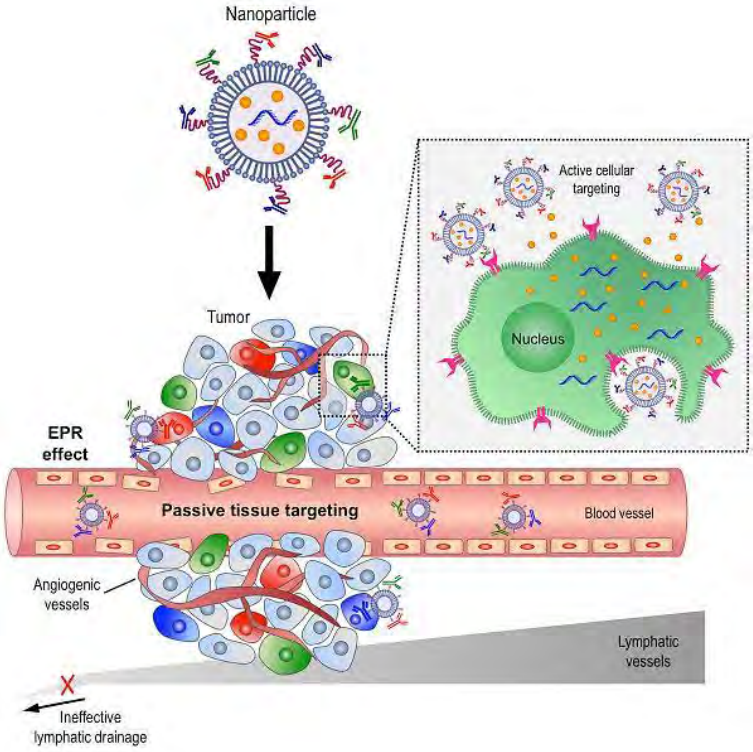

Figure 11. Representation of passive and active targeting approaches. Passive targeting is achieved by extravasation of nanoparticles through increased permeability of the tumor vasculature and ineffective lymphatic drainage (EPR effect). Active cellular targeting (inset) can be achieved by decorating the surface of nanoparticles with multiple targeting moieties that promote cell-specific recognition and binding. Reprinted with permission of Mol. Cell Ther. **2014**, *2*, 5. Copyright © Peer; licensee BioMed Central Ltd. 2014.

1.3.2 Targeting and cellular uptake of mesoporous silica nanoparticles

Once assessed the interactions of nanoparticles with the organism during their transit, it is also important to recognize how nanoparticles interact with targeted cells and the cellular uptake mechanism of these nanomaterials. When

nanoparticles are circulating into the organism, they are exposed to many types of cells which can internalize nanoparticles. This includes the internalization by a variety of mammalian cells, including cancerous (cancer cells) and non-cancerous cells (endothelial, fibroblast and inflammatory cells).[63] The uptake process is influenced by the cell-membrane characteristics and the unique features of the designed nanoparticles. Moreover, the interactions with the cell membrane determine the cellular trafficking of the nanoparticles, their accumulation in intracellular compartments, their retention in the target area and thus the efficacy of the encapsulated drugs.[64] Specific cellular uptake to damaged cells or tissues can be achieved by the nanoparticles passive and/or active targeting effect.[65]

Despite the fact that mechanisms for cellular uptake of nanoparticles are not well-understood yet, it is described that in the majority of cases MSNs are internalized by cells through endocytosis pathways and several uptake mechanisms can be acting simultaneously, with different efficiencies. Factors, such as the size, shape and surface functional groups present in silica nanoparticles (which determine the charge and hydrophobicity) influence the cellular uptake pathways (Figure 13).[58a,66] Besides, the active targeting interactions, promoted through the attachment of targeting molecules (such as antibodies, aptamers, proteins, peptides and small molecules) to the nanoparticle surface, facilitates the specific and active nanocarrier binding to certain receptors overexpressed on the cellular surface with the subsequent

[63] a) D. R. Radu, C. -Y. Lai, K. Jeftinija, E. W. Rowe, S. Jeftinija, V. S. -Y. Lin, *J. Am. Chem. Soc.* **2004,** *126*, 13216; b) I. I. Slowing, B. G. Trewyn, V. S. -Y. Lin, *J. Am. Chem. Soc.* **2006**, *128*,14792; c) I. I. Slowing, B. G. Trewyn, V. S. -Y. Lin, *J. Am. Chem. Soc.* **2007**, *129*, 8845.

[64] a) I. M. Adjei, B. Sharma, V. Labhasetwar, *Nanomaterial*s **2014**, *811*, 73; b) Ž. Krpetić, S. Anguissola, D. Garry, P. M. Kelly, K. A. Dawson, *Nanomaterial*s **2014**, *811,* 135.

[65] a) F. Danhier, O. Feron, V. Préat, *J. Control. Release* **2010**, *148*, 135; b) T. S. P. Grandhi, K. Rege, *Nanomaterial*s **2014**, *811*, 157.

[66] a) F. Lu, S. -H. Wu, Y. Hung, C. -Y. Mou, *Small*, **2009**, *5*, 1408; b) A. Verma, F. Stellacci, *Small,* **2010**, *6,* 12.

receptor-mediated cellular uptake. Below, are described the common pathways by which nanoparticles are internalized by cells.

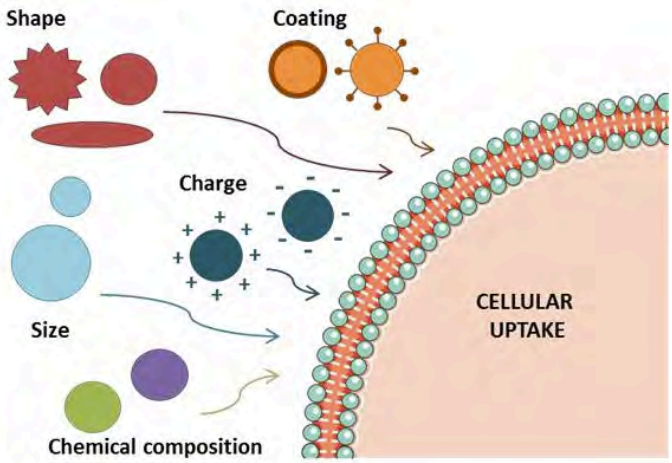

Figure 13. Scheme of the principal features of nanoparticles which determine the cellular interactions and the subsequent internalization mechanism.

The most common internalization pathway of nanoscale materials is the ***pinocytosis*** which is an energy-dependent complex mode of endocytosis in which small particles present in the extracellular fluid are internalized upon the formation of an invagination of the cell membrane which leads to the formation of a vesicle inside the cell containing the ingested material (see Figure 14). In general, these vesicles are fused with the endosomes, from early endosomes (pH 6.5) to late endosomes (pH 5.5.-6), which then mature into lysosomes and become still more acidic (pH ca. 5) and acquire lysosomal enzymes to finally degrade, recycle and modulate the endocytosed materials.[67] On the other hand, ***phagocytosis*** is an endocytic process carried out by specialized phagocytes cells

[67] a) F. Zhao, Y. Zhao, Y. Liu, X. Chang, C. Chen, Y. Zhao, Small, 2011, 7, 1322-1337; b) O. Nuri, J.H. Park, Int J. Nanomedicine 2014, 9, 51.

which facilitate the ingestion of large particles (such as microorganisms or dead cells) via large vesicles (see also Figure 14).

The pynocytic pathways are divided into macropynocytosis, clatrhin-mediated endocytosis, caveole-mediated endocytosis and clathrin-caveolae-independent endocytosis[68] (see Figure 14). Of all the four pathways, the ***clathrin-mediated endocytosis*** is the predominant for MSNs.[69] This process involves the formation of clathrin-coated vesicles (ca. 100 nm in diameter) able to fuse with early endosomes. The ingested materials can be recycled to the cellular membrane or retained in endosomes and transferred into lysosomes. Moreover, this mechanism is used to internalize ligand-functionalized nanoparticles which target specific cells. In this case, the clathrin-mediated endocytosis is known as *receptor-mediated endocytosis* and is started by the recognition of the ligand to the specific cellular membrane receptors. The clatrhin-coated vesicles are fused with the endosomal compartments, however the subsequent steps of this endocytic pathway are diverse and internalized receptors could either remain bound to their ligands or change their conformation and release the ligand into the early endosomes with the subsequent degradation in lysosomal compartments.

The ***caveolae-dependent endocytosis*** mechanism is less understood, and mainly associated to transport molecules across endothelial cells. It is believed that materials are invaginated though the evolution of caveolae-derivatives of the subdomains of sphingolipid and cholesterol-rich cell membrane fractions. Then the caveolae-vesicles are fused to endosome compartments, transported to the endoplasmic reticulum/Golgi apparatus or recycle the plasma membrane.

[68] c) SD. Conner, SL. Schmid, *Nature*, **2003**, *422,* 37–44; d) GJ. Doherty, HT. Mcmahon, *Annu Rev Biochem*, **2009**, *78*, 857–902.
[69] a) A. Kumari, SK. Yadav SK, *Expert Opin Drug Deliv*, **2011**, *8*, 141-151; b) J. Rejman, V. Oberle, IS. Zuhorn, D. Hoekstra, *Biochem. J.*, **2004**, *377*, 159-169;

Another less common mechanism is the ***macropinocytosis***, which is a non-selective uptake process in which large amounts of particles and membranes are internalized in large intracellular vacuoles (> 0.2 µm).

Finally, ***clathrin-caveolae-independent endocytosis*** routes could be constitutive or triggered by specific signals, facilitating large micrometer-scale and a smaller (<200 nm) scale processes of endocytosis. However, the mechanism, vesicle formation, associated molecular machinery and destination of ingested material are very different and the regulatory mechanism remains still unclear.

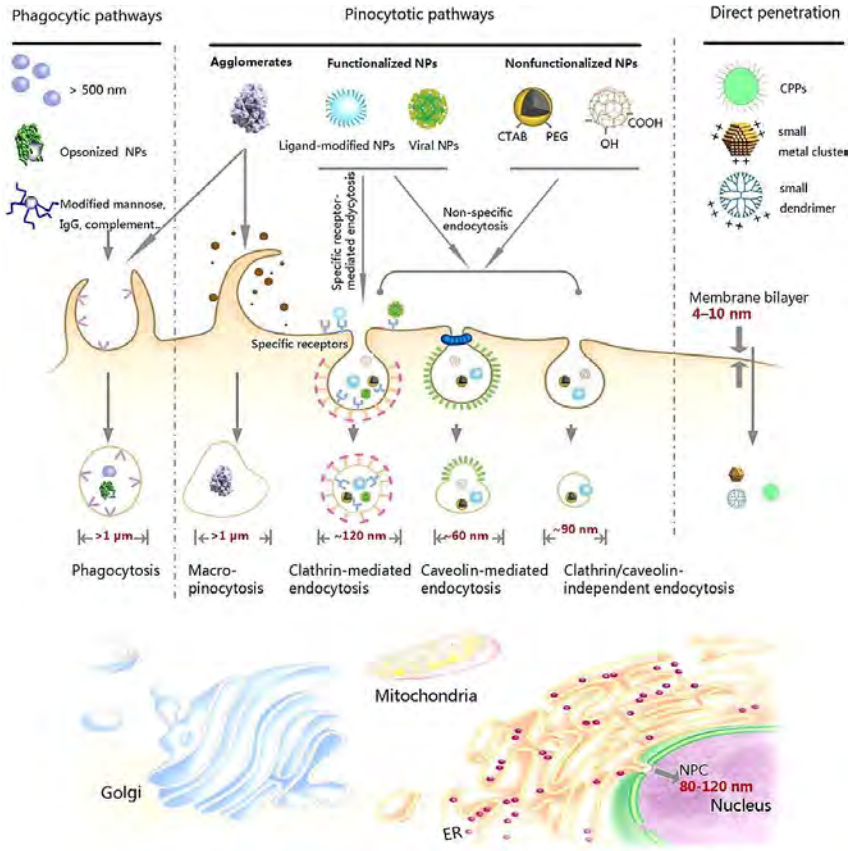

Figure 14. Illustration of the different internalization pathways to nanomaterials. Reprinted with permission of *Acc. Chem. Res.* **2013**, 46, 622. Copyright © 2012 American Chemical Society.

We have already seen how endocytosed materials that reach the late endosomes become fuse with lysosomes. However, in some cases such as in gene delivery approaches, it is mandatory to deliver the nanoparticles and its cargo into the cytoplasm. For this purpose, nanoparticles have to be designed to escape from the endolysosomal compartments.[70] The most common strategy employed involves the use of cationic polymers such as polyethyelenimine (PEI) which act as "proton sponges". These polymers have a high buffering capacity in the pH 5-7 range preventing the acidification of the endosomes and, at the same time, are also able to swell when protonated, facilitating the rupture of the endosomal membrane and the release of the nanoparticles.[71] In addition, some strategies involve the use of cell penetrating peptides (such as the transactivator of transcription (TAT) peptide) that facilitate the direct entry of the nanoparticles into the cytoplasm.[72]

1.3.3 Stimuli responsive gated mesoporous silica nanoparticles

Once described the interactions of nanoparticles with cells and thus cellular uptake, the relevance of molecules acting as gatekepeers and targeting effectors anchored onto mesoporous silica nanoparticles, needed for providing controlled drug release to specific cells, are described here.[73] The design of these gated materials represents a promising opportunity to improve the solubility and bioavailability of drugs and the delivery of an accurate amount of drug specifically

[70] a) A. K. Varkouhi, M. Scholte, G. Storm, H. J. Haisma, *J. Control. Release* **2011**, 151, 220; b) I. Nakase, S. Kobayashi, S. Futaki, *Biopolymers* **2010**, *94*, 763.
[71] a) X. Wang, D. Niu, C. Hu, P. Li., *Curr. Pharm. Des.* **2015,** *21,* 6140; b) R. A. Jones, C. Y. Cheung, F. E. Black, J. K. Zia, P. S. Stayton, A. S. Hoffman, M. R. Wilson, *Biochem. J.* **2003**, *372*, 65.
[72] a) J. P. Richard, K. Melikov, E. Vives, C. Ramos, B. Verbeure, M. J. Gait, L. V Chernomordik, B. Lebleu, *J. Biol. Chem*. **2003**, *278*, 585; b) E. Vivès, J. P. Richard, C. Rispal, B. Lebleu, *Curr. Protein. Pept. Sci.* **2003**, *4*, 125.
[73] a) J. Florek, R. Caillard, F. Kleitz, *Nanoscale* **2017**, *9*, 15252; b) K. E. Bremmell, C. A. Prestidge, *Drug Dev. Ind. Pharm.* **2019**, *45*, 349.

to specific sites, thus reducing side effect and increasing the therapeutic outcome when compared with the free drug.

As we described above, numerous nanocarriers have been designed and applied in drug delivery protocols, such as liposomes, micelles, polymers, dendrimers, quantum dots, gold or metal oxide nanoparticles and silica-based materials.[74] All these systems are able to store drugs and deliver them passively or in a controlled way. Passive systems include nanocarriers in which the drug is released by simply diffusion or by degradation of the material.[75] These types of passive systems are characteristic of organic nanoparticles (such as liposomes, micelles or polymers) and the timing of release is fundamental to reach the target site and achieve the desired drug effect. In contrast, a more sophisticated delivery strategy is based on on-command drug delivery, in which nanocarriers are tailored to deliver their cargo in the presence of external stimuli. While organic-based nanoparticles are used today in several biomedical applications, most of the studies with capped MSNs have been focused on the design of new gating ensembles.[76] However, the number of *in vivo* studies regarding gated MSNs has increased dramatically in last years.[77]

[74] a) V. Kozlovskaya, B. Xue, E. Kharlampieva, *Macromolecules* **2016**, *49*, 8373; b) D. K. Mishra, R. Shandilya, P. K. Mishra, *Nanomedicine* **2018**, *14*, 2023; c) F. Seidi, R. Jenjof, T. Phakkeeree, D. Crespy, *J. Control. Release* **2018**, *284*, 188; d) W. Chen, S. Zhou, L. Ge, W. Wu, X. Jiang, *Biomacromolecules* **2018**, *19*, 1732; e) M. Vazquez-Gonzalez, I. Willner, *Langmuir* **2018**, *34*, 14692; f) R. M. Farid, N. A. H. A. Youssef, A. A. Kassem, *Curr. Pharm. Des.* **2017**, *23*, 6613; g) D. Lombardo, P. Calandra, D. Barreca, S. Magazu, M. A. Kiselev, *Nanomaterials* **2016**, *6*, 125/1; h) A. Bansal, Y. Zhang, *Acc. Chem. Res.* **2014**, *47*, 3052.

[75] N. Kamaly, B. Yameen, J. Wu, O. C. Farokhzad, *Chem. Rev.* **2016**, *116*, 2602.

[76] a) C. Coll, A. Bernardos, R. Martínez-Máñez, F. Sancenón, *Acc. Chem. Res.* **2013**, *46*, 339; b) S. Yi, J. Zheng, P. Lv, D. Zhang, X. Zheng, Y. Zhang, R. Liao, *Bioconjug. Chem.* **2018**, *29*, 2884; c) N. Song, Y. –W. Yang, *Chem. Soc. Rev.* **2015**, *44*, 3474; d) C. Argyo, V. Weiss, C. Bräuchle, T. Bein, *Chem. Mater.* **2014**, *26*, 435.

[77] a) J. L. Vivero-Escoto, I. I. Slowing, B. G. Trewyn, V. S. –Y. Lin, *Small* **2010**, *6*, 1952; b) B. Murugan, U. M. Krishnan, *Int. J. Pharm.* **2018**, *553*, 310; c) A. F. Moreira, D. R. Dias, I. J. Correia, *Mesopor. Micropor. Mater.* **2016**, *236*, 141; d) T. L. Nguyen, Y. Choi, J. Kim, *Adv. Mater.* **2018**, *30*, 1803953; e) Y. Chen, H. Chen, J. Shi, *Adv. Mater.* **2013**, *25*, 3144.

Stimuli to which gated nanoparticles respond and induce cargo delivery can be classified as ***endogenous*** (such as pH, redox reactions, enzymes, etc) or ***exogenous*** (such as light, magnetic fields, ultrasounds). [78] An overview of gated mesoporous silica nanoparticles used in drug delivery applications in relevant biomedical applications is described below attending to the triggered stimuli.

Endogenous stimuli

Most of the reported gated nanocarriers for controlled drug delivery in *in vivo* models in the last years, respond to endogenous cellular stimuli such as changes in pH, the presence of a reducing intracellular environment, enzymes or other biomolecules. These stimuli are present in living organisms and the use of gated nanocarriers sensitive to these intrinsic conditions provide an autonomous controlled delivery in more realistic settings. Most of the reported studies are applied to cancer, and in most cases, an enhancement of the therapeutic effect of the drug delivered in *in vivo* models with diminished undesired side effects, compared with the effect observed for the free drugs at similar concentrations, is observed.[79]

- pH triggered drug delivery

Among different stimuli used to trigger cargo release in gated materials, pH is, perhaps, the most commonly employed. pH-triggered gated materials provide a tool to prepare nanodevices for drug delivery applications taking into account the pH differences between the extracellular environment (neutral pH) and that of endosomes/lysosomes (slightly acidic pH), which allows drug release inside cells minimizing undesired drug delivery in the extracellular media. Besides,

[78] B. Yang, Y. Chen, J. Shi, *Adv. Healthcare Mater.* **2018**, *7*, 1800268.
[79] S. Mura, J. Nicolas, P. Couvreur, *Nat. Mater.,* **2013**, *12*, 991.

the acidic microenvironment found in certain tumours, due to the overproduction of lactic acid, can also be used for the targeted drug release.[80] Several approaches have been used for the preparation of pH-triggered gated supports. One common approach is the inclusion of pH-hydrolysable linkages (such as imine, hydrazone, acetals, ketals, amides and esters) on the capping ensemble. The hydrolysis of such bonds induces the detachment of the cap with subsequent pore opening and payload delivery.[81] Another approach consists of coating the nanoparticles with different ionisable polymers or biomolecules that use electrostatic interactions as main assembly forces. For these systems, protonation/deprotonation of the coating components induce disruption of the electrostatic interactions, detachment of the polymers from the mesoporous surface and cargo delivery.[82] Finally, some few examples takes advantage of protonation-induced conformation changes in the gating ensemble to induce payload release.[83] Besides, the use of lipid bilayers as gating ensembles, resembling those founds in living cells has also been extensively explored. For this purpose several simple or complex (functionalized with polymers or targeting biomolecules) phospholipids can be used for the preparation of bilayers which coated the external surface of the loaded nanoparticles inhibiting cargo release.[84] These lipid bilayers facilitate the cellular uptake of nanoparticles and subsequent cargo delivery upon cell membrane fusion or disruption of the coating in the lysosome acidic environment.

[80] a) Y. Kato , S. Ozawa , C. Miyamoto , Y. Maehata , A. Suzuki , T. Maeda, Y. Baba , *Cancer Cell Int.*, **2013**, *13* , 89; b) O. Warburg, *Naturwissenschaften*, **1924**, *12*, 1131.

[81] a) D. Yang, N. Wang, H. Ji, S. Sun, J. Dong, Y. Zhong, C. Qian, H. Xu. *RSC Adv*., **2018**, *8*, 38987; b) J. Liu, Z. Luo, J. Zhang, T. Luo, J. Zhou, X. Zhao. K. Cai, *Biomaterials,* **2016**, *83*, 51; c) S. Yang, D. Chen, N. Li, Q. Xu, H. Li, F. Gu, J. Xie, J. Lu, *Small,* **2016**, *12*, 360.

[82] a) C. Murugan, S. Venkatesan, S. Kannan, ACS Omega 2017, 2, 7959; b) Y. Li, Y. Duo, P. Zhai, L. He, K. Zhon, Y. Zhang, K. Huang, J. Luo, H. Zhang, X. Yu, *Nanomedicine* **2018**, *13*.

[83] a) J. Shen, H. Liu, C. Mu, J. Wolfram, W. Zhang, H. –C. Kim, G. Zhu, Z. Hu, L. –N. Ji, X. Liu, M. Ferrari, Z. –W. Mao, H. Shen, *Nanoscale*, **2017**, *9*, 5329.

[84] A. E. La Bauve, T. E. Rinker, A. Noureddine, R. E. Serda, J. Y. Howe, M. B. Sherman, A. Rasley, C. J. Brinker, D. Y. Sasaki, O. A. Negrete, *Sci. Rep.* **2018**, *8*, 13990.

For instance, Yang and co-workers reported the use of cadmium telluride quantum dots (CdTe QDs) integrated into hollow MSNs loaded with doxorubicin and capped with the vascular endothelial growth factor (VEGF) antibody for cancer detection and treatment.[85] The nanoparticles were functionalized with amino groups and then reacted with succinimidyl-PEG_{5000}-maleimide to include PEG_{5000}-maleimide moieties onto the external surface of the nanoparticles through amide linkages. Finally a thiol-modified VEGF antibody was attached onto the nanoparticles through a Michael addition reaction (see Figure 15). Drug release was confirmed by the authors at 37° in simulated physiological conditions at pH 6.5 and 5.0 whereas at pH 7.4 a non-significant drug delivery was observed. The drug delivery mechanism is attributed to the hydrolysis of the amide bonds, thus resulting in the detachment of the gatekeeper with the subsequent cargo release, opening and payload delivery. Confocal laser scanning microscopy *in vitro* studies (measuring the fluorescence of the CdTe QDs) carried out with VEGF-positive HeLa cells and VEGF-negative L929 fibroblast cells showed preferential internalization of the nanodevice in the VEGF-positive cells. *In vivo* studies were carried out with HeLa cells tumours in female nude mice. Intravenously administration of the prepared material showed the preferentially accumulation of the nanoparticles in tumours attributed to the EPR effect and the active targeting by VEGF antibody.

[85] D. Yang, N. Wang, H. Ji, S. Sun, J. Dong, Y. Zhong, C. Qian, H. Xu. *RSC Adv*. **2018**, *8*, 38987.

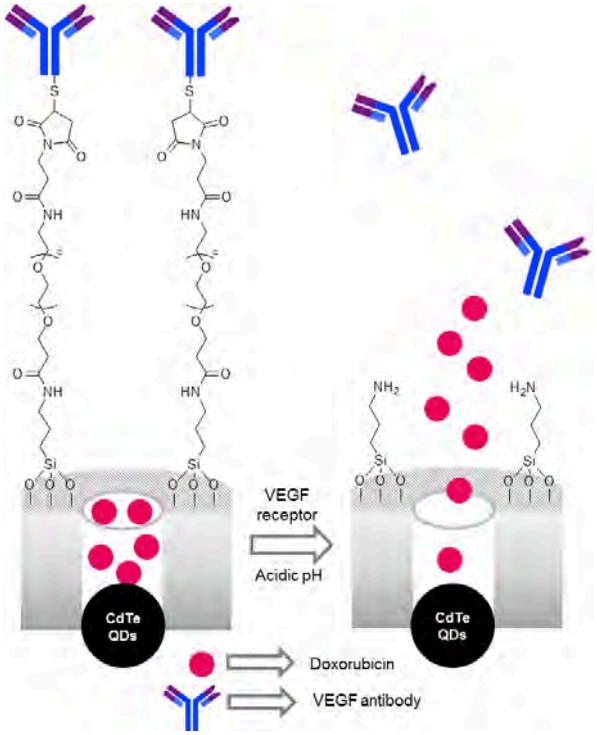

Figure 15. CdTe quantum dots integrated into hollow MSNs loaded with doxorubicin and capped with polyethylene glycol functionalized with VEGF antibody.

Lee and co-workers designed multifunctional magnetic core-shell MSNs able to deliver simultaneously in cancer cells the let-7a miRNA, which has the ability to repress DNA repair mechanism and downregulate drug efflux pumps, and the chemotherapeutic drug doxorubicin.[86] Magnetic $ZnFe_2O_4$ nanoparticles were coated with a mesoporous silica shell. The mesoporous coating was functionalized with trihydroxysilylpropylmethyl phosphonate and the pores loaded with doxorubicin. Afterward, PEI was absorbed through electrostatic interactions onto the external negatively charged surface of the doxorubicin-loaded nanoparticles. Next, let-7a miRNA was adsorbed, through electrostatic

[86] P. T. Yin, T. Pongkulapa, H. –Y. Cho, J. Han, N. J. Pasquale, H. Rabie, J. –H. Kim, J. –W. Choi, K. –L. Lee, *ACS Appl. Mater. Interfaces* **2018**, *10*, 26954.

interactions, onto the PEI layer. Lastly, the external surface was again coated with a PEI layer in which PEG containing the internalizing RGD peptide (which binds with α_v integrins) was covalently linked (Figure 16). In this case, the protonation of the PEI at acidic pH resulted in the disruption of the electrostatic interactions of the coating with the subsequent controlled drug release. The prepared nanoparticles were evaluated in MDA-MB-231 breast cancer cells (which overexpressed integrins) and in *in vivo* assays using MDA-MB-231 xenografted BALB/c nude mice. A significant decrease in cancer cell viability and tumour volume was observed with the nanoparticles, compared to free drug, due to the combined action of let-7a miRNA and doxorubicin. Fluorescence imaging and magnetic resonance imaging (MIR) measurements showed the accumulation of nanoparticles in tumours.

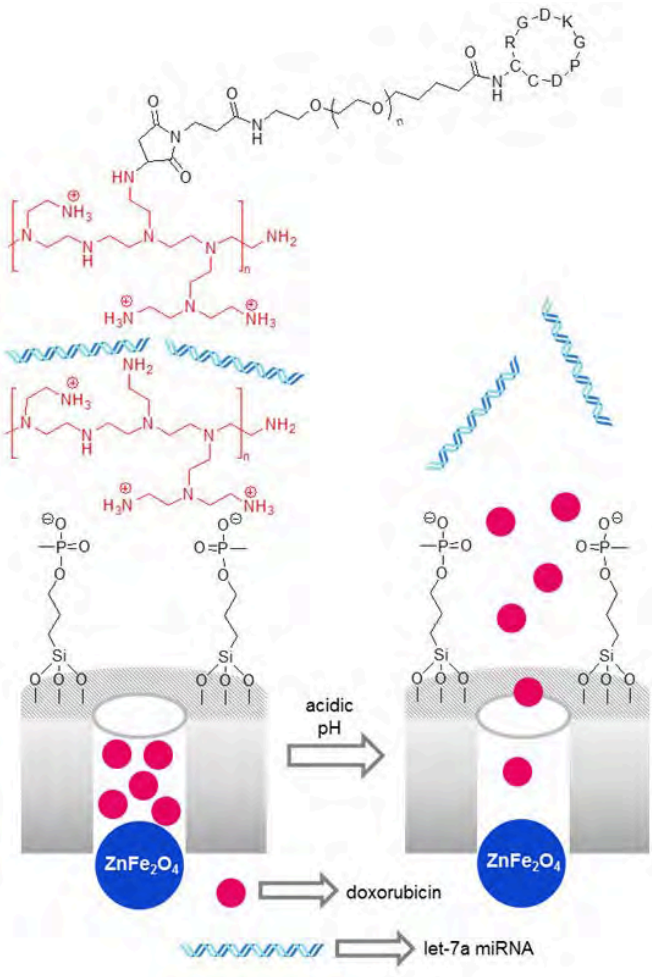

Figure 16. $ZnFe_2O_4$ core-shell MSNs loaded with doxorubicin, grafted with PEI in which let-7a miRNA was adsorbed. Finally there is a PEI layer modified with PEG containing the RGD peptide.

Zeng and co-workers prepared polydopamine (PDA) coated MSNs for targeted cancer therapy.[87] For the preparation of the functional material MSNs were loaded with doxorubicin and then coated with a PDA shell. Then, a

[87] W. Cheng, J. Nie, L. Xu, C. Liang, Y. Peng, G. Liu, T. Wang, L. Mei, L. Huang, X. Zheng, *ACS Appl. Mater. Interfaces* **2017**, *9*, 18462.

poly(ethylene glycol) derivative containing folic acid (FA) and thiol moieties was linked onto the PDA shell through a Michael addition reaction (Figure 17). Aqueous suspensions of the prepared nanoparticles showed a moderate doxorubicin release at pH 7.4 that was increased at acidic pH (pH 5.0 and 2.0) attribute to the degradation of PDA coating at acidic pH. The proper activity of the prepared nanoparticles was first evaluated in vitro in HeLa cervical cancer cells. *In vivo* studies carried out in nude mice bearing HeLa cells and intravenously injected with the nanoparticles showed accumulation of the solid in the tumour and a marked reduction in tumour size was observed due to doxorubicin release confirming the therapeutic benefit of the nanoformulation compared to the free drug.

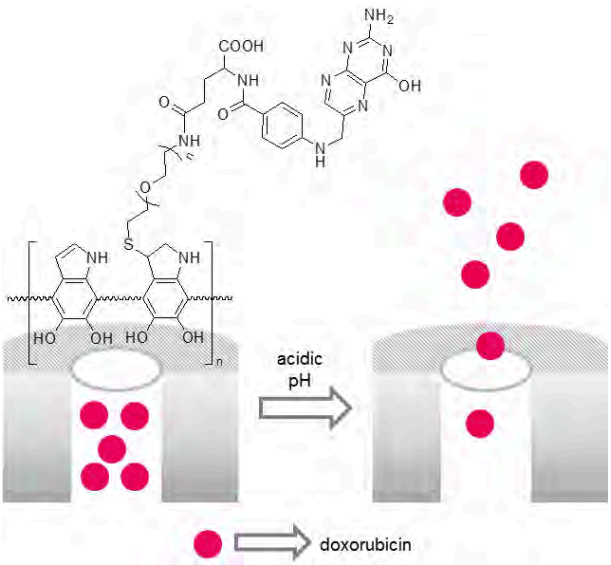

Figure 17. MSNs loaded with doxorubicin, capped with PDA attached to a poly(ethylene glycol) derivative containing folic acid.

- Redox-responsive drug delivery systems

Oxidation and reduction reactions have an important role in the design and development of gated nanomaterials. In biological applications, the different concentration of reducing agents within the intracellular environment and the bloodstream can be exploited to release drugs efficiently by their encapsulation in nanocarriers equipped with redox-responsive (supra)molecular capping machinery. In addition, it is known that in tumours and cancer cells there is a significant increase in redox activity compared to normal cells. In the examples described below the mechanisms that control pore uncapping are two, (i) the cleavage of disulphide bonds, and (ii) bonds cleaved by the presence of reactive oxygen species (ROS).

The most commonly used redox capping ensembles are formed by bulky (bio)molecules containing disulphide linkages. These bulky capping ensembles block mesopores, yet in the presence of reducing agents (such as glutathione, GSH) the disulphide bonds are cleaved with the subsequent cap detachment and cargo delivery. The first example of this gating mechanism was described by Lin and co-workers, who developed redox-sensitive MSNs functionalised with CdS nanocrystals through disulphide bonds.[88] Since then, this has been a rather popular approach to design gated nanosystems.

Wang et al. designed redox-responsive MSNs as drug delivery carrier to overcome drug resistance in lung cancer.[89] Drug resistance (DR) to tyrosine kinase inhibitor (TKI) is the main drawback for an efficient treatment of epidermal growth factor receptor (EGFR)-mutant lung cancer. To overcome this drug resistance, MSNs were used for the design of a nanodevice to target EGFR with

[88] C. Y. Lai, B. G. Trewyn, D. M. Jeftinija, K. Jeftinija, S. Xu, S. Jeftinija, V. S. –Y. Lin, *J. Am. Chem. Soc.* **2003**, *125*, 4451.
[89] Y. Wang, H. -Y. Huang, L. Yang, Z. Zhang, H. Ji, *Sci. Rep.* **2016***, 6*, 25468.

the anti-EGFR antibody cetuximab (CET) as cap and loaded with the anticancer drug doxorubicin or the TKI drug gefitinib (GEF). For the preparation of the nanodevice the surface of MSNs was modified with mercaptopropyl groups and then doxorubicin or GEF were loaded. Finally, the CET antibody was anchored onto the external surface through the formation of disulfide bonds (Figure 18). After the CET binding to EGFR on the cell surface the nanoparticles are internalized and the capping ensemble disrupted through the cleavage of disulfide bonds by intracellular glutathione (GSH). In the absence of GSH, a negligible doxorubicin release was registered whereas in the presence of high levels of GSH or dithiothreitol (DTT) an increased delivery of the drug was observed. The specific targeting mediated by CET was confirmed in PC9 lung cancer cells, which overexpressed EGFR in comparison with epithelial Beas2B lung cells and accompanied by a marked growth inhibition of cancer cells. The therapeutic application of the GEF loaded nanoparticles was analyz ed *in vivo* in PC9-DR tumour bearing mice after intravenously administration of the free drug or the nanoparticles. The nanoparticles showed a significant effect in targeting the tumour site with the subsequent inhibition of the PC9-DR tumour growth. The results showed a better therapeutic effect of the nanoformulation and reduced undesired side effects, when compared with the free drugs.

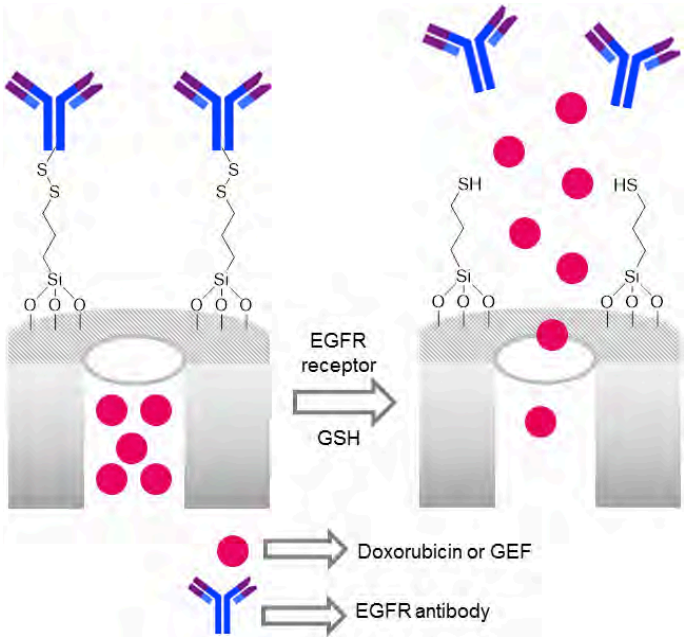

Figure 18. MSNs loaded with doxorubicin or with gefitinib (GEF) and capped with anti-EGFR antibody cetuximab (CET) attached by disulphide bonds.

On the other hand, reactive oxygen species (ROS) are increased in pathological conditions such as in cancer cells. In the field of nanomedicine, this biochemical property has been exploited to design capped MSNs with sensitive groups that are broken in the presence of ROS. The molecules acting as gatekeepers are based on bonds such as thioketals, ketals and diselenides that are cleaved in the presence of ROS species such as hydrogen peroxide H_2O_2, superoxide anion O_2^- and hydroxyl radical HO. Examples of such ROS-responsive nanomaterials have been reported in the literature although very few examples have been tested in *in vivo* models. For instance, Hu and co-workers used MSNs for the preparation of a ROS-cleavable nanodevice.[90] For this purpose, MSNs were functionalized with aminopropyl moieties. Then the amino groups were reacted

[90] J. -J. Hu, Q. Lei, M. -Y. Peng, D. -W. Zheng, Y. -X. Chen, X. -Z. Zhang, *Biomaterials* **2017**, *128*, 136.

with a thioketal linker which was synthesized by the reaction between acetone and 3-mercaptopropionic acid. Afterward, doxorubicin and the ROS generator α-tocopheryl succinate (α-TOS) were co-encapsulated. Finally, the nanoparticles were functionalized with β-cyclodextrin derivatized with amino groups, through the formation of amide bonds, and then the pores capped upon addition of adamantane-containing PEG via host-guest interactions (Figure 19). The system was designed to respond to intracellular ROS present in cancer cells, which mediated the release of doxorubicin and α-TOS from the inner of the pores after ROS-induced thioketal cleavage. The α-TOS delivered had the capability of self-regenerate the intracellular ROS, which facilitated the cleavage of the thioketal linkers and the subsequent release of more α-TOS, self-accelerating the release of doxorubicin. The ROS-responsive properties of the nanoparticles were tested in the presence of H_2O_2 (as a typical ROS). The results demonstrated that in the presence of different concentrations of H_2O_2; the thioketal linkage was cleaved and the supramolecular inclusion complex removed with subsequent doxorubicin and α-TOS delivery. The ROS generating capability and ROS-triggered release was confirmed in MCF-7 breast cancer cells (with high amounts of ROS) compared to normal cells as control group. The high efficiency of drug release of the nanoparticles in ROS abundant tumour MCF-7 cells was demonstrated. Finally, the antitumour efficacy was studied in MCF-7 tumour-bearing nude mice with the intravenously administration of nanoparticle samples compared to free drug treatments. The material showed a high inhibition in tumour growth promoted by the self-accelerating drug release strategy, which maximized the antitumour activity resulting in a higher apoptosis of cancer cells compared to free drug, with lower side effects.

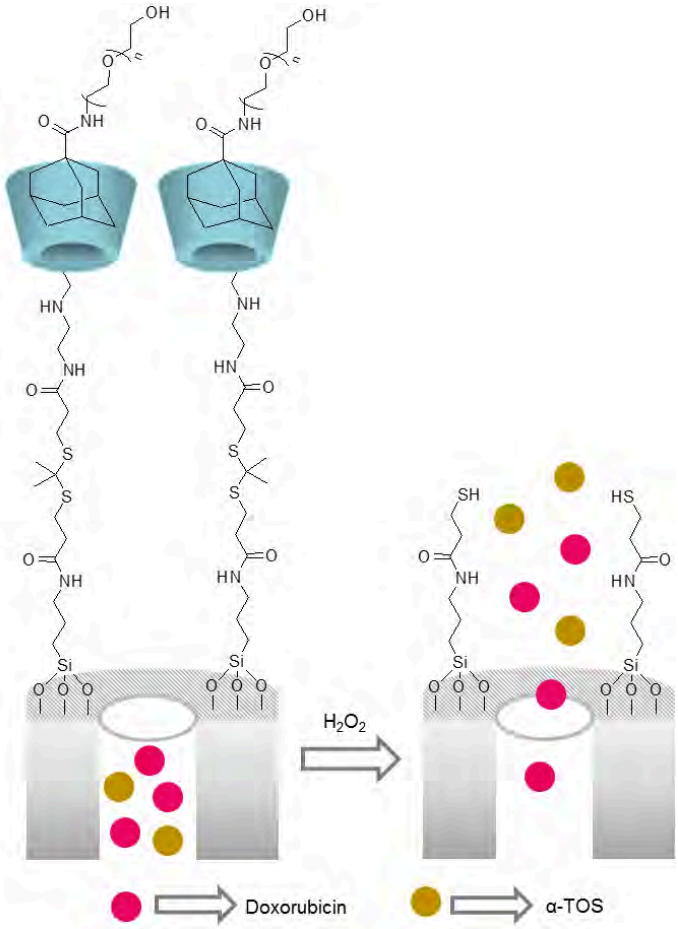

Figure 19. MSNs loaded with doxorubicin and α-tocopheryl succinate (α-TOS) and capped with β-cyclodextrin-adamantane-containing PEG and a ROS-cleavable thioketal linker.

- Enzymatic triggered release

Enzyme-responsive gated materials have attracted much attention in the last years in drug delivery applications.[34b] In pathological conditions, from cancer to inflammation disorders, the activity of some enzymes is upregulated and this fact could be used to design gated materials. Typical enzymes used to uncap the pores in different pathological scenarios are hydrolases, lipases, nucleases,

phosphatases, glycosidases, oxidoreductases and transferases. In these nanoparticles bulky (bio)molecules, able to block the mesopores, contain functional groups that could be hydrolysed by selected enzymes. As we detailed below, some of these nanomaterials have successfully been applied in realistic biological environments in *in vivo* models, being the protease-responsive and hyaluronidase-responsive nanocarriers the most widely used.

Specific proteases present in different tissues or cancer cells, such as cathepsins or metalloproteinases (MMPs), have been used to design tailor-made enzyme-sensitive gated systems. For instance, Li and co-workers reported an enzyme-responsive nanodevice for real-time diagnosis by magnetic resonance imaging (MRI) and tumour treatment in living animals.[91] For the preparation of the nanodevice the anticancer drug doxorubicin was loaded onto magnetic iron oxide nanoparticles coated with a mesoporous silica layer. The surface of the nanoparticles was modified with mercaptopropyl moieties and the thiol groups were reacted with 3-(maleimido)propionic acid *N*-hydroxysuccinimide ester through a Michael addition reaction. This procedure yielded nanoparticles with the surface functionalized with *N*-hydroxysuccinimide ester groups. The system was finally capped, through the formation of amide bonds with the *N*-terminus, with a peptide substrate of the matrix metallopeptidase-2 (MMP-2), overexpressed in cancer cells (Figure 20). The authors found that the nanodevice remained capped in the absence of MMP-2 enzyme, whereas doxorubicin release was clearly observed when the MMP-2 enzyme was present. The antitumoural activity and selectivity of the nanomaterial was evaluated *in vitro* in studies with HT-1080 cancer cells. Moreover, MRI-chemotherapy experiments were carried out in HT-1080 tumour-bearing mice by nanoparticle administration by tail vein injection. T_2-weight MRI imaging measurements showed accumulation of the

[91] E. Li, Y. Yang, G. Hao, X.Yi, S. Zhang, Y. Pan, B. Xing, M. Gao, *Nanotheranostics* **2018**, *2*, 233.

nanoparticles in tumours which was enhanced after the application of a magnet. Besides, a marked inhibition of tumour growth was observed for mice treated with the nanoparticles alone or with nanoparticles + magnet.

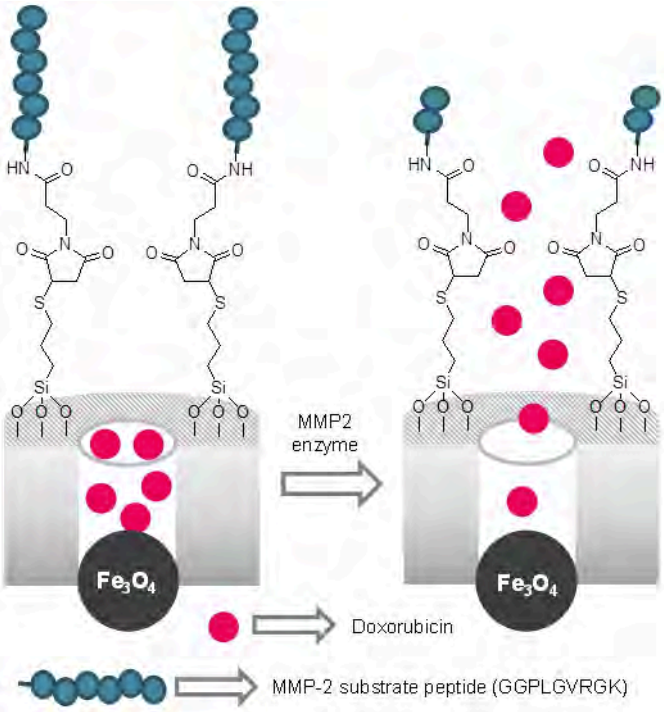

Figure 20. Fe_3O_4 nanoparticles coated with a mesoporous silica shell loaded with doxorubicin and capped with a peptide substrate of the matrix metallopeptidase-2 (MMP-2) enzyme.

Hyaluronic acid (HA)-capped nanomaterials have been widely used in biomedicine due to its good biocompatibility and the targeting properties of HA. In this scenario, it has been reported that members of the HA signalling pathway (HYAL-1 hyaluronidase, HA synthases and HA receptors) are overexpressed in a variety of carcinomas. Following this concept, Yang et al. prepared sulfhydryl and amino-co-functionalized MSNs loaded with doxorubicin and capped upon addition

of a HA derivative (HA-His-SS-Py) through a disulphide bond exchange reaction (Figure 21).[92] Nanoparticles were designed to respond to the presence of intracellular hyaluronidase (HAase), which degrades HA, and GSH that reduces disulfide bonds. In fact, the authors found that the nanoparticles were able to release the entrapped doxorubicin in the presence of HAase or GSH. Besides, when both stimuli are present, a more marked doxorubicin release was observed. In contrast, when nanoparticles were suspended in water in the absence of any stimuli a negligible doxorubicin release was found, confirming the function of the HA as a cap to prevent premature drug release. The targeting ability and antitumour efficacy of the nanoparticles was demonstrated *in vivo* in a doxorubicin-resistant human breast adenocarcinoma (MCF-7/ADR) mouse model. For this purpose mice were administered with the prepared nanoparticles (through intravenous injection) or with free doxorubicin. Nanoparticles showed a stronger cytotoxicity in the MCF-7/ADR cells and enhanced therapeutic effect to reverse multi drug resistance in a MCF-7/ADR tumour-bearing xenograft mouse model compared to the free drug, attending to the superior pharmacokinetics and targeting effect to reach the tumour site.

[92] D. Yang, T. Wang, Z. Su, L. Xue, R. Mo, C. Zhang, *ACS Appl. Mater. Interfaces* **2016**, *8*, 22431.

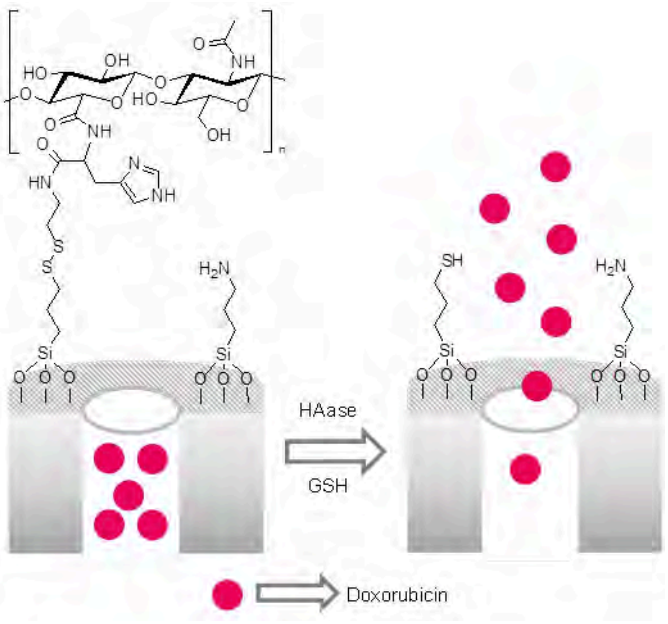

Figure 21. MSNs loaded with doxorubicin and capped with a hyaluronic acid derivative through disulphide bonds.

- Temperature responsive drug delivery

Temperature-responsive systems can be used simply to protect by encapsulation a drug until it reaches the body at 37°C or used to deliver selectively drugs in tissues with higher temperature such as inflamed tissues or tumoral cells. Temperature can be also considered an external stimulus. In this case, metallic nanoparticles able to transform light in heat or superparamagnetic nanoparticles able to generate heat when are exposed to an alternating magnetic fields (AMF) can be used, as discussed in the next section. Regarding the design of this kind of nanodevices, thermosensitive polymers with temperature-phase transition, and especially those which contain *N*-isopropylacrylamide units, have been widely used as part of the gating mechanism. These polymers have the

ability to exchange its conformation between a hydrated state and a more compact dehydrated state, which makes them ideal as capping moieties.

Yang and Wu took advantage of polymer shrinkage to design nanoparticles for controlled drug delivery.[93] MSNs were functionalized with 3-methacryloxypropyltrimethoxysilane that reacted with *N*-isopropylacrylamide and methacrylic acid through seed precipitation polymerization to form a capping co-polymer with a low critical solution temperature (LCST) of 39°C, which indicates a collapsed conformation above this temperature and an hydrated and bulky state below this temperature. Pores were loaded with berberine and evodiamine was adsorbed onto the responsive polymer. Berberine and evodiamine are active components of *Coptidis rhizoma* and *Euodiae fructus*, respectively, which are used in Traditional Chinese medicine to induce a synergistic antitumoral effect. Finally, a lipid bilayer using 1,2-distearoyl-*sn*-glycero-3-phosphoethanolamine-*N*-[methoxy(polyethylene glycol)$_{2000}$] (DSPE-PEG$_{2000}$) was formed around the nanoparticle. The solid showed no significant release of any of the drugs at neutral pH (7.4) and at 37°C. However, drug release increased when pH decreased to 5 or when temperature rose until 41°C, which represented tumoral microenvironment. Below LCST, the polymer forms a dense layer onto the solid surface that hinders berberine release while the lipid bilayer prevents evodiamine leakage. At high temperature lipid bilayer destabilization and polymer shrinkage allowed the escape of the drugs (Figure 22). Additionally, when pH decreases, lipid bilayer permeation and polymer degradation triggered drugs release. *In vitro* cytotoxicity of the gated nanoparticles was studied in tumoral HepG2, HCT-8 and HeLa cells and in non-tumoral HUVEC cells. While treatment with unloaded nanoparticles underwent high viability (>90%), treatment with the drug-loaded system led to an important toxicity. Moreover, a good inhibition of cell migration

[93] Y. Feng, N. Li, H. Yin, T. Chen, Q. Yang, M. Wu, *Mol. Pharm.* **2019**, *16*, 422.

and invasion was observed in wound-healing and transwell assays when HepG2 and HCT-8 tumoral cells were treated with the capped NPs. In contrast, the same nanoparticles were able to inhibit the formation of capillary tubes in normal HUVEC as a model of tumour angiogenesis. Finally, nude mice injected with EMT-6 cells to generate a breast tumour model were treated with the gated nanoparticles via tail vein. Free Taxol was used as control. Taxol showed the strongest tumour inhibition, but animal body weight was importantly decreased due to side effects. Free evodiamine and free berberine showed rapid clearance. In contrast, the prepared nanoparticles showed great tumour inhibition without body weight loss. The study also showed that the efficacy of the nanoparticles was significantly better than the free drug combination.

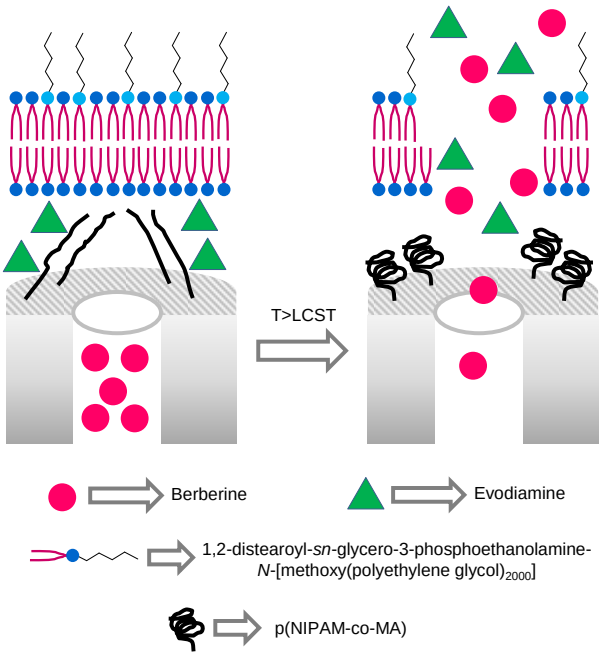

Figure 22. MSNs loaded with berberine and evodiamine and capped with a p(NIPAM-co-MA) polymer and DSPE derivatized with polyethylene(glycol) lipid bilayer.

Exogenous stimuli

Gated nanoparticles taking advantage of externally applied stimuli to drug delivery represent a potential tool to on-command drug release in biomedical applications. Although this strategy seems more complex compared to endogenous stimuli, the application of external stimuli has gained interest in the last years and some examples using gated nanoparticles externally activated for drug delivery have been reported. These nanodevices provide a major control of the premature cargo release and thus can enhance the therapeutic effect of the drugs in target organs reducing undesirable side effects. Examples reported of drug delivery from gated nanoparticles triggered by light, magnetic fields and ultrasounds are described below.

- Light triggered release

Since the first example developed by Fujiwara and coworkers in 2003,[40] light has been an appealing external stimulus to trigger cargo release in gated nanoparticles. In biological applications, light can be applied from outside in a noninvasive manner and it is possible to have a fine control in time and in the area when light is applied. However, an important drawback of light as stimulus in biological models is that UV-vis light does not penetrate deep in tissues. A solution to this shortcoming is the use of the more tissue-penetrating near-infrared radiation (NIR). In fact, most examples of application in living models use NIR light to trigger the release of the entrapped cargo in gated nanoparticles. Examples using up-converting nanoparticles to transform a low-energy irradiation in a high energetic irradiation or the use of photosensitizers to generate ROS have also been applied.

Regarding NIR light as stimuli, Zhao and Xu developed an imaginative gated material able to perform photodynamic therapy, controlled drug release and gene therapy combined with photoacoustic imaging.[94] In their work, the authors used rattle-structured nanoparticles which consisted of hollow MSNs with gold nanorods (AuNRs) synthesized *in situ* inside the hollow cavity of the nanoparticle. The nanoparticles were functionalized with amino groups and then adamantanecarboxylic moieties were incorporated to the surface by and amidation reaction. After loading the nanoparticles with the antiproliferative and antiangiogenic drug sorafenib, pores were capped with a polycation designed with two-armed ethanolamine-functionalized poly(glycidylmethacrilate) units with one β-cyclodextrin core. Finally, a plasmid corresponding to the antioncogene p53 was condensed by electrostatic interaction with the capping polycation (see Figure 23). NIR-triggered sorafenib release was also demonstrated. Negligible sorafenib release was found in the absence of NIR light (5% at 250 min). In contrast, massive drug release was obtained when the suspension was irradiated due to the detachment of β-cyclodextrin containing polycation from the solid surface. When HepG2 cells were treated with the complete system including p53 antioncogene and irradiated with NIR laser light a cell viability of 22% was obtained due to the combined effect of gene, chemo- and photothermal therapy. Additionally, thanks to the AuNRs cores, photoacoustic and computed tomography imaging was also verified. In a final step, hepatoma-bearing nude mice were treated with the final nanoparticles. Tumour growth in animals treated with the complete nanoparticles and irradiated was highly suppressed and tumour size was visibly reduced compared to control groups.

[94] X. Chen, Q. Zhang, J. Li, M. Yang, N. Zhao, F.-J. Xu, *ACS Nano* **2018**, *12*, 5646.

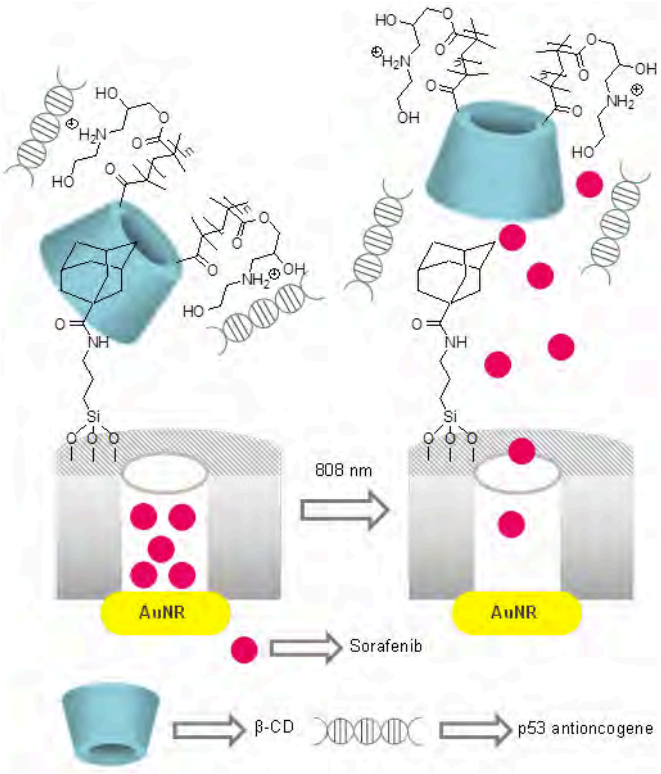

Figure 23. AuNRs coated with mesoporous silica loaded with sorafenib, capped with a photosensitive inclusion complex with p53 antioncogene.

In the following work, Xuan and co-workers developed a similar system but including magnetic functionality in its design.[95] MSNs were functionalized with (3-aminoproyl)triethoxysilane (APTES) and citrate-stabilized iron oxide nanoparticles were incorporated to the mesoporous surface by electrostatic interaction with the protonated amino groups in MSNs. In a further step, the material was loaded with the photosensitizer hypocrellin B and capped with a red-blood cell membrane (Figure 24). The main advantage of the magnetic functionalization is related with the possibility of guiding the nanoparticles to a specific site. After assessing good performance of the nanoparticles in HeLa cells,

[95] M. Xuan, J. Shao, J. Zhao, Q. Li, L. Dai, J. Li, *Angew. Chem. Int. Ed.* **2018**, *57*, 6049.

Balb/c bare mice with tumors created by the injection of 4T1 cancer cells in their right-hind leg were treated intravenously with the nanoparticles. Tumour eradication was achieved when the tumour was covered with a magnet for 1 h to accumulate the nanoparticles in the tumoral environment, and then irradiated with 560 nm light for 30 min for ROS generation.

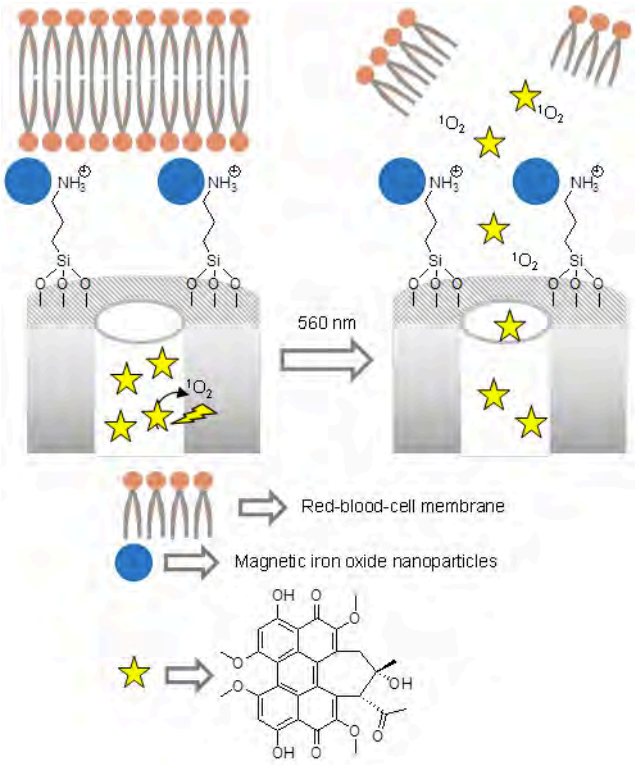

Figure 24. MSNs loaded with hyprocellin A and capped a red-blood cell membrane. Hypocrellin A induced ROS generation upon irradiation with 560 nm light.

- Magnetic field triggered release

In recent years, the possible use of magnetic field to trigger the release of drugs is a pursued goal to obtain a completely spatio-temporal controlled delivery

with minimal invasion and high safety even in the same visualization moment. Additionally, the reorientation of magnetic cores when exposed to AMF generates heat which can induce a synergic thermal effect to destroy for example cancerous cells. Based on these concepts, AMF-driven delivery nanosytems combine thermosensitive moieties such as polymers and superparamagnetic domains to design devices able to trigger the release of the species through the heat dissipated by the superparamagnetic core. Due to the requirements to generate AMFs such as high energy without external heating and good signal control, this stimulus has not been developed as others. Currently, the obtained internal heating is not very high because of the rapid heat dissipation in tissues among others. However, magnetic hyperthermia can be considered a promising alternative to prepare AMF-driven systems able to exert a synergic effect due to the obvious heating of the tissues plus controlled release of drugs.

Vallet-Regí et al. validated AMF-sensitive nanoparticles for tumour reduction.[96] The system consisted of superparamagnetic iron oxide nanoparticle embedded in a mesoporous silica matrix and coated with a thermosensitive polymer. Specifically, the external surface of the nanoparticles were first functionalized with both, small poly(ethyleneglycol) chains for colloidal stability and 3-[tris(trimethylsiloxy)silyl]propyl methacrylate. In a further step, radical polymerization was performed using the monomers *N*-isopropylacrylamide, *N*-(hydroxymethyl)acrylamide and *N*'-methylenebis(acrylamide) and ammonium persulfate as radical initiator (Figure 25). The thermosensitive layer had a LCST of 42°C. When the temperature is above this fixed temperature, the polymer chains collapse and a cargo can diffuse from the pore voids to the exterior. The authors validated their nanoparticles in an allograft model using murine melanoma EL4 cells injected subcutaneously in 7-week-old female immunocompetent C57/BL6

[96] E. Guisasola, L. Asín, L. Beola, J.M. de la Fuente, A. Baeza, M. Vallet-Regí, *ACS Appl. Mater. Interfaces* **2018**, *10*, 12518.

mice. The study revealed that nanoparticles deeply penetrated within all tumor parts. In a subsequent study the activity of the doxorubicin-loaded MSNs was evaluated when an AMF (H x f: 1.89 x 10^9 $Am^{-1}s^{-1}$) was applied. Two groups, i) with and ii) without application of magnetic hyperthermia were used as control and mice treated with doxorubicin-loaded nanoparticles iii) with and iv) without application of AMF were studied. Finally, mice treated with v) free doxorubicin and with vi) unloaded nanoparticles and with AMF were included in the study. The researchers only found tumour growth inhibition in mice treated with doxorubicn-loaded nanoparticles and treated with AMF, which can be explained in terms of the synergic effect obtained due to the local heating and drug release.

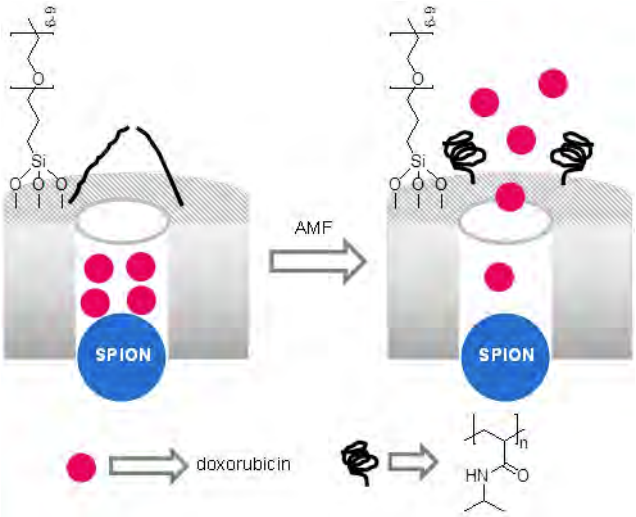

Figure 25. PEG-functionalized magnetic MSNs loaded with doxorubicin and capped with NIPAM thermosensitive polymer. Upon the application of AMF the polymer collapsed allowing doxorubicin release.

- Ultrasounds triggered release

Ultrasounds (US) are an attractive exogenous stimulus to trigger cargo release from gated particles. This type of irradiation is known to penetrate deep

inside tissues by an appropriate selection of the frequency. Additionally, the use of US induces an enhanced particle uptake in cells and a synergic killing effect due to membrane fluidification and ROS generation. US can be also used as a safe, easy and affordable visualization technique. Microbubbles, usually generated by perflorocarbons, give a specific contrast which improves significantly the US image. All these features envision that US-driven MSNs could be an excellent theranostic system which combines localized drug administration and superior imaging capability. Typical US-induced cavitation process or the presence of US-sensitive molecules (mechanophores) can be used to design such ingenious nanosystems.

Zhang and coworkers developed a multifunctional system including MSNs in microbubbles which can be selectively disrupted by US.[97] MSNs were first functionalized with APTES and then FA was incorporated by coupling folic acid- *N*-hydroxysuccinimide with the amino functionalized nanoparticles by means of an amidation reaction. Finally the solid was loaded with coumarin 6 or with the apoptosis inducer diterpenoid tanshinone IIA (TAN). In a final step, nanoparticles where included in a microbubble formed by mixing 1,2-dipalmitoyl-*sn*-glycero-3-phosphocholine (DPPC) and 1,2-dipalmitoyl-*sn*-glycero-3-phosphoethanolamine (DPPE) lipids and injecting perfluorocarbon octafluoropropane during the shearing process (Figure 26). Right encapsulation of coumarin 6-loaded nanoparticles in microbubbles was confirmed using confocal laser scanning microscopy. Also, the ultrasound imaging contrast enhancement ability of the final nanoparticles was confirmed. Nanoparticles were injected in a gel mold and in H22 tumor-baring mice. In both cases, image contrast enhancement was significantly higher after administration of nanoparticles in comparison with the models before nanoparticles administration due to the microbubbles and thanks to its specific

[97] Y. Lv, Y. Cao, P. Li, J. Liu, H. Chen, W. Hu, and L. Zhang, *Adv. Healthcare Mater.* **2017**, *6*, 1700354.

ultrasonic response. Preferential internalization of TAN-loaded MSNs in cells containing folate receptors (FR) was also confirmed using HeLa cells, with high expression of FR compared to A549 cells, with low levels of FR. Finally, TAN-loaded MSNs included in microbubbles were injected in kumming mice with H22 tumors. Authors found remarkable tumor growth suppression when mice were treated with the nanoparticles and subsequently irradiated for 6 min with ultrasounds using a working intensity of 2 Wcm^{-2} and a frequency of 1 MHz. The efficacy of the nanoparticles was associated to US-induced membrane permeation combined with microbubble rupture and FA targeting.

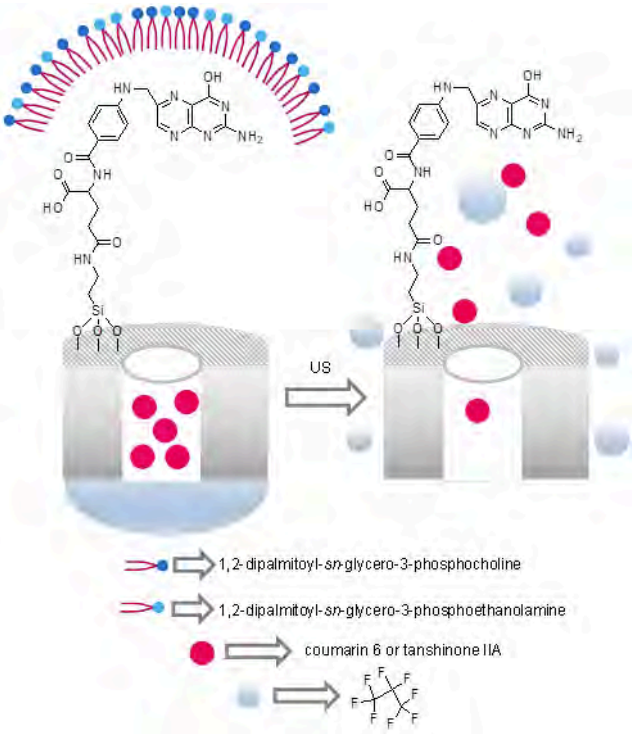

Figure 26. Folic acid-functionalized MSNs loaded with coumarin 6 or tanshinone IIA and octaperfluoropropane and included in a phospholipid microbubble. Upon the application of US, the microbubble was broken and coumarin 6/tanshinone IIA was released.

1.3.4 Clinical relevance of gated mesoporous silica nanoparticles

As we described above, MSNs are promising vehicles for drug delivery therapy in order to enhance the efficacy of therapeutics *in vivo* from a biocompatibility perspective, improving the targeting and controlling the biodistribution of the entrapped drug and thus reducing the drug-related undesired side effects. The advantage of using gated MSNs has been widely demonstrated with promising results in both *in vitro* and *in vivo* studies. However, till date, clinical translation remains challenging. While FDA approved materials are mainly based on polymeric and liposomal nanoformulations, there is an increasing interest in the development and application of novel nanomaterials which include micelles, protein-based nanoparticles and a diversity of metallic and inorganic particles in clinical trials (see Figure 27). In this scenario, more than 50 nanomedices are FDA-approved being ca. 40% of clinical trials listed started in the last five years.[98]

Despite FDA classified silica as "generally recognized as safe" (GRAS) and approved its use in cosmetics and as a food-additive[99] in the field of nanomedicine, no clinical trials have been completed with MSNs. However, recently, some clinical trials have started using silica-based nanoparticles (Table 1), one of them successfully completed and two of them yet in recruiting state.

[98] a) D. Bobo, KJ Robinson, J. Islam, KJ, Thurecht, SR. Corrie, *Pharm. Res.* **2016**, *33*, 2373; b) T. Tagami, T. Ozek, *J. Pharm. Sci.* **2017**, *106*, 2219.

[99] US Food and Drug Administration GRAS Substances (SCOGS) Database—Select Committee on GRAS Substances (SCOGS) Opinion: Silicates. Available online: https://www.fda.gov/food/ingredientspackaginglabeling/gras/scogs/ucm260849.htm

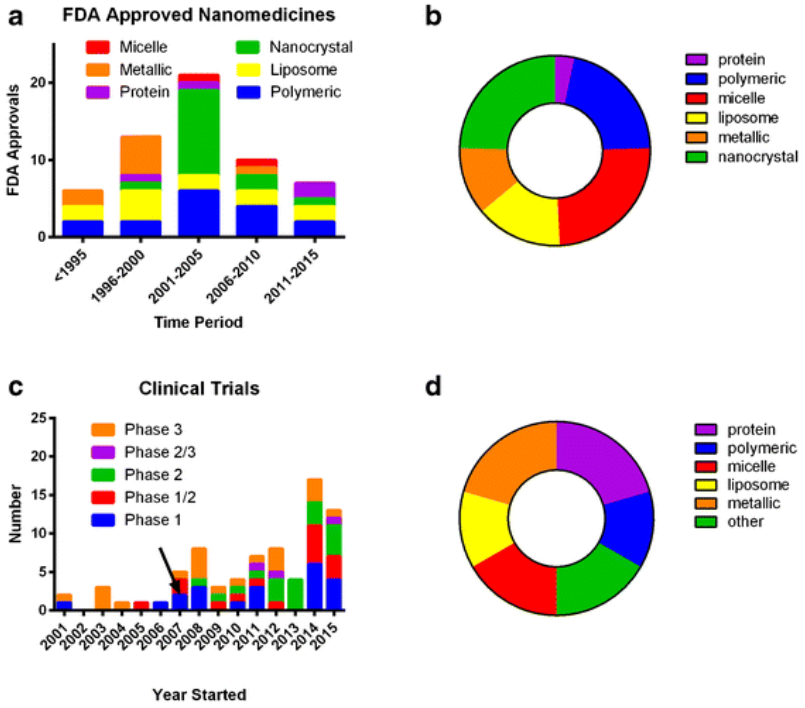

Figure 27. Date recompilation of the development of nanomedicines until 2015 (a) FDA-approved nanomedicines stratified by category; (b) FDA-approved nanomedicines stratified by category overview; (c) clinical trials described in clinicaltrials.gov from 2001 to 2015, the arrow indicate the start date of US law (FDAAA 801) requiring reporting to FDA database; (d) nanomedicines under clinical trial investigation stratified by category overview. Reprinted with permission of *Pharm. Res.* **2016**, *33*, 2373. Copyright © 2016, Springer Science Business Media New York.

The first study completed was Plasmonic Nanophotothermic Therapy of Atherosclerosis (NANOMFIM) (ClinicalTrials.gov Identifier: NCT01270139). This study (phases 1 and 2) explored the treatment of coronary atherosclerosis using nanotechnology. A bioengineered scaffold containing silica-gold nanoparticles and stem cells was transplanted to conduct photothermal therapy, remove the atherosclerosis plaque and remodel blood vessels. Moreover, the researchers also developed CD68-targeted microbubbles based on silica-gold iron nanoparticles to

target macrophages in atherosclerosis plaque and combined with stem cells. In this case, ultrasounds were used to destroy the microbubbles patch and release the nanoparticles which were guided to the target using a magnetic field. The group of individuals treated with the scaffold showed great decrease in atherosclerosis plaque volume allowing quick recover without major complications.[65,100]

The other promising study in early phase of clinical trials is Targeted Silica Nanoparticles for Real-Time Image-Guided Intraoperative Mapping of Nodal Metastases (ClinicalTrials.gov Identifier: NCT02106598). This work developed[124] I-cRGDY-PEGylated core-shell silica nanoparticles for image-guided operative sentinel lymph node mapping in the primary tumour site for breast and colorectal malignancies (phase 1) and melanoma (phase 2) applications.[101] Another study performed at the present using silica-based materials is involved in the field of odontology in which nano-crystalline hydroxyapatite silica gel is employed for the management of periodontal defects. Finally, it should be noted that prior to these studies the use of gold nanoparticles with silica-iron oxide shells to plasmonic photothermal therapy achieved early phase 1 trial, however the study had to be finished before getting results for political pressure.[65,102]

[100] A. N. Kharlamov, J. L. Gabinsky, *Rejuvenation Res*. **2012**, *15*, 222.
[101] S. Michelle, E. P. Bradbury, P. H. Montero, S. M. Cheal, H. Stambuk, J. C. Durack, C. T. Sofocleous, R. J. Meester, U. Wiesner, S. Patel, *Intregr. Biol.* **2013**, *5*, 74.
[102] A. Watermann, J. Brieger, *Nanomaterials* **2017**, *7*, 189.

Table 1. List of MSNs in clinical trials identified in clinicaltrials.gov

TITLE	NANOPARTICLES TYPE	CONDITIONS	PHASE OF CLINICAL TRIALS	STATE	REFERENCE
Plasmonic Photothermal and Stem Cell Therapy of Atherosclerosis Versus Stenting (NANOM PCI)	Gold nanoparticles with silica-iron oxide shells	•Coronary Artery Disease •Atherosclerosis	Phase 1	Terminated 2011-2015	NCT01436123
Plasmonic Nanophotothermal Therapy of Atherosclerosis (NANOM-FIM)	Silica-gold iron-bearing nanoparticles	•Stable Angina •Heart Failure •Atherosclerosis •Multivessel Coronary Artery Disease	Phase 1 Phase 2	Completed 2011-2019	NCT01270139
Evaluation of Nano-crystalline Hydroxyapatite Silica Gel in Management of Periodontal Intrabony Defects	Nano-crystalline hydroxyapatite silica gel	•Chronic Periodontitis	Clinical attachment level	Recruiting 2015-Present	NCT02507596
Targeted Silica Nanoparticles for Real-Time Image-Guided Intraoperative Mapping of Nodal Metastases	124I-cRGDY-PEG-ylated core-shell silica nanoparticles	•Head and Neck Melanoma •Breast Cancer •Colorectal Cancer	Phase 1 Phase 2	Recruiting 2014-Present	NCT02106598

As described before, the increasing progress in nanotechnology and nanomedicine fields has leaded to the development of new nanocarriers, which are arriving to clinical trials as more conventional nanomedicines such as liposomes. Drug delivery nanosystems have resulted useful in the treatment of various diseases, being cancer the most benefited in this field. In addition, infectious diseases, age-related mental diseases and inflammatory disorders which are high cause of mortality are also attractive therapeutic targets for drug delivery systems, in which gated mesoporous silica nanoparticles could play a crucial role.

1.4 Gated mesoporous silica nanoparticles as drug delivery systems in inflammatory disorders

1.4.1 Inflammation and inflammatory response

Inflammation is a biological response of the immune system in response to infectious agents and injury such as pathogens, damaged cells and toxic compounds (see Figure 28). Inflammation is a complex process in which different mechanism of induction, regulation and resolution are involved. The spectrum of persistence of inflammatory conditions determines the type of inflammatory response from acute inflammation (which includes injuries and infections) to chronic inflammatory processes (present in disorders such as type 2 diabetes, atherosclerosis, respiratory disorders, neurodegenerative diseases and cancer).[103] Acute inflammatory response is associated with the rapidly mitigation and reparation of damaged tissues thus restoring their homeostasis and reducing the acute inflammation. However, when acute inflammation is uncontrolled or dysregulated it becomes chronic prevailing along the time and contributing to diverse chronic inflammatory diseases.[104]

In general terms, the inflammatory process is regulated by the activation of signalling pathways which control the levels of inflammatory mediators in the cells present in the damaged tissue (fibroblasts, vascular endothelial cells, and resident inflammatory cells) and in inflammatory cells recruited from the blood (leukocytes, such as neutrophils and macrophages, and plasma cells). This process is mainly coordinated by four components: inflammatory inducers, sensors to detect the inducers, inflammatory mediators activated by the sensors and the

[103] a) R. Medzhitov, *Cell* **2010**, *140*, 771; b) P. Libby, *Nutr. Rev.* **2007**, *65*, S140.

[104] L. Chen, H. Deng, H. Cui, J. Fang, Z. Zuo, J. Deng, Y. Li, X. Wang, L. Zhao, *Oncotarget* **2018**, *9,* 7204.

target tissues affected by the inflammatory mediators (see Figure 29).[105] In order to describe this complex process, in which multitude of elements participate, a detailed explanation attending the different checkpoints and the different regulatory signals is shown below.

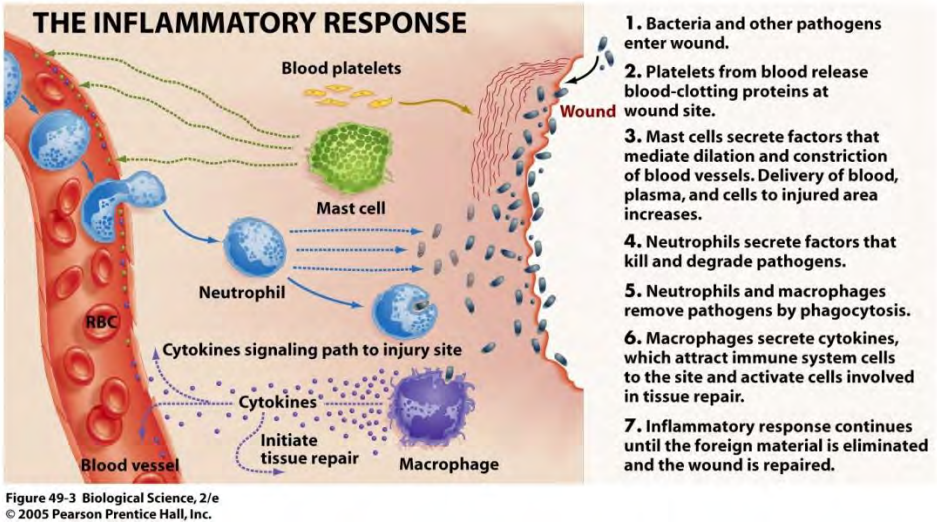

Figure 28. Illustration of the main phases in the inflammatory response process**.**

In a first place, the inducers are the responsible of triggering the inflammatory response upon the activation of germline-encoded pattern-recognition receptors (PRRs), the sensors, expressed in immune and nonimmune cells. The inducers are divided into exogenous signals, in which microbial structures (bacterial DNA and wall components as lipopolysaccharide (LPS)) known as pathogen-associated molecular patterns (PAMPs), virulence factors and other non-microbial factors are included,[106] or endogenous signals derived from tissue or cell damage (host released biomolecules) known as danger-associated molecular patterns

[105] R. Medzhitov, *Nature* **2008**, *454*, 428.
[106] G. Brusselle, K. Bracke, *Ann. Am. Thorac. Soc.* **2014**, *11*, S322.

(DAMPs).[107] Otherwise, the PRRs sensors are located both at cellular surface (Toll-like receptors (TLRs)), in the cytoplasm (NOD-like receptors (NLRs)) or secreted in the tissues surroundings.[108]

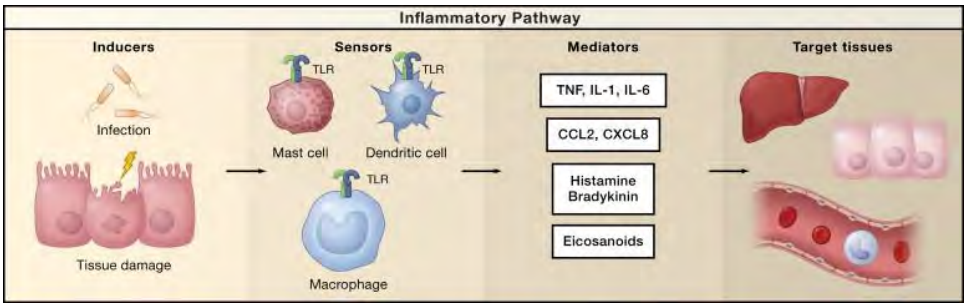

Figure 29. Scheme of inflammatory pathway components: inducers, sensors, mediators and effectors. Reprinted with the permission of *Cell* **2010**, *140*, 771. Copyright © 2010 Elsevier Inc. All rights reserved.

After their activation, PRRs oligomerize and recruit multi-subunit complexes that trigger intracellular signal cascades, as the mitogen-activated protein kinases (MAPK) or nuclear factor kappa-B (NF-κB) signalling pathways.[109] Activation leads to the expression of genes which encode the different inflammatory mediators such as, cytokines (Tumour necrosis factor-alpha (TNF-α) and interleukins (ILs)), chemokines (CCLs and CXCLs), vasoactive molecules (histamine and bradykinin), lipid mediators (eicosanoids) and proteolytic enzymes (elastin and metalloproteinases). The release of these factors promotes the vasodilation and recruitment of inflammatory cells, as well as activates the different cell types to secrete new inflammatory mediators. These tissues and

[107] A. V. Gudkov, E. A. Komarova, *CSH Perspect. Med*. **2016**, *6*, a026161.
[108] a) O. Takeuchi, S. Akira, *Cell*, **2010**, *140*, 805; b) C. A. Janeway, R. Medzhitov, *Annu. Rev. immunol.* **2002**, *20*, 197.
[109] a) S. F. Hendrayani, B. Al-Harbi, M. M. Al-Ansari, G. Silva, A. Aboussekhra, *Oncotarget* **2016**, *7*, 41974; b) J. M. Kyriakis, J. Avruch, *Physiol. Rev.* **2001**, *81*, 807; c) C. Henríquez-Olguín, F. Altamirano, D. Valladares, J. R. López, P. D. Allen, E. Jaimovich, *BBA-Mol. Basis Disc.* **2015**, *1852*, 1410.

cells, among blood vessels endothelial cells and/or hepatocytes are include, act as effectors altering their functional status in response to the inflammatory mediators, to finally resolve the inflammatory event and recover the initial homeostasis of the affected tissue.[90,92,110]

1.4.2 Inflammasomes

The term inflammasome was recently defined by Tschopp in 2002.[111] The inflammasomes are multiprotein complexes which recognize diverse signals of danger, including PAMPs and DAMPs, which trigger the inflammatory response regulated by the activation of caspase-1 and production of pro-inflammatory cytokines such as interleukin-1β (IL-1β) and IL-18.[112] These complexes are mainly formed by proteins of NOD-like receptors (NLRs) acting as a sensors, the adaptor protein apoptosis-associated speck-like protein containing a caspase-recruitment domain called ASC and the pro-inflammatory protease pro-caspase 1. Once recruited pro-caspase 1, it is activated into caspase-1 which processes the pro-inflammatory cytokines (pro-IL-1β and pro-IL-18) into their active forms (IL-1β and IL-18) and leads to inflammation.[113] Besides, the release of the activated cytokines and the cleaved caspase-1 promote the inflammatory cell death called pyroptosis, in which the cellular membrane is disrupted and the intracellular content released (Figure 30).[114]

[110] a) J. S. Pober, W. C. Sessa, *Nat. Rev. Immunol.* **2007**, *7*, 803; b) A. Mantovani, M. A. Cassatella, C. Costantini, S. Jaillon, *Nat. Rev. Immunol*. **2011**, *11*, 519; c) C. N. Serhan, N. Chiang, *Curr. Opin. Pharmacol*. **2013**, *13*, 632.

[111] F. Martinon, K. Burns, J. Tschopp, *Mol. Cell* **2002**, *10*, 417.

[112] a) K. Schroder, J. Tschopp, *Cell* **2010**, *140*, 821; b) B. K. Davis, H. Wen, J. P. Ting, *Annu. Rev. Immunol*. **2011**, *29*, 707.

[113] a) C. Conforti-Andreoni, P. Ricciardi-Castagnoli, A. Mortellaro, *Cell. Mol. Immunol.* **2011**, *8*, 135; b) M. Lamkanfi, V. M. Dixit, *Cell* **2014**, *157*, 1013.

[114] C.A. Dinarello, *Ann. N. Y. Acad. Sci.* **1998**, *856*, 1.

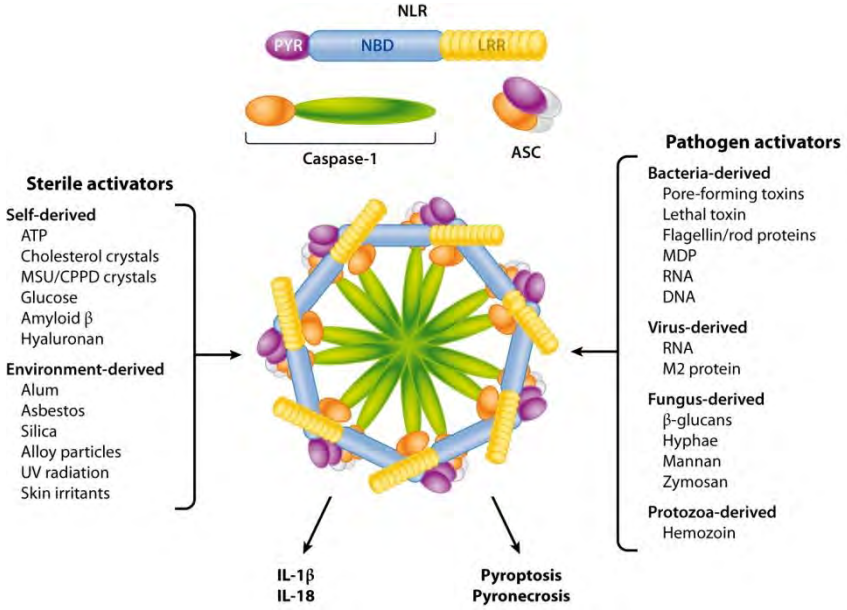

Figure 30. Inflammasome activation and components. Activators of the inflammasome are divided into two categories: Sterile activators and pathogen-associated activators. The assembly of the NLRs, ASC and caspase-1 constitutes the formation of the penta-or heptamer structure called inflammasome. The inflammasome activation leads to the secretion of pro-inflammatory cytokines as well asinflammatory cell death. Reprinted with the permission of *Ann. Rev. Immunol.* **2011**, *29*, 707, Copyright © 2011 by Annual Reviews. All rights reserved.

Since it was first described, the constitution of inflammasome complexes with the subsequent inflammatory cascade activation has been studied and multitude sensors proteins, ligands and activation mechanisms have been identified, as well as the diverse functions carried out by these complexes which involves from antimicrobial responses to multifaceted diseases.[115] On one side, the inflammasomes are classified attending to the receptor that coordinates the assembly of the complex (Figure 31). The NLR family (nucleotide-binding

[115] T. Strowig, J. Henao-Mejia, E. Elinav, R. Flavell, *Nature*, **2012**, *481*, 278-286

domain and leucine-rich repeat containing receptor) is the most representative, being the first sensor proteins described to form inflammasomes. This family is constituted by 23 genes in humans and 34 in mice, and it is also divided in five subfamilies in accordance to the N-terminal domain, being the NLRP family the most important.[116] Besides, recent studies have identified additional receptor families: the AIM2-like receptor (ALR)[117], and the RIG-I-like receptor (RLR) family.[118]

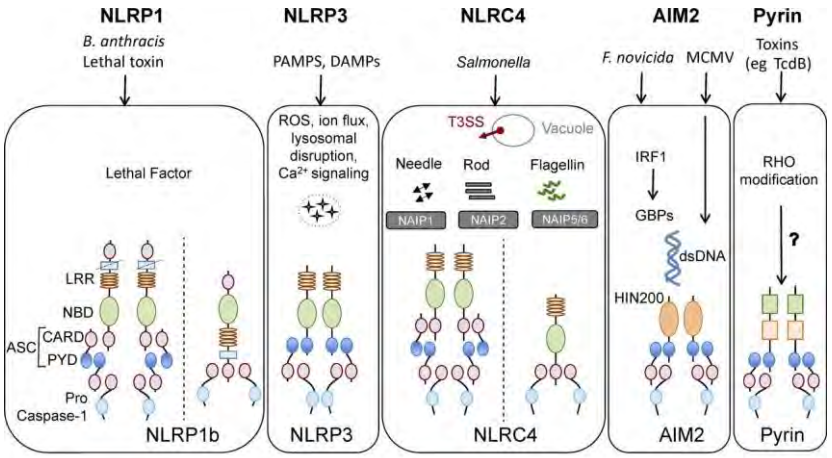

Figure 31. Main inflammasome family subtypes. Reprinted from *J. Cell. Biol.* **2016**, *213*, 617.

In addition, since recent studies remarked the involvement of other caspases in the process, inflammasomes were divided into canonical or non-canonical as a function of the caspases activated in the process (Figure 32). The ***canonical inflammasomes*** include all the receptors which form caspase-1 activating inflammasomes, referred to the canonical function described in the

[116] a) J. C. Reed, K. Doctor, A. Rojas, J.M. Zapata, C. Stehlik, L. Fiorention, J. Damiano, W. Roth, S. Mastuzawa, R. Newman, *Genome. Res*, **2003**, *13*, 1376-1388; b) J.P. Ting, R.C. Lovering, E.S. Alnemri, J. Bertin, J.M. Boss, B.K. Davis, R.A. Flavell, S.E. Girardin, A.Godzik, J.A. Harton, *Immunity*, **2008**, *28*, 285–287.

[117] S. A. Schattgen, K. A. Fitzgerald, *Immunol. Rev.* **2011**, *243*, 109.

[118] R. C. Ireton, M. Gale, *Viruses* **2011**, *3*, 906.

early stages of the inflammasome field. In this classification are included the caspase-1 dependent inflammasome such as NLRP-1, NLRP-3 and AIM-2 being the NLRP3 the most widely described and best characterized (Figure 33).[119] In the case of ***non-canonical inflammasomes***, complexes formed through inflammasome-independent mechanisms or alternative caspases, such as murine pro-caspase 11 murine or human pro-caspase 4 and pro-caspase 5, are described.[120] The triggering of this non-canonical pathway is still not well-understood, although recent studies described the direct interaction of LPS with these pro-caspases.

Regarding pyroptosis, the programmed cell death downstream of inflammatory caspase (1, 4, 5 and 11) activation from canonical or non-canonical inflammasomes, recent findings determine the crucial role of the Gasdermin D (GSDMD) protein as the molecular effector that link the inflammatory downstream processes (see also Figure 33).[121] This protein is formed by an N-terminal fragment which is cleaved and forms pores into the cell membrane, facilitating the release of pro-inflammatory cytokines and the subsequent cell lysis.

[119] J. M. Platnich, D. A. Muruve, *Arch. Biochem. Biophys.* **2019**, *18*, 30994.

[120] N. Kayagaki, S. Warming, M. Lamkanfi, L. Vande Walle, S. Louie, J. Dong, K. Newton, Y. Qu, J. Liu, S. Heldens, J. Zhang, W. P. Lee, M. Roose-Girma, V. M. Dixit, *Nature* **2011**, *479*, 117.

[121] a) N. Kayagaki, I.B. Stowe, B.L. Lee, K. O'Rourke, K. Anderson, S. Warming, T. Cuellar, B. Haley, M. Roose-Girma, Q.T. Phung, P.S. Liu, J.R. Lill, H. Li, J. Wu, S. Kummerfeld, J. Zhang, W.P. Lee, S.J. Snipas, G.S. Salvesen, L.X. Morris, L. Fitzgerald, 870 Y. Zhang, E.M. Bertram, C.C. Goodnow, V.M. Dixit, *Nature,* **2015***, 526*, 2015, 666-671. b) J. Shi, Y. Zhao, K. Wang, X. Shi, Y. Wang, H. Huang, Y. Zhuang, T. Cai, F. Wang, F. Shao, *Nature*, **2015**, *526*, 660-665.

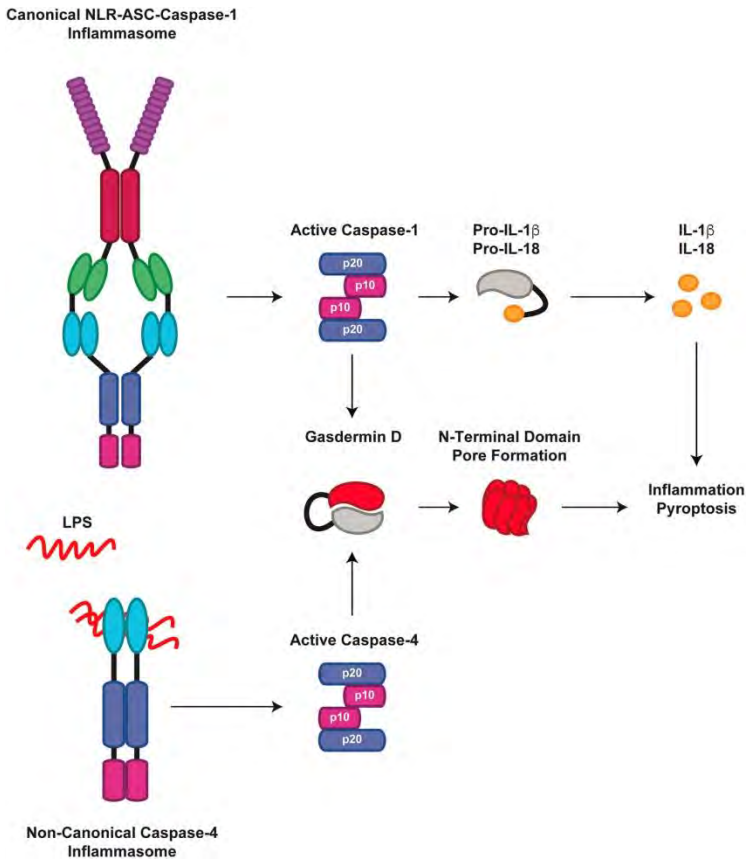

Figure 32. Representation of the Canonical and Non-Canonical Inflammasome components. Activation leads to the cleavage of caspases-1 and 4, which in turn triggers the cleavage of gasdermin D and the induction of pyroptotic cell death. Caspase-1 also results in the maturation of the IL-1β and IL-18 into their active and secreted forms to drive inflammation. Reprinted from *Arch. Biochem. Biophy,* **2019***, 670,* 4 © 2019 Elsevier Inc. All rights reserved.

The better understanding of inflammatory cell death pyroptosis with the findings in the last two decades about inflammasome complexes have provided important data of their role in inflammation and their crucial implication in infectious, autoimmune and autoinflammatory diseases progression, resulting of

special interest for the development of new therapeutic approaches focused on targeting inflammasome components to deal with inflammatory disorders.

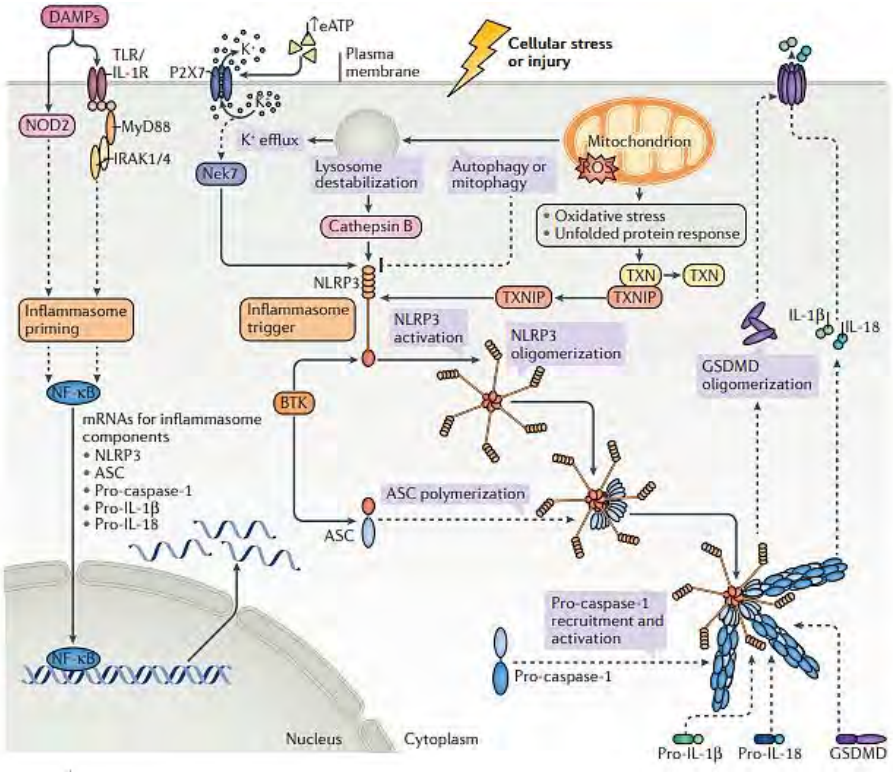

Figure 33. NLPR3 inflammasome pathway. The inflammasome activation is developed after the recognition of damage priming and triggering signals. The cells respond to the injury by increasing the production of inflammasome components and the associated cytokines. The active NLRP3 oligomerizes and recruits ASC which polymerized into filaments. Finally caspase 1 is recruited and activated, forming a star-like structure. Active caspase 1 cleaves the pro-inflammatory cytokines into their active forms, IL-1β and IL-18. Besides, Gasdermin D (GSDMD) is cleaved by caspase 1, oligomerizes and forms pores in the cell membrane with the N-terminal fragments. The activation of GSDMD allows the extracellular release of active IL-1β and IL-18 and subsequent cell lysis or pyroptosis. Reprinted with permission of *Nat. Rev. Cardiol.* **2018**, *15*, 203. Copyright © 2017, Springer Nature.

1.4.3 Drug delivery systems as therapeutic approaches in inflammatory disorders

Inflammatory diseases involve a large group of conditions and disorders characterized by inflammation. Acute and chronic inflammation are identified as important sources of disease which concern many organs systems, including from heart, lung, liver, kidney, pancreas, brain to intestinal tract. Moreover, recent studies related chronic infection and inflammation to some cancers. The common basis of these inflammatory disorders underlies in the insufficient ability to solve inflammation, either produced by pathogens, tissue damage or endogenous signals such as apoptotic or necrotic events.[90,122] An imbalance in the population of inflammatory cells, the elevated presence of inflammatory mediators and chemokines have been identified as essential factors contributing to the progression of the uncontrolled inflammation, and therefore to the inflammatory diseases (Figure 34).

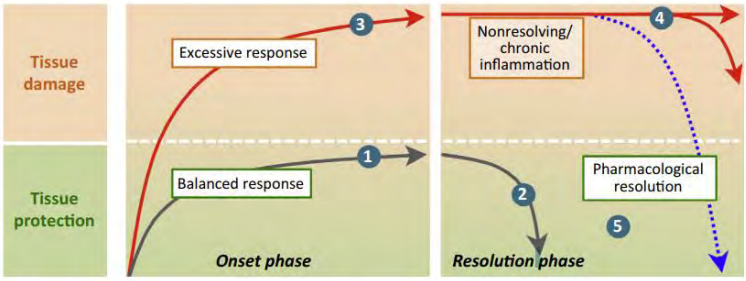

Figure 34. Time phase of inflammatory process resolution compared to non-resolved inflammatory process. Reprinted with permission of *Trends Pharmacol. Sci.* **2015**, *36*, 737. Copyright © 2015 Elsevier Ltd. All rights reserved.

The clinical therapies for the treatment of inflammatory diseases are mainly based on the use of drugs which inhibit specific enzymes or/and

[122] L. Ferrero-Miliani, O. Nielsen, P. Andersen, S. Girardin, *Clin. Exp. Immunol.* **2007**, *147*, 227.

antagonising specific receptors or/and blocking their ligands. These therapies predominantly facilitate the amelioration of the inflammatory-derived symptoms without achieving a complete cure. Among the drugs available to decrease injury and inflammation, and thus minimizing the progression of the inflammatory diseases, the most frequently used are the nonsteroidal anti-inflammatory drugs (NSAIDs) and corticosteroids.[123] NSAIDs, such as aspirin or ibuprofen, are nonselective inhibitors of the cyclooxygenase (COX) enzyme involved in the reduction of pain and inflammation in different inflammatory conditions.[124] On the other hand, corticosteroids are referred to steroid hormones called glucocorticoids (such as prednisone and dexamethasone) used in the suppression of inflammation and immunity in rheumatic diseases, respiratory syndromes and multiple sclerosis among other inflammatory disorders.[125]

Besides, due to the improved understanding of the inflammatory process and the molecular and cellular mechanisms involved, a number of biological agents have been developed to actively resolve inflammation (Figure 35).[126] These new therapeutics include from small-molecules drugs, proteins, nucleic acids to antibodies whose main function is focused on reducing the levels of specific inflammatory cytokines (such as IL-1β and TNF-α) or their receptors (IL-1R and TNF-R), blocking the interaction of immune cells with vessel endothelial cells and reducing the arrival of more immune cells into the injured tissue.[127] In this scenario, the IL-1R antagonist Anakinra,[128] which interferes in the IL-1 binding to

[123] M. Perretti, X. Leroy, E. J. Bland, T. Montero-Melendez, *Trend. Pharm. Sci.* **2015**, *36*, 737.
[124] a) P. G. Conaghan, *Rheumatol. Int*. **2012**, *32*, 1491; b) F. Díaz-González, F. Sánchez-Madrid, *Eur. J. Immunol*. **2015**, *45*, 679.
[125] a) R. H. Straub, M. Cutolo, *Rheumatology* **2016**, *55*, ii6; b) D. W. Cain, J. A. Cidlowski, *Nat. Rev. Immunol.* **2017**, *17*, 233.
[126] A. L. Alessandri, L. P. Sousa, C. D. Lucas, A. G. Rossi, V. Pinho, M. M. Teixeira, *Pharmacol. Ther.* **2013**, *139*, 189.
[127] C. Nathan, A. Ding, *Cell*, **2010**, *140*, 871.
[128] J. Ramírez, J. D. Cañete, *Expert. Opin. Drug. Saf*. **2018**, *17*, 727.

IL-1 receptor, and the IL-1β antagonist Canakinumab,[129] which is and monoclonal antibody that neutralizes the circulating IL-1β, were FDA approved in the last years and since that have been widely used to reduce the inflammation in several disorders. However, despite their notable effectiveness, the inhibition of downstream cytokines in the inflammatory pathway is not enough in some cases to completely deal with inflammation. Thereby, new strategies to block directly inflammasome components have emerged in the recent years. At this respect, inhibitors of caspase-1, such the small molecules VX-765 (Belnacasan)[130] or VX-740 (Pralnacasan)[131], exhibited promising results in the inhibition of inflammation by preventing IL-1β secretion, and they are also being tested in clinical trials.[132]

On the other hand, other strategies have focused their efforts in the prevention of inflammasome formation. In this scenario, there are five inhibitors described (such as MCC950 and Tranilast) to target directly NLPR3 and thus perverting their oligomerization which results in the blockage of both canonical and noncanonical inflammasome activation and the inhibition of interleukins secretion. These compounds showed encouraging therapeutic properties and they are already used in clinical trials (see also Figure 35).[133]

However, as previously mentioned the success of these therapies is limited despite the remarkable activity of some of them in the reduction of inflammation and the continuously progress in the development of new therapeutics.[134] The major limitation is the poor bioavailability of these drugs, which need of repeated and high dosages to achieve the therapeutic effect in the

[129] J. M. Rondeau, P. Ramage, M. Zurini, H. Gram, *MAbs*. **2015**, *7*, 1151.
[130] W. Wannamaker, R. Davies, M. Namchuk, J. Pollard, P. Ford, G. Ku, C. Decker, P. Charifson, P. Weber, U. A. Germann, K. Kuida, J. C. Randle, *J. Pharmacol. Exp. Ther.* **2007**, *321*, 509.
[131] K. Rudolphi, D. V. M. Rudolphi, N. Gerwin, N. Verzijl, P. van der Kraan, W. van den Berg, *Osteoarthr. Cartilage* **2003**, *11*, 738.
[132] M. Lamkanfi, V. M. Dixit, *Cell* **2014**, *157*, 1013.
[133] Y. Yang, H. Wang, M. Kouadir, H. Song, F. Shi, *Cell Death Dis.* **2019***, 10,* 128.
[134] F. A. Khaja, O. M. Koo, H. Onyuksel, *Methods Enzymol.* **2012**, *508*, 355.

desired inflamed tissue. Besides, the broad distribution of these types of immunosuppressive drugs in multiple cells and tissues causes off-target serious side effects and systemic toxicities.[135] According to these premises, the development of drug delivery systems for the treatment of inflammatory diseases has attracted great attention in order to enhance the therapeutic efficacy of the drugs by achieving a specific and sustained delivery to the inflamed tissues thus reducing undesired derived-side effects.[136]

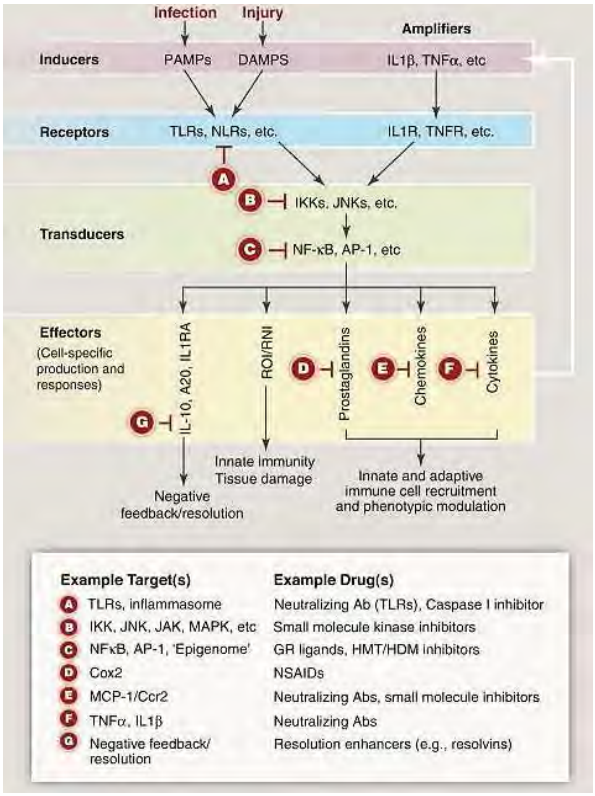

Figure 35. Therapeutic targets and drugs for the inflammatory therapy**.** Reprinted with permission of *Science* **2013**, *339*, 166. Copyright © 2013, American Association for the Advancement of Science.

[135] F. Yuan, L. D. Quan, L. Cui, S. R. Goldring, D. Wang, *Adv. Drug Deliv. Rev*. **2012**, *64*, 1205.
[136] T. H. Tran, M. M Amiji, *Expert Opin. Drug Deliv*. **2015**, *12*, 393.

The principal strategies are based on the use of nanocarriers targeting, both passive and active, macrophages and monocytes and modulate their activity in order to control the inflammatory response. As described in previous sections, inflamed tissues present increased vascular permeability and inflammatory cells the ability to internalize foreign bodies that transport to inflamed site of action (Figure 36). Most of the developed nanocarriers take advantage of this phenomenon, the ELVIS mechanism, and the passively targeting of the inflamed focus with the subsequent drug delivery has been described in models of inflammatory diseases such as rheumatoid arthritis and multiple sclerosis.[123,137] Besides, numerous inflammatory markers have been identified and have been used to developed nanoparticles that actively interact with receptors or ligands present in the inflammatory cells or inflamed tissues. In this scenario, an increase in the design and application of novel targeted drug delivery systems for selective regulation of pro-inflammatory cytokines in chronic autoimmune and inflammatory diseases has remarkably arisen.[138] A multitude of drug delivery systems based on liposomes, polymers and gold and silica based inorganic nanoparticles have being used in the last decade for inflammatory therapy, being this area an intensely active field of research.

[137] a) E. Koziolová, K. Venclíková, T. Etrych, *Physiol. Res*. **2018**, *67*, S281; b) J. Schmidt, J. M. Metselaar, M. H. Wauben, K. V. Toyka, G. Storm, R. Gold, *Brain* **2003**, *126*, 1895; c) D. Wang, S. C. Miller, X. M. Liu, B. Anderson, X. S. Wang, S. R. Goldring, *Arthritis Res. Ther.* **2007**, 9, R2.

[138] a) M. Talekar, T. H. Tran, M. Amiji, *AAPS J.* **2015**, *17*, 813; b) H. Lee, M. Y. Lee, S. H. Bhang, B. S. Kim, Y. S. Kim, J. H. Ju, K. S. Kim, S. K. Hahn, *ACS Nano* **2014**, *8*, 4790; c) K. Tahara, S. Samura, K. Tsuji, H. Yamamoto, Y. Tsukada, Y. Bando, H. Tsujimoto, R. Morishita, Y. Kawashima, *Biomaterials* **2011**, *32*, 870; d) M. D. Bhavsar, M. M. Amiji, *Gene Ther.* **2008**, *17*, 1200; e) I. Kim, S. O. Moon, S. H. Kim, H. J. Kim, Y. S. Koh, G. Y. Koh, *J. Biol. Chem.* **2001**, *276*, 7614; f) J. C. Fernandes, H. Wang, C. Jreyssaty, M. Benderdour, P. Lavigne, X. Qiu, F. M. Winnik, X. Zhang, K. Dai, Q. Shi*, Mol. Ther.* **2008**, *16*, 1243.

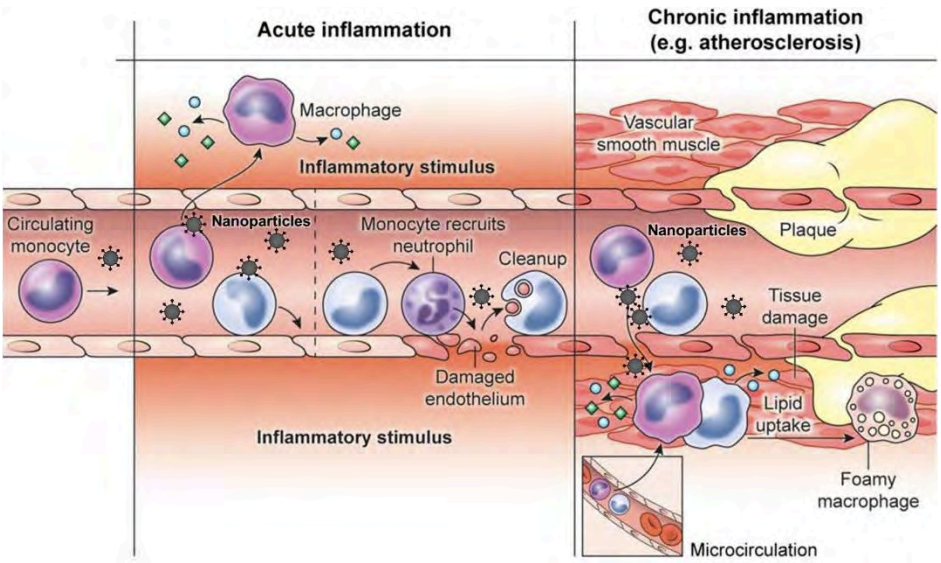

Figure 36. Nanoparticles circulation taking advantage of the ELVIS mechanism in order to modulate the inflammatory response upon the controlled release of anti-inflammatory and immunosuppressive drugs. Adapted from *J. Leukoc. Biol.* **2015**, *98*, 319. With permission © Society for Leukocyte Biology.

In the case of MSNs, despite the smaller number of inflammatory studies using this type of solids compared to liposomes or polymeric nanoparticles, in the last years the interest has increased and the number of studies applying MSNs for inflammatory drug delivery are growing. The limited uses of the silica-based materials in inflammatory applications until time were determined by their controversial immunological effect due to its active surface.[139] Some studies associated an increase of the intracellular oxidative stress and the levels of pro-inflammatory mediators after silica-based nanoparticles exposure. However, most studies concluded that the possible immunological effect depends to the

[139] a) I. Lynch, C. Weiss, E. Valsami-Jones, *Nano Today*, **2014**, *9,* 266; b) T. Gebel, H. Foth, G. Damm, A. Freyberger, P. J. Kramer, W. Lilienblum, C. Röhl, T. Schupp, C. Weiss, K. M. Wollin, J. G. Hengstler, *Arch. Toxicol.* **2014**, *88*, 2191.

physiochemical properties of the nanomaterials. The nanoparticle size, shape and surface functionalization have a crucial role in the cytotoxicity,[140] being the surface modification a key strategy to overcome this immunogenicity. In this aspect, some studies demonstrated that the molecules attached to the nanoparticles surface determine the interaction with serum proteins (corona effect), thus reducing the possible adverse effects and pro-inflammatory response in the different cell types.[141]

Despite the potential drawbacks underlying the immunological effect of silica-based materials, strategies targeting inflammation using gated mesoporous silica nanoparticles, which are commonly modified with biomolecules onto their external surface, is a realistic alternative for immunosuppressive therapies in inflammatory disorders by exploiting the immunological response to nanomaterials and fight with inflammation from the inside using anti-inflamamtory or immunosuppresvive loaded silica nanoparticles as drug delivery systems.[142] In fact MSNs have already been applied in various models of neuroinflammatory diseases, rheumatoid arthritis, inflammatory bowel diseases and several other inflammatory disorders. For example, Xie and co-workers used MSNs loaded with an analgesic (Δ9-tetrahydrocannabinol) and capped with the anti-inflammatory peptide ARA290 (an erytrhopoietin-derived peptide) and polyethylene-glycol (PEG). The therapeutic effect of the nanocarrier was evaluated in microglial cells as *in vitro* model of neuronal inflammation and *in vivo* in a chronic constriction injury of the sciatic nerve in mice as peripheral nerve pain model. The nanoparticles showed a great potential in the suppression of

[140] P. Khanna, C. Ong, B. H. Bay, G. H. Baeg, *Nanomaterials* **2015**, *5*, 1163.

[141] a) A. Lesniak, F. Fenaroli, M. P. Monopoli, C. Aberg , K. A. Dawson, A. Salvati, *ACS Nano* **2012**, *6*, 5845; b) R. Leibe, I. L. Hsiao, S. Fritsch-Decker, U. Kielmeier, A. M. Wagbo, B. Voss, A. Schmidt, S. D. Hessman, A. Duschl, G. J. Oostingh, S. Diabaté, *Arch Toxicol.*, **2019**, DOI: 10.1007/s00294-019-02422-9.

[142] a) D. M. Smith, J. K. Simon, J. R. Baker, *Nat. Rev. Immunol.* **2013**, *13*, 592; b) Q. Jiao, L. W. Li, Q. Z. Mu, Q. Zhang, *Biomed. Res. Int.* **2014**, 2014, 1.

inflammation *in vivo*; the neuropathic pain responses were significantly attenuated and protective effects were higher with the nanoformulation compared to single drugs controls.[143] On the other hand, Martínez-Máñez and co-workers prepared micrometric magnetic mesoporous silica particles loaded with hydrocortisone and capped with a bulky azoderivative for the treatment of inflammatory bowel diseases.[144] The therapeutic effect of the nanomaterials was evaluated *in vivo* in Wistar rats treated with 2,4,6-trinitrobenzene sulfonic acid in order to induce colon inflammation. Hydrocortisone-loaded capped nanoparticles were orally administered to the animals and a remarkable decrease was observed in colon inflammation followed by an intensive regeneration of the mucosa structure.

These results clearly demonstrate the possible use of MSNs as drug delivery systems for inflammatory therapy. In most cases, the studies of the therapeutic effect resulted superior when compared to the free administered drug in cell culture or animal studies with no significant derived side effects. Based on the above, MSNs are candidates as drug delivery vehicles that could be exploited in anti-inflammatory or immunopresive therapies from inflammatory disorders, cancer-related inflammation and complimentary treatments for regenerative medicine and transplantation.

[143] J. Xie, D. Xiao, J. Zhao, N. Hu, Q. Bao, L. Jiang, L. Yu, *Adv. Healthcare Mater*. **2016**, *5*, 1213.

[144] A. H. Teruel, E. Pérez-Esteve, I. González-Álvarez, M. González-Álvarez, A. M. Costero, D. Ferri, M. Parra, P. Gaviña. V. Merino, R. Martínez-Máñez, F. Sancenón, *J. Control. Release* **2018**, *281*, 58.

Chapter 2 | Objectives

Given the relevance of gated nanomaterials in drug delivery applications, the present PhD thesis aims to contribute to the field of biomedicine upon the desing, synthesis, characterization and *in vitro* and *in vivo* evaluation of different nanodevices based on mesoporous silica nanoparticles functionalized with different biomolecules acting as molecular gates for controlled drug release in order to manage inflammatory disorders.

The specific objectives referred to each chapter are:

- To develop a drug delivery system to target inflammation taking advantage of the intrinsic passive targeting effect of mesoporous silica nanoparticles for inflamed tissue.

- To design a targeted-lung delivery system based on gated mesoporous silica nanoparticles, for glucocorticoid-controlled release, for acute lung injury treatment.

- To evaluate an alternative pharmacological treatment for acute lung injury based on the use of the inflammasome inhibitor QM-378 encapsulated in targeted-lung mesoporous silica nanoparticles.

Chapter 3 | Targeting inflammasome using mesoporous silica nanoparticles

Targeting inflammasome by the inhibition of caspase-1 activity using capped mesoporous silica nanoparticles

Alba García-Fernández [a,b,c,] Guillermo García-Laínez [d,] María Luisa Ferrándiz [a,e,] Elena Aznar [a,b,c,] Félix Sancenón [a,b,c,] María José Alcaraz [a,e,*,] José Ramón Murguía [a,b,c,] María D. Marcos [a,b,c,] Ramón Martínez-Máñez [a,b,c,**,] Ana M. Costero [a,c,f,] Mar Orzáez [d,***]

[a] Instituto Interuniversitario de Investigación de Reconocimiento Molecular y Desarrollo Tecnológico (IDM), Universitat Politècnica de València, Universitat de València, Camino de Vera s/n. Valencia
46,022, Spain

[b] Departamento de Química, Universitat Politècnica de València, Camino de Vera s/n, Valencia, 46, ,022, Spain

[c] CIBER de Bioingeniería, Biomateriales y Nanomedicina (CIBER-BBN), Spain

[d] Centro de Investigación Príncipe Felipe, Eduardo Primo Yúfera, 3. Valencia 46,012, Spain

[e] Departamento de Farmacología, Facultat de Farmàcia, Universitat de València, Av. Vicente Andrés, s/n. 46,100, Burjassot, Valencia, Spain

[f] Departamento de Química Orgánica, Universitat de València, Dr. Moliner 50, 46,100, Burjassot, Valencia, Spain

Published online: January 6, 2017

(Reprinted with permission from *J.Control. Release,* **2017**, *248*, 60.

3.1 Abstract

Acute inflammation is a protective response of the body to harmful stimuli, such as pathogens or damaged cells. However, dysregulated inflammation can cause secondary damage and could thus contribute to the pathophysiology of many diseases. Inflammasomes, the macromolecular complexes responsible for caspase-1 activation, have emerged as key regulators of immune and inflammatory responses. Therefore, modulation of inflammasome activity has become an important therapeutic approach. Here we describe the design of a smart nanodevice that takes advantage of the passive targeting of nanoparticles to macrophages and enhances the therapeutic effect of caspase-1 inhibitor VX-765 *in vivo*. The functional hybrid systems consisted of MCM-41-based nanoparticles loaded with anti-inflammatory drug VX-765 (S2-P) and capped with poly-L-lysine, which acts as a molecular gate. **S2-P** activity has been evaluated in cellular and *in vivo* models of inflammation. The results indicated the potential advantage of using nanodevices to treat inflammatory diseases.

3.2 Introduction

The use of gated materials in biomedical applications has increased in the past few years thanks to their ability to release therapeutic drugs upon the application of external stimuli. These nanodevices have attracted much attention as candidates for the development of potential new therapies to improve drug efficacy and safety, and are potential alternatives to liposomes and polymeric carriers, which usually release their cargo via simple diffusion-controlled processes or through container degradation [1-7]. Gated nanoparticles have been

used for controlled delivery applications since the first report by Fujiwara and co-workers [8, 9]. To date, several examples of gated systems capable of delivering their cargo have been described [10] upon the application of specific chemical [11-14] physical [15-17] and biochemical [18-20] stimuli.

The unique properties of mesoporous silica nanoparticles (MSNs), such as large loading capacity, low toxicity, stability, biocompatibility and easy functionalization, make them most appealing as carriers for drug storage and on-command delivery [21-23]. Moreover, gated MSNs are also suitable nanocarriers of poor soluble drugs and are able to protect drugs from degradation [24-27]. The combination of the remarkable properties of MSNs as nanocarriers and the use of polymers as caps has been proven a feasible procedure to develop drug delivery systems for applications in a more biological and realistic environment. In this subfield of research, several examples have been reported in the literature on MSNs with polymers capable of delivering the payload by changes in temperature, pH, redox activity and by presence of target enzymes [10] [28].

From another point of view, the intrinsic capacity of macrophages to internalize foreign bodies evidences their potential use for targeting drug delivery using nanoparticles [29-31]. Accordingly, efforts made to develop innovative therapies have been reported that use nanomaterials as intramacrophagic vectors to enhance the antimicrobial effects of antibiotics, based mainly on liposomes [32, 33], polymeric [34, 35] and carbon nanotube [36, 37] carriers. While the use of liposomes, solid lipid particles and biodegradable nanoparticles has been described to target macrophages and deal with infectious diseases, the use of gated silica nanoparticles as a delivery platform to manage inflammation by taking advantage of targeting passive for macrophages has not been previously reported. Very few recent reports have been found that describe the use of MSNs

in the inflammation field that lead to infectious diseases [38] and neuroinflammation [39].

Macrophages are cells implicated in host defense that attack harmful substances through destruction and ingestion associated with an inflammatory response to limit harm to the body [40]. Dysregulated macrophage function and, thus dysregulated inflammation, have been implicated in the pathophysiology of a wide range of disorders, including chronic ulcers, allergic asthma, atherosclerosis, autoimmune disorders and fibrotic diseases, Alzheimer's disease, etc. [41]. Inflammation initiates upon the sensing of signs of acute damage or disturbances in tissue homeostasis, which results in the synthesis and activation of potent pro-inflammatory cytokines, such as pro-Interleukin-1 beta (pro-IL-1β) [42]. This activation is a proteolytic process controlled by interleukin-1 beta (IL-1β)-converting enzyme, caspase-1, which cleaves key pro-inflammatory cytokine IL-1β to trigger inflammation [43]. The protein complexes responsible for caspase-1 activation are inflammasomes [44]. Inflammasomes are molecular platforms formed by an inflammasome sensor molecule (the NLR protein), adaptor protein ASC and protease caspase-1. The formation of these multiprotein oligomers activates caspase-1 that triggers the maturation of pro-inflammatory cytokines IL-1β and IL-18 [45]. Another consequence of caspase-1 activation in macrophages is a pro-inflammatory form of caspase-1-dependent cell death, known as pyroptosis [46, 47]. Alterations in inflammasome components are involved in the physiopathology of several of the above-mentioned inflammatory diseases [48]. Therefore, modulation of inflammasome activity is an important target to develop effective therapeutics to treat inflammation and related inflammatory diseases.

One emerging strategy to treat inflammatory diseases consists of drugs that target caspase activity. One specific inhibitor of caspase-1 is VX-765, a prodrug converted efficiently into the potent and selective inhibitor of ICE/caspase-1 VRT-

043198 with the action of esterases. The therapeutic effect of this drug has already been demonstrated in preclinical studies and clinical trials to treat inflammatory and autoimmune conditions. Former studies have shown their therapeutic potential effect by reducing disease severity and inflammatory response in mouse models of rheumatoid arthritis and skin inflammation. Reducing cytokines production by inhibiting caspase-1, using drugs like VX-765, is a promising approach to consider the important role of these cytokines in inflammatory diseases [49, 50].

Here we report the synthesis, characterization and controlled release behavior of gated-MSNs in both *in vitro* and *in vivo* models of inflammation. MSNs nanodevices were loaded with rhodamine B (**S1**) or drug VX-765 (**S2**), and were capped with polymer ε-poly-L-lysine. Nanoparticles showed "zero release", yet cargo was delivered in the presence of a target stimulus (presence of pronase enzymes). Nanoparticles' behavior was studied in the THP-1 acute monocytic leukemia cell line stimulated, or not, with lipopolysaccharide (LPS) and muramyl dipeptide (MDP) to produce the synthesis of pro-IL1-β and the activation of pro-caspase-1 by the inflammasome. Capped nanoparticles were also evaluated in a subcutaneous air pouch inflammation mouse model.

3.3 Materials and methods

3.3.1. General methods

Powder X-ray diffraction (PXRD), thermogravimetric analysis (TGA), transmission electron microscopy (TEM), N_2 adsorption-desorption and elemental analyses were run to characterize synthesized materials. PXRD measurements were taken with a Philips D8 Advance Diffractometer using CuKα radiation. TGAs were carried out on a TGA/SDTA 851e Mettler Toledo balance in an oxidant

atmosphere (air, 80 mL/min) with a heating program that consisted of a heating ramp of 10°C per minute from 25°C to 100°C. Then the temperature was kept at 100°C for 60 min. Finally, a new heating ramp of 10°C per minute from 100°C to 1000°C was applied and an isothermal heating step at the final temperature for 30 min. TEM images were obtained under a 100 KV JEM-1010 microscope. N_2 adsorption-desorption isotherms were recorded with a Micromeritics ASAP2010 automated sorption analyzer. Samples were degassed at 120°C in vacuum overnight. Specific surface areas were calculated from the adsorption data within the low pressure range using the BET model. Pore size was determined following the BJH method. To determine the zeta potential of the bare and functionalised MSPs, a Zetasizer Nano ZS equipment (Malvern Instruments, Malvern, UK) was used. Samples were dispersed in distilled water at a concentration of 1 mg/mL. Before each measurement, samples were sonicated for 2 min to preclude aggregation. The zeta potential was calculated from the particle mobility values by applying the Smoluchowski model. The average of five recordings was reported as zeta potential. The measurements were performed at 25°C and performed in triplicate. Dynamic light scattering (DLS) studies for the determination of particle size were conducted at 25°C in a Malvern Zetasizer Nano ZS instrument; all the measurements were taken in triplicate on previously sonicated highly dilute water dispersions. Fluorescence spectroscopy was carried out with a JASCO spectrofluorometer FP-8300. HPLC analyses were performed with a Merck Hitachi L-2130 HPLC pump and an L-2200 autosampler using a Lichrospher® 100 C18 (150 x 3.9 mm) column, and different acetonitrile gradients in aqueous 0.1 % TFA as the mobile phase. Live cellular internalization studies were carried out with a Cytomics FC 500 (Beckman Coulter, Inc.). Cell viability and fluorescence spectroscopy measurements were taken with a Wallac 1420 workstation. Silicon determination in mice was made by ICP-MS 7900 from Agilent.

3.3.2. Chemicals

Chemicals tetraethylorthosilicate (TEOS), *n*-cetyltrimethylammonium bromide (CTABr), sodium hydroxide, (3-isocyanatopropyl)triethoxysilane, rhodamine B, trimethylamine, dimethyl sulfoxide (DMSO) and the pronase enzyme from *Streptomyces griseus* were purchased from Sigma Aldrich Química (Madrid, Spain). VX-765 was provided by AdooQ Bioscience. ε-Poly-L-lysine was purchased from Chengdu Jinkai Biology Engineering CO., Ltd. All the other reagents were of a general laboratory grade and were purchased from Merck, unless otherwise stated. For the cell biology studies, RPMI-1640, fetal bovine serum (FBS), Dulbecco's phosphate-buffered saline (PBS), lipopolysaccharides (LPS) from *Escherichia coli* 055:B55 (*in vitro* experiments), 0111:B4 (*in vivo* experiments), adenosine 5'- triphosphate disodium salt (ATP), *N*-acetylmuramyl-L-alanyl-D-isoglutamine hydrate (MDP), peroxidase conjugate goat anti-rabbit and anti-mouse and tetramethylammonium hydroxide (TMAH) solution 25% wt were obtained from Sigma Aldrich. Cell proliferation reagent WST-1 was obtained from Roche Applied Science (Madrid, Spain). LDH activity was measured by the Lactate Assay Kit II by BioVision. The human IL-1β ELISA Set II and skin milk powder were purchased from BD Biosciences. The caspase-1 (2225) and cleaved caspase-1 antibodies (4199) were purchased from Cell Signaling, while the α-tubulin antibody (#T8203) was obtained from Sigma-Aldrich. ECL Western blotting detection reagents were purchased from Amersham Pharmacia Biotech. Mouse IL-1β ELISA and TNF-α ELISA were purchased from R&D Systems (Minneapolis, MN, USA) Mouse IL-18 Platinum ELISA and Mouse IL-10 ELISA Ready-Set-Go were purchased from eBioscience.

3.3.3. Synthesis of gated mesoporous silica nanoparticles

3.3.3.1. Synthesis of MCM-41 mesoporous silica nanoparticles

CTABr (1.00 g, 2.74 mmol) was dissolved in 480 mL of deionized H_2O before adding a solution of NaOH (3.5 mL, 2.00 M). The solution temperature was adjusted to 80°C and then TEOS (5.00 mL, 2.57×10^{-2} mol) was added dropwise to the surfactant solution at maximum stirring. The mixture was stirred for 2 h to give a white precipitate. The solid was isolated by centrifugation and washed with deionized H_2O until a neutral pH was obtained. Finally, the solid was dried at 60°C. To prepare the final porous material, MSNs were calcined at 550°C in an oxidant atmosphere to remove the template phase.

3.3.3.2. Synthesis of S1.

In a typical synthesis, calcined MCM-41 nanoparticles (200 mg) and rhodamine B (76.64 mg, 0.16 mmol, 0.8 mmol/g solid) were suspended in CH_3CN (7 mL). The suspension was stirred at room temperature for 24 h. Then an excess of (3 isocyanatopropyl)triethoxysilane (200 µl, 0.85 mmol, 4.25 mmol/g solid) was added, and the final mixture was stirred at room temperature for 5.5 h. The resulting pink solid (**S1**) was finally isolated by centrifugation, washed twice with CH_3CN (5 mL) and dried at 37°C. Taking into account the amount of rhodamine B used and the content in the loaded solid (see Table 2) a load efficiency of 54% was calculated.

3.3.3.2. Synthesis of S1-P.

First, **S1** (200 mg) and ε-poly-L-lysine (200, mg, 1 mmol, 5 mmol of polymer/g solid) were dissolved in CH_3CN (9 mL) and H_2O (4 mL), followed by the addition of rhodamine B (50 mg) to avoid dye delivery from pores. Triethylamine (400 µl) was added and the final mixture was stirred for 2 h. Nanoparticles were

centrifuged and washed thoroughly with water. The resulting solid **S1-P** was dried at 37°C.

3.3.3.3. Synthesis of S2.

First calcined MSNs (1 g) and VX-765 (80, mg, 0.16 mmol, 0.16 mmol/g solid) were suspended in 10 mL of DMSO (VX-765 solubility in DSMO at 10 mg/mL). The suspension was stirred at room temperature for 24 h to yield solid **S2**. Then excess (3 isocyanatopropyl)triethoxysilane (1 mL, 4.25 mmol, 4.25 mmol/g solid) was added to a suspension that contained solid **S2** (1 g) in CH_3CN (25 mL).The final mixture was stirred at room temperature for 5.5 h and the resulting white solid (**S2**) was isolated by centrifuging, washed twice with CH_3CN (5 mL) and dried at 37°C. Taking into account the amount of VX-765 used and the content in the loaded solid (see Table 2) a load efficiency of 81% was calculated.

3.3.3.4. Synthesis of S2-P.

First, **S2** (1 g) and ε-poly-L-lysine (1 g, 5 mmol, 5 mmol of polymer/g solid) were dissolved in a mixture of CH_3CN (50 mL) and H_2O (30 mL). Triethylamine (1.6 mL) was added, and the final mixture was stirred for 5.5 h. Nanoparticles were centrifuged and washed thoroughly with water. The resulting solid **S2-P** was dried at 37°C.

3.3.4. Cargo release studies.

To investigate the stimuli-responsive gating properties of the solid, rhodamine B and VX-765 delivery studies were performed in each case in water and in a highly competitive media (PBS buffer).

In a first step, 2 mg of **S1-P** were placed in 1 mL of water at pH 8, and separated into two aliquots of 500 µl. Both samples were added to a volume of

2.5 mL of water at pH 8 in the absence or presence of the pronase enzyme (0.12 mg/mL) from *Streptomyces Griseus*, respectively. Suspensions were stirred at 37°C. At certain time aliquots were separated and centrifuged to eliminate the solid and dye delivery was monitored by the fluorescence emission band of rhodamine B at 575 nm (λ_{ex} = 555 nm) in the aqueous phase. In a second step, studies in PBS were also performed. In this case, 2 mg of **S1-P** were placed in 1 mL of PBS 1X at pH 7.5, and separated into two aliquots of 500 µl. Both samples were added to a volume of 2.5 mL of PBS at pH 7.5 in the absence or presence of the pronase enzyme (0.12 mg/mL) from *Streptomyces Griseus*, respectively. In addition, experiments with denatured pronase (0.12 mg/mL) were also performed to assess the role played by the enzyme in the gating mechanism of **S1-P**. Suspensions of **S1-P** in PBS were stirred at 37°C. At certain time aliquots were separated and centrifuged to eliminate the solid and dye delivery was monitored by the fluorescence emission band of rhodamine B at 575 nm (λ_{ex} = 555 nm) in the aqueous phase.

In the **S2-P** delivery studies, 10 mg of the solid were suspended in 2 mL of water at pH 8. The suspension was separated into two aliquots and each was added to 4 mL of water at pH 8 in the absence or presence of the pronase enzyme (0.12 mg/mL) from *Streptomyces Griseus*, respectively. Suspensions were stirred at 37°C. At certain time aliquots were separated and centrifuged to eliminate the solid. Drug delivery was monitored by analytical RP-HPLC with a UV detector using a mobile phase of CH_3CN-H_2O mixtures that contained 0.1% TFA at 1mL/min. Compound VX-765 was monitored at 220 nm.

3.3.5. Cell culture conditions.

THP-1 human leukemic monocyte cells were purchased from the German Resource Centre for Biological Materials (DSMZ) and were grown in RPMI-1640

supplemented with 10% of FBS. Cells were incubated at 37°C in an atmosphere of 5% carbon dioxide and 95% air, and underwent passage twice a week. For the experiments, THP-1 cells were seeded at 10^6 cell/mL in RPMI-medium at 1% of FBS.

3.3.6. Cytotoxicity cell assays.

THP-1 cells were seeded in a 96-well plate and treated at different **S1-P** concentrations (0 (control), 25, 50, 100 and 150 μg/mL in PBS). Cells were incubated for 6 h and 24 h, and then viability was determined by a WST-1 assay and a lactate dehydrogenase (LDH) activity assay. For cell viability, WST-1 was added for 30 min and then absorbance was measured at 595 nm. The cytotoxicity of mesoporous silica nanoparticles against THP-1 was addressed by measuring the LDH activity in cell culture supernatants with the Lactate Assay Kit II following the manufacturer's instructions. In this case cells were treated with 1% triton-X100, in the absence of nanoparticles, as a control positive of the LDH activity.

3.3.7. Cellular uptake.

In a first step, flow cytometry experiments were carried out to test the uptake of nanoparticles by THP-1 cells. For this purpose, cells were seeded in a 6 well-plate and treated with **S1-P** at the 0 (control), 25 and 50 μg/mL concentrations (in PBS) for 30 min. Then cells were washed with PBS and quantification of rhodamine B fluorescence was performed by flow cytometry and analyzed using version 2.9 of the WinMDI program. To assess **S1-P** nanoparticle's uptake by THP-1 cells, studied were carried out by confocal microscopy by means of rhodamine B associated fluorescence. THP-1 cells were seeded in a 6-well assay and treated with 50 μg/mL of nanoparticles and incubated at 37°C for 1h. Then, cells were

washed several times with PBS, and the fluorescence intensity was monitored using a Leica TCS SP2 confocal microscope. Two independent experiments that contained triplicates were performed.

Finally, a solid containing covalently attached fluorescein was prepared and internalization studies were performed by flow cytometry and confocal microscopy as described above (see supporting information Fig.S2).

3.3.8. VX-765 loaded nanoparticles activity cellular assays.

Inhibition of inflammatory response by **S2-P** was studied in THP-1 human leukemic monocyte cells. For this purpose, cells were seeded in a 6-well plate and were then treated with **S2-P** at the 0 (control), 50, 75 and 100 μg/mL concentrations (in PBS). Free VX-765 was used as a reference at 1 and 2 μM (in DMSO) and with **S2-P** at 100 μg/mL as a nanoparticles control, respectively. After 30 min, NLPR-3 inflammasome was activated with lipopolysaccharide (LPS) from *Escherichia coli* (100 ng/mL) and muramyl dipeptide (MDP) (50 μg/mL) stimulus, and was incubated for 6 h. Finally, the cell suspension was centrifuged and separated into the supernatant and pellet.

The amount of IL-1β secreted in the cell culture supernatants of THP-1 was measured by an enzyme-linked immunosorbent assay (ELISA) kit in accordance with the manufacturer's instructions (Human IL-1β ELISA Set II from BD Biosciences).

Western blot analyses were performed to detect the amount of active caspase-1 secreted into supernatants. Samples were concentrated by methanol/chloroform precipitation [51]. To determine the amount of pro-caspase 1 as a control, whole cell extracts were obtained by lysing cells in a buffer that contained 25 mM Tris-HCl pH 7.4, 1 mM EDTA, 1 mM EGTA, and 1% SDS, plus protease and phosphatase inhibitors. Supernatants and lysates were resolved by

SDS-PAGE, transferred to nitrocellulose membranes, blocked with 5% non-fat milk, washed with 0.1% Tween/PBS and incubated overnight with a specific primary antibody against caspase 1 and cleaved caspase 1 (2225 C1 and 4199 cleaved C1 from Cell Signalling). α-Tubulin was detected in cell lysates as the reference control. Membranes were washed and probed with the appropriate secondary antibody conjugated with horseradish peroxidase for enhanced chemiluminescence detection.

3.3.9. Characterization of the ε-poly-L-lysine-capped nanoparticles activity in *in vivo* models of inflammation.

All the studies were performed in accordance with European Union regulations for the handling and use of laboratory animals. Protocols were approved by the institutional Animal Care and Use Committee. Air pouches were produced by subcutaneous injections of 10 mL of sterile air into the back of male C57BL/6J mice (25-30 g). Three days later, 5 mL of sterile air were injected into the same cavity. Six days after the formation of air pouches, inflammation was induced by an injection of 1 mL of LPS (1μg/mL) into physiological saline [52-54].

As a preliminary assay to test the activity of the solid, gated nanoparticles and free VX-765 were injected locally into the air pouch. Mice were treated with **S2-P** at 0.8 and 1.6 mg/kg or with the reference VX-765 at 0.008 mg/kg (in 0.5 mL PBS + 0.1% DMSO). Air pouches in the control mice were treated with sterile physiological saline and 0.5 mL of PBS + 0.1% DMSO. Two hours after injecting LPS, mice were killed by cervical dislocation and the exudate in the pouch was collected with 1 mL of sterile physiological saline. After centrifuging exudates, supernatants were used to measure the amount of IL-1β, IL-18, IL-10 and TNF-α by ELISA kit according to the manufacturer's instructions.

Then the same experiment was performed systemically by intravenous tail injection of nanoparticles and free drug. **S2-P** was injected at 75 mg/kg and VX-765 at 10 mg/kg (in 0.150 mL PBS + 0.1% DMSO). Control mice were treated with 0.150 mL of vehicle. In this case supernatants were used to measure the amount of IL-1β and IL-18. One part of the exudate sample from the blank and the mice treated with LPS and **S2-P** was used to study the presence of silica nanoparticles at the inflammation focus.

To determine the effect of targeting, presence of MSNs was determined by measuring the amount of silicon in the exudate from the air pouches by ICP-MS, which obtained the exudate, as described above, of three groups of mice. A control group was treated with 0.150 mL of vehicle, a second group was treated with **S2-P** (75 mg/kg, intravenous) and a third group with the LPS stimulus (1 µg/mL, subcutaneous) and **S2-P** (75 mg/kg, intravenous). Then 100 µl of air pouch exudate were introduced into 15 mL of polytetrafluoroethylene (PTFE) tubes and 1 mL of TMAH 25% was added. The digestion temperature was set at 80°C and was kept for 2 h. After cooling digests were diluted to 10 mL in polystyrene tubes. Finally 0.5 mL of the samples was diluted in a mixture of 10 mL of nitric acid 2% and hydrochloric acid 1%, and was measured in the 7900 ICP-MS in H_2 mode using germanium as an internal standard.

3.4 Results and discussion

3.4.1. Gated materials

As stated above, the combination of polymers and MSNs is an appealing approach to design gated nanocarriers for controlled release applications. In this context we used ε-poly-L-lysine as the capping system in MSNs as a suitable polymer anchored covalently to the silica surface in order to develop gated

nanodevices capable of selectively releasing the cargo (rhodamine B or VX-765) in the presence of a target stimulus (pronase enzymes). A representation of the designed nanoparticles is provided in Scheme 1.

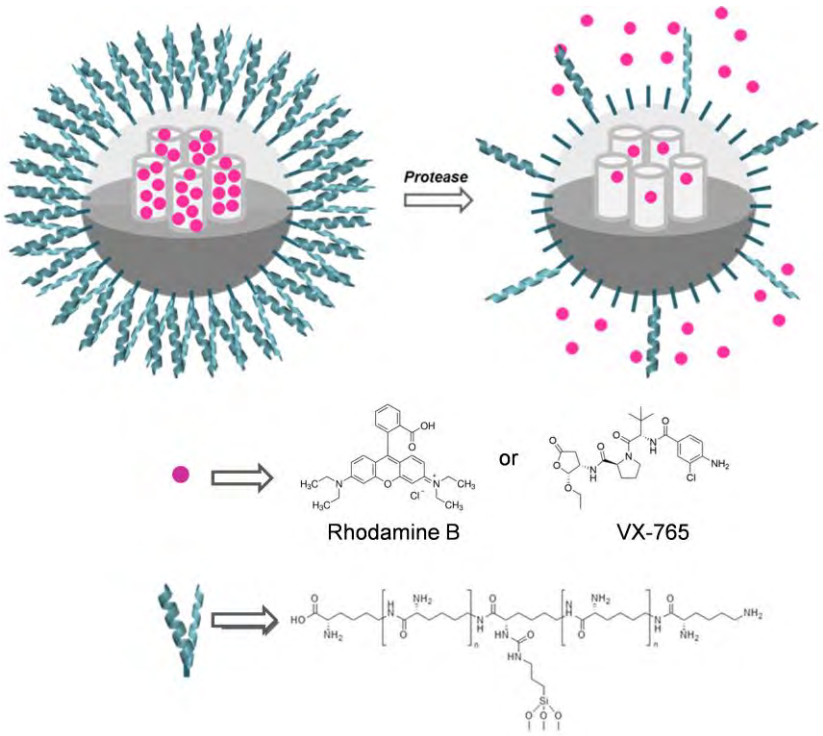

Scheme 1. Representation of the prepared gated material capped with randomly attached ε-poly-L-lysine.

MSNs were obtained following well-known procedures, loaded with the corresponding cargo and functionalized with 3-(triethoxysilyl)propyl isocyanate (solids **S1** loaded with rhodamine B and **S2** loaded with VX-765, see the Experimental Section). Another reaction with ε-poly-L-lysine allowed pores to be capped via the formation of urea bonds between the isocyanate groups in the

nanoparticles and amine groups in the polymer (see Scheme 1) [55]. Following this simple procedure, solids **S1-P** and **S2-P** were obtained.

3.4.2. Characterization of nanoparticles

The prepared solids were characterized by standard procedures. The powder X-ray patterns (PXRD) of the as-synthesized MCM-41, MCM-41 calcined, **S1**, **S1-P** and **S2-P** nanoparticles are shown in Figure 1. The X-ray pattern of the as-synthesized MCM-41 solid presents the four mesoporous characteristic low-angle peaks of a hexagonal-ordered array, which can be indexed as (100), (110), (200) and (210) Bragg reflections. A significant shift of (100) reflection is observed in the MCM-41 calcined nanoparticles pattern, which corresponds to an approximate cell contraction of 4 Å induced by the condensation of silanol groups in the calcination step. In the PXRD pattern of solid **S1-P** and **S2-P**, a slight intensity reduction in the (100) reflection and loss of the (110) and (200) reflections (especially for **S2-P**) are observed, most likely due to the reduced contrast after the loading/functionalization process. Nevertheless, the permanence of the (100) reflection in the X-ray patterns strongly evidences that the mesoporous scaffold is maintained in the final gated nanoparticles.

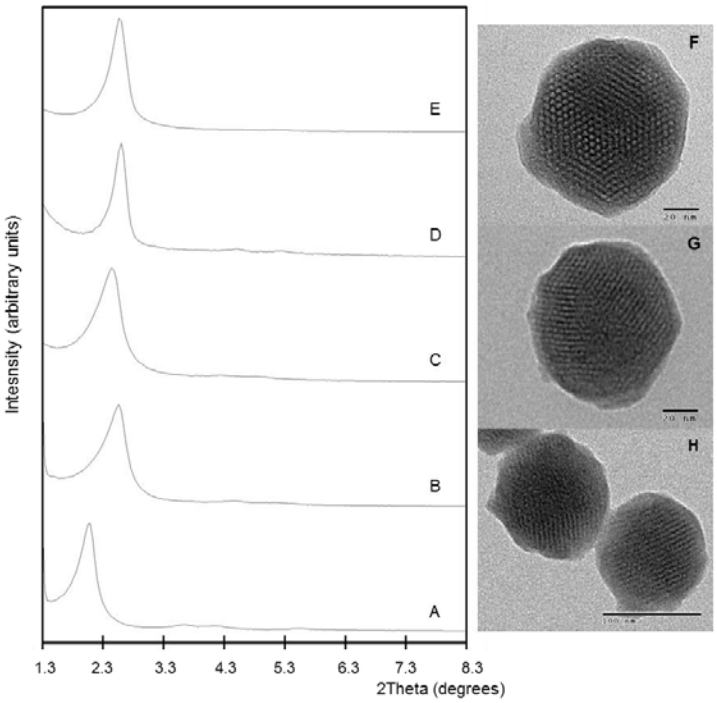

Fig. 1. Powder X-ray patterns of solids A) as-synthesized MCM-41 nanoparticles; B) MCM-41 calcined nanoparticles, C) **S1** solid, D) **S1-P** solid and E) **S2-P** solid. TEM images of F) MCM-41 calcined nanoparticles, G) **S1-P** and H) solid **S2-P** showing the typical hexagonal porosity of the MCM-41 type mesoporous matrix**.**

Furthermore, presence of the mesoporous structure was also confirmed by TEM analyses (Fig. 1, right). In the representative images, spherical nanoparticles were observed, with a mean diameter of 100 nm (92±9, 109±10 and 103±7 nm for calcined MCM-41, **S1-P** and **S2-P** solids respectively) and the loaded and functionalized **S1-P** and **S2-P** solids maintained the initial morphology of the mesoporous silica starting matrix. The typical channels of mesoporous MCM-41 support were easily observed as either alternate black and white stripes or as a pseudo-hexagonal array of pores in the images.

Dynamic light scattering (DLS) studies were also carried out. The results showed particles with a mean diameter of 90±15 nm for the starting calcined MCM-41 nanoparticles and of 122±16 and 114±8 for **S1-P** and **S2-P**, respectively (Fig. 2). The dynamic diameter of the functionalized nanoparticles was larger than that of the bare nanoparticles due to the presence of the capping ε-poly-L-lysine polymer.

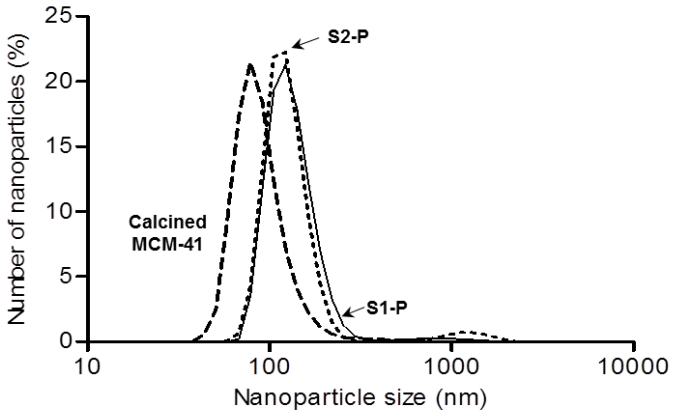

Fig. 2. Size distribution per number of particles obtained by the DLS studies for calcined MCM-41 nanoparticles, **S1-P** and **S2-P**.

The N_2 adsorption-desorption isotherm of the MCM-41 calcined nanoparticles is shown in Figure 3. The curve for the starting calcined nanoparticles displays an adsorption step with intermediate P/P_0 values between 0.1 and 0.3, which correspond to a type IV isotherm that is typical of mesoporous MCM-41-type materials. This step can be related to nitrogen condensation that takes place inside mesopores by capillarity. The specific area was obtained by applying the BET model. From the BJH model on the adsorption curve of the isotherm ($P/P_0 < 0.8$), pore diameter and pore volume were calculated (Table 1). A second feature of the N_2 adsorption-desorption isotherms of the MCM-41 calcined nanoparticles

was the characteristic H1 hysteresis loop that appeared on the curve at a high relative pressure ($P/P_0 > 0.8$), which corresponded to the filling of the large pores between nanoparticles due to textural porosity. In this case, curves showed, in addition to the characteristic H1 hysteresis loop, a wide pore size distribution.

For nanoparticles **S1-P** and **S2-P** (Fig. 3), the adsorption-desorption isotherms are typical of mesoporous systems with partially filled mesopores and the N_2 volume adsorbed and the specific surface area significantly decrease compared with the starting MCM-41 material (see Table 1).

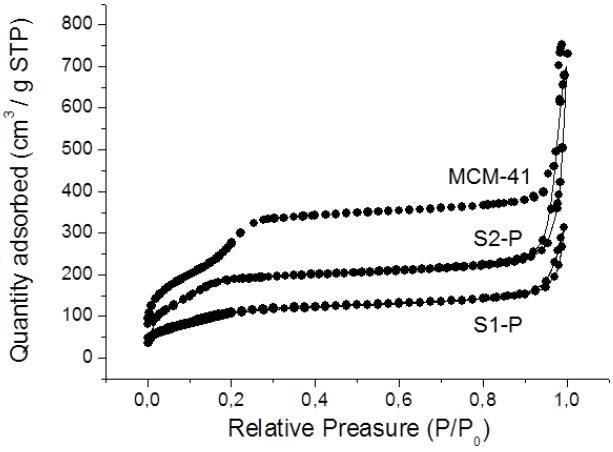

Fig. 3. Nitrogen adsorption-desorption isotherm for: MCM-41 calcined mesoporous nanoparticles, **S1-P**, and **S2-P** solids.

Table 1. BET specific surface values, pore volumes and pore sizes calculated from the N_2 adsorption-desorption isotherms for selected materials.

Solid	S_{BET} (m^2 g^{-1})	Pore volume (cm^{-3} g^{-1})	Pore size (nm)
Calcined MCM-41	1020 ± 28	0.63	2.2
S1-P	413 ± 9	0.27	-
S2-P	745 ± 40	0.20	-

The contents of grafted molecules and cargoes in solids **S1**, **S1-P**, **S2** and **S2-P** were determined by elemental and thermogravimetric analyses (see Table 2). The isocyanatopropyl contents in solids **S2** and **S2-P** (0.42 mmol/g SiO_2) are nearly the same than those measured for **S1** and **S1-P** solids (0.39 mmol/g SiO_2) and subtle differences in contents could be ascribed to the different grafting and loading process used to prepare the solids (see Experimental section). In the case of the synthesis of **S1** and **S1-P** the loading and the grafting processes were carried out in a one pot fashion using acetonitrile as solvent. On the other hand, solid **S2** was loaded with VX-765 in DMSO and then isolated because the functionalization with isocyanatopropyl moieties was carried out in acetonitrile. The amount of polymer in both groups of materials is also quite similar (0.018 g/g SiO_2 for **S1-P** and 0.014 g/g SiO_2 for **S2-P**).

Table 2. Content of molecular gate ε-poly-L-Lysine, the isocyanate group and the guest molecule in the different synthesized nanoparticles.

Solid	Rhodamine B	VX-765	NCO	ε-Poly-L-Lysine
	mmol/g SiO_2	mmol/g SiO_2	mmol/g SiO_2	g/ g SiO_2
S1	0.33	-	0.39	-
S1-P	0.14	-	0.39	0.018
S2	-	0.14	0.42	-
S2-P	-	0.14	0.42	0.014

Finally, in order to assess the charge of the different prepared nanomaterials (calcined MCM-41, **S1**, **S1-P**, **S2** and **S2-P**), the zeta potential were measured. As expected, calcined MCM-41 showed a zeta potential value of -29±1 mV due to the presence of silanolate moieties onto the external surface of the nanoparticles. The rhodamine B loaded solid had a positive value of zeta potential (21±1 mV) induced by the presence of the positively charged dye into the porous network of the nanoparticles. When the external surface of **S1** was coated with poly-lysine (soild **S1-P**) the zeta potential increased to 35±4 mV due to the fact that biopolymer is positively charged at neutral pH. In the case of solid **S2**, a negative zeta potential was measured (-20±6 mV) probably due to the smaller quantity of VX-765 loaded inside the pores when compared to the rhodamine B presented in **S1**. Solid **S2-P** showed a positive zeta potential value (28±5 mV) due to the grafting of poly-lysine onto the external surface of the VX-765-loaded nanoparticles.

3.4.3. Cargo release studies.

In a first step we tested the controlled release performances of **S1-P** nanoparticles in water (pH 8.0). In a typical experiment, 1 mg of solid was suspended in 1 mL of water at pH 8.0 in the absence and in the presence of pronase from *Streptomyces griseous*. Aliquots were taken at scheduled times, centrifuged to remove nanoparticles, and the cargo release was evaluated by measuring the emission band of rhodamine B at 575 nm (λ_{ex} = 555 nm). The obtained results are shown in Fig. 4. A poor rhodamine B delivery occurred in the absence of the enzyme (less than 20%), which is indicative of remarkable pore closure (Fig. 4, curve B). Conversely in the presence of pronase pores opened due to the hydrolysis of the peptide bonds in the polymer with the subsequent dye delivery (Fig. 4, curve E). Nearly the same behavior was observed in a highly competitive media such as PBS. As expected, negligible rhodamine B release was observed in the absence of pronase (Fig. 4, curve A) whereas a marked dye delivery was observed when enzyme was present (Fig. 4, curve D). Moreover, to assess the crucial role played by the enzyme in the release mechanism, cargo release for solid **S1-P** in the presence of denatured pronase was studied. As could be seen in curve C in Fig. 4 a negligible rhodamine B delivery was observed in the presence of denatured pronase. This result demonstrated the specific enzyme response of the gated nanoparticles. Besides, we analysed by HPLC the content of the aliquots obtained at scheduled times after solid **S1-P** was treated with pronase. HPLC measurements showed the presence of lysine in the aliquots, pointing toward a pronase-induced poly(lysine) hydrolysis as mechanism that governed rhodamine B release (see Supporting information).

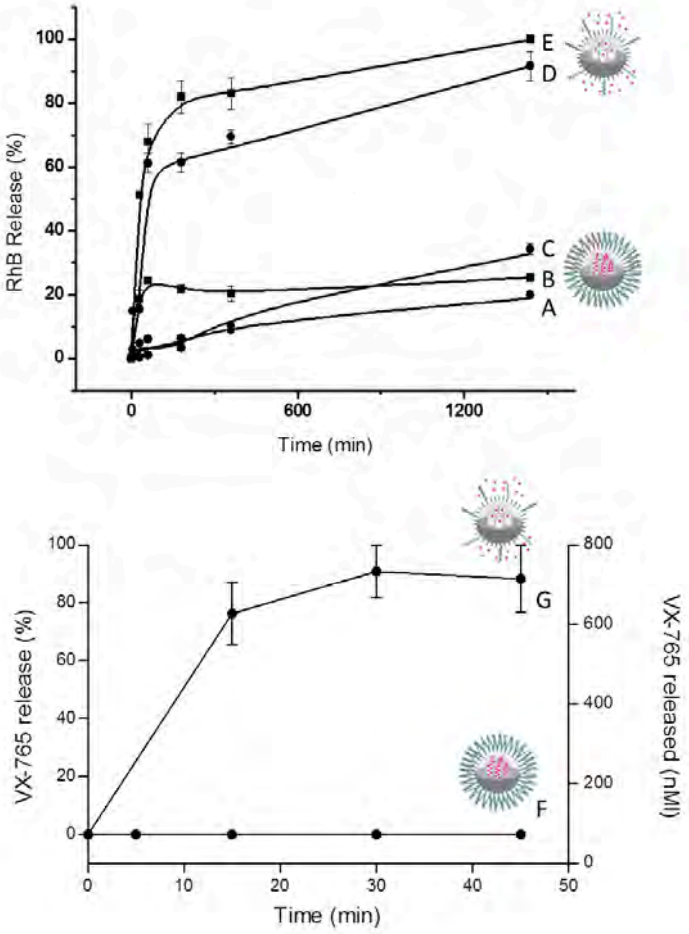

Fig. 4. Top: Enzyme-responsive rhodamine B release form solid **S1-P**: (A) in the absence of pronase in PBS at pH 7.5; (B) in the absence of pronase in water at pH 8.0; (C) in the presence of denatured pronase in PBS at pH 7.5; (D) in the presence of pronase in PBS at pH 7.5; (E) in the presence of pronase in water at pH 8.0. Down: Enzyme-responsive VX-765 release from solid **S2-P** in water at pH 8.0 (F) in the absence and (G) in the presence of pronase.

Similar release experiments were carried out with solid **S2-P**. In this case, delivery of VX-765 from nanoparticles was determined by HPLC analyses. A near-zero release was observed in the absence of pronase, whereas clear drug delivery was detected when enzymes were present (see Fig. 4, curves F and G). The VX-765 concentration reached (after 45 min of pronase addition) was ca. 700 nM, which is a value higher than the IC_{50} reported for this drug (ca. 100 nM). This indicated that relevant therapeutic concentrations of VX-765 can be reached using solid **S2-P**. The delivery experiments also showed that after 1 h, the VX-765 concentration lowered in the medium (data not shown), which was most likely due to an enzyme-mediated hydrolysis or drug degradation.

As it can also be observed in Fig. 4 an apparent faster payload release was observed for solid **S2-P** when compared with **S1-P** in the presence of enzyme and most likely ascribed to the fact that VX-765 is hydrolyzed by the enzyme used to trigger cargo release. This hydrolysis/degradation process of VX-765 avoids the detection of the real maximum delivery peak because after 1 h the amount of payload release began to decrease (the hydrolysis of VX-765 began to be faster than its release from **S2-P**). This is why maximum VX-765 delivery appears at ca. 30 min. A second potential explanation that may also account for the different payload release observed for solids **S1-P** (loaded with rhodamine) and **S2-P** (loaded with VX-765) is, as noted above, the different physical properties of both molecules (such as solubility, polarity, etc). It is well known that delivery from silica mesoporous materials is highly influenced by the nature of the cargo.

3.4.4. Characterization of ε-poly-L-lysine-capped nanoparticles activity in cellular models of inflammation.

Cytotoxicity and cellular uptake studies with the dye-loaded **S1-P** nanoparticles in the THP-1 acute monocytic leukemia cell line were carried out as a preliminary step to further characterize **S2-P** nanoparticles in an *in vivo* anti-inflammatory model (*vide infra*). Cell viability studies that measured mitochondrial activity (WST-1 assays) in the presence of **S1-P** indicated that nanoparticles were well-tolerated by THP-1 cells at concentrations up to 150 μg/mL (Fig. 5 A) after 6 and 24 h of exposure. Furthermore, a non significant LDH release, indicative of the absence of cellular necrosis or pyroptosis, was observed within the 25-150 μg/mL concentration range (see Fig. 5 B) both for 6 and 24 h of treatments.

To evaluate the cellular uptake of rhodamine B-loaded, ε-poly-L-lysine-capped **S1-P** solid by THP-1 cells, internalization of nanoparticles was evaluated by flow cytometry and by confocal microscopy (Fig. 5 C and D). These studies demonstrated that up to 80% of the cellular population internalized **S1-P** 30 min upon treatment, which suggests that these nanoparticles can be used for delivery applications in THP-1 cells. Based on previous published results obtained with similar MSNs capped with enzyme degradable caps [39], it has been postulated that **S1-P** nanoparticles internalize by endocytosis. The resulting endosomal vesicles would fuse to lysosomes, where the activity of lysosomal enzymes would induce ε-poly-L-lysine hydrolysis and entrapped cargo delivery.

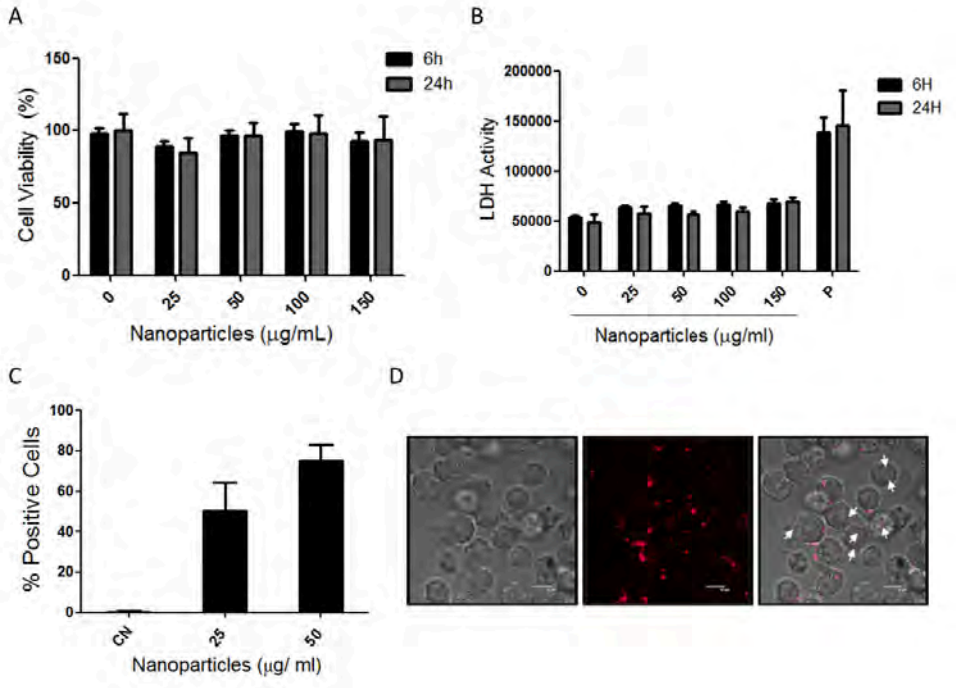

Fig. 5. Cytotoxicity and internalization studies of S1-P at different concentrations of nanoparticles in THP-1 cells. A) Cell viability by the WST-1 assay, B) LDH-activity in the presence of nanoparticles. The positive control of LDH activity (P) was obtained by cellular lysis in 1%Triton-X100 (P) in the absence of nanoparticle. C) Percentage of fluorescent cells analyzed by flow cytometry in internalization studies D) **S1-P** uptake (in red) by THP-1 cells analyzed by confocal microscopy. Confocal images of cells treated with the **S1-P** nanoparticle at 50 μg/mL for 1 h. Data represent the mean±SEM of at least three independent experiments.

3.4.5. Anti-inflammatory activity of S2-P nanoparticles and free VX-765 in a cellular model of inflammation.

After performing internalization studies of **S1-P** nanoparticles in THP-1 cells, further assays to test the anti-inflammatory activity of the **S2-P** nanoparticles in the same cell line were carried out. In a first step, it was verified that stimulation of THP-1 cells with LPS and MDP produced synthesis of pro-IL1-β and activation of pro-caspase-1 by the inflammasome. Under these conditions, an increase in processed IL-1β and activated caspase-1 (casp-1 p20 subunit) in the supernatant of cell cultures was observed (Fig. 6A and B, third line). Treatment of stimulated THP-1 with encapsulated VX-765 (**S2-P** nanoparticles) at the 50, 75 and 100 μg concentrations of solid/mL, or free VX-765 (1 and 2 μM), diminished the release of both IL-1β and activated caspase-1 to the medium (Fig. 6A and B, lines 5-7 and 8-9, respectively). Fig. 6 shows that the activity of **S2-P** nanoparticles at a concentration of 100 μg/mL is similar to that obtained using 1 μM of free VX-765. Moreover, the HPLC studies found that a concentration of 100 μg/mL of **S2-P** corresponded to an equivalent concentration of VX-765 of 13.7 μM (considering that all the encapsulated VX-765 can be released). This indicated that for a similar drug concentration, nanoparticles were less effective than the free drug in assays using THP-1 cells. However, these results strongly contrast with the *in vivo* studies carried out in a mouse model of inflammation in which nanoparticles **S2-P** displayed much more effective anti-inflammatory activity than the free drug (*vide infra*).

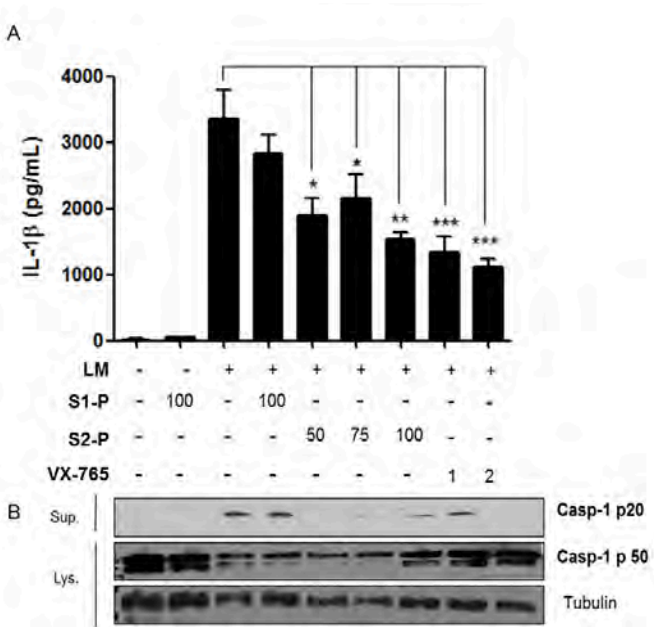

Fig. 6. Inhibition of IL-1β and caspase-1 release induced by **S2-P** treatment in a cellular model of inflammation. Quantification of inflammatory markers in the THP-1 cells stimulated with LPS+MDP. A) IL-1β Levels from cell supernatants measured by enzyme-linked immunosorbent assay (ELISA). B) Levels of active caspase-1 (p-20) detected in the supernatants, inactive fraction of caspase 1 (p50) in cell lysates and, tubulin in cell lysates as a control by Western Blot. Data represent the mean±SEM of at least three independent experiments (* $p< 0.005$, ** $p<0.0025$, *** $p<0.0001$).

3.4.6. Anti-inflammatory activity of S2-P nanoparticles and free VX-765 in the *in vivo* model of inflammation.

Having demonstrated the activity of **S2-P** nanoparticles in cellular assays, we moved one step forward to characterize the anti-inflammatory properties of nanoparticles in an *in vivo* model of inflammation.

In particular, firstly, **S2-P** activity was evaluated in a subcutaneous air pouch inflammation mouse model. In this model, injection of LPS into the air pouch induced an inflammatory response that was easily quantified by the increase in exudates of inflammatory mediators IL-1β, IL-18, TNF-α and IL-10. To confirm that in the air pouch in vivo model of inflammation, release of IL-1 β is dependent of the inflammasome, we have demonstrated caspase-1 activation in the animal exudates by western blot analysis (see Supporting Information Fig. S2). After the intra-pouch administration of free VX-765 at 0.01 mg/kg or **S2-P** at 0.8 and 1.6 mg/kg (which corresponded to amounts of 0.05 and 0.1 mg/kg of VX-765, respectively) in the mouse model, both inflammasome-dependent interleukins IL-1β and IL-18 significantly reduced in exudates (Fig. 7A and B). The therapeutic effect of VX-765 in all cases was the inhibition of ca. 50% of inflammatory activity, and agreed with the cellular model results. In this case no significant differences in activity were found at similar concentrations of VX-765 free or encapsulated in **S2-P**. These results corroborated that treatment with VX-765-loaded mesoporous silica nanoparticles **S2-P** in an animal model was possible and that the inflammatory response properly reduced. In addition, levels of TNF-α and IL-10 were also analyzed as a control of inflammasome-independent cytokines. As expected, no significant differences between the group treated only with LPS and the different treatments with the drug were observed (Fig. 7C and D). These data suggest that a reduction in the IL-1β and IL-18 levels resulted from the specific effect of VX-765 on caspase-1 activity.

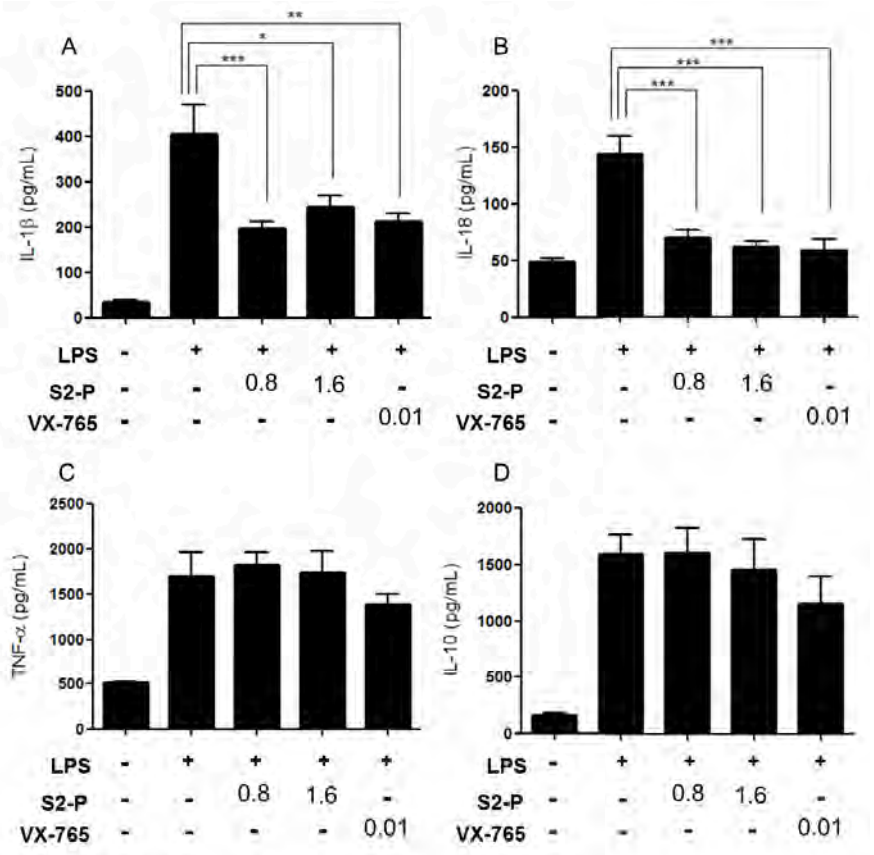

Fig. 7. *In vivo* inhibition of cytokines production by local administration of **S2-P**. Upon air pouch induction, the mice stimulated with LPS were treated with **S2-P** at 0.8 and 1.6 mg/kg (which corresponded to 0.05 and 0.1 mg/kg of VX-765, respectively) or with VX-765-free drug (0.01 mg/kg) for 2 h. Then presence of the cytokine in the air pouch exudates was analyzed by ELISA. Quantification of the assays (n=8) for IL-1β, IL-18, TNF-α and IL-10 is showed in A), B), C) and D) panels, respectively. Data represent the mean±SEM of at least three independent experiments (* p< 0.005, ** p<0.0025, *** p<0.0001).

In another step, the activity of VX-765, either free or encapsulated (**S2-P**), was also analyzed in the same subcutaneous air pouch inflammation mouse model by an intravenous tail injection of VX-765 and **S2-P**. For the intravenous

administration of VX-765, doses were adjusted according to previous reports [56]. As described above, the subcutaneous injection of LPS into the air pouch induced the secretion of IL-1β and IL-18 inflammatory cytokines in exudates. The treatment of LPS-stimulated mice with **S2-P** at 75 mg/kg i.v. (which corresponded to 4.2 mg/kg of VX-765) or free VX-765 at 10 mg/kg, which clearly reduced inflammatory cytokines levels in both cases. In this systemic approach, significant differences were also observed in the IL-1β and IL-18 release upon treatment with nanoparticles. By taking advantage of drug protection and the preferential systemic distribution of nanoparticles to inflamed tissues, in this case the therapeutic effect of the encapsulated drug upon intravenous administration was noteworthily better than that of the free drug (Fig. 8). In particular, a significant reduction in LPS-induced inflammation (ca. 50% of interleukins inhibition) was observed when **S2-P** was used, while differences were not significant for the free drug (around 20-25% of inhibition). Note that in these experiments the amount of loaded VX-765 in **S2-P** (4.2 mg/kg) was lower than the dose of free drug administrated intravenously (10 mg/kg), which indicated that, in this case, VX-765 was almost 4-fold more effective when encapsulated; i.e. the therapeutic effect clearly increased with nanoformulation. These results demonstrated the effectiveness of capped nanoparticles as passively targeted drug delivery systems to inhibit inflammatory response.

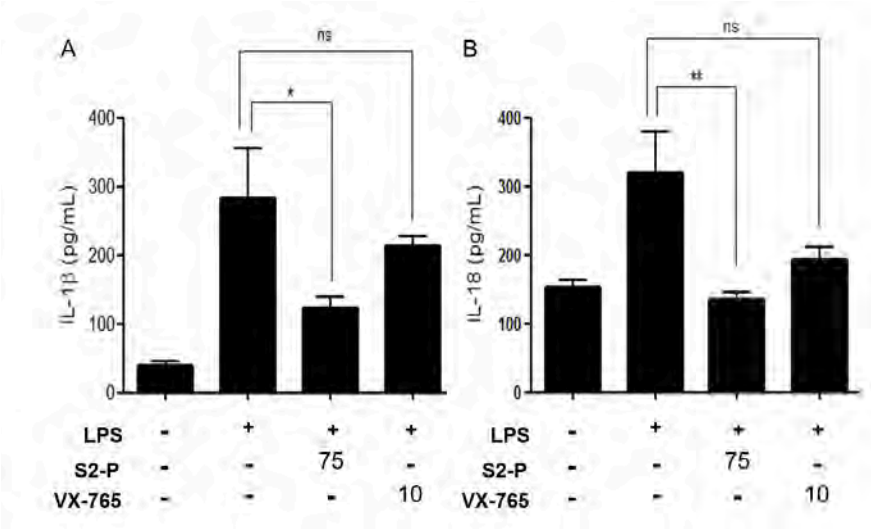

Fig. 8. Anti-inflammatory effects of an intravenous administration of **S2-P** at 75 mg/kg (corresponds to 4.2 mg/kg of VX-765) in the air pouch inflammation model. IL-1β (A) and IL-18 (B) quantification from the exudates of the systemic assay in the air pouch mouse model in different mice groups (n=8). Data represent the mean±SEM of at least three independent experiments (* p< 0.005, ** p<0.0025, *** p<0.0001).

Analyses of silica content in exudates (Fig. 9) confirmed our hypothesis. Similar background Si levels were detected in mice with no induced inflammation (not treated with LPS) in the exudate samples from the air pouch mouse when no nanoparticles or **S2-P** were intravenously injected (2.2 and 2.8 µg of Si/ g exudate, respectively). Conversely in the **S2-P**-treated group (75 mg/kg by intravenous injection), where inflammation was induced by LPS, a clear 2-fold increase in the Si concentration was observed in exudates (5.33 µg of Si/g exudate). These results suggested some specific targeting of nanoparticles at the inflammation focus.

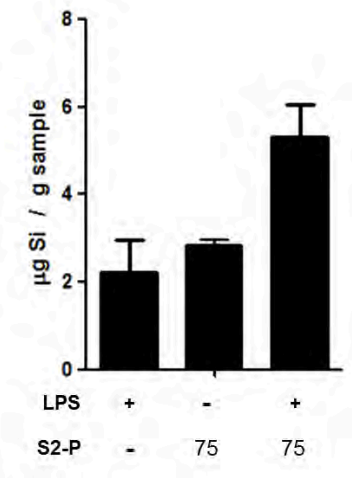

Fig. 9. Silica quantification in the exudate samples from the air pouch mouse. Quantification was performed in groups of mice not submitted to any nanoparticles treatment, **S2-P** treatment (without LPS) and from the air pouch mouse treated with LPS and **S2-P** by intravenous injection.

3.5 Conclusions

Our results demonstrate that delivery of anti-inflammatory drugs using gated mesoporous silica nanoparticles is a suitable tool to develop therapeutic strategies to treat inflammatory diseases. In particular, we developed a drug delivery system to inhibit the inflammatory response in an inflammatory model. The carrier consists in ε-poly-L-lysine-gated mesoporous silica nanoparticles capable of delivering the VX-765 drug in macrophages in *in vitro* and *in vivo* models of inflammation. Our design employs two basic concepts: (a) it is possible to take advantage of the passive targeting of nanoparticles to macrophages and (b) capped materials can deliver modulators of inflammasome in macrophages present at the inflammation focus. ε-poly-L-lysine-functionalized nanoparticles are efficiently taken up by macrophage cells, most likely via endocytosis, and

further reach autolysosomes where the polymer is degraded by lysosomal enzymes and cargo is released. We corroborate that using mesoporous silica nanoparticles in non toxic doses does not trigger an anti-inflammatory response in either macrophages or an *in vivo* air pouch mouse model. We prove that the nanoparticles which encapsulate VX-765 can be intravenously injected into the *in vivo* inflammation model and that the drug is able to reach the inflammation focus. The drug therapeutic effect is enhanced by a significant reduction in the inflammatory response when **S2-P** is injected, compared with the free drug in the animal model. In particular, VX-765 is ca. 4-fold more effective when encapsulated. The demonstration that gated mesoporous silica materials can release drugs selectively at the inflammatory focus is state of the art and, as far as we know, no similar systems to those described herein to treat inflammatory-based diseases have been reported.

ACKNOWLEDGEMENTS. The authors wish to express their gratitude to the Spanish government (Projects MAT2015-64139-C4-1-R and SAF2014-52614-R (MINECO/FEDER)) and the Generalitat Valencia (Projects PROMETEOII/2014/061and PROMETEOII/2014/047) for support. A.G-F. is grateful to the Spanish government for an FPU grant.

3.6 References

[1] K. Hoste, K. De Winne, E. Schacht, Polymeric prodrugs, International Journal of Pharmaceutics, 277 (2004) 119-131.

[2] S. Liu, R. Maheshwari, K.L. Kiick, Polymer-Based Therapeutics, Macromolecules, 42 (2009) 3-13.

[3] T. Traitel, R. Goldbart, J. Kost, Smart polymers for responsive drug-delivery systems. , J. Biomater. Sci. Polym. Ed. , 19 (6) (2008) 13.

[4] F. Puoci, F. Iemma, N. Picci, Stimuli-responsive molecularly imprinted polymers for drug delivery: A review, Current Drug Delivery, 5 (2008) 85-96.

[5] F. Siepmann, J. Siepmann, M. Walther, R.J. MacRae, R. Bodmeier, Polymer blends for controlled release coatings, Journal of Controlled Release, 125 (2008) 1-15.

[6] L.S. Nair, C.T. Laurencin, Biodegradable polymers as biomaterials, Progress in Polymer Science (Oxford), 32 (2007) 762-798.
[7] D. Schmaljohann, Thermo- and pH-responsive polymers in drug delivery, Advanced Drug Delivery Reviews, 58 (2006) 1655-1670.
[8] N.K. Mal, M. Fujiwara, Y. Tanaka, Photocontrolled reversible release of guest molecules from coumarin-modified mesoporous silica, Nature, 421 (2003) 350-353.
[9] N.K. Mal, M. Fujiwara, Y. Tanaka, T. Taguchi, M. Matsukata, Photo-switched storage and release of guest molecules in the pore void of coumarin-modified MCM-41, Chemistry of Materials, 15 (2003) 3385-3394.
[10] E. Aznar, M. Oroval, L. Pascual, J.R. Murguía, R. Martínez-Máñez, F. Sancenón, Gated Materials for On-Command Release of Guest Molecules, Chemical Reviews, 116 (2016) 561-718.
[11] B. Zhang, Z. Luo, J. Liu, X. Ding, J. Li, K. Cai, Cytochrome c end-capped mesoporous silica nanoparticles as redox-responsive drug delivery vehicles for liver tumor-targeted triplex therapy in vitro and in vivo, Journal of Controlled Release, 192 (2014) 192-201.
[12] C. Wang, Z. Li, D. Cao, Y.-L. Zhao, J.W. Gaines, O.A. Bozdemir, M.W. Ambrogio, M. Frasconi, Y.Y. Botros, J.I. Zink, J.F. Stoddart, Stimulated Release of Size-Selected Cargos in Succession from Mesoporous Silica Nanoparticles, Angewandte Chemie International Edition, 51 (2012) 5460-5465.
[13] C. Théron, A. Gallud, C. Carcel, M. Gary-Bobo, M. Maynadier, M. Garcia, J. Lu, F. Tamanoi, J.I. Zink, M. Wong Chi Man, Hybrid Mesoporous Silica Nanoparticles with pH-Operated and Complementary H-Bonding Caps as an Autonomous Drug-Delivery System, Chemistry – A European Journal, 20 (2014) 9372-9380.
[14] R. Liu, P. Liao, J. Liu, P. Feng, Responsive Polymer-Coated Mesoporous Silica as a pH-Sensitive Nanocarrier for Controlled Release, Langmuir, 27 (2011) 3095-3099.
[15] Z. Yu, N. Li, P. Zheng, W. Pan, B. Tang, Temperature-responsive DNA-gated nanocarriers for intracellular controlled release, Chemical Communications, 50 (2014) 3494-3497.
[16] J. Croissant, M. Maynadier, A. Gallud, H. Peindy N'Dongo, J.L. Nyalosaso, G. Derrien, C. Charnay, J.-O. Durand, L. Raehm, F. Serein-Spirau, N. Cheminet, T. Jarrosson, O. Mongin, M. Blanchard-Desce, M. Gary-Bobo, M. Garcia, J. Lu, F. Tamanoi, D. Tarn, T.M. Guardado-Alvarez, J.I. Zink, Two-Photon-Triggered Drug Delivery in Cancer Cells Using Nanoimpellers, Angewandte Chemie International Edition, 52 (2013) 13813-13817.
[17] C. de la Torre, A. Agostini, L. Mondragon, M. Orzaez, F. Sancenon, R. Martinez-Manez, M.D. Marcos, P. Amoros, E. Perez-Paya, Temperature-controlled release by changes in the secondary structure of peptides anchored onto mesoporous silica supports, Chemical Communications, 50 (2014) 3184-3186.
[18] C.-H. Lu, I. Willner, Stimuli-Responsive DNA-Functionalized Nano-/Microcontainers for Switchable and Controlled Release, Angewandte Chemie International Edition, 54 (2015) 12212-12235.
[19] C. De La Torre, L. Mondragõn, C. Coll, A. García-Fernández, F. Sancenõn, R. Martínez-Máñez, P. Amorõs, E. Pérez-Payá, M. Orzáez, Caspase 3 Targeted Cargo Delivery in Apoptotic Cells Using Capped Mesoporous Silica Nanoparticles, Chemistry - A European Journal, 21 (2015) 15506-15510.
[20] R. Qian, L. Ding, H. Ju, Switchable Fluorescent Imaging of Intracellular Telomerase Activity Using Telomerase-Responsive Mesoporous Silica Nanoparticle, Journal of the American Chemical Society, 135 (2013) 13282-13285.

[21] J.S. Beck, J.C. Vartuli, W.J. Roth, M.E. Leonowicz, C.T. Kresge, K.D. Schmitt, C.T.W. Chu, D.H. Olson, E.W. Sheppard, S.B. McCullen, J.B. Higgins, J.L. Schlenker, A new family of mesoporous molecular sieves prepared with liquid crystal templates, Journal of the American Chemical Society, 114 (1992) 10834-10843.
[22] G. Kickelbick, Hybrid Inorganic–Organic Mesoporous Materials, Angewandte Chemie International Edition, 43 (2004) 3102-3104.
[23] D. Tarn, C.E. Ashley, M. Xue, E.C. Carnes, J.I. Zink, C.J. Brinker, Mesoporous Silica Nanoparticle Nanocarriers: Biofunctionality and Biocompatibility, Accounts of Chemical Research, 46 (2013) 792-801.
[24] C. Argyo, V. Weiss, C. Bräuchle, T. Bein, Multifunctional Mesoporous Silica Nanoparticles as a Universal Platform for Drug Delivery, Chemistry of Materials, 26 (2014) 435-451.
[25] D. Peer, J.M. Karp, S. Hong, O.C. Farokhzad, R. Margalit, R. Langer, Nanocarriers as an emerging platform for cancer therapy, Nature Nanotechnology, 2 (2007) 751-760.
[26] R.A. Petros, J.M. DeSimone, Strategies in the design of nanoparticles for therapeutic applications, Nat Rev Drug Discov, 9 (2010) 615-627.
[27] V. Wagner, A. Dullaart, A.K. Bock, A. Zweck, The emerging nanomedicine landscape, Nature Biotechnology, 24 (2006) 1211-1217.
[28] F. Sancenón, L. Pascual, M. Oroval, E. Aznar, R. Martínez-Máñez, Gated Silica Mesoporous Materials in Sensing Applications, ChemistryOpen, 4 (2015) 418-437.
[29] K.H. Chen, D.J. Lundy, E.K.W. Toh, C.H. Chen, C. Shih, P. Chen, H.C. Chang, J.J. Lai, P.S. Stayton, A.S. Hoffman, P.C.H. Hsieh, Nanoparticle distribution during systemic inflammation is size-dependent and organ-specific, Nanoscale, 7 (2015) 15863-15872.
[30] N.K. Jain, V. Mishra, N.K. Mehra, Targeted drug delivery to macrophages, Expert Opinion on Drug Delivery, 10 (2013) 353-367.
[31] O.M. Koo, I. Rubinstein, H. Onyuksel, Role of nanotechnology in targeted drug delivery and imaging: a concise review, Nanomedicine: Nanotechnology, Biology and Medicine, 1 (2005) 193-212.
[32] S.P. Vyas, M.E. Kannan, S. Jain, V. Mishra, P. Singh, Design of liposomal aerosols for improved delivery of rifampicin to alveolar macrophages, International Journal of Pharmaceutics, 269 (2004) 37-49.
[33] S. Chono, T. Tanino, T. Seki, K. Morimoto, Efficient drug targeting to rat alveolar macrophages by pulmonary administration of ciprofloxacin incorporated into mannosylated liposomes for treatment of respiratory intracellular parasitic infections, Journal of Controlled Release, 127 (2008) 50-58.
[34] M. Nahar, N.K. Jain, Preparation, Characterization and Evaluation of Targeting Potential of Amphotericin B-Loaded Engineered PLGA Nanoparticles, Pharmaceutical Research, 26 (2009) 2588-2598.
[35] R. Kalluru, F. Fenaroli, D. Westmoreland, L. Ulanova, A. Maleki, N. Roos, M. Paulsen Madsen, G. Koster, W. Egge-Jacobsen, S. Wilson, H. Roberg-Larsen, G.K. Khuller, A. Singh, B. Nyström, G. Griffiths, Poly(lactide-co-glycolide)-rifampicin nanoparticles efficiently clear Mycobacterium bovis BCG infection in macrophages and remain membrane-bound in phago-lysosomes, Journal of Cell Science, 126 (2013) 3043-3054.

[36] J. Pruthi, N.K. Mehra, N.K. Jain, Macrophages targeting of amphotericin B through mannosylated multiwalled carbon nanotubes, Journal of Drug Targeting, 20 (2012) 593-604.
[37] V.K. Prajapati, K. Awasthi, S. Gautam, T.P. Yadav, M. Rai, O.N. Srivastava, S. Sundar, Targeted killing of Leishmania donovani in vivo and in vitro with amphotericin B attached to functionalized carbon nanotubes, Journal of Antimicrobial Chemotherapy, 66 (2011) 874-879.
[38] D.L. Clemens, B.-Y. Lee, M. Xue, C.R. Thomas, H. Meng, D. Ferris, A.E. Nel, J.I. Zink, M.A. Horwitz, Targeted Intracellular Delivery of Antituberculosis Drugs to Mycobacterium tuberculosis-Infected Macrophages via Functionalized Mesoporous Silica Nanoparticles, Antimicrobial Agents and Chemotherapy, 56 (2012) 2535-2545.
[39] J. Xie, D. Xiao, J. Zhao, N. Hu, Q. Bao, L. Jiang, L. Yu, Mesoporous Silica Particles as a Multifunctional Delivery System for Pain Relief in Experimental Neuropathy, Advanced Healthcare Materials, (2016) n/a-n/a.
[40] F. Krombach, S. Münzing, A.M. Allmeling, J.T. Gerlach, J. Behr, M. Dörger, Cell size of alveolar macrophages: an interspecies comparison, Environmental Health Perspectives, 105 (1997) 1261-1263.
[41] P.J. Murray, T.A. Wynn, Protective and pathogenic functions of macrophage subsets, Nat Rev Immunol, 11 (2011) 723-737.
[42] R. Medzhitov, C.A. Janeway Jr, Innate Immunity: The Virtues of a Nonclonal System of Recognition, Cell, 91 (1997) 295-298.
[43] M. Keller, A. Rüegg, S. Werner, H.-D. Beer, Active Caspase-1 Is a Regulator of Unconventional Protein Secretion, Cell, 132 (2008) 818-831.
[44] F. Martinon, K. Burns, J. Tschopp, The Inflammasome: A Molecular Platform Triggering Activation of Inflammatory Caspases and Processing of proIL-β, Molecular Cell, 10 (2002) 417-426.
[45] K. Schroder, J. Tschopp, The Inflammasomes, Cell, 140 (2010) 821-832.
[46] T. Bergsbaken, S.L. Fink, B.T. Cookson, Pyroptosis: host cell death and inflammation, Nat Rev Micro, 7 (2009) 99-109.
[47] S.L. Fink, B.T. Cookson, Caspase-1-dependent pore formation during pyroptosis leads to osmotic lysis of infected host macrophages, Cellular Microbiology, 8 (2006) 1812-1825.
[48] T. Strowig, J. Henao-Mejia, E. Elinav, R. Flavell, Inflammasomes in health and disease, Nature, 481 (2012) 278-286.
[49] W. Wannamaker, R. Davies, M. Namchuk, J. Pollard, P. Ford, G. Ku, C. Decker, P. Charifson, P. Weber, U.A. Germann, K. Kuida, J.C.R. Randle, (S)-1-((S)-2-{[1-(4-Amino-3-chloro-phenyl)-methanoyl]-amino}-3,3-dimethyl-butanoyl)-pyrrolidine-2-carboxylic acid ((2R,3S)-2-ethoxy-5-oxo-tetrahydro-furan-3-yl)-amide (VX-765), an Orally Available Selective Interleukin (IL)-Converting Enzyme/Caspase-1 Inhibitor, Exhibits Potent Anti-Inflammatory Activities by Inhibiting the Release of IL-1β and IL-18, Journal of Pharmacology and Experimental Therapeutics, 321 (2007) 509-516.
[50] J.H. Stack, K. Beaumont, P.D. Larsen, K.S. Straley, G.W. Henkel, J.C.R. Randle, H.M. Hoffman, IL-Converting Enzyme/Caspase-1 Inhibitor VX-765 Blocks the Hypersensitive Response to an Inflammatory Stimulus in Monocytes from Familial Cold Autoinflammatory Syndrome Patients, The Journal of Immunology, 175 (2005) 2630-2634.
[51] C. Jakobs, E. Bartok, A. Kubarenko, F. Bauernfeind, V. Hornung, Immunoblotting for Active Caspase-1, in: M.C. De Nardo, E. Latz (Eds.) The Inflammasome: Methods and Protocols, Humana Press, Totowa, NJ, 2013, pp. 103-115.

[52] D.B. Duarte, M.R. Vasko, J.C. Fehrenbacher, Models of Inflammation: Carrageenan Air Pouch, in: Current Protocols in Pharmacology, John Wiley & Sons, Inc., 2001.
[53] V. Escrig, A. Ubeda, M.L. Ferrandiz, J. Darias, J.M. Sanchez, M.J. Alcaraz, M. Paya, Variabilin: A Dual Inhibitor of Human Secretory and Cytosolic Phospholipase A2 With Anti-inflammatory Activity, Journal of Pharmacology and Experimental Therapeutics, 282 (1997) 123-131.
[54] A. Araico, M.C. Terencio, M.J. Alcaraz, J.N. Domínguez, C. León, M.L. Ferrándiz, Evaluation of the anti-inflammatory and analgesic activity of Me-UCH9, a dual cyclooxygenase-2/5-lipoxygenase inhibitor, Life Sciences, 80 (2007) 2108-2117.
[55] L. Mondragón, N. Mas, V. Ferragud, C. De La Torre, A. Agostini, R. Martínez-Máñez, F. Sancenón, P. Amorós, E. Pérez-Payá, M. Orzáez, Enzyme-responsive intracellular-controlled release using silica mesoporous nanoparticles capped with ε-poly- L -lysine, Chemistry - A European Journal, 20 (2014) 5271-5281.
[56] C. Thomas, M.B. Boxer, Caspase inhibitors, in, Google Patents, 2011.

3.7 Supporting Information

Kinetic measurements of ε-poly-L-lysine hydrolysis

To determine the crucial role played by the enzyme in the release mechanism, 1 mg of solid **S1-P** was suspended in 1 ml of water at pH 8.0 in the absence and in the presence of pronase enzyme (0.12 mg/ml) from *Streptomyces Griseus*, respectively. Suspensions were stirred at 37°C. At certain time aliquots were separated and centrifuged to eliminate the solid. Drug delivery was monitored by analytical RP-HPLC with a UV detector using a mobile phase of CH_3CN-H_2O mixtures that contained 0.1% TFA at 1 ml/min. Generated lysine was monitored at 220 nm.HPLC measurements showed the presence of lysine in the aliquots, pointing toward a pronase-induced poly(lysine) hydrolysis as mechanism that governed rhodamine B release (see Figure S1).

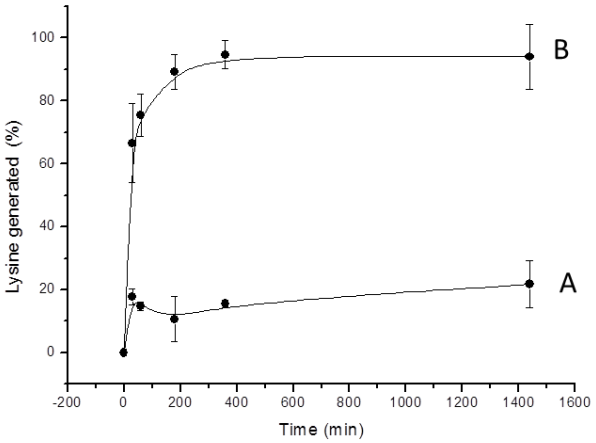

Fig. S1. Enzyme-responsive lysine generated form solid **S1-P**: (A) in the absence and (B) in the presence of pronase in water at pH=8.

Cellular uptake of FITC-MSNs in THP-1 cells

In order to corroborate that the observed **S1-P** internalization was assessed to the nanoparticles and not only to the rhodamine B release a solid covalently labelled with fluorescein isothiocyanate (FITC) was prepared (FITC-MSNs). For this purpose, to graft FITC onto mesoporous silica nanoparticles, 2 mg of FITC were covalently linked to 20 µl of (3-aminopropyl)triethoxysilane (APTES) in 2 ml of anhydrous ethanol. The mixture was stirred in the dark overnight at room temperature. Then, 20 mg of MCM-41 nanoparticles were dispersed in 5 ml of anhydrous ethanol and then 500 µl of FITC/APTES mixture was added. The suspension was maintained in dark for 24 h at room temperature. Finally the nanoparticles were washed and dried yielding the FITC-MSNs.

The cellular uptake studies were performed seeding THP-1 cells in a 6 well-plate and treated with FITC-MSNs at the 0 (control), and 50 µg/ml concentrations (in PBS) for 2 h. Then cells were washed with PBS and quantification of fluorescein was performed by flow cytometry and analyzed using version 2.9 of the WinMDI program (Fig S2.A). Confocal microscopy internalization experiments were performed by means of fluorescein associated fluorescence using a Leica TCS SP2 confocal microscope (Fig. S2.B).

Flow cytometry studies demonstrated that around 50% of the cellular population internalized FITC-MSNs after 2 h of treatment (Fig. S2.A). Moreover, confocal studies were carried out to ensure the internalization in addition to the **S1-P** uptake studies. The cellular uptake of the solid in this case was monitored by FITC associated fluorescence, as could be observed in figure S2.B. After the treatment with FITC-MSNs before 2 h, an appreciable presence of fluorescein (in green) associated to the prepared nanoparticles. These studies demonstrated that the observed rhodamine B fluorescence in cellular uptake studies performed (Fig.

5C and D in the manuscript) was associated to the presence of the nanoparticles, and thus that nanoparticle were endocytosed by THP-1 cells.

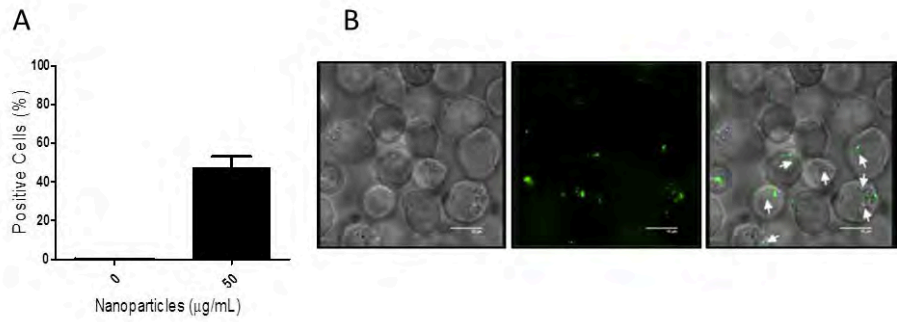

Fig. S2. A) Percentage of fluorescent cells analyzed by flow cytometry in internalization studies with FITC-MSNs and D) FITC-MSNs uptake (in green) by THP-1 cells analyzed by confocal images.

Activation of caspase-1

To confirm that in the air pouch in vivo model of inflammation, release of IL-1β was dependent of the inflammasome, we have studied caspase-1 activation, through the treatment or not with the LPS stimulus, in the collected animal exudates of the air pouch by western blot analysis.

The activation of the inflammasome component caspase-1 was demonstrated in the air pouch model. As we observed in the figure S3, the LPS administration resulted in the formation of the inflamasome and caspase-1 activation. Whereas in untreated mice the activation was not observed. Caspase-1 is a constituent of the inflammasome and, as far as we know, inflammasome-independent modes of caspase-1 activation have not been yet described [1]. Due to caspase-1 triggers the maturation of pro-inflammatory cytokines IL-1β and IL-18, and their easier

detection; the effect on our target, inflammasome activity, was studied through onto the levels of these cytokines.

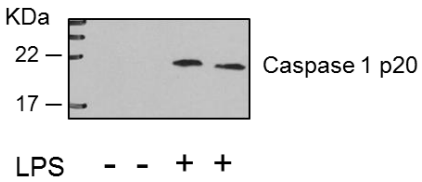

Fig. S3. Activation of caspase-1 in the exudates of LPS-treated mice. Protein from mice exudates was precipitated and the presence of active caspase-1 (p20) was analyzed by western blotting in untreated or LPS treated mice.

References

[1] L. Franchi, T. Eigenbrod, R. Munoz-Planillo, G. Nunez, The inflammasome: a caspase-1 activation platform that regulates immune responses and disease pathogenesis, Nat Immunol, 10 (2009) 241-247 .

Chapter 4 | Targeted-lung delivery of glucocorticoids for acute lung injury

Targeted-lung delivery of glucocorticoids using gated mesoporous silica nanoparticles. A new therapeutic approach for acute lung injury treatment

Alba García-Fernández,[1,3,5] Mónica Sancho,[5,6] Viviana Bisbal-Velasco[6], Ramón Martínez-Máñez,[1,2,3,4,5]* Mar Orzáez,[5,6] and Félix Sancenón[1,2,3,4,5]

[1] Instituto Interuniversitario de Investigación de Reconocimiento Molecular y Desarrollo Tecnológico (IDM), Universitat Politècnica de València, Universitat de València, Spain. E-mail: rmaez@qim.es

[2] Departamento de Química, Universitat Politècnica de València, Camino de Vera s/n, 46022 Valencia, Spain.

[3] CIBER de Bioingeniería, Biomateriales y Nanomedicina (CIBER-BBN).

[4] Unidad Mixta de Investigación en Nanomedicina y Sensores. Universitat Politècnica de València, IIS La Fe, Valencia, Spain

[5] Unidad Mixta UPV-CIPF de Investigación en Mecanismos de Enfermedades y Nanomedicina, Valencia, Universitat Politècnica de València, Centro de Investigación Príncipe Felipe, València, Spain.

[6] Centro de Investigación Príncipe Felipe. Eduardo Primo Yúfera, 3. Valencia 46012, Spain.

Submitted

4.1 Abstract

Acute lung injury (ALI) is a critical inflammatory syndrome, characterized by increased diffuse inflammation and severe lung damage, which represent a clinical concern due to the high morbility and mortality in critical patients. In last years, the need in development of more effective treatments to ALI has arisen, and targeted drug delivery to inflamed lungs has become an attractive research field. Here, we present two nanodevices based on mesoporous silica nanoparticles loaded with rhodamine B or with dexamethasone (a glucocorticoid extensively used for ALI treatment) and capped with a peptide that targets the TNFR1 receptor expressed in pro-inflammatory macrophages (solids **TNFR-RhB-MSNs** and **TNFR-Dex-MSNs**). **TNFR-RhB-MSNs** suspended in PBS shows negligible rhodamine B release, whereas cargo delivery is observed when suspended in lysosomal extract due to the enzymatic hydrolysis of the capping peptide. **TNFR-RhB-MSNs** is preferentially internalized by THP-1 and pro-inflammatory M1 macrophages which overexpressed TNFR1 receptor. Moreover, **TNFR-Dex-MSNs** are able to reduce the levels of TNF-α and IL-1β cytokines in activated pro-inflammatory M1 macrophages. The anti-inflammatory effect of **TNFR-Dex-MSNs** is also tested in an *in vivo* ALI mice model. The administered nanodevice accumulated in the injured lungs and the controlled dexamethasone release reduces markedly the inflammatory response (TNF-α IL-6 and IL-1β levels). The attenuation in lung damage, after treatment with **TNFR-Dex-MSNs**, is also confirmed by histopathological studies. These results suggest that **TNFR-Dex-MSNs** could potentially be used for the treatment in ALI and could help to overcome the clinical limitations of current treatments.

4.2 Introduction

Acute lung injury (ALI) is a severe inflammatory disease, main cause of morbility and mortality in critical patients in which acute diffuse inflammation develops as well as alterations in lung function and structure, resulting in many cases in a severe respiratory failure.[1–3] ALI is characterized, especially in the early stages, for an increase in lung permeability leading to interstitial and alveolar edema with the subsequent formation and accumulation of alveolar hyaline membranes.[4,5] The inflammatory response is also activated and multiple inflammatory cytokines (TNF-α, IL-6, IL-1β, etc.) are released in concert with neutrophil influx to the alveolar space of injured lung.[6–8] The advances in the understanding of pathophysiology of ALI have led to the development of numerous pharmacological treatments.[9] However, clinical trials revealed that these are not as effective as expected, mainly limited to the difficulty of the drugs to reach the injured lungs.[10,11] Thus, there is a real interest for the development of more effective treatments for ALI and the preparation of systems for the direct delivery of drugs in lung has become an active research area.[12,13]

In this scenario, several nanotechnological-based strategies to specifically delivery drugs in lungs based on the use of lipids, organic polymers, nanogels and inorganic nanoparticles have been developed in the last years.[14–20] Among different nanoparticles, mesoporous silica nanoparticles (MSNs) are excellent candidates as scaffold for drug storage and on-command delivery due to the possibility of decorate their external surface with (supra)molecular or biomolecular entities (gating ensembles), which controlled cargo release upon application of an external stimuli.[21–23] This is a clear advantage, when compared with nanodevices constructed using liposomes and polymeric carriers, which usually release their cargo by carrier-degradation or diffusion-controlled processes.[24,25] Besides, MSNs also possess several remarkable features such as

high surface area, homogenous and tuneable pore size, easy functionalization, good biocompatibility, prolonged retention time and physiological stability.[26–29] In fact, gated MSNs have been successfully used in several applications and their capability to improve the availability and pharmacokinetics of encapsulated drugs, reducing undesired side effects, has been demonstrated in *in vivo* models.[30–36]

Regarding ALI, MSNs could be suitable nanocarriers to direct drug delivery for the treatment of ALI due to their preferential accumulation on lungs as well as to inflamed tissue.[37–39] It has been widely demonstrated that the vascular nature, high permeability and retention capacity of the lungs facilitate the preferential accumulation of MSNs.[40–45] This preferential accumulation is ascribed to a passive targeting called ELVIS mechanism (Extravasation through Leaky Vasculature and Inflammatory cell-mediated Sequestration) that can be exploited for the treatment of inflammatory diseases.[46,47] In addition to passive targeting, an active targeting strategy can also be used to make the nanoparticles more specific to the target site. In relation to acute lung injury, one common approach is to target the inflamed endothelium in lungs. In this scenario, some studies described the use of lipid carriers or polymers modified with antibodies to target the pulmonary vascular-endothelium by targeting ICAM (intercellular adhesion molecule 1) receptor.[48–50] Moreover, some recent approaches to deal with ALI have focoused on the use of antibodies, in the absence of nanoparticles, against the CD64 (Fc ϒ receptor I) or tumour necrosis factor receptor (TNFR) which are overexpressed in pro-inflammatory macrophages.[51–54]

On the other hand, glucocorticosteroids (GCs), as strong anti-inflammatory drugs, are widely used to ameliorate ALI clinical symptoms by limiting tissue injury and acute inflammatory response.[55,56] Among GCs, dexamethasone (Dex) is one of the most used for ALI treatment and its administration induces a decrease of the pro-inflammatory cytokines, a reversal in lung tissue injury and a reduction in the

pulmonary edema.[57,58] However, despite the potent therapeutic effect of Dex and the improvement of ALI outcome, its use remains a serious concern due to their undesired side-effects attributed to its broad spectrum of action.[59,60] In order to overcome these drawbacks efficient GCs delivery strategies using appropriate vehicles have been described in numerous inflammatory diseases.[61–65] However, focusing on the treatment of ALI, only two reports described the encapsulation of Dex and efficient lung delivery in acute lung injury model using lipid nanocarriers.[66,67]

Based on the above, we report herein the preparation of lung-targeted drug delivery nanodevice (**TNFR-Dex-MSNs**) for the treatment of ALI. The nanodevice consists of MSNs loaded with RhB or Dex and capped with a peptide containing the binding sequence to the tumour necrosis factor receptor 1 (TNFR1)[68] which is expressed in pro-inflammatory macrophages and is involved in the progress of the inflammatory response. The nanodevice is designed to take advantage of the MSNs intrinsic passive targeting to inflammation and lungs in combination with an active targeting to TNFR. Here, we demonstrate the activity of **TNFR-Dex-MSNs** nanodevice *in vitro* in inflammatory macrophages and *in vivo* in an ALI mice model, confirming lung targeting and anti-inflammatory effect. While different nanomaterials have been developed for GCs encapsulation and ALI treatment independently, only few nanocarriers have been used for GCs delivery in ALI. Moreover, and as far as we know, our report herein describes the first use of MSNs as drug delivery system in an acute lung injury model.

4.3 Results and discussion

Design, synthesis and characterization of TNFR-gated nanodevices

For the synthesis of the **TNFR-gated** nanodevices MSNs were selected as inorganic scaffold. The pores were loaded with rhodamine B or dexamethasone and the external surface functionalised with isocyanatopropyl moieties (solids **NCO-RhB-MSNs** and **NCO-Dex-MSNs**). Then, the TNFR1 peptide (GGGGFIGLMYRYQRWKSKLY) was anchored onto the external surface of the silica nanoparticles, through the formation of urea bonds, yielding the **TNFR-RhB-MSNs** and **TNFR-Dex-MSNs** nanoparticles. An illustration showing the structure of the nanodevices is depicted in Scheme 1A. The nanoparticles are expected to be endocytosed in pro-inflammatory macrophages through a TNFR1 mediated endocytosis and deliver the cargo (i.e. rhodamine B or dexamethasone) due to degradation of the capping ensemble in the endocytic compartment (Scheme 1B). Besides, in order to evaluate the targeting ability of TNFR1 peptide-functionalised nanoparticles, a similar nanodevice loaded with rhodamine B but capped with a random peptide sequence (i.e. KKRSLFGSLLVVGAVTMGTLFWRKK), unable to bind with TNFR1 receptor, was also prepared (**Random-RhB-MSNs**).

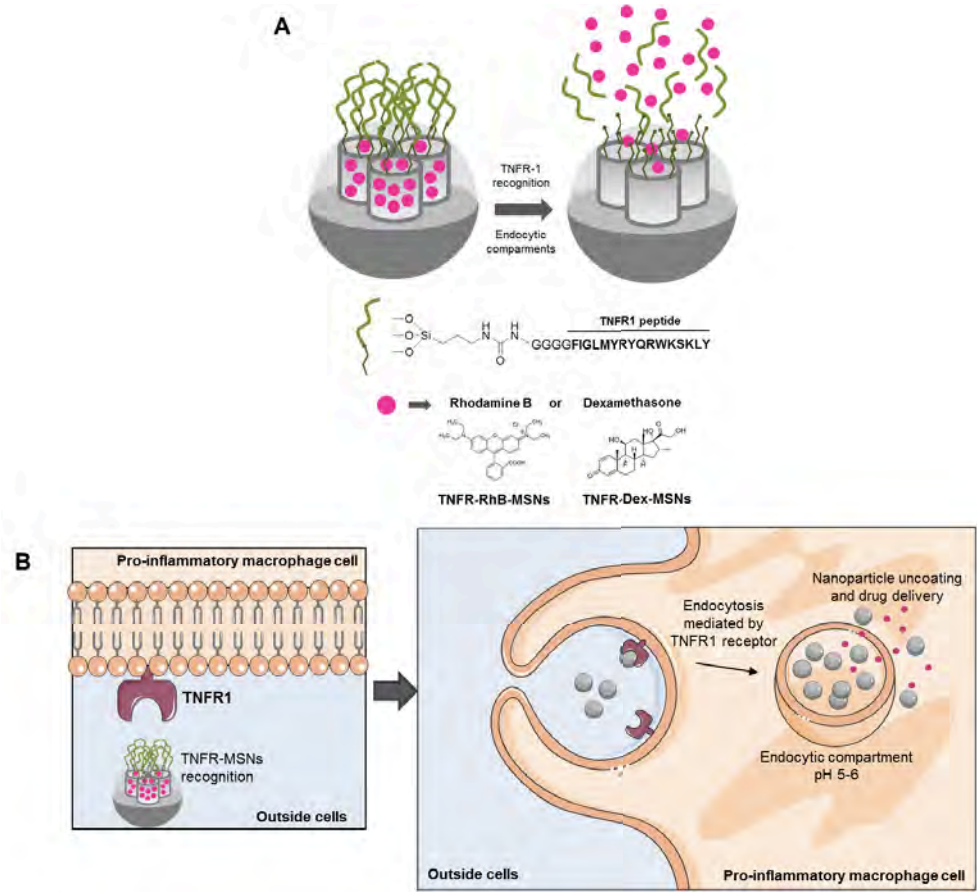

Scheme 1. Illustration of the TNFR-MSNs nanodevices. A) Representation of the designed TNFR-gated nanodevices. MSNs were loaded with rhodamine B or with dexamethasone, functionalized with (3-isocyantopropyl)triethoxysilane and capped with a peptide which recognized TNFR1 in macrophages. B) Schematic representation of TNFR1 mediated endocytosis of the nanodevices and subsequent controlled drug delivery in pro-inflammatory macrophages.

The prepared nanoparticles were characterized by power X-ray diffraction (PXRD), TEM, N_2 adsorption-desorption curves, dynamic light scattering and zeta potential. The PXRD patterns of the starting MSNs showed low angle reflexions

typical of mesoporous materials with a hexagonal order (see Supporting Information) which is preserved in the nanoparticles **NCO-RhB-MSNs** and **TFNR-RhB-MSNs.** TEM images of the starting MSNs (Figure 1A) show the nanoparticles as spheres of ca. 100 nm and the mesopores as alternate black and white channels. The same morphology was also observed in the final and intermediate solids. N_2 adsorption-desorption isotherms of the starting MSNs showed a type IV isotherm, typical of the mesoporous silica materials and a BET specific surface area of 1167 m^2/g. In contrast N_2 adsorption-desorption isotherm of the final nanodevice **TNFR-RhB-MSNs** was typical of mesoporous systems with partially filled mesopores with reduced specific surface areas (Table 1 and Supporting Information).

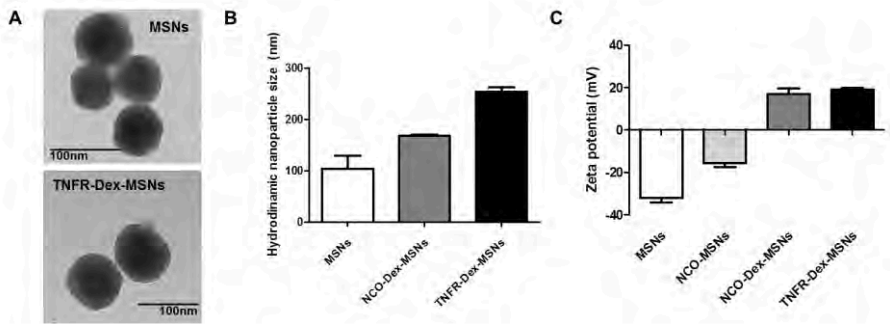

Figure 1. Nanomaterials characterization. A) Representative images from TEM from MSNs and **TNFR-Dex-MSNs** B) Hydrodynamic size distribution determined by dynamic light scattering for MSNs, **NCO-Dex-MSNs** and **TNFR-Dex-MSNs**; C) Zeta potential for MSNs, **NCO-Dex-MSNs** and **TNFR-Dex-MSNs**.

Table 1. Textural properties of calcined MSNs and TNFR-RhB-MSNs.

Solid	BET (m^2/g)	Pore Volume (cm^3/g)	Pore size (nm)
MSNs	1167	0.96	2.55
TNFR-RhB-MSNs	480	0.23	2.50

We also monitored the preparation process by zeta pontential and hydrodynamic diameter using dynamic light scattering (DLS). Zeta potential changed from -32 ± 3mV for the starting **MSNs** to 19 ± 1mV for the final **TNFR-Dex-MSNs** solid loaded with dexamethasone and capped with the targeting peptide, with and additional value of 17 ± 4mV for the intermediate NCO-Dex-MSNs (Figure 1C). Moreover, the hydrodynamic diameter increased after each preparation step (103 ± 25, 168 ± 4 and 253 ± 12 nm for MSNs, NCO-Dex-MSNs and TNFR-Dex-MSNs, respectively) (Figure 1B). A single population distribution was observed for all nanoparticles suggesting the particles were not aggregated, even after the loading and capping process with the targeting peptide.

Moreover, the amount of Dex (340 μg/mg SiO_2, 0.86 mmol/g SiO_2) and TNFR peptide (0.05 mmol/g SiO_2) in **TNFR-Dex-MSNs** solid were determined by thermogravimetric analysis and HPLC measurements. The same techniques were used to determine rhodamine B (0.16 mmol/g SiO_2) and TNFR peptide (0.04 mmol/g SiO_2) in **TNFR-RhB-MSNs**.

Controlled release and cytotocicity studies

In order to study the gating ability of the capping peptide, payload delivery from **TNFR-RhB-MSNs** was studied in PBS at pH 7.4 (mimicking physiological conditions) and in lysosomal extract at mildly acidic conditions (pH in the 5.0-6.0 interval simulating the endocytic compartments). PBS suspension of **TNFR-RhB-**

MSNs at pH 7.4 showed negligible rhodamine B release (Figure 2). However, a marked delivery was observed when the nanodevice was suspended in lysosomal extract reaching ca. 80% of the maximum rhodamine B delivery after 60 min. The observed release is attributed to the action of lysosomal enzymes that hydrolysed the TNFR capping peptide.

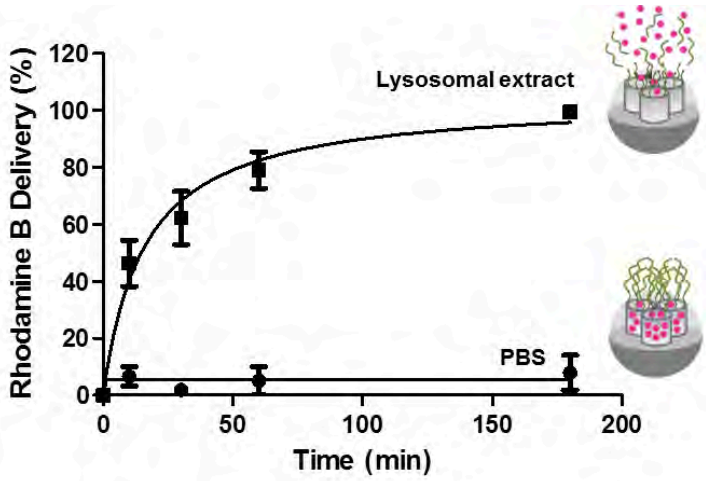

Figure 2. Drug delivery studies. Release profiles of rhodamine B from **TNFR-RhB-MSNs** in PBS at pH 7.4 (bottom) and in lysosomal extract at pH 5.0-6.0 (up). Data represent the means ± SD of at least three independent experiments.

Once assessed the gating ability of the TNFR peptide, the biocompatibility of the nanodevices was determined. For this purpose, cell viability studies in the presence of **TNFR-RhB-MSNs** at different concentrations were performed in THP-1 monocytes and A549 epithelial lung cells (Figures 3A and 3C). After 24 h of treatment, cell viability was kept in all cases up to 80% even at the highest **TNFR-RhB-MSNs** concentrations (150 µg/mL).

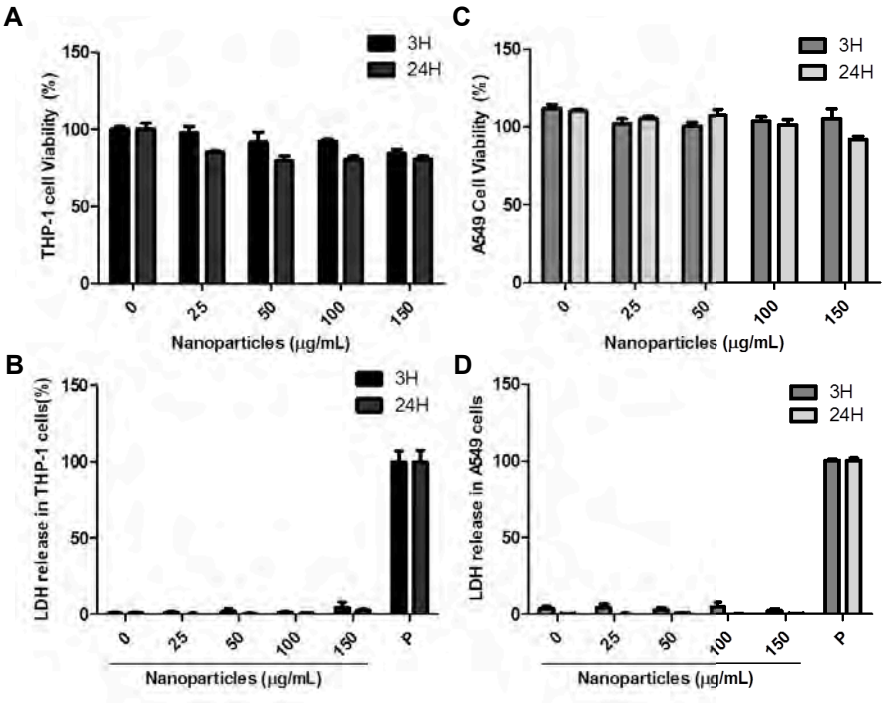

Figure 3. Cytotoxicity profile of TNFR-MSNs in THP-1 cells and A549 lung cells. A) THP-1 cell viability and B) LDH release in THP-1 cells at different concentrations of nanoparticles at 3 h (black bars) and 24 h (dark grey bars). C) A549 cell viability and D) LDH release at 3 h (grey bars) and 24 h (light grey bars) in the presence of different nanoparticles dosages. P represents the positive control of lysate cells. Data represent the means ± SEM of at least three independent experiments.

In order to discard the non-desired pro-inflammatory activity of our nanodevices we studied the induction of inflammatory cell death by treatment with **TNFR-RhB-MSNs.** For this purpose the release of the intracellular lactate dehydrogenase (LDH) enzyme to the extracellular media was measured demonstrating that **TNFR-RhB-MSNs** were unable induce pro-inflammatory cell death neither in THP-1 monocytes nor in A549 lung cells(Figures 3B and 3D).

Targeted cellular uptake studies

As stated above, the nanoparticles are capped with a peptide designed to target the TNFR1 receptor in the inflammatory cells. The TNFR1 receptor is expressed both in THP-1 monocytes and pro-inflammatory M1 macrophages (Figure 4A). Then, cellular uptake of **TNFR-RhB-MSNs** in THP-1 monocytes and pro-inflammatory M1 macrophages, was studied by confocal microscopy (Figure 4A). In both cell lines, a clear increase in rhodamine B fluorescence signal was observed inside cells (see Figure 4B) after 4 h of treatment. Besides, the intensity of fluorescence observed in pro-inflammatory M1 macrophages treated with **TNFR-RhB-MSNs** was higher than that found for THP1 cells, which is tentatively attributed to the higher level of expression of TNFR1 in activated M1 macrophages.

In order to demonstrate the targeting ability of the capping peptide in **TNFR-RhB-MSNs**, similar cell internalization studies were performed with the nanoparticles capped with a random peptide (**Random-RhB-MSNs)**. In this case a weaker fluorescence emission signal of rhodamine B was observed both in THP-1 monocytes and pro-inflammatory M1 macrophages (Figure 4B). Flow cytometry experiments also confirmed preferential internalization of **TNFR-RhB-MSNs** in inflammatory cells, especially in M1 macrophages, when compared with the uptake of **Random-RhB-MSNs** (Figure 4C). These results demonstrate the targeting ability of **TNFR-RhB-MSNs** to inflammatory THP-1 and M1 macrophages due to the selective interaction between the capping TNFR peptide and the TNFR1 receptor in the cell membrane.

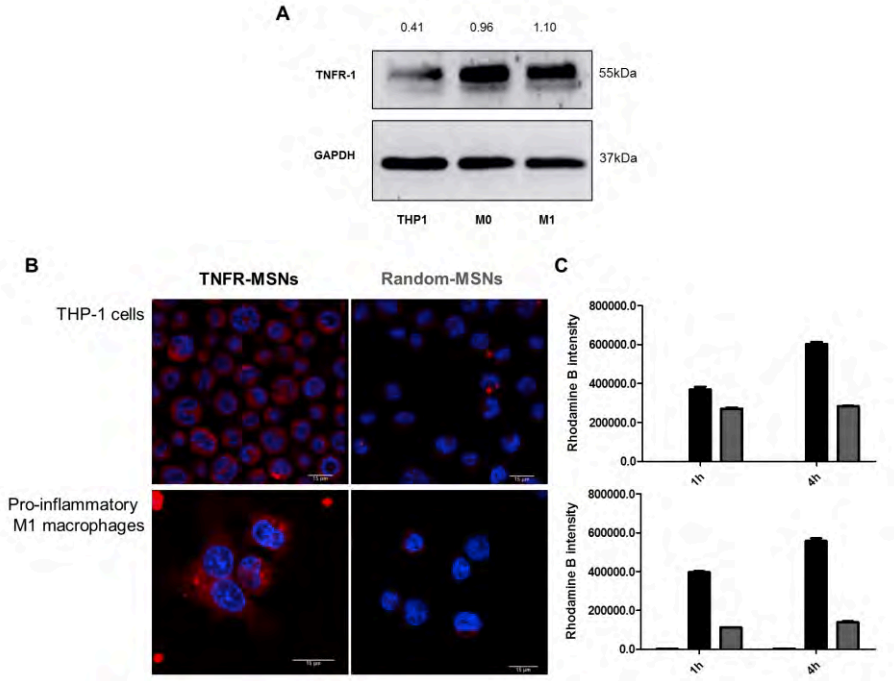

Figure 4. Targeting studies of TNFR-RhB-MSNsin inflammatory cells. A) Western blot analysis of TNFR1 expression in the different inflammatory cells; monocytes THP-1, non-differentiate M0 macrophages and pro-inflammatory M1 macrophages. B) Confocal images of nanoparticles uptake in THP-1 cells (up) and in pro-inflammatory M1 macrophages (below) in the presence of **TNFR-RhB-MSNs** (left) or **Random-RhB-MSNs** (right) after 4 h. Rhodamine B associated fluorescence in red and DNA Hoechst 33342 in blue. C) Fluorescence intensity of THP-1 cells (up) and pro-inflammatory M1 macrophages (below) analyzed by flow cytometry after **TNFR-RhB-MSNs** (black bars) or **Random-RhB-MSNs** (grey bars) treatment for 1 and 4 h. Data represent the means ± SEM of at least three independent experiments.

Anti-inflammatory activity of TNFR-Dex-MSNs in inflammatory cells

Once assessed the targeting ability of the nanodevices, we tested the use of **TNFR-Dex-MSNs** to modulate the inflammatory response. Dexamethasone is a potent immunosuppressant that reduces the release of TNF-alpha[69] and IL-1beta.[70] In order to analyse the anti-inflammatory activity of the nanodevices, the NLPR3 inflammasome was activated in pro-inflammatory M1 macrophages by treatment with LPS and nigericin. This treatment produces the release of the pro-inflammatory cytokines TNF-α and IL-1β (figure 5A and B). Under this conditions M1 macrophages were treated with **TNFR-RhB-MSNs** (as control, 2 μg/mL), **TNFR-Dex-MSNs** (2 μg/mL), and free dexamethasone (1 μM) and the levels of IL-1β and TNF-α measured by ELISA. A marked and similar reduction in IL-1β level was found when activated pro-inflammatory M1 macrophages were treated with **TNFR-Dex-MSNs** and free dexamethasone (Figure 5A and 5B) while as expected no changes were observed upon treatment with TNFR-RhB-MSNs. Along the same lines, IL-1β and TNF-α levels in stimulated THP-1 monocytes markedly diminished when treated with **TNFR-Dex-MSNs** nanoparticles and remained unchanged using **TNFR-RhB-MSNs** (see Supporting Information).

Upon treatment with LPS and nigericin caspase-1 is cleaved by the inflammasome and released to the media (Figure 5 D and E), contributing to inflammatory signal spreading. Interestingly, treatment with **TNFR-Dex-MSNs** and free dexamethasone produces a significant reduction in active caspase-1 in the cell supernatants (Figure 5E). Despite caspase-1 is not a direct target of dexamethasone treatment, its reduction could be related to TNF-α and IL-1β inhibition as this enzyme is involved in the production of pro-inflammatory cytokines and some of the responses of TNF-α are mediated by caspase-1.[71]

We also corroborated that **TNFR-RhB-MSNs**, **TNFR-Dex-MSNs** and free dexamethasone are unable to induce pro-inflammatory signalling and the

associated cell death by pyroptosis by themselves (Figure 5C) reinforcing the biocompatibility of the nanomaterials (*vide ante*).

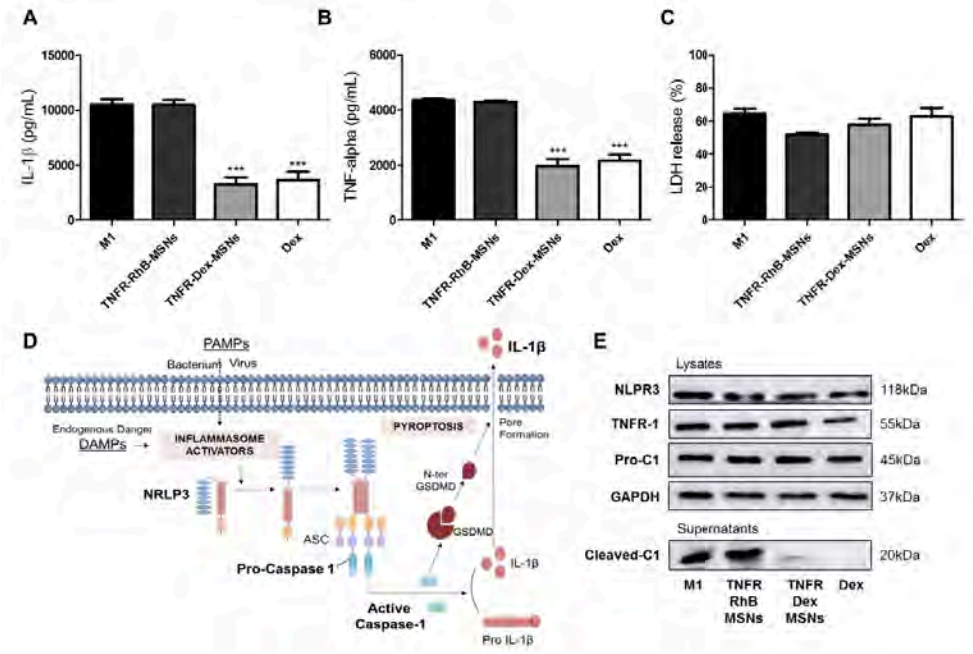

Figure 5. Analysis of inflammatory response in activated pro-inflammatory M1 macrophages in the presence of TNFR-Dex-MSNs. A) IL-1β and B) TNF-α cytokines levels from cell supernatants measured by ELISA. C) LDH release profile detected in cell supernatants as inflammatory cell death marker. D) Schematic representation of inflammasome activation pathway and the involved proteins. E) Western blot detection cleaved capase-1 measured in cell supernatants and NLPR3, TNFR1, pro-Caspase 1, detected in cell lysates using GAPDH as reference protein. Data represent the means ± SEM of at least three independent experiments. Statistical significance was determined using a one-way ANOVA.

Anti-inflammatory activity of TNFR-Dex-MSNs in acute lung injury model

Once confirmed the activity of **TNFR-Dex-MSNs** *in vitro*, we moved one step forward and tested the therapeutic efficiency of the nanodevice in an acute lung injury inflammatory mice model. The ALI model was developed by the intratracheally administration of LPS (2.5 mg/kg in saline) to CD-1 mice for 24h. Nanoparticles were intravenously administered by tail vein injection (25 mg/kg in PBS) to equivalent dose of 10 mg/kg of free dexamethasone. Moreover, **TNFR-RhB-MSNs** were also administered at 25 mg/kg as control in the presence and the absence of LPS. The inflammation in the ALI model for all groups was characterized by determining the amount of leukocytes and pro-inflammatory cytokines in bronchoalveolar fluid (BALF). Moreover, to determine the severity of lung injury, alterations in alveolar capillary barrier and histological evidence of tissue injury were also studied.

After LPS exposure, TNF-α, IL-6 and IL-1β were up-regulated in lungs as quantified in BALF by ELISA. As could be seen in Figure 6A, 6B and 6C high levels of cytokines were also observed in the LPS and LPS+**TNFR-RhB-MSNs** groups which are the evidence of the activation of a strong inflammatory response. Besides, negligible inflammatory effect was found when mice were treated only with **TNFR-RhB-MSNs** (Figures 6A, 6B and 6C) discarding any inflammatory adverse effect from the inorganic mesoporous scaffold. In contrast, the levels of TNF-α, IL-6 and IL-1β were significantly reduced in mice treated with LPS+**TNFR-Dex-MSNs** when compared to untreated LPS mice (Figure 6A, 6B, 6C light grey bars). Moreover, a higher effect in the reduction of pro-inflammatory interleukins was achieved in mice treated with **TNFR-Dex-MSNs** than in those treated with free dexamethasone at equivalent doses.

Moreover, a significant influx of leukocytes in BALF was found in the groups treated with LPS and LPS+**TNFR-RhB-MSNs** (Figure 6D) and ascribed to leukocytes migration to the lungs in response to the inflammatory stimuli. As clear contrast, after **TNFR-Dex-MSNs** treatment a marked 5.5-fold reduction in the total amount of leukocytes was observed when compared with LPS-treated mice. Besides, the reduction in leukocytes observed when mice were treated with free dexamethasone (3.5-fold) was smaller, pointing out to a higher therapeutic effect of the nanodevice when compared with the free drug. Changes in lung permeability were studied determining the total protein concentration in BALF. The accumulation of protein in BALF is correlated with the increase in vascular permeability induced by inflammation. Protein concentration in BALF drastically increased when LPS was administered (Figure 6E), whereas levels of proteins decreased upon treatment with **TNFR-Dex-MSNs** or dexamethasone.

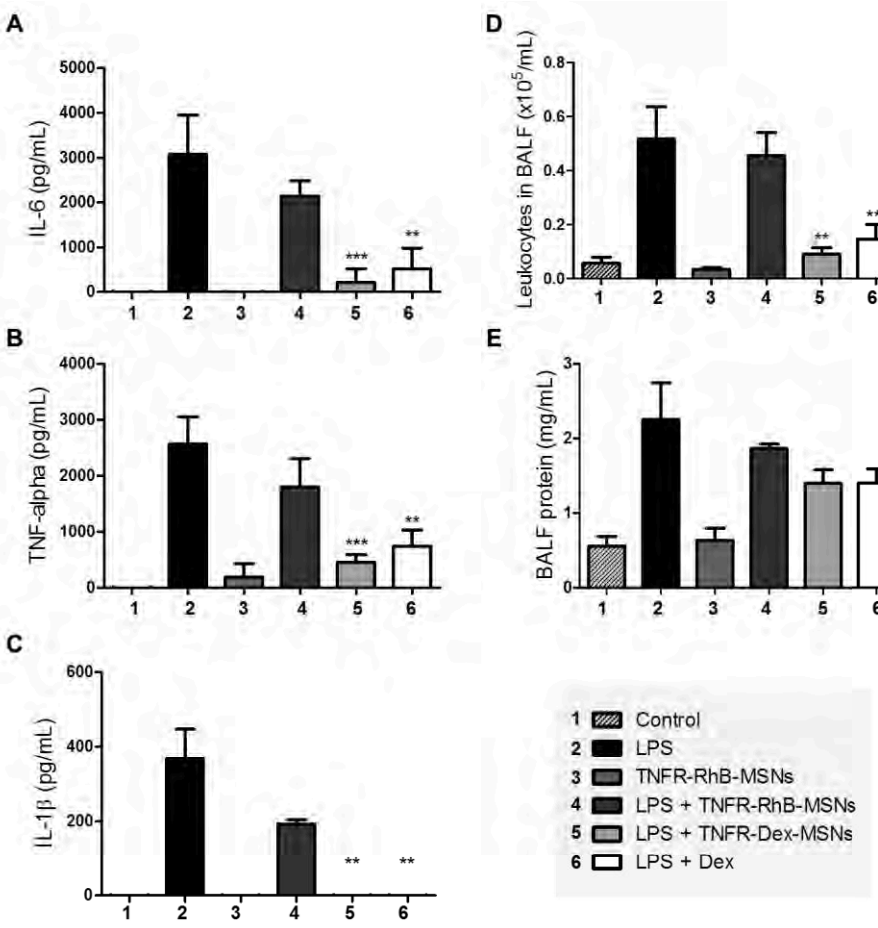

Figure 6. Evaluation of inflammatory response in BALF obtained from LPS-ALI mice. Levels of A) IL-6, B) TNF-α and C) IL-1β of pro-inflammatory cytokines in BALF measured by ELISA. D) Leukocytes account in BALF analysed by flow cytometry as indicator of inflammation focus. E) Total amount of protein in BALF, as lung permeability marker, measured by BCA assay. The data represent the mean ± SEM (n=6-8) and statistical significance was determined using a one-way ANOVA.

The severity in lung damage was studied by histology of tissues for all groups (Figure 7A). The most important hallmark of ALI is the diffuse alveolar damage in lung tissue characterized by: (i) neutrophil accumulation in vascular, interstitial

and alveolar spaces, (ii) the presence of hyaline membranes (proteins and dead cells) and other proteinaceous debris, and (iii) the interstitial thickening. Healthy lung section was composed by thin alveolar walls (control in Figure 7A) whereas LPS treated mice presented serious tissue injury (LPS and LPS+**TNFR-RhB-MSNs** groups) distinguished by remarkable congestion and disruption of the alveolar architecture. Despite some alteration in the lung architecture was observed with the administration of **TNFR-RhB-MSNs** (without LPS exposure), this alteration was very low when compared to LPS treated groups. On the other hand, dexamethasone and **TNFR-Dex-MSNs** administration remarkable attenuated lung injury (LPS+Dex and LPS+**TNFR-Dex-MSNs** in Figure 7A). In mice treated with LPS+**TNFR-Dex-MSNs** and LPS+Dex the pulmonary architecture is almost similar to control groups, despite the impairment in the alveolar walls attributed to LPS instillation. These results were also assessed following a standard scoring system (Figure 7B and supporting information for details). ALI score for groups 2 and 4 (i.e. LPS and LPS+ **TNFR-RhB-MSNs)** was in the 0.7-0.8 interval indicating a strong lung injury, whereas mice treated with free dexamethasone of **TNFR-Dex-MSNs** (groups 5 and 6) showed a marked reduction of the ALI score (ca. 0.4) indicative of a noticeable decrease of lung injury.

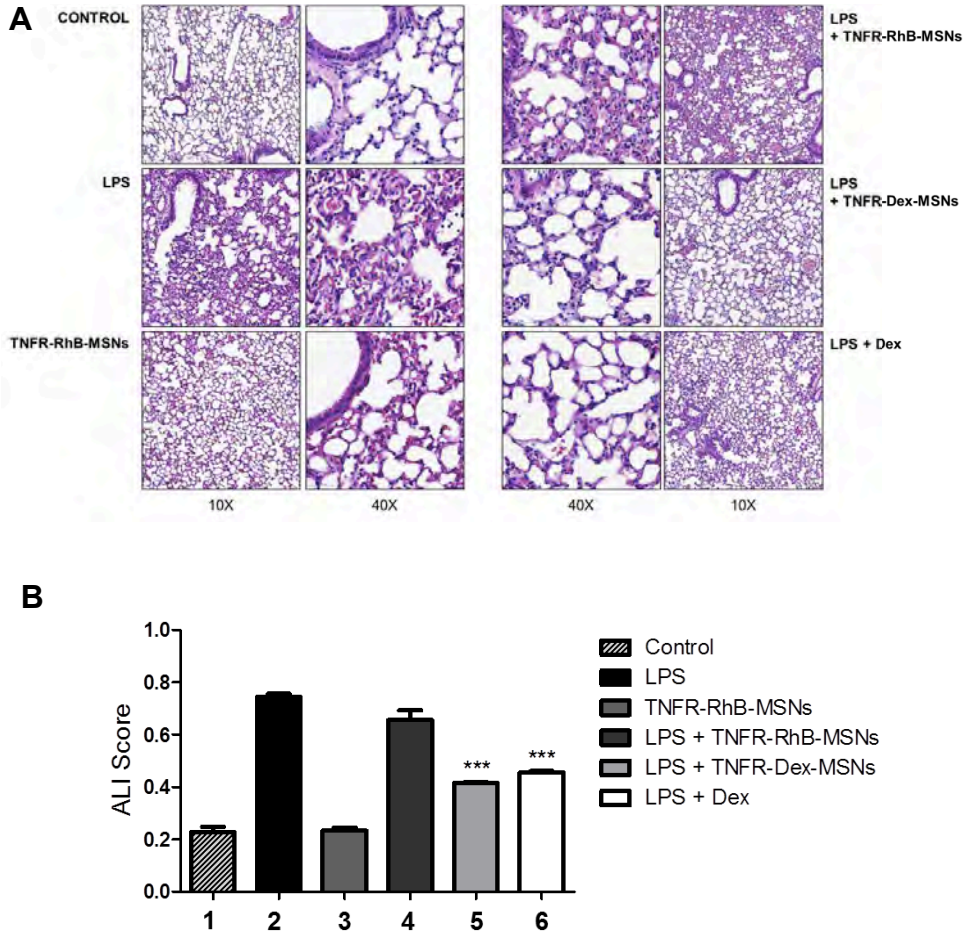

Figure 7. Histopathological examination of lungs. A) Representative images of H&E stain of lung tissue from mice at different zoom amplitudes and with the different treatments. B) Histological assessment of the acute lung injury determined by ALI score for groups 1-6. The data represent the mean ± SEM (n=4-6) and statistical significance was determined using a one-way ANOVA.

TNFR-MSNs biodistribution in ALI mouse model

To evaluate the targeting effect of **TNFR-RhB-MSNs** nanoparticles to inflamed lungs, rhodamine B emission after 24 h of treatment in mice instilled or not with LPS was evaluated. Lungs were collected and visualized by fluorescence optical imaging using an IVIS Spectrum (Figure 8). A remarkable fluorescent signal attributed to rhodamine B presence was registered in the case of inflamed lungs treated with **TNFR-RhB-MSNs**. In contrast, lungs treated with LPS or with **TNFR-RhB-MSNs** alone showed negligible fluorescence. The rhodamine B emission was also quantified using the Living Image software (Figure 8B). As could be seen, the highest rhodamine B fluorescence was obtained for individuals treated with LPS+ **TNFR-RhB-MSNs** when compared with the other groups in which a weak fluorescence was detected. These results indicate the targeting effect of **TNFR-RhB-MSNs** and cargo delivery to inflamed lungs in an acute lung injury mice model.

Finally, a biodistribution study was performed by measuring the levels of silicon in lungs and other selected organs (kidney, liver, spleen, tail) for all six groups after 24h upon treatment. A silicon pattern was clearly identified in individuals treated with nanoparticles compared to other groups. A preferential accumulation of the nanoparticles in lungs was also confirmed when compared with spleen, liver and kidney. Moreover, biodistribution studies confirmed that a higher silicon content was detected in lungs of individuals treated with LPS + **TNFR-RhB-MSNs** or LPS + **TNFR-Dex-MSNs** when compared with mice treated alone with **TNFR-RhB-MSNs** group in which silicon was detected in less quantity. The results demonstrated the preferential targeting of the nanoparticles to inflamed lungs in an acute lung injury mice model.

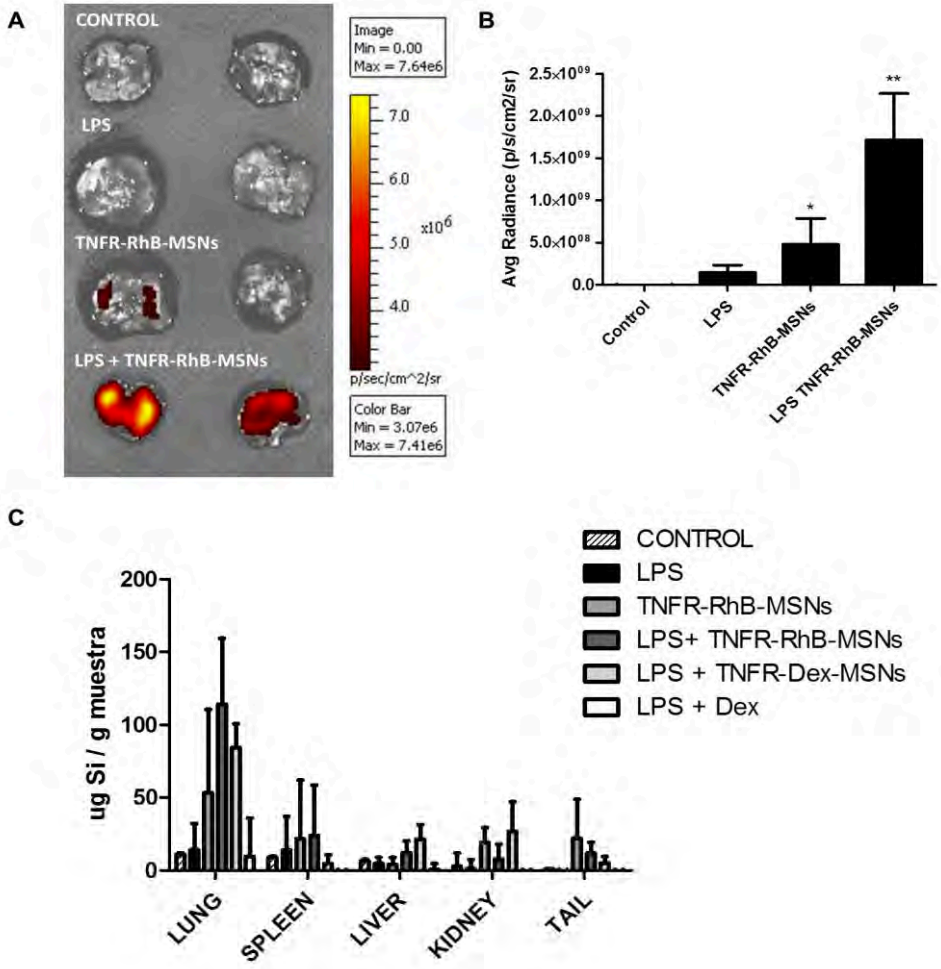

Figure 8. Evaluation of TNFR-RhB-MSNs in the inflamed lungs in an acute lung injury mice model. A) Representative lung images obtained using an IVIS spectrum equipment and B) quantification of rhodamine B associated fluorescence. C) Bidiostribution of the **TNFR-RhB-MSNs** and **TNFR-Dex-MNSs** silica scaffold in lung, liver, spleen, kidney and tail. The graph exhibited the µg Si per g of sample detected by Inductively Coupled Plasma Mass Spectroscopy (ICP-MS) in the indicated organs. The data represent the mean ± SEM and statistical significance was determined using a one-way ANOVA (n=4-5).

Impact of the encapsulation on the adverse side effects derived from dexamethasone treatment

A remarkable drawback of dexamethasone use is the high dosage needed to achieve the desired therapeutic effect in the site of action. As a result, different side adverse effects are developed in critical patients (*vide ante*). For this reason, in order to mimic side effects of dexamethasone in clinic cases, the progression of undesired effects (hyperglycaemia, thrombosis and systemic toxicity) was followed in group 6 (i.e. LPS+dexamethasone) and compared with mice treated with LPS and **TNRF-Dex-MSNs** (group 5).

Hyperglycaemia is caused as a result of an increase in the glucose levels since glucocorticoids stimulate glucogenesis.[72,73] Figure 9A shows that although glucose levels were altered in mice treated with **TNFR-Dex-MSNs** and free dexamethasone, **TNFR-Dex-MSNs** administration induced a noticeable reduction (ca. 1.7-fold) in the concentration of the free monosaccharide when compared to that found when free dexamethasone was used.

Some studies have demonstrated that the use of glucocorticoids increases the risk of thrombosis because glucocorticoids promote the synthesis of different factors involved in coagulation.[74] In order to evaluate the risk of thrombosis associated with the use of dexamethasone and **TNFR-Dex-MSNs** platelet levels were evaluated. The obtained results are depicted in Figure 9B. As could be seen, a marked increase in the platelet levels was observed for the treatment with free dexamethasone, whereas mice treated with **TNFR-Dex-MSNs** presented platelet levels in the normal range for healthy individuals. Additionally, the inflammatory response at systemic level by measuring the percentages of neutrophils, lymphocytes and monocytes was assessed. Figure 9C shows that levels of neutrophils for individuals instilled with LPS, and treated with **TNFR-RhB-MSNs**, **TNFR-Dex-MSNs** and free dexamethasone, are in the expected range for

individuals that present an acute inflammatory response (neutrophils > 40% and lymphocytes < 60%). However, in the case of **TNFR-Dex-MSNs**, the amount of neutrophils is lower and the lymphocytes population is much closer to the healthy conditions when compared to other groups. Moreover, a major misbalance in the leukocyte population was observed in the group treated with free dexamethasone (neutrophils ca. 85% and lymphocytes ca. 15%). All these results indicated that the encapsulation of dexamethasone into the capped mesoporous matrix attenuate some of the undesired side effects related with the use of free dexamethasone due to its systemic and unspecific biodistribution.

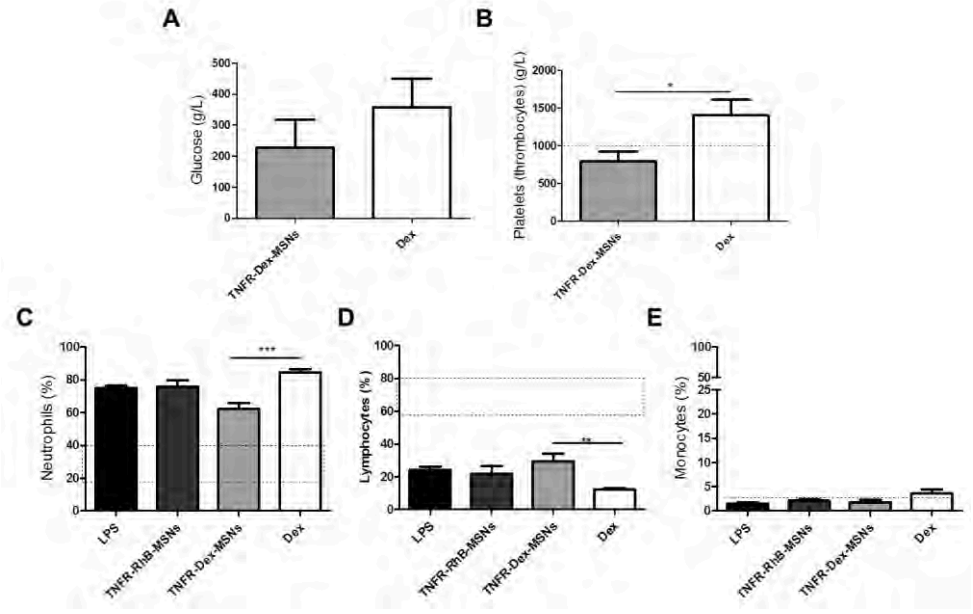

Figure 9. Evaluation of systemic dexamethasone effects. A) Hyperglicaemia evaluation by measuring glucose levels. B) Thrombosis effect determined by platelets levels. C, D, E) Percentage of neutrophils, lymphocytes and monocytes as systemic inflammation indicators. The dashed lines indicate the values for healthy individuals. The data represent the mean ± SEM (n=6-8) and statistical significance was determined using Student's t-test.

4.4 Conclusions

Two nanodevices based on mesoporous silica nanoparticles loaded with rhodamine B (**TNFR-RhB-MSNs**) or with dexamethasone (**TNFR-Dex-MSNs**) and capped with a peptide that target TNFR1 receptor were prepared and characterized. **TNFR-RhB-MSNs** nanoparticles are preferentially internalized by pro-inflammatory M1 macrophages, which overexpressed TNFR1 receptor and are able to release the cargo after the enzymatic hydrolysis of the capping peptide. Besides, **TNFR-Dex-MSNs** nanoparticles reduce cytokine levels *in vitro* in activated pro-inflammatory M1 macrophages and *in vivo* in an ALI mice model. Reduction of inflammation and attenuation of lung injuries with **TNFR-Dex-MSNs** nanoparticles is assessed also by histopathological studies. Moreover, **TNFR-Dex-MSNs** exhibited greater therapeutic effect leading with the inflammatory response in inflamed lungs with lower adverse side effects compared to free dexamethasone. Targeting of the nanoparticles is confirmed by IVIS analysis using **TNFR-RhB-MSNs** as well as by silicon biodistribuion studies in mice treated with **TNFR-RhB-MSNs** or **TNFR-Dex-MSNs**. The nanomaterials exhibited a preferential accumulation in inflamed lungs. Based on the above, we demonstrated that targeted-delivery of glucocorticoids using gated-mesoporous silica nanoparticles is an attractive tool for direct and specific drug release to inflamed lungs in ALI by taking advantage of the passive and active targeting provided by engineered MSNs, while reducing dosages and undesired drug side effects. These results might find application for the controlled delivery of glucocorticoids in other pathologies such as Chronic Pulmonary Obstructive Disease (COPD), asthma and pulmonary fibrosis, for which new therapies are urgently demanded. In addition, in most cancer treatments glucocorticoids are also used for long periods to deal with inflammatory tumour microenvironment.

4.5 Materials and methods

Synthesis of MSNs. In a typical synthesis CTABr and TEOS were used to prepare the as-synthetized MSNs. For this purpose, a CTABr solution (1 g, 2.74 mmol) was prepared in deionized H_2O and then NaOH (3.5 mL, 2 M) solution was added. The surfactant solution was stirred at 80ºC and then TEOS was added (5 mL, 2.57 x 10^{-2} mol)) dropwise. The finally mixture was stirred for 2 h to give a white precipitate. The solid was isolated by centrifugation and washed with deionized H_2O until neutral pH. The material was dried at 60ºC and then was calcined at 550ºC in an oxidant atmosphere, to remove the surfactant template, obtaining the porous scaffold (MSNs).

Synthesis of NCO-RhB-MSNs. The pores of the calcined MSNs were loaded with rhodamine B. For this purpose, MSNs (100 mg) were suspended in an acetonitrile solution containing rhodamine B (38.3 mg, 0.8 mmoles/g solid) and stirred overnight. Then, an excess of (3-isocyanatopropyl)triethoxysilane (124.93 µL, 5 mmoles/g solid) were added to the mixture, and stirred for 5.5 h at room temperature. Finally the solid was isolated by centrifugation, washed twice with CH_3CN and dried at 37ºC to yield a pink solid.

Synthesis of TNFR-RhB-MSNs. The TNFR1 peptide (GGGGFIGLMYRYQRWKSKLY), which binds with TNFR1 receptor in pro-inflammatory macrophage cell surface, was covalently anchored onto the external surface of **NCO-RhB-MSNs** through urea bond formation. At this respect, **NCO-RhB-MSNs** (40 mg) were suspended in CH_3CN (2 mL) and the peptide (40 mg) was dissolved in H_2O (2 mL). Finally, the peptide solution was added to the **NCO-RhB-MSNs** suspension which contained also triethylamine (80 µL). The mixture was stirred at room temperature for 2 h and then nanoparticles were centrifuged and

washed with water and PBS. Finally, the solid was dried at 37ºC to obtain the final **TNFR-RhB-MSNs** nanodevice.

Synthesis of NCO-Dex-MSNs. A saturated solution of dexamethasone (26 mg in 1 mL of methanol) was prepared. The solution was separated in two aliquots, and added in two different cycles to calcined MSNs. The MSNs (50 mg) were extended on a plate and the first dexamethasone aliquot was added dropwise. Then, the mixture was dried at 37ºC and a second step of impregnation was carried out. The material was finally dried at 37ºC. Afterward, dexamethasone-loaded MSNs were suspended in anhydrous CH_3CN with an excess of (3-isocyanatopropyl)triethoxysilane (32.48 µL, 5 mmoles/g solid) and the mixture was stirred at room temperature for 5.5 h. The nanoparticles were isolated by centrifugation and washed twice with CH_3CN. Finally the resulting **NCO-Dex-MSNs** were dried at 37ºC.

Synthesis of TNFR-Dex-MSNs. The TNFR1 peptide (GGGGFIGLMYRYQRWKSKLY), which binds with TNFR1 receptor in pro-inflammatory macrophage cell surface, was covalently anchored onto the external surface of **NCO-Dex-MSNs** through urea bond formation. At this respect, **NCO-Dex-MSNs** (40 mg) were suspended in CH_3CN (2 mL) and the peptide (40 mg) was dissolved in H_2O (2 mL). Finally, the peptide solution was added to the **NCO-Dex-MSNs** suspension which contained also triethylamine (80 µL). The mixture was stirred at room temperature for 2 h and then nanoparticles were centrifuged and washed with water and PBS. Finally, the solid was dried at 37ºC to obtain the final **TNFR-Dex-MSNs** nanodevice.

Standard characterization procedures of prepared materials. Powder XRD, TEM, N_2 adsorption-desorption, thermogravimetric analysis and HPLC measurements were employed to characterize the prepared materials. Powder X-ray measurements were performed on a Seifert 3000TT diffractometer using CuKα radiation. Transmission electron microscope (TEM) images were performed in a Philips CM-10. N_2 adsorption-desorption isotherms were recorded on a Micromeritics ASAP2010 automated sorption analyser. Thermogravimetric analysis were carried out on a TGA/SDTA 851e Mettler Toledo equipment, using an oxidant atmosphere (air, 80 mL/min) with a heating program consisting on a heating ramp of 10 °C per minute from 393 K to 1273 K and an isothermal heating step at this temperature for 30 min. HPLC analysis was carried out with a Merck Hitachi L-2130 HPLC pump and an L-2200 autosampler using a Lichrospher®100 C18 (150 × 3.9 mm) column, and different acetonitrile gradients in aqueous 0.1% TFA as the mobile phase.

Drug delivery studies. To assess the proper working of the capping ensemble **TNFR-RhB-MSNs** were suspended in PBS (pH 7.4) or in lysosomal extract (pH 5.0) and the release of rhodamine B evaluated by fluorescence measurements. Lysosomal extract was obtained from animal tissues and purified using the Lysosome Isolation Kit (LYSISO1) following supplier's instructions. In a typical assay, 1 mg of **TNFR-RhB-MSNs** was suspended in 2 mL of PBS or 2 mL of lysosomal extract and stirred at 37ºC. At certain time aliquots were separated and centrifuged to eliminate the solid and dye delivery was monitored by the fluorescence emission band of rhodamine B at 575 nm (λ_{ex} = 555 nm).

Cell culture conditions. Human leukemic monocyte (THP-1) cells were purchased from the German Resource Centre for Biological Materials (DSMZ) and

were grown in RPMI-1640 supplemented with 10% of FBS. Cells were incubated at 37 °C in an atmosphere of 5% carbon dioxide and 95% air, and underwent passage twice a week. For macrophage derivation, THP-1 cells were seeded in a 6-well plate at 800,000 cells/mL and differentiated into non-polarized macrophages with the addition of 50 ng/mL of phorbol 12-myristate 13-acetate (PMA) followed by 24 h of incubation in RPMI medium. When a differentiated non-polarized phenotype (M0) was achieved, the PMA-containing medium was removed, and replaced with complete RPMI 1640 supplemented with 1% FBS for another 24 h. Finally, macrophages were polarized into pro-inflammatory (M1) or anti-inflammatory (M2) macrophages. For M1 polarization, macrophages cells were incubated with 20 ng/ml of interferon-ϒ (IFN-ϒ) for 24 h and finally incubated with LPS (100 ng/mL) for 3 h. In the case of M2 derivation, the cells were incubated with 20 ng/mL of IL-4 and IL-13 for 48 h.

Macrophage phenotype characterization. As a first step of phenotype characterization, THP-1 cells were derived onto macrophages cells and pro-inflammatory (IL-1β) and anti-inflammatory (IL-10) cytokines levels were determined in cell supernatants by ELISA assay. In addition, pyroptosis cell death was determined by measuring LDH activity in cell supernatants with the Lactate Assay Kit II following the manufacturer's instructions. Moreover, phenotypes were confirmed via QRT-PCR analysis of gene expressions in commonly used cell protein markers CCR7, and CXCL10 for M1 and mannose receptor CD206 for M2 (See supporting information).[75] For this purpose, THP-1, M0, M1 and M2 cells were cultured in a 6-well plate to prepare RNA extracts. Total RNA was extracted using the RNA isolation RNeasy Mini Kit (Qiagen) and then reverse transcribed (RT) into mRNA using super script first strand synthesis system for RT-PCR (Invitrogen). Equal amounts of cDNA were taken from each RT reaction mixture

for PCR amplification. The qPCR analysis was performed on the Roche Light Cycler 480 using the SYBRGreen reagent kit and primers for CCR7, CXCL10, CD206 (100 nM) were used. Besides, GAPDH expression was used as the reference gene for normalization. Non-template controls were included for each primer pair to discard any contaminant and the specificity of the amplified PCR products was confirmed by melting-curve analysis. Finally, the mRNA abundance was quantified using Roche Applied Science software using the threshold cycle (C_T) method and the level expressions were expressed as relative-fold change versus the GAPDH expression.

TNFR1 characterization in pro-inflammatory macrophages. In order to evaluate the proper working of **TNFR-RhB-MSNs** and **TNFR-Dex-MSNs** nanodevices, the expression of TNFR1 on the different inflammatory cells was studied by western blot analysis. For this purpose, THP-1 cells were cultured in a 6-well plate, derived in M0 macrophages and polarized to M1 pro-inflammatory macrophages respectively, as we described above. To prepare whole cell extracts, cells were scrape-harvested in 50 µL of lysis buffer (25 mM Tris-HCl pH 7.4, 1 mM EDTA, 1 mM EGTA and 1% SDS plus protease and phosphatase inhibitors). Lysates were separated by SDS-PAGE electrophoresis, electrophoretically transferred to nitrocellulose membranes, blocked with 5% non-fat milk and incubated overnight with the specific primary antibody against TNFR1 (C25C1 from Cell Signalling). The expression of GAPDH (MA5-15738 from Invitrogen) was detected in cell lysates as reference protein for normalization. Membranes were washed and incubated with the horseradish peroxidase-conjugated secondary antibody. Chemiluminescence detection of the bound antibody was carried out using Amersham Imager 600 equipment.

Cytotoxicity cell studies with TNFR-RhB-MSNs. The biocompatibility of **TNFR-RhB-MSNs** was evaluated in the THP-1 monocytes and A549 lung cancer cells. The cytotoxic effect was determinate by WST-1 assay and inflammatory cell-death called pyroptosis by LDH activity assay. The THP-1 cells and A549 cells were seeded in a 96-well plate and treated with different concentrations of **TNFR-RhB-MSNs** (0, 25, 50, 100 and 200 μg/mL in PBS) for 3 and 24 h. For cell viability, WST-1 was added for 30 min and then absorbance at 595 nm was registered in a Wallac 1420 workstation. In the case of LDH activity was measured in cell supernatants with the Lactase Assay Kit II following the manufacturer's instructions. A positive control was used to normalize the LDH activity in THP-1 cells under the addition of 1% triton-x100 in the absence of nanoparticles.

Targeted cellular uptake studies. The targeting features of the prepared nanodevices were evaluated in THP-1 cells and polarized pro-inflammatory (M1) macrophages. For this purpose, MSNs loaded with rhodamine B and capped with a random peptide (**Random-RhB-MSNs**) were prepared as control solid to study the selective targeting of **TNFR-RhB-MSNs**. In a first step, flow cytometry experiments were performed to test the efficiency uptake of nanoparticles in the inflammatory cells. For this purpose, THP-1 cells were seeded in a 6-well plate and derived to M1 macrophages as described above. The THP-1 cells and the pro-inflammatory (M1) macrophages were treated with 50 μg/mL of **TNFR-RhB-MSNs** and **Random-RhB-MSNs** nanodvices and, after 30 min, cells were washed with PBS to remove the non-internalized nanoparticles. Finally, the cells were incubated for a total time of 1 and 4 h in the presence of nanoparticles. Then the cells were washed and collected for rhodamine B quantification by flow cytometry. The single-cell fluorescence measurements were performed in CytoFLEX S (Beckman-Coulter, USA) equipped with 4 lasers and 13 fluorescence

detectors and analysed in the CytoFLEX software. In addition, nanodevice internalization was followed in THP-1 cells and pro-inflammatory (M1) macrophages by confocal microscopy. The cells were seeded over glass-cover slips in 6-well plates and treated with of **TNFR-RhB-MSNs** and **Random-RhB-MSNs** (50 μg/mL) for 30 min. Then cells were washed with PBS and new media was added until complete 1 and 4 h of nanoparticles incubation. Finally, the cells were washed several times with PBS, Hoechst 33342 nuclei stain was added at 2μg/mL and the fluorescence intensity was monitored using a Leica TCS SP8 confocal microscope.

Anti-inflammatory activity of TNFR-Dex-MSNs in inflammatory cells. The proper anti-inflammatory activity of **TNFR-Dex-MSNs** was evaluated in the pro-inflammatory (M1) macrophages and in THP-1 cells. The THP-1 cells were seeded in a 6 well-plate at 800,000 cells/mL in RPMI 1% FBS and after 24 h of incubation, the cells were treated with **TNFR-Dex-MSNs** at 2 μg/mL (in PBS). Free dexamethasone was used as a reference at equivalent concentration of 1 μM (in ethanol) and **TNFR-RhB-MSNs** at 2 μg/mL was used as control. The NLPR3 inflammasome was activated, after 30 min of treatments, by the addition of lipopolysaccharide (LPS) from *Escherichia coli* (100 ng/mL) for 3 h and nigericin addition (20 μM) during the last 30 min of incubation. On the other hand, pro-inflammatory (M1) macrophages were polarized from THP-1 cells. THP-1 were seeded at 800,000 cells/mL in RPMI 10%FBS and PMA was added at 50 ng/mL for 24 h. After 24 h, media was replace for RPMI 1% FBS and IFN-ϒ at 20 ng/mL was added for 24 h. Once pro-inflammatory macrophages were derived, treatments were added as described above for THP-1 cells for 30 min. The NLPR3 inflammasome was activated, after 30 min of treatments, by the addition of

lipopolysaccharide (LPS) from *Escherichia coli* (100 ng/mL) for 3 h and nigericin addition (10 μM) during the last 30 min of incubation.

The anti-inflammatory activity of nanodvices was evaluated by the amount of IL-1β and TNF-α secretion in the cell culture supernatants of inflammatory cells by enzyme-linked immunosorbent assay (ELISA) kit in accordance with the manufacturer's instructions. The pyroptosis cell death was also measured by the LDH activity in the cell supernatants using the LDH Assay Kit II following the supplier's instructions. Finally, western blot analysis was performed to characterize the inflammasome components in cell lysates and supernatants from THP-1 cells and pro-inflammatory (M1) macrophages. The proteins studied in cell lysate were NLPR3, TNFR1 and pro-Caspse-1. GAPDH was used as protein reference to normalize the expression levels. Active Caspase 1 (p20) was also analysed in the cell supernatants. To determine the amount of proteins in cell lysates, whole cell extracts were obtained by lysing the cells in a lysis buffer (25 mM Tris-HCl pH 7.4, 1 mM EDTA, 1 Mm EGTA and 1% SDS plus protease and phosphatase inhibitors). Supernatants samples were also collected and concentrate by lyophilisation and finally suspended in loading electrophoresis buffer. The samples were resolved by SDS-PAGE, transferred to nitrocellulose membranes, blocked with 5% non-fat milk and incubated overnight with the specific primary antibody in each case (Table 2). Membranes were washed and the correspondent secondary antibody conjugated with horseradish peroxidase was added in order to chemiluminescence detection of the bounded antibody.

TNFR-Dex-MSNs In vivo studies in ALI mouse model. These studies were carried out in strict accordance with the recommendations in the Guide for Care and Use of Laboratory and were approved by the Ethical Committee for Animal Experiments at Centro de Investigación Príncipe Felipe (Valencia, Spain). Female

and male CD-1 mice (10-12 weeks of age) were purchased from Charles River (France) and were maintained in polyethylene cages with stainless steel lids with access to food and water in a temperature-controlled room with a 12h light/dark cycle. The animals were allocated into six groups of 8-10 animals, formed by 4-5 male and 4-5 female mice in each case. The group's distribution was: (1) control; (2) treated with LPS; (3) administered with **TNFR-RhB-MSNs**; (4) treated with LPS + **TNFR-RhB-MSNs**; (5) administered with LPS + **TNFR-Dex-MSNs**; (6) treated with LPS + dexamethasone. Nanoparticles were intravenously administered by tail vein injection (25 mg/Kg) in 200 µL of PBS corresponding to equivalent dose of 10 mg/kg of dexamethasone. Free dexamethasone was administered at 10 mg/Kg in 200 µL of PBS and 200 µL of PBS vehicle was administered in the control and LPS animals. Moreover, **TNFR-RhB-MSNs** were administered at 25 mg/kg as nanoparticle control. After 30 min, the acute lung injury (ALI) model was established by the intratracheally administration of LPS (*E. coli* 055:B5, 2.5 mg/kg) in 50 µL of saline for 24 h. The animals were previously anesthetized with ketamine (75 mg/kg) and dexmedetomidine (1 mg/kg) and reversals from anaesthesia with 1 mg/kg of atipamezole. After 24 h of ALI induction the animals were euthanized by sodium pentobarbital overdose. Bronchoalveolar lavage (BAL), blood extraction and dissection of different organs were carried out in order to evaluate the pulmonary injury and inflammatory response.

Bronchoalveolar lavage analysis. Inside of each group the lungs from 6 of the 10 animals were lavage intra-tracheally with two injections of 250 µL of PBS to obtain the bronchoalveolar lavage. The bronchoalveolar lavage fluid (BALF) was collected and supernatant was separated from cells by centrifugation at 1200 rpm for 5 min at 4ºC. The cell pellet was suspended in PBS for counting the total leukocyte number and analysed in laboratory of veterinary analytical clinic

(ACVLAB). BAL supernatants were used to measure the cytokines and protein level. TNF-α, IL-6 and IL-1β were quantified using ELISA kit following the manufacturer's instructions. The protein concentration in the BAL fluid was determined by BCA protein assay kit.

Histopathology analysis. The lungs from 4 of the 10 animals were obtained and fixed with 4% paraformaldehyde. After fixation, lungs were embedded in paraffin, cut with a microtome into 2 μm sections and mounted on coated glass slides for histological evaluation and stained by hematoxylin and eosin to determine the ALI score. The slides were registered in the Leica ASP300 tissue processor and analysed with the CaseViewer program. At least 20 random high-power fields were independently analysed for each condition and ALI score was evaluated in different gradations of severy for main histological findings (neutrophils in the alveolar space, neutrophils in the interstitial space, hyaline membranes, proteinaceous debris filling the airspaces and alveolar septal thickening). Moreover, the sections were stained with different markers to study the myeloperoxidase activity associated to neutrophil presence, the accumulation of carbohydrate macromolecules with PAS (Periodic Acid Schiff) stainer to determine alveolar proteinosis, the deposition of collagen with Masson's trichrome as fibrosis marker and factor VIII/Von Willebrand factor to determine vascular inflammation. For this purpose, sections were processed in a DAKO PT link with the Dako 3-in-1 AR buffer EDTA pH 9.0 after a rehydration and antigen retrieval procedure. Then, the tissue sections were prepared with the Envision Flexþ kit (DAKO) for finally incubate with the correspondent primary antibody. The endogenous peroxidase activity was previously blocked for 5 min. The primary antibodies used were anti-myeloperoxidase (Dako, IR511 for 20 minutes), anti-Von Willebrand Factor (Dako, IR527 for 20 minutes), Masson's trichrome

(Dako, AR173) and Periodic Acid Schiff (PAS) (Dako AR165) were added using the Artisan LinkPro de Dako. Finally, the reaction was visualized by adding Envision Flexþ horseradish peroxidase for 20 min and diaminobenzidine for 10 min. Sections were counterstained with Mayer's hematoxylin (DAKO, S3309, ready-to-use) for 5 min. The slides were registered in the Leica ASP300 tissue processor and analysed with the CaseViewer program.

Nanodevices biodistribution in ALI mouse model. To determine the targeting effect to inflamed lungs by **TNFR-RhB-MSNs**, lungs were collected after the sacrifice and were analysed immediately after harvesting. Rhodamine B fluorescence was registered by an IVIS spectrum imaging system (PerkinElmer Inc) using excitation wavelength of 535 nm and emission wavelength of 580 nm. Moreover, presence of nanodevices was determined by silicon quantification in selected organs (lungs, liver, kidneys, spleen, tail and BAL) by ICP-MS. The samples were introduced into 15 mL of polytetrafluorethylene (PTFE) tubes and 1 mL of TMAH 25% was added. The digestion temperature was set at 80º for 2 h using a Bloc digest 20 (Selecta). For the analysis, digested samples were diluted in a mixture of nitric acid 2% and hydrochloric acid 1% to 10 mL and were measured in the 7900 ICP-MS in H_2 mode using germanium as an internal standard.

Acknowledgements

A. García-Fernández thanks the Spanish government for her FPU fellowship. The authors are grateful to the Spanish Government (project RTI2018-100910-B-C41 (MCUI/AEI/FEDER, UE) and the Generalitat Valencia (Project PROMETEO/2018/024 and PROMETEOII/2014/061) for support. The authors would like to thank I. Borred and J. Forteza from Instituo Valenciano de Patología for its technical support in the histopathology analysis and Animal Facilities from

Centro de Investigación Principe Felipe for its support in the animal research and procedures.

4.6 References

(1) Bernard, G. R.; Artigas, A.; Brigham, K. L.; Carlet, J.; Falke, K.; Hudson, L.; Lamy, M.; Legall, J. R.; Morris, A.; Spragg, R. The American-European Consensus Conference on ARDS. Definitions, Mechanisms, Relevant Outcomes, and Clinical Trial Coordination. *Am. J. Respir. Crit. Care Med.* **1994**, *149*, 818–824.

(2) Johnson, E. R.; Matthay, M. A. Acute Lung Injury: Epidemiology, Pathogenesis, and Treatment. *J. Aerosol Med. Pulm. Drug Deliv.* **2010**, *23*, 243–252.

(3) Matthay, M. A.; Zemans, R. L.; Zimmerman, G. A.; Arabi, Y. M.; Beitler, J. R.; Mercat, A.; Herridge, M.; Randolph, A. G.; Calfee, C. S. Acute Respiratory Distress Syndrome. *Nat. Rev. Dis. Prim.* **2019**, *5*, 1-22.

(4) Matthay, M. A.; Wiener-Kronish, J. P. Intact Epithelial Barrier Function Is Critical for the Resolution of Alveolar Edema in Humans. *Am. Rev. Respir. Dis.* **1990**, *142*, 1250–1257.

(5) Matthay, M. A.; Fukuda, N.; Frank, J.; Kallet, R.; Daniel, B.; Sakuma, T. Alveolar Epithelial Barrier: Role in Lung Fluid Balance in Clinical Lung Injury. *Clin. Chest Med.* **2000**, *21*, 477–490.

(6) Meduri, G. U.; Kohler, G.; Headley, S.; Tolley, E.; Stentz, F.; Postlethwaite, A. Inflammatory Cytokines in the BAL of Patients With ARDS: Persistent Elevation Over Time Predicts Poor Outcome. *Chest* **1995**, *108*, 1303–1314.

(7) Zemans, R. L.; Colgan, S. P.; Downey, G. P. Transepithelial Migration of Neutrophils. *Am. J. Respir. Cell Mol. Biol.* **2009**, *40*, 519–535.

(8) Ward, P. A. Acute Lung Injury: How the Lung Inflammatory Response Works. *Eur. Respir. J.* **2003**, *22*, 22s LP-23s.

(9) Raghavendran, K.; Pryhuber, G. S.; Chess, P. R.; Bruce, A.; Knight, P. R.; Notter, R. H. NIH Public Access. **2009**, *15*, 1911–1924.

(10) Cepkova, M.; Matthay, M. A. Pharmacotherapy of Acute Lung Injury and the Acute Respiratory Distress Syndrome. *J. Intensive Care Med.* **2006**, *21*, 119–143.

(11) Matthay, M. A.; Zemans, R. L. The Acute Respiratory Distress Syndrome: Pathogenesis and Treatment. *Annu. Rev. Pathol. Mech. Dis.* **2011**, *6* , 147–163.

(12) Carolina, N. Nanomedicine for Treatment of Acute Lung Injury and Acute Respiratory Distress Syndrome. **2017**, *2*, 477086.

(13) Iyer, R.; Nguyen, C. C. W. H. and K. T. Nano-Therapeutics for the Lung: State-of-the-Art and Future Perspectives. *Current Pharmaceutical Design*. **2015**, *21*, 5233–5244.

(14) Bailey, M. M.; Berkland, C. J. Nanoparticle Formulations in Pulmonary Drug Delivery. *Med. Res. Rev.* **2009**, *29*, 196–212.

(15) Kim, S.-W.; Park, J.-Y.; Lee, S.; Kim, S.-H.; Khang, D. Destroying Deep Lung Tumor Tissue through Lung-Selective Accumulation and by Activation of Caveolin Uptake Channels Using a Specific Width of Carbon Nanodrug. *ACS Appl. Mater. Interfaces* **2018**, *10*, 4419–4428.

(16) Elmowafy, E.; Ishak, R. O. and R. A. H. Polymer-Based Novel Lung Targeted Delivery Systems.

Current Pharmaceutical Design. **2017**, *23*, 373–392.

(17) Mangal, S.; Gao, W.; Li, T.; Zhou, Q. (Tony). Pulmonary Delivery of Nanoparticle Chemotherapy for the Treatment of Lung Cancers: Challenges and Opportunities. *Acta Pharmacol. Sin.* **2017**, *38*, 782-797.

(18) van Rijt, S. H.; Bölükbas, D. A.; Argyo, C.; Wipplinger, K.; Naureen, M.; Datz, S.; Eickelberg, O.; Meiners, S.; Bein, T.; Schmid, O.; et al. Applicability of Avidin Protein Coated Mesoporous Silica Nanoparticles as Drug Carriers in the Lung. *Nanoscale* **2016**, *8*, 8058–8069.

(19) Hussain, S.; Ji, Z.; Taylor, A. J.; Degra, L. M.; George, M.; Tucker, C. J.; Chang, C. H.; Li, R.; Bonner, J. C.; Garantziotis, S. Multiwalled Carbon Nanotube Functionalization with High Molecular Weight Hyaluronan Signi Fi Cantly Reduces Pulmonary Injury. **2016**, *10*, 7675-7688.

(20) Bohr, A.; Tsapis, N.; Andreana, I.; Chamarat, A.; Foged, C.; Delomenie, C.; Noiray, M.; Brahmi, N. El; Majoral, J.; Mignani, S.; et al. Anti-In Fl Ammatory Effect of Anti-TNF - α SiRNA Cationic Phosphorus Dendrimer Nanocomplexes Administered Intranasally in a Murine Acute Lung Injury Model. **2017**, *18*, 2379-2388.

(21) Aznar, E.; Oroval, M.; Pascual, L.; Murguía, J. R.; Martínez-Máñez, R.; Sancenón, F. Gated Materials for On-Command Release of Guest Molecules. *Chem. Rev.* **2016**, *116*, 561–718.

(22) Llopis-Lorente, A.; de Luis, B.; García-Fernández, A.; Jimenez-Falcao, S.; Orzáez, M.; Sancenón, F.; Villalonga, R.; Martínez-Máñez, R. Hybrid Mesoporous Nanocarriers Act by Processing Logic Tasks: Toward the Design of Nanobots Capable of Reading Information from the Environment. *ACS Appl. Mater. Interfaces* **2018**, *10*, 26494–26500.

(23) Llopis-Lorente, A.; Díez, P.; Sánchez, A.; Marcos, M. D.; Sancenón, F.; Martínez-Ruiz, P.; Villalonga, R.; Martínez-Máñez, R. Interactive Models of Communication at the Nanoscale Using Nanoparticles That Talk to One Another. *Nat. Commun.* **2017**, *8*, 15511.

(24) Mura, S.; Nicolas, J.; Couvreur, P. Stimuli-Responsive Nanocarriers for Drug Delivery. *Nat. Mater.* **2013**, *12*, 991-1003.

(25) Kamaly, N.; Yameen, B.; Wu, J.; Farokhzad, O. C. Degradable Controlled-Release Polymers and Polymeric Nanoparticles: Mechanisms of Controlling Drug Release. *Chem. Rev.* **2016**, *116*, 2602–2663.

(26) Yang, P.; Gai, S.; Lin, J. Functionalized Mesoporous Silica Materials for Controlled Drug Delivery. *Chem. Soc. Rev.* **2012**, *41*, 3679–3698.

(27) Wu, S.-H.; Mou, C.-Y.; Lin, H.-P. Synthesis of Mesoporous Silica Nanoparticles. *Chem. Soc. Rev.* **2013**, *42*, 3862–3875.

(28) Pascual, L.; Cerqueira-Coutinho, C.; García-Fernández, A.; de Luis, B.; Bernardes, E. S.; Albernaz, M. S.; Missailidis, S.; Martínez-Máñez, R.; Santos-Oliveira, R.; Orzaez, M.; et al. MUC1 Aptamer-Capped Mesoporous Silica Nanoparticles for Controlled Drug Delivery and Radio-Imaging Applications. *Nanomedicine Nanotechnology, Biol. Med.* **2017**, *13*, 2495–2505.

(29) Giménez, C.; de la Torre, C.; Gorbe, M.; Aznar, E.; Sancenón, F.; Murguía, J. R.; Martínez-Máñez, R.; Marcos, M. D.; Amorós, P. Gated Mesoporous Silica Nanoparticles for the Controlled Delivery of Drugs in Cancer Cells. *Langmuir* **2015**, *31*, 3753–3762.

(30) Pu, X.; Li, J.; Qiao, P.; Li, M.; Wang, H.; Zong*, L.; Duan*, Q. Y. and S. Mesoporous Silica Nanoparticles as a Prospective and Promising Approach for Drug Delivery and Biomedical

Applications. *Current Cancer Drug Targets*. **2019**, *19*, 285–295.

(31) Castillo, R. R.; Vallet-Regí, M. Functional Mesoporous Silica Nanocomposites: Biomedical Applications and Biosafety. *International Journal of Molecular Sciences* . **2019**, 20, 929-959.

(32) Muñoz-Espín, D.; Rovira, M.; Galiana, I.; Giménez, C.; Lozano-Torres, B.; Paez-Ribes, M.; Llanos, S.; Chaib, S.; Muñoz-Martín, M.; Ucero, A. C.; et al. A Versatile Drug Delivery System Targeting Senescent Cells. *EMBO Mol. Med.* **2018**, *10*, e9355.

(33) Yin, P. T.; Pongkulapa, T.; Cho, H.-Y.; Han, J.; Pasquale, N. J.; Rabie, H.; Kim, J.-H.; Choi, J.-W.; Lee, K.-B. Overcoming Chemoresistance in Cancer via Combined MicroRNA Therapeutics with Anticancer Drugs Using Multifunctional Magnetic Core-Shell Nanoparticles. *ACS Appl. Mater. Interfaces* **2018**, *10*, 26954–26963.

(34) Zhang, L.; Chen, Y.; Li, Z.; Li, L.; Saint-Cricq, P.; Li, C.; Lin, J.; Wang, C.; Su, Z.; Zink, J. I. Tailored Synthesis of Octopus-Type Janus Nanoparticles for Synergistic Actively-Targeted and Chemo-Photothermal Therapy. *Angew. Chemie Int. Ed.* **2016**, *55*, 2118–2121.

(35) Hu, J.-J.; Lei, Q.; Peng, M.-Y.; Zheng, D.-W.; Chen, Y.-X.; Zhang, X.-Z. A Positive Feedback Strategy for Enhanced Chemotherapy Based on ROS-Triggered Self-Accelerating Drug Release Nanosystem. *Biomaterials* **2017**, *128*, 136–146.

(36) Teruel, A. H.; Pérez-Esteve, É.; González-Álvarez, I.; González-Álvarez, M.; Costero, A. M.; Ferri, D.; Gaviña, P.; Merino, V.; Martínez-Máñez, R.; Sancenón, F. Double Drug Delivery Using Capped Mesoporous Silica Microparticles for the Effective Treatment of Inflammatory Bowel Disease. *Mol. Pharm.* **2019**, *16*, 2418–2429.

(37) Manzano, M.; Vallet-Regí, M. Mesoporous Silica Nanoparticles in Nanomedicine Applications. *J. Mater. Sci. Mater. Med.* **2018**, *29*, 65.

(38) Wu, T.; Tang, M. Review of the Effects of Manufactured Nanoparticles on Mammalian Target Organs. *J. Appl. Toxicol.* **2018**, *38*, 25–40.

(39) Tang, F.; Li, L.; Chen, D. Mesoporous Silica Nanoparticles: Synthesis, Biocompatibility and Drug Delivery. *Adv. Mater.* **2012**, *24*, 1504–1534.

(40) García-Fernández, A.; García-Laínez, G.; Ferrándiz, M. L.; Aznar, E.; Sancenón, F.; Alcaraz, M. J.; Murguía, J. R.; Marcos, M. D.; Martínez-Máñez, R.; Costero, A. M.; et al. Targeting Inflammasome by the Inhibition of Caspase-1 Activity Using Capped Mesoporous Silica Nanoparticles. *J. Control. Release* **2017**, *248*, 60–70.

(41) Teruel, A. H.; Pérez-Esteve, É.; González-Álvarez, I.; González-Álvarez, M.; Costero, A. M.; Ferri, D.; Parra, M.; Gaviña, P.; Merino, V.; Martínez-Mañez, R.; et al. Smart Gated Magnetic Silica Mesoporous Particles for Targeted Colon Drug Delivery: New Approaches for Inflammatory Bowel Diseases Treatment. *J. Control. Release* **2018**, *281*, 58–69.

(42) Xie, J.; Xiao, D.; Zhao, J.; Hu, N.; Bao, Q.; Jiang, L.; Yu, L. Mesoporous Silica Particles as a Multifunctional Delivery System for Pain Relief in Experimental Neuropathy. *Adv. Healthc. Mater.* **2016**, *5*, 1213–1221.

(43) Kwon, D.; Cha, B. G.; Cho, Y.; Min, J.; Park, E.-B.; Kang, S.-J.; Kim, J. Extra-Large Pore Mesoporous Silica Nanoparticles for Directing in Vivo M2 Macrophage Polarization by Delivering IL-4. *Nano Lett.* **2017**, *17*, 2747–2756.

(44) Yu, T.; Hubbard, D.; Ray, A.; Ghandehari, H. In Vivo Biodistribution and Pharmacokinetics of Silica Nanoparticles as a Function of Geometry, Porosity and Surface Characteristics. *J. Control. Release* **2012**, *163*, 46–54.

(45) Chen, Y.; Chen, H.; Shi, J. In Vivo Bio-Safety Evaluations and Diagnostic/Therapeutic Applications of Chemically Designed Mesoporous Silica Nanoparticles. *Adv. Mater.* **2013**, *25*, 3144–3176.

(46) Yuan, F.; Quan, L.; Cui, L.; Goldring, S. R.; Wang, D. Development of Macromolecular Prodrug for Rheumatoid Arthritis. *Adv. Drug Deliv. Rev.* **2012**, *64*, 1205–1219.

(47) KOZIOLOVÁ, E.; VENCLÍKOVÁ, K.; ETRYCH, T. Polymer-Drug Conjugates in Inflammation Treatment. *Physiol. Rev.* **2018**, *67*, S281–S292.

(48) Jiang, S.; Li, S.; Hu, J.; Xu, X.; Wang, X.; Kang, X.; Qi, J.; Lu, X.; Wu, J.; Du, Y.; et al. Combined Delivery of Angiopoietin-1 Gene and Simvastatin Mediated by Anti-Intercellular Adhesion Molecule-1 Antibody-Conjugated Ternary Nanoparticles for Acute Lung Injury Therapy. *Nanomedicine Nanotechnology, Biol. Med.* **2019**, *15*, 25–36.

(49) Li, S.-J.; Wang, X.-J.; Hu, J.-B.; Kang, X.-Q.; Chen, L.; Xu, X.-L.; Ying, X.-Y.; Jiang, S.-P.; Du, Y.-Z. Targeting Delivery of Simvastatin Using ICAM-1 Antibody-Conjugated Nanostructured Lipid Carriers for Acute Lung Injury Therapy. *Drug Deliv.* **2017**, *24*, 402–413.

(50) Zhang, C. Y.; Lin, W.; Gao, J.; Shi, X.; Davaritouchaee, M.; Nielsen, A. E.; Mancini, R. J.; Wang, Z. PH-Responsive Nanoparticles Targeted to Lungs for Improved Therapy of Acute Lung In Fl Ammation / Injury. *ACS Appl. Mater. Interfaces* **2019**, *11*, 16380–16390.

(51) Weifeng, Y.; Li, L.; Yujie, H.; Weifeng, L.; Zhenhui, G.; Wenjie, H. Inhibition of Acute Lung Injury by TNFR-Fc through Regulation of an Inflammation- Oxidative Stress Pathway. **2016**, 1–13.

(52) Wilson, M. R.; Wakabayashi, K.; Bertok, S.; Oakley, C. M.; Lucas, R.; Mcguire, J. Inhibition of TNF Receptor P55 By a Domain Antibody Attenuates the Initial Phase of Acid-Induced Lung Injury in Mice. **2017**, *8*, 1–12.

(53) Hristodorov, D.; Mladenov, R.; Felbert, V. Von; Huhn, M.; Fischer, R.; Barth, S.; Thepen, T.; Hristodorov, D.; Mladenov, R.; Felbert, V. Von; et al. Targeting CD64 Mediates Elimination of M1 but Not M2 Macrophages in Vitro and in Cutaneous Inflammation in Mice and Patient Biopsies Targeting CD64 Mediates Elimination of M1 but Not M2 Macrophages in Vitro and in Cutaneous in Fl Ammation in Mice and Pati. **2015**, *7*, 853-862.

(54) Chronic, M. M. M.; Akinrinmade, O. A.; Chetty, S.; Daramola, A. K.; Islam, M. CD64 : An Attractive Immunotherapeutic Target For M1-type Macrophage Mediated Chronic Inflammatory Diseases. *Biomedicines*, **2017**, *5*, 1–18.

(55) Zhang, Z.; Chen, L.; Ni, H. The Effectiveness of Corticosteroids on Mortality in Patients with Acute Respiratory Distress Syndrome or Acute Lung Injury : A Secondary Analysis. *Sci Rep.* **2015**, *5*, 17654-17665.

(56) Peter, J. V.; John, P.; Graham, P. L.; Moran, J. L.; George, I. A.; Bersten, A. Corticosteroids in the Prevention and Treatment of Acute Respiratory Distress Syndrome (ARDS) in Adults: Meta-Analysis. *BMJ,* **2008**, *336*, 1006 LP-1009.

(57) Aktas, M. S.; Kandemir, F. M.; Ozkaraca, M.; Hanedan, B.; Kirbas, A. Protective Effects of Rutin on Acute Lung Injury Induced by Oleic Acid in Rats. *Kafkas Univ Vet Fak Derg* **2017**, *23*, 445–451.

(58) Al-Harbi, N. O.; Imam, F.; Al-Harbi, M. M.; Ansari, M. A.; Zoheir, K. M. A.; Korashy, H. M.; Sayed-Ahmed, M. M.; Attia, S. M.; Shabanah, O. A.; Ahmad, S. F. Dexamethasone Attenuates LPS-Induced Acute Lung Injury through Inhibition of NF-KB, COX-2, and Pro-Inflammatory

Mediators. *Immunol. Invest.* **2016**, *45*, 349–369.

(59) Moghadam-Kia, S.; Werth, VP. Prevention and treatment of systemic glucocorticoid side effects, *Int. J. Dermatol.* **2011**, *49*, 239–248.

(60) Caplan, A.; Fett, N.; Rosenbach, M.; Werth, V. P.; Micheletti, R. G. Prevention and Management of Glucocorticoid-Induced Side Effects: A Comprehensive Review: Ocular, Cardiovascular, Muscular, and Psychiatric Side Effects and Issues Unique to Pediatric Patients. *J. Am. Acad. Dermatol.* **2017**, *76*, 201–207.

(61) Lühder, F.; Reichardt HM. Novel Drug Delivery Systems Tailored for Improved Administration of Glucocorticoids. *Int. J. Mol. Sci*. **2017**, *18*, 1836-1855.

(62) Bartneck, M.; Marie, F.; Warzecha, K. T.; Bienert, M.; Bloois, L. Van; Trautwein, C.; Lammers, T.; Tacke, F. Liposomal Encapsulation of Dexamethasone Modulates Cytotoxicity , Inflammatory Cytokine Response , and Migratory Properties of Primary Human Macrophages. *Nanomedicine Nanotechnology, Biol. Med.* **2014**, *10*, 1209–1220.

(63) Quan, L.; Zhang, Y.; Crielaard, B. J.; Dusad, A.; Lele, S. M.; Rijcken, C. J. F.; Metselaar, J. M.; Kostková, H.; Etrych, T.; Ulbrich, K.; et al. Nanomedicines for Inflammatory Arthritis: Head-to-Head Comparison of Glucocorticoid-Containing Polymers, Micelles, and Liposomes. *ACS Nano* **2014**, *8*, 458–466.

(64) Bartneck, M.; Scheyda, K. M.; Warzecha, K. T.; Rizzo, L. Y.; Hittatiya, K.; Luedde, T.; Storm, G.; Trautwein, C.; Lammers, T.; Tacke, F. Fluorescent Cell-Traceable Dexamethasone-Loaded Liposomes for the Treatment of Inflammatory Liver Diseases. *Biomaterials* **2015**, *37*, 367–382.

(65) Montes-Cobos, E.; Ring, S.; Fischer, H. J.; Heck, J.; Strauß, J.; Schwaninger, M.; Reichardt, S. D.; Feldmann, C.; Lühder, F.; Reichardt, H. M. Targeted Delivery of Glucocorticoids to Macrophages in a Mouse Model of Multiple Sclerosis Using Inorganic-Organic Hybrid Nanoparticles. *J. Control. Release* **2017**, *245*, 157–169.

(66) Li, N.; Weng, D.; Wang, S.-M.; Zhang, Y.; Chen, S.-S.; Yin, Z.-F.; Zhai, J.; Scoble, J.; Williams, C. C.; Chen, T.; et al. Surfactant Protein-A Nanobody-Conjugated Liposomes Loaded with Methylprednisolone Increase Lung-Targeting Specificity and Therapeutic Effect for Acute Lung Injury. *Drug Deliv.* **2017**, *24*, 1770–1781.

(67) Li, S.; Chen, L.; Wang, G.; Xu, L.; Hou, S.; Chen, Z.; Xu, X. Anti - ICAM - 1 Antibody - Modified Nanostructured Lipid Carriers : A Pulmonary Vascular Endothelium - Targeted Device for Acute Lung Injury Therapy. *J. Nanobiotechnology.* **2018**, *16*, 1–14.

(68) Kluger, M. S.; Li, J. H.; Al-lamki, R.; Bradley, J. R.; Pober, J. S. Targeting of Tumor Necrosis Factor Receptor 1 to Low Density Plasma Membrane Domains in Human Endothelial. **2010**, *285*, 23868–23879.

(69) Ting-Yun Chuang, An-Jie Cheng, I-Ting Chen, Tien-Yun Lan, I-Hsuan Huang, Chung-Wai Shiau, Chia-Lin Hsu, Ya-Wen Liu, Zee-Fen Chang, Ping-Hui Tseng, ean-C. K. Suppression of LPS-Induced Inflammatory Responses by the Hydroxyl Groups of Dexamethasone. *Oncotarget,* **2017**, *8*, 49735–49748.

(70) Jeon, Y. J.; Han, S. H.; Lee, Y. W.; Lee, M.; Yang, K. H.; Kim, H. M. Dexamethasone Inhibits IL-1β Gene Expression in LPS-Stimulated RAW 264.7 Cells by Blocking NF-KB/Rel and AP-1 Activation. *Immunopharmacology*. **2000**, *48*, 173–183.

(71) Jain, N.; Sudhakar, C.; Swarup, G. Tumor Necrosis Factor-α-Induced Caspase-1 Gene

Expression. *FEBS J.* **2007**, *274*, 4396–4407.

(72) Clore, J.; Thurby-Hay, L. Glucocorticoid-Induced Hyperglycemia. *Endocr. Pract.* **2009**, *15*, 469–474.

(73) Elena*, C.; Chiara, M.; Angelica, B.; Chiara, M. A.; Laura, N.; Chiara, C.; Claudio, C.; Nicola, F. A. and G. Hyperglycemia and Diabetes Induced by Glucocorticoids in Nondiabetic and Diabetic Patients: Revision of Literature and Personal Considerations. *Current Pharmaceutical Biotechnology*. **2018**, *19*, 1210–1220.

(74) Van Zaane, B.; Nur, E.; Squizzato, A.; Gerdes, V. E. A.; Büller, H. R.; Dekkers, O. M.; Brandjes, D. P. M. Systematic Review on the Effect of Glucocorticoid Use on Procoagulant, Anti-Coagulant and Fibrinolytic Factors. *J. Thromb. Haemost.* **2010**, *8*, 2483–2493.

(75) Snapper, C. M. Immunology and Immunotherapy ClinMed. **2016**, *3*, 2–5.

4.7 Supporting Information

Characterization of the TNFR-MSNs materials

Mesoporous silica nanoparticles were synthetized following well-known procedures (as made MSNs). Surfactant was removed by calcination yielding calcined MSNs. The prepared solids were characterized by power X-ray diffraction (PXRD), TEM and N_2 adsorption-desorption curves. The pattern of as made MSNs corresponds to a hexagonal-ordered array (present in MCM-41 mesoporous silica nanoparticles) showing the characteristic peaks indexed as (100), (110), (200) and (210) (Figure S1 A). After calcination a significant shift of (100) reflection is observed in calcined MSNs (see Figure S1 B). The observed shift was ascribed to cell contraction induced by the condensation of silanol groups in the calcination step. The PXRD patterns for **NCO-RhB-MSNs** and **TNFR-RhB-MSNs** are showed in Figure S1 C and D. After the functionalization steps the low-angle reflections at (110), (200) and (220) were lost and the characteristic peak (100) reflection presented a slightly reduction in the intensity, associated to the reduced contrast after functionalization process. Nevertheless, the representative (100) reflection is maintained in all the cases, evidencing that the permanence of mesoporous scaffold in the gated nanoparticles.

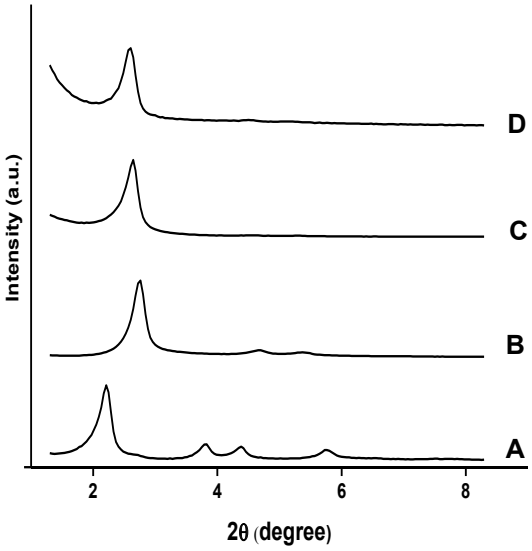

Figure S1. PXRD patterns from (A) as made MSNs (B) calcined MSNs (C) **NCO-RhB-MSNs** and (D) **TNFR-RhB-MSNs**.

In addition, the porosity of the prepared materials was studied by N_2 adsorption-desorption isotherms. The typical isotherm curve for calcined MSNs is shown in Figure S2 A. The curve corresponds to IV isotherm type in which an adsorption step at low P/P_0 values between 0.1 and 0.3 could be observed. This step indicated that nitrogen condensation takes place inside the mesopores by capillary and the specific area could be obtained by applying BET model. In addition, applying BJH model on the adoption curve at $P/P_0 < 0.8$, pore diameter and pore volume were calculated. The porosity features of MSNs are shown in Table 1 (see manuscript). Finally, the porosity of **TNFR-RhB-MSNs** was compared with the calcined MSNs, to confirm the proper loading and functionalization process. The adsorption-desorption isotherms of **TNFR-RhB-MSNs** are shown in Figure S2 B. The isotherm for **TNFR-RhB-MSNs** represents a typical curve of

systems with filled mesopores. The N_2 volume adsorbed, and thus the specific surface area, significantly decreases in comparison with the starting material.

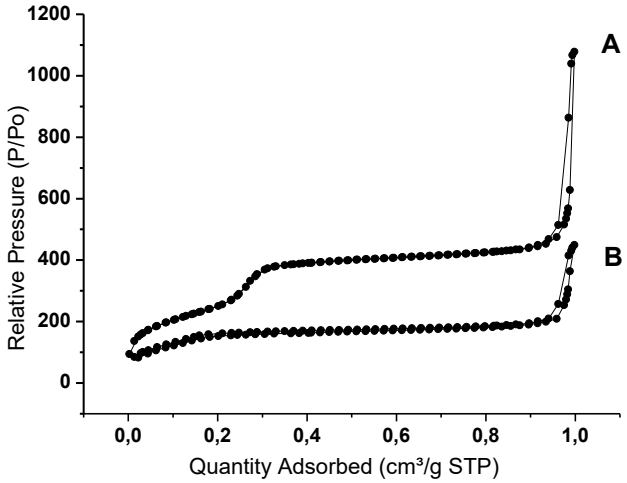

Figure S2. N_2 adsorption-desorption isotherms of (A) calcined MSNs and (B) **TNFR-RhB-MSNs** .

Macrophages polarization and phenotype characterization

Table 1. Macrophage markers used for qPCR.

Gene	Primer
CCR7	F 5'-TGGTGGTGGCTCTCCTTGTC-3'
	R 5'-TGTGGTGTTGTCTCCGATGTAATC-3'
CXCL10	F 5'-GAAAGCAGTTAGCAAGGAAAGGTC-3'
	R 5'-ATGTAGGGAAGTGATGGGAGAGG-3'
CD206	F 5'-ACCTCACAAGTATCCACACCATC-3'
	R 5'-CTTTCATCACCACACAATCCTC-3'

To study the activity of **TNFR-Dex-MSNs** in pro-inflammatory macrophages, first we established and characterized a model of macrophages polarization. The

THP-1 monocytes, M0 macrophages, pro-inflammatory M1 macrophages and anti-inflammatory M2 macrophages were established as we described above. In order to discriminate the pro-inflammatory macrophages we compared different inflammatory markers through gene expression and the levels of soluble cytokines in the different cell types.

Macrophage M1 polarization was then assessed by measuring the expression of the M1marker IL-1β, which is a pro-inflammatory cytokine, and CCR7 and CXCL10 as pro-inflammatory marker proteins at the mRNA level using RT-qPCR (Figures S3 C and E). As we expected, after IFN-γ combined with LPS treatment, an increased pro-inflammatory expression profile was obtained for M1 pro-inflammatory macrophages. IL-1β were expressed in M0 macrophages and M2 anti-inflammatory macrophages at less level, this could be due to PMA used for monocyte-to-macrophage differentiation, which has been described to up-regulate their expression. We also observed significant expression of the CCR7 and CXCL10 genes. In contrast, the anti-inflammatory M2 profile was characterized by studying the mRNA abundance of the mannose receptor CD206 mainly characteristic of M2 macrophages and the anti-inflammatory cytokine IL-10 was measured by ELISA. The expression pattern of CD206 was confirmed and high levels of IL-10 were observed for M2 polarized cells. In contrast, no expression of pro-inflammatory markers was evidenced in anti-inflammatory M2 macrophages and no anti-inflammatory pattern was exhibited by M1 macrophages. Moreover, the inflammatory cell death called pyroptosis was characterized in the different cell types by measuring the LDH activity. As could observe in Figure S3 D a higher level of LDH was achieved by pro-inflammatory M1 macrophages attributed to their IFN-γ and LPS activation. In contrast, low levels of LDH were registered in no activated THP-1 and M0 macrophages and no evidence of pyroptosis was observed in anti-inflammatory M2 macrophages. In

conclusion, polarizing THP-1 monocytes with PMA for 24h then treated with IFN-Ɣ for another 24 h and finally with LPS during 3 h, induced their differentiation into pro-inflammatory M1 macrophages.

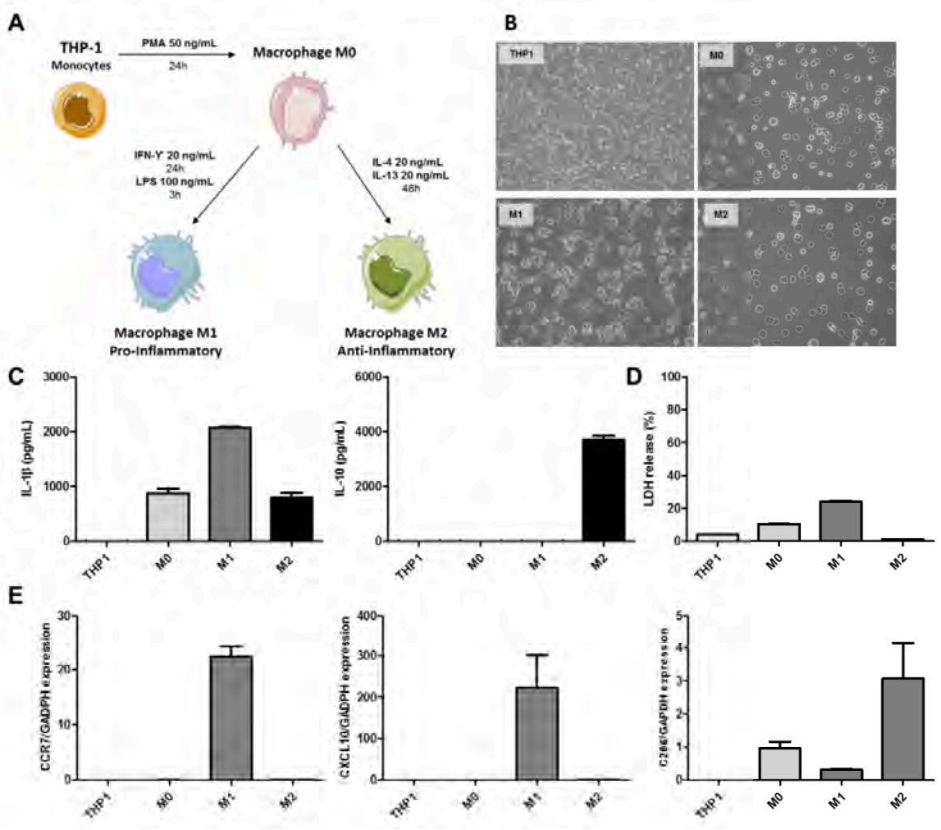

Figure S3. Macrophage polarization from THP-1 monocyte cells. (A) Schematic representation of THP-1 derived macrophages. (B) Phase contrast microscope image of THP-1, M0 macrophages, pro-inflammatory M1 macrophages and anti-inflammatory M2 macrophages. (C) Pro-inflammatory IL-1β levels (left) and anti-inflammatory IL-10 levels (right and D) pyroptosis inflammatory cell death levels in the different cell populations. (E) Relative gene expression of CCR7, CXCL10 and CD206 markers (from left to right) in inflammatory cells.

Anti-inflammatory activity of TNFR-Dex-MSNs in THP-1 monocytes cells

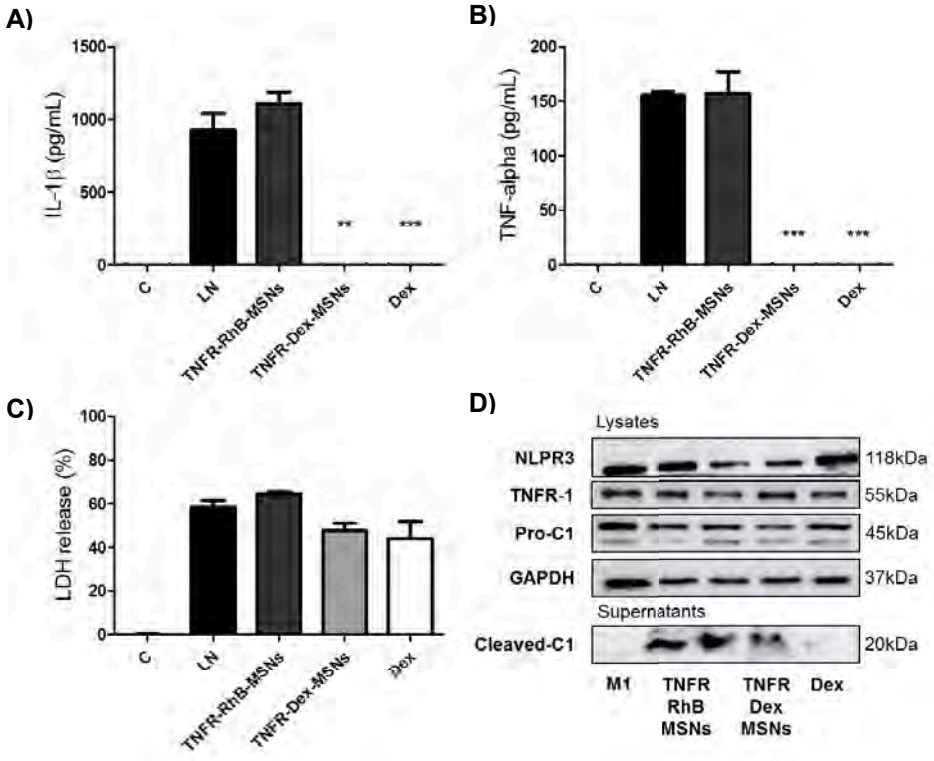

Figure S4. Analysis of inflammatory response in THP-1 cells in the presence of TNFR-Dex-MSNs stimulated with LPS + NG. (A) IL-1β and (B) TNF-α cytokines levels from cell supernatants measured by ELISA. (C) LDH release profile detected in cell supernatants as inflammatory cell death marker. (D) Western blot detection of proteins involved in the inflammatory response. Levels of cleaved capase-1 measured in cell supernatants and NLPR3, TNFR1, pro-Caspase 1, detected in cell lysates using GAPDH as reference protein. Data represent the means ± SEM of at least three independent experiments.

Table 2. Primary antibody used in western blot

Protein	*Antibody*	*Molecular weight (kDa)*
NLPR3	NLRP3 (D4D8T) Rabbit mAb #15101 from Cell Signaling	118
TNFR1	TNF-R1 (C25C1) Rabbit mAb #3736S from Cell Signaling	55
Pro-Caspase 1	Caspase-1 antibody, Rabbit, #2225 from Cell Signaling	45
GAPDH	Anti-GAPDH antibody, Mouse monoclonal, G8795 from Sigma Aldrich	37
Cleaved Caspase 1	Cleaved Caspase-1 (Asp297) (D57A2) Rabbit mAb, #4199 from Cell Signaling	20

Histopathological analysis of lungs. Determination of ALI score

In order to determine the degree of acute lung injury, the lung slides were stained with haematoxylin and at least 20 random high-power fields were independently analysed for each condition. ALI score was evaluated in different gradations of severity for main histological findings (neutrophils in the alveolar space, neutrophils in the interstitial space, hyaline membranes, proteinaceous debris filling the airspaces and alveolar septal thickening).

Table 3. Lung injury score system

	Score per field		
Parameter	0	1	2
A. Neutrophils in the alveolar space	None	1-5	>5
B. Neutrophils in the interstitial space	None	1-5	>5
C. Hyaline membranes	None	1	>1
D. Proteinaceous debris filling the airspaces	None	1	>1
E. Alveolar septal thickening	<2x	2x-4x	>4x

Score = [(20 x A) + (14 x B) + (7 x C) + (7 x D) + (2 x E)]/(number of fields 100)

Histopathological analysis of lungs with specific staining markers

Histopathological analysis of lung the sections were carried out with different markers to study the myeloperoxidase (MPO) activity associated to neutrophil infiltration, to determine the presence of alveolar proteinuria by the accumulation of macromolecules with PAS (Periodic Acid Schiff) stainer, to evaluate the deposition of collagen with Masson's trichrome as fibrosis marker and to determine the development of vascular inflammatrion upon the factor VIII/Von Willebrand factor staining.

In the case of myeloperoxidase marker, in normal conditions the sections are stained in a light blue colour whereas a brown or dark yellow staining characterized the activity of myeloperoxidase. As colud be observed in Figure S5, lungs sections from LPS and LPS+**TNFR-RhB-MNSs** were positive to myeloperoxidase and therefore indicating the accumulation of inflammatory cells, polymorphonuclear leukocyte type, in the lungs. In contrast, the melyoperoxidase activity was decreased in the LPS+**TNFR-Dex-MSNs** and LPS+Dex conditions, reflecting a reduced inflammation.

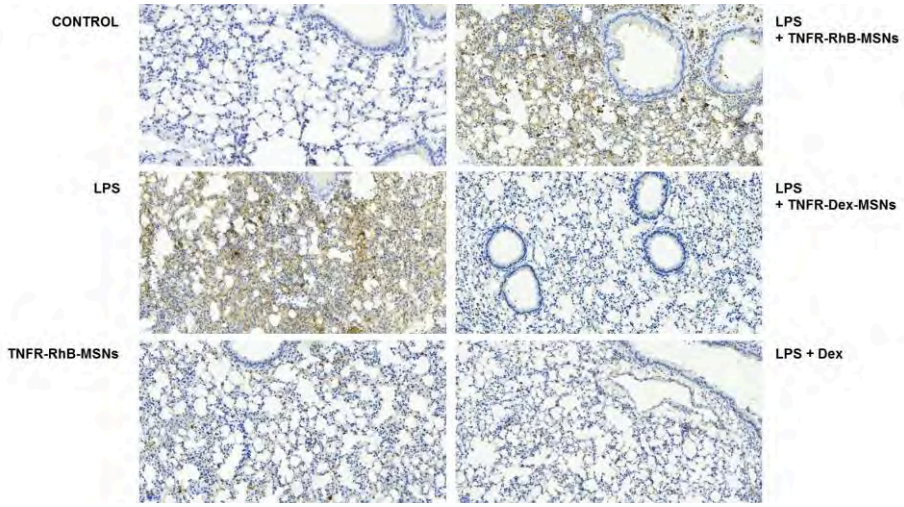

Figure S5. Representative images of myeloperoxidase stain of lung tissue from mice (n = 4-6).

Acute lung injury is characterized by an early exudative phase followed by a subacute proliferative phase and late fibrotic phase with alveolar epithelial cell hyperplasia and interstitial fibrosis. In our case, an acute phase was developed and Masson's staining was carried out to discard the proliferative and fibrotic stage. In non-fibrotic conditions the section is stained in a dark red colour whereas the presence of fibrotic associated fibres was marked in bright dark blue.

In this case the fibrotic deposition is discarded and therefore the fibrosis. All the sections showed a predominant dark red staining despite in some cases slightly blue fibres were founded and these little findings were considered non-significant due to the early stage includes intraalveolar edema with variable amounts of hemorrhage and fibrin deposition.

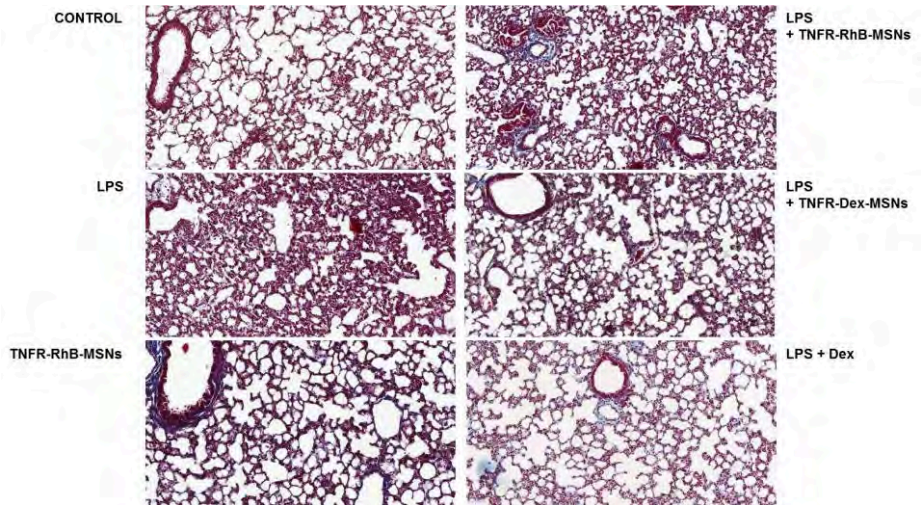

Figure S6. Representative images of Masson's marker of lung tissue from mice (n = 4-6).

The factor VIII/Von Willebrand factor was used to evaluate the platelet aggression and adhesion. When the factor VIII is marked a characteristic dark yellow or brown is observed. The bloods vessels from the endothelium usually appear marked due to they are a kind of internal control. Attending to the acute inflammatory processes could be related with a local vascular inflammation and in some cases lead to thrombosis, we evaluated the increase of factor VIII in blood vessels and in the alveolar septum and bronchoalveolar epithelium. The images from LPS and LPS+**TNFR-RhB-MSNs** exhibited the development of an acute inflammation with some microtrhombosis complication. It should be noted that in the case of LPS+Dex treatment a major factor VIII positive staining was observed

compared to LPS+**TNFR-Dex-MSNs** treatment, this fact could be associated to the dexamethasone derived side effects.

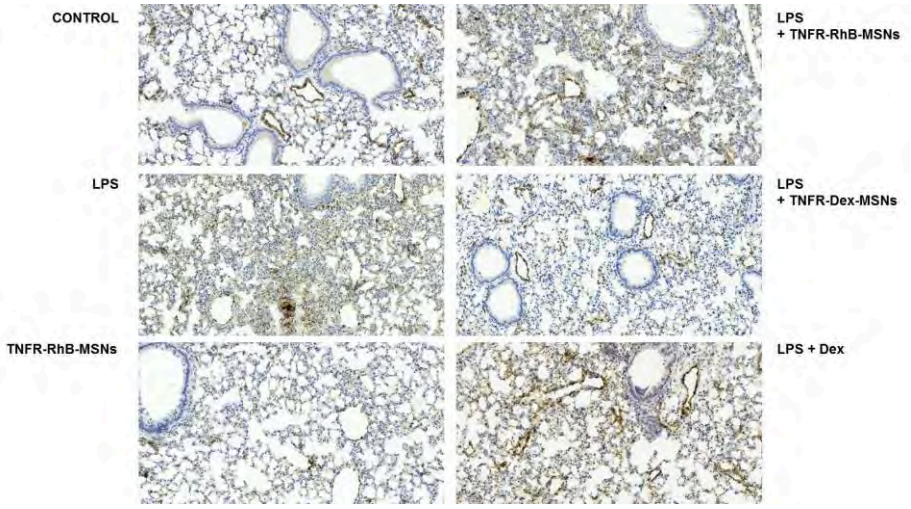

Figure S7. Representative images of factor VIII/von Willebrand factor staining of lung tissue from mice (n = 4-6).

Finally, the PAS marker was used to evaluate the alveolar proteinuria characteristic in the exudative phase of acute lung injury. The presence of this proteinuria is marked in pink or fuchsia and it is above all founded filling the alveolus and bronchial terminations. The images from LPS and **TNFR-RhB-MSNs** exhibited the high inflammation with desquamation to alveolar space (marked in pink), associated to the alveolar detriment with the subsequent accumulation of cellular debris.

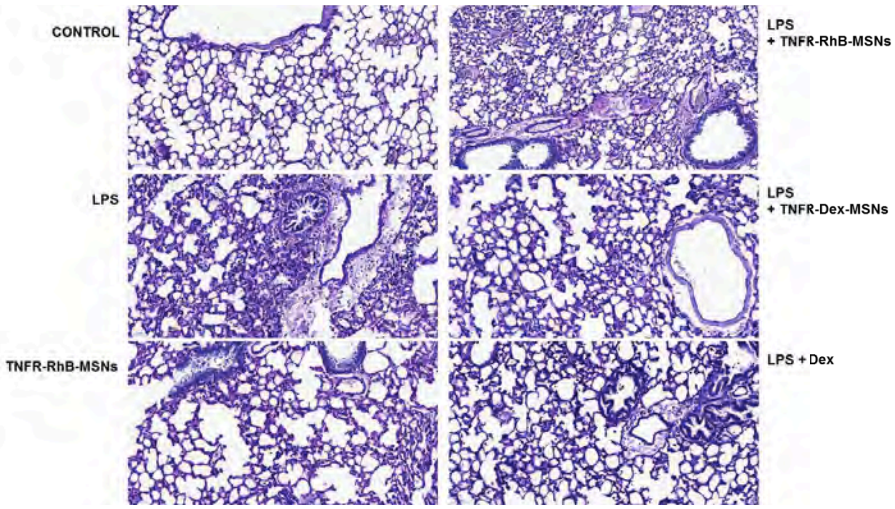

Figure S8. Representative images of PAS staining of lung tissues from mice (n = 4-6).

Chapter 5 | Targeted-lung delivery of QM-378 for acute lung injury treatment

Targeted delivery of the novel inhibitor of inflammasome QM-378 as alternative approach to acute lung injury therapy

Alba García-Fernández,[1,3,5] Mónica Sancho,[5,6] Viviana Bisbal-Velasco[6], Ramón Martínez-Máñez,[1,2,3,4,5]* Félix Sancenón[1,2,3,4,5] and Mar Orzáez,[5,6*]

[1] Instituto Interuniversitario de Investigación de Reconocimiento Molecular y Desarrollo Tecnológico (IDM), Universitat Politècnica de València, Universitat de València, Spain. E-mail: rmaez@qim.es

[2] Departamento de Química, Universitat Politècnica de València, Camino de Vera s/n, 46022 Valencia, Spain.

[3] CIBER de Bioingeniería, Biomateriales y Nanomedicina (CIBER-BBN).

[4] Unidad Mixta de Investigación en Nanomedicina y Sensores. Universitat Politècnica de València, IIS La Fe, Valencia, Spain

[5] Unidad Mixta UPV-CIPF de Investigación en Mecanismos de Enfermedades y Nanomedicina, Valencia, Universitat Politècnica de València, Centro de Investigación Príncipe Felipe, València, Spain.

[6] Centro de Investigación Príncipe Felipe. Eduardo Primo Yúfera, 3. Valencia 46012, Spain. E-mail: morzaez@cipf.es

Submitted

5.1 Abstract

Acute lung injury (ALI) is a complex and severe pulmonary disorder responsible for a high percentage of mortality and morbidity in intensive care unit patients. Current treatments are ineffective so the development of new efficient and specific therapies is an unmet medical need. The NLRP3 inflammasome, a macromolecular complex from the innate immune system, is strongly associated with the pathophysiology of this disease. Activation of the inflammasome, during ALI produces the release of the pro-inflammatory factors, such as interleukin-1β, and pyroptosis, a pro-inflammatory form of cell death that contributes to lung-damage spreading.

In this work, we present a novel inhibitor of the inflammasome, QM-378, as alternative pharmacotherapy to lead with the uncontrolled inflammation in ALI. Furthermore, attending to the need of specific therapies with improved capacity to deliver drugs to the inflamed lungs, the QM-378 drug is incorporated into mesoporous silica nanoparticles capped with a peptide (**TNFR-QM-MSNs**) to target the TNFR-1 receptor in pro-inflammatory macrophages. The prepared **TNFR-QM-MSNs** nanoparticles are able to deliver the cargo in a controlled manner after the preferentially uptake by pro-inflammatory macrophages and exhibit anti-inflammatory activity in activated THP-1 monocytes and pro-inflammatory M1 macrophages. Finally, the therapeutic effect of **TNFR-QM-MSNs** to inhibit inflammatory response and lung injury was successfully demonstrated in a LPS-mouse model of ALI. The results suggest the potential of **TNFR-QM-MSNs** as candidate to lead with ALI. Moreover, the encapsulation of QM-378 has a crucial role to enhance the therapeutic effect, which could help to overcome clinical limitations of current treatments.

5.2 Introduction

Inflammatory pulmonary disorders are a major health concern due to the high morbidity and mortality in critical ill patients. In particular, acute lung injury (ALI) is an early phase of acute respiratory distress syndrome (ARDS) characterized by severe lung inflammatory response and pulmonary injury with mortality values that reach the 39- 46% of hospitalized patients.[1–4] The main treatments for ALI are focused on supportive therapies based on mechanical ventilation and pharmacological medication with corticosteroids.[5–7] Although many research efforts have been carried out in last years, the molecular and cellular mechanisms involved in ALI development still remain unclear and the effective prevention and treatment has not been successfully achieved.[8] The progression of the disease to the uncontrolled lung inflammation is regulated by the activated alveolar macrophages and aggravated by the associated pro-inflammatory cell death in the lung tissue[9,10]. In particular, interleukin-1β (IL-1β) is a key player in disease evolution being responsible of increased lung vascular permeability and pulmonary edema.[11] Recent studies have demonstrated the role of the NLR family pyridine domain 3 (NLPR3) inflammasome in ALI.[12–15] NLRP3 is an intracellular receptor from the innate immune system that, in response to diverse damage signals, binds to the adaptor apoptosis-associated speck-like protein containing a CARD domain (ASC) to finally recruit and activate the inflammatory protease procaspase-1. Once activated, capase-1 cleaves pro-IL-1β and -18 to their active forms that are released from the cell contributing to inflammation.[16,17] Besides, caspase-1 also cleaves gasdermin D resulting in the formation of pores in the cellular membrane, which induces the pro-inflammatory form of cell death known as pyroptosis.[18,19] Due to the critical role of NLRP3 in the pathogenesis of ALI, the inflammasome key mediators have become promising pharmacological targets[13,20,21] and in recent years inhibitors of

caspase-1 activity,[22,23] antagonists of interleukin-1 receptor[24] and other anti-inflammatory compounds (such as flavonoids or antioxidants) have been analysed in ALI animal models with positive results.[25–28]

An important issue to be taken into account for the development of effective ALI treatments is the fact that the efficient delivery of drugs to the inflamed lungs is still an unresolved challenge.[29,30] In this scenario, the development of nanomedicines to target lungs in ALI has become an intensive area of research.[31,32] The use of nanoparticles as reservoirs provides an improvement in the bioavailability of the drug to target organs, especially when poorly soluble drugs are used, resulting in an enhanced therapeutic effect that usually results in minimizing drug toxicity. In the last years, several nanoparticulated systems based on organic polymers,[33,34] lipid nanocarriers[35,36] and inorganic materials[37] have been developed to deliver drugs to treat ALI. However, among them mesoporous silica nanoparticles (MSNs) have been poorly studied for this application. MSNs have been widely used in different biomedical applications due to their unique properties, such as high loading capacity, stability, biocompatibility and easy surface functionalization.[38–40] Moreover, the possibility of functionalize the external surface of MSNs make them excellent candidates for the preparation of gated materials, which display cargo delivery only upon the presence of certain chemical, biochemical or physical stimuli.[41–43] Moreover, when working with nanoparticles one can take advantage of the intrinsic capacity of macrophages to take nanomaterials and transport them to the inflamed site of action.[44–47] This effect is known as the Extravasation through Leaky Vasculature and Inflammatory cell-mediated Sequestration (ELVIS) mechanism. Moreover, two additional properties of MSNs make them suitable nanocarriers for the design of nanomedicines for ALI treatment. One is described the preferentially accumulation of MSNs in lungs[48–50] and the other is the possibility of anchoring

targeting (bio)molecules in the nanodevice to target selected cells/organs. At this respect, the use of antibodies or peptides to target pro-inflammatory macrophages has been widely described and some examples described their use for ALI treatment.[51–53]

Dealing with ALI treatments, some of us have recently described the inflammasome inhibition features of a 1,3-dihydro-2*H*-indol-2-one derivative (QM-378), which interferes with the binding of ASC to procaspase-1. One of the main advantages of this inhibitor is the point of action, which circumvents caspase-1 activation, thus producing the inhibition of IL-1β release and, more interestingly, interfering with pyroptosis more efficiently than caspase-1 direct inhibitors. Hence, QM-378 blocks pro-inflammatory signalling spread (unpublished results). Attending to the fact that some therapies blocking inflammatory cytokines are only partially successful and the need to improve the drug biodistribution in lungs,[54–56] the combination of QM-378 therapy with targeted nanodevices is an attractive strategy to limit injury and inflammation in ALI.

Taking into account the above mentioned facts, we report herein the preparation of MSNs loaded with the anti-inflammatory drug QM-378 and capped with a peptide containing the binding sequence of the tumour necrosis factor receptor (TNFR)-1 (**TNFR-QM-MSNs**) aiming to target macrophages in inflamed lungs.[57] The nanomedicine is tested *in vitro* in pro-inflammatory macrophages and *in vivo* in an LPS-induced ALI model.

5.3 Materials and methods

5.3.1. Synthesis of MSNs

A CTABr solution in deionized water (1 g, 2.74 mmol) was prepared and then NaOH (3.5 mL, 2 M) was added. The solution was stirred and the temperature adjusted to 80ºC. Then TEOS (5 mL, 2.57 x 10^{-2} mol) was added dropwise to yield the as-made MSNs. The finally mixture was stirred for 2 h yielding a white precipitate, which was isolated by centrifugation and washed until neutral pH with deionized H_2O. The material was dried and the final MSNs were obtained after calcination process at 550ºC in an oxidant atmosphere to remove the surfactant template.

5.3.2. Synthesis of NCO-RhB-MSNs

For MSNs loading, 38.32 mg of rhodamine B (0.8 mmoles/g solid) were suspended in anhydrous CH_3CN (10 mL) and stirred overnight at room temperature. Then (3 isocyanatopropyl) triethoxysilane (124.93 µL, 5 mmoles/g solid) was added and the suspension stirred 5.5 h in order to functionalize the external surface of MSNs. The solid was isolated by centrifugation, washed with CH_3CN and dried at 37ºC obtaining a pink solid.

5.3.3. Synthesis of TNFR-RhB-MSNs

The TNFR-1 peptide (GGGGFIGLMYRYQRWKSKLY) was covalently attached onto the grafted MSNs through the formation of urea bonds. For this purpose **NCO-RhB-MSNs** (30 mg) were suspended in CH_3CN (2 mL). On the other hand, a solution of the peptide (30 mg) was prepared in H_2O (2 mL) and added to the nanoparticles suspension together with triethylamine (80 µL). The mixture was

stirred at room temperature for 2 h and then the solid was isolated by centrifugation, washed with water and with PBS. Finally, the final solid was dried at 37ºC.

5.3.4. Synthesis of NCO-QM-MSNs

The pores of the MSNs were loaded with QM-378 using an impregnation method. For this purpose, a saturated solution of QM-378 (26 mg in 1 mL of DMSO) was prepared and separated in two aliquots. 50 mg of MSNs were extended on a plate and a first 500 µL of QM-378 suspension was added dropwise. The mixture was dried at 37ºC and then a second cycle of impregnation was carried out. The QM-378-loaded MSNs were obtained after drying the solid at 37ºC. Then, the loaded nanoparticles were suspended in anhydrous CH_3CN and an excess of (3-isocyanatopropyl) triethoxysilane (32.48 µL, 5 mmoles/g solid) was added to the suspension. The solid was stirred at room temperature for 5.5 h and then was collected by centrifugation, washed with CH_3CN and dried at 37ºC to obtain **NCO-QM-MSNs**.

5.3.5. Synthesis of TNFR-QM-MSNs

The TNFR-1 peptide (40 mg) was dissolved in H_2O (2 mL) and then added to a **NCO-QM-MSNs** suspension (40 mg in 2 mL of CH_3CN). Finally, triethylamine (80 µL) was added and the mixture was stirred at room temperature for 2 h. The resulting solid was obtained by centrifugation, washed with water and PBS and finally, dried at 37ºC to yield **TNFR-QM-MSNs**.

5.3.6. Standard characterization procedures of prepared materials

The prepared materials were characterized by standard techniques. Powder X-ray diffraction patterns were obtained on a Seifert 3000TT diffractometer using CuKα radiation. Transmission electron microscopy (TEM) images were obtained in a Philips CM-10. Micromeritics ASAP2010 automated sorption analyser was used to record N_2 adsorption-desorption isotherms. Thermo-gravimetric analysis were performed on a TGA/SDTA 851e Mettler Toledo equipment, using an oxidant atmosphere (Air, 80 mL/min) with a heating program consisting on a heating ramp of 10°C per min from 393 K to 1273 K and an isothermal heating step at this temperature for 30 min. HPLC studies were carried out with a Merck Hitachi L-2130 HPLC pump, an L-2200 autosampler and a Lichrospher®100 C18 (150 × 3.9 mm) column using gradients of CH_3CN-H_2O with 0.1% TFA as the mobile phase.

5.3.7. Drug delivery studies

To evaluate the capping features of TNFR1 peptide, **TNFR-RhB-MSNs** were suspended in PBS at pH 7.4 (mimicking physiological conditions) or in lysosomal extract at pH 5 (to mimic endocytic cellular compartments). Lysosomal extract was purified from animal tissues in accordance to Lysosome Isolation Kit (LYSISO1) following the provided instructions. To perform the delivery studies, 1 mg of the nanoparticles were suspended in 2 mL of PBS or 2 mL of lysosomal extract and stirred at 37ºC respectively. At scheduled times aliquots were isolated by centrifugation and dye release was followed by the fluorescence emission band of rhodamine B at 575 nm (λ_{ex} =555 nm).

5.3.8. Cell culture conditions

Human leukemic monocyte THP-1 cells were obtained from the German Resource Centre for Biological Materials (DSMZ) and were maintained in RPMI-1640 supplemented with 10% of FBS at 37°C in an atmosphere of 5% carbon dioxide and 95% air. For macrophage polarization from THP-1 cells, 800,000 cells/mL were seeded in a 6-well plate and derived into non-polarized macrophages with the addition of 50 ng/mL phorbol 12-myristate 13-acetate (PMA) for 24 h of incubation in RPMI medium. Then, medium was replaced with complete RPMI 1640 supplemented with 1% FBS to differentiate macrophages to pro-inflammatory (M1) or anti-inflammatory (M2) macrophages phenotype. For M1 polarization, 20 ng/mL of interferon-ϒ (IFN-ϒ) was added and cells were incubated for 24 h, and finally incubated with LPS (100 ng/Ml) for 3 h. For M2 polarization, IL-4 and IL-13 were added (20 ng/mL) for 48 h.

5.3.9 TNFR-1 characterization in pro-inflammatory macrophages

In order to confirm the TNFR-1 expression profile western blot analysis in the different inflammatory cells were performed. For this purpose, THP-1 cells were cultured and polarized to M0 macrophages and M1 pro-inflammatory macrophages as described in section 2.8. Whole cell extracts were obtained by scrape-collecting in 50 µL of lysis buffer (25 mM Tris-HCl pH 7.4, 1 mM EDTA, 1 mM EGTA and 1% SDS plus protease and phosphatase inhibitors). Lysates were separated by SDS-PAGE electrophoresis, transferred to nitrocellulose membranes, blocked with 5% non-fat milk and incubated with TNFR-1 (C25C1 from Cell Signalling) antibody overnight. GAPDH expression (MA5-15738 from Invitrogen) was also analysed in cell lysates as reference protein for normalization. Membranes were washed and incubated with the correspondent secondary

antibody. Finally horseradish peroxidase-conjugated secondary antibody was incubated with the membranes and chemiluminescent signal was detected using Amersham Imager 600 instrument.

5.3.10. Cytotoxicity cell studies with TNFR-MSNs

The cytotoxic effect of **TNFR-RhB-MSNs** was assessed in biocompatibility studies by WST-1 assay and LDH activity assay measuring the inflammatory cell-death pyroptosis. For this purpose, THP-1 and lung A549 cells were seeded in a 96-well plate and treated with **TNFR-RhB-MSNs** at 0, 25, 50, 100 and 200 µg/mL for 24 h. To determine cell viability, WST-1 was added and after 1 h absorbance at 595 nm was registered in a Wallac 1420 workstation. For LDH activity measurement, cell supernatants were collected and Lactase Assay Kit II was used following the manufacturer's instructions. THP-1 cells were treated 1% Triton-X100 as positive control to normalize LDH activity.

5.3.11. Targeted cellular uptake studies

The targeting effect of the **TNFR-RhB-MSNs** was evaluated in THP-1 cells and polarized pro-inflammatory (M1) macrophages by confocal microscopy and flow cytometry studies. Moreover, to confirm the selectivity of **TNFR-RhN-MSNs**, a similar solid containing a scrambled-peptide sequence (**Rd-RhB-MSNs**) was prepared. THP-1 cells were seeded in a 6-well plate and polarized to M1 macrophages as previously described. Then, flow cytometry studies were carried out to determine the nanoparticles uptake by the inflammatory cells. THP-1 monocytes and M1 macrophages were treated with **TNFR-RhB-MSNs** and **Rd-RhB-MSNs** solids (50 µg/mL) and, after 30 min, cells were washed with PBS and media replaced to remove the non-internalized nanoparticles. Then, cells were

incubated for a total time of 1 and 4 h in the presence of nanoparticles. Finally, cells were washed and collected for rhodamine B detection by flow cytometry. The single-cell fluorescence determinations were realized using CytoFLEX S instrument (Beckman-Coulter, USA) equipped with 4 lasers and 13 fluorescence detectors and analysed in the CytoFLEX software. Nanoparticle internalization was confirmed in THP-1 cells and pro-inflammatory (M1) macrophages by confocal microscopy. For this purpose cells were seeded over glass-cover slips in 6-well plates and treated with **TNFR-RhB-MSNs** and **Rd-RhB-MSNs** (50 μg/mL) for 30 min. Then non-internalized nanoparticles were removed by replacing media and cells were incubated for a total time of 1 and 4 h. For confocal microscopy analysis, cells were washed with PBS and Hoechst 33342 nuclei stain was added at 2 μg/mL. The fluorescence signal was followed using a Leica TCS SP8 confocal microscope.

5.3.12. Anti-inflammatory activity of TNFR-QM-MSNs in inflammatory cells

The anti-inflammatory activity of **TNFR-QM-MSNs** was studied in the pro-inflammatory (M1) macrophages and in THP-1 cells. In the case of THP-1, cells were seeded in a 6 well-plate at 800,000 cells/mL in RPMI 1% FBS and incubated for 24 h. Then, cells were treated with **TNFR-QM-MSNs** at 25 μg/mL suspended in PBS (being an equivalent dose of 6 μM of QM-378) and free-formulated QM-378 was added at 20 μM in DMSO as reference. Moreover, **TNFR-RhB-MSNs** (25 μg/mL) were used as control. After 30 min of treatments, lipopolysaccharide (LPS) from *Escherichia coli* (100 ng/mL) was added for 3 h and Nigericin at 20 μM during the last 30 min of incubation in order to activate the NLPR3 inflammasome. In the case of pro-inflammatory (M1) macrophages, THP-1 were derived with PMA as described above and after 24 h of incubation, media was replace for RPMI 1% FBS

and IFN-Ɣ at 20 ng/mL was added for 24 h. Then, treatments were added in a similar manner as THP-1 cells. After 30 min of the addition, lipopolysaccharide (LPS) from Escherichia coli (100 ng/mL) was added for 3 h and Nigericin (10 µM) during the last 30 min of incubation.

The activity of **TNFR-QM-MSNs** was examined by measuring the amount of IL-1β and TNF-α secreted in the cell culture supernatants of inflammatory cells by ELISA kit following supplier's instructions. In addition, LDH activity was measured in cell supernatants to determine the pyroptosis cell death using the LDH Assay Kit II following manufacturer instructions. Finally, the inflammasome components were characterized by western blot analysis both in cell lysates and supernatants from THP-1 cells and pro-inflammatory (M1) macrophages. The proteins studied in cell lysate were NLPR3, TNFR-1, pro-Caspase-1, pro-Gasdermin D (GSDMD), N-ter Gasdermin D and GAPDH as protein reference to normalize the expression levels. In cell supernatants, cleaved Caspase-1 (p20) was analysed. Whole extracts were obtained from cells using a lysis buffer (25 mM Tris-HCl pH 7.4, 1 mM EDTA, 1 Mm EGTA and 1% SDS plus protease and phosphatase inhibitors) and supernatants samples were collected and concentrate by lyophilisation. The samples were separated by SDS-PAGE, transferred to nitrocellulose membranes, blocked with 5% non-fat milk and incubated with the different primary antibody in each case (see supporting information) overnight at 4°C. Finally, membranes were incubated with correspondent secondary antibody conjugated with horseradish peroxidase and chemiluminescence detection of the bounded antibody was carried out in Amersham Imager 600 instrument.

5.3.13. Animals

Female and male CD-1 mice (10-12 weeks of age) were obtained from Charles River (France) and were maintained in a temperature-controlled room with a 12 h

light/dark cycle with access to food and water. The study was approved by the Ethical Committee for Animal Experiments at Centro de Investigación Príncipe Felipe (Valencia, Spain) and was performed in strict accordance with the recommendations in the Guide for Care and Use of Laboratory. Mice were distributed to six groups of 8-10 animals, formed by 4-5 male and 4-5 female. The different groups were: (1) control, (2) LPS treated, (3) administered with **TNF-RhB-MSNs**, (4) treated with LPS + **TNFR-RhB-MSNs**, (5) administered with LPS + **TNFR-QM-MSNs** and, (6) treated with LPS + QM-378.

The acute lung injury (ALI) was established upon LPS (*E.coli* 055:B5, 2.5 mg/kg) intra-tracheal instillation in 50 µL of saline for 24 h. Prior to LPS administration, the nanoparticles **TNFR-QM-MSNs** were administered intravenously by tail vein injection at 50 mg/kg in 200 µL of PBS, being equivalent of 3.6 mg/kg of free formulated QM-378. The free-drug was administered at 10 mg/kg in 200 µL of PBS and PBS vehicle was administered in the control and LPS animals. Moreover, **TNFR-RhB-MSNs** were administered at 50 mg/kg as nanoparticle control in 200 µL of PBS. For LPS instillation, the animals were previously anesthetized with ketamine (75 mg/kg) and dexmedetomidine (1 mg/kg) and then anaesthesia was reverted using 1 mg/kg of atipamezole. After 24 h of ALI development, the animals were euthanized with overdose of sodium pentobarbital. Bronchoalveolar lavage fluid (BALF), blood extraction and dissection of different organs were realized in order to examine the inflammatory response and pulmonary injury.

5.3.14. BALF analysis

For BALF obtaining we selected 6 of the 10 animals per group to perform a lung lavage using intra-tracheal injections of 250 µL of PBS. BALF was collected and centrifuged at 1,200 rpm for 5 min at 4°C to separate supernatant from cells. The cell pellet was suspended in PBS and total leukocyte number was analyzed by

flow cytometri by Acvlab (Valencia). BALF supernatants were used to measure the expression of TNF-α, IL-6 and IL-1β cytokines using ELISA kit following the supplier's instructions. Finally, the total protein expression in BALF was determined by BCA protein assay kit.

5.3.15. Histopathology analysis

Lungs from 4 of the 10 animals were selected and embedded with 4% paraformaldehyde. After this treatment, lungs were fixed in paraffin, cut with a microtome into 2 µm sections, placed on coated glass slides and stained by hematoxylin and eosin for histological evaluation to determine the ALI Score. The Leica ASP300 tissue processor was used to register the slides and the analysis was performed with the CaseViewer software. For ALI score evaluation, at least 20 random high-power fields were independently examined for each group. ALI score was examined in different gradations attending to mainly histological findings (neutrophils in the alveolar space, neutrophils in the interstitial space, hyaline membranes, proteinaceous debris filling the airspaces and alveolar septal thickening). In addition, the sections were analysed with different markers to evaluate the neutrophil presence by myeloperoxidase activity, the determination of alveolar proteinosis evaluating the accumulation of carbohydrates using PAS (Periodic Acid Schiff) stainer, the fibrosis development using Masson's trichrome to analyse the deposition of collagen and the vascular inflammation by factor VIII/Von Willebrand factor staining.

5.3.16. TNFR-RhB-MSNs biodistribution in ALI mouse model

The targeting features to inflamed lungs of **TNFR-RhB-MSNs** were confirmed *in vivo* monitoring the rhodamine B fluorescence in an IVIS spectrum imaging system

(PerkinElmer Inc.). For this purpose, lungs were harvested after the euthanasia and immediately analysed in the IVIS equipment using excitation wavelength of 535 nm and emission wavelength of 580 nm. In addition, the silicon presence, associated to MSNs, was quantified in selected organs (lungs, liver, kidneys, spleen and tail) by ICP-MS. The samples were digested with 1 mL of TMAH 25% into polytetrafluorethylene (PTFE) tubes. The digestion process was established at 80ºC for 2 h using a Bloc Digest 20 (Selecta). Finally, samples were diluted to 10 mL of water and filtered to measure Si in 7900 ICP-MS system in H_2 mode using germanium as an internal standard.

5.4 Results and discussion

5.4.1 Synthesis, characterization and cellular biocompatibility of the prepared nanodevices

With the aim of developing alternative pharmaceuticals and better formulations to treat ALI, we synthesized a nanoformulation based on gated MSNs loaded with the novel inflammasome inhibitor QM-378. MSNs were prepared using a well known synthetic procedure which used cetyltrimethylammonium bromide as structure directing agent and TEOS as silica source. The as-made MSNs were then calcined in order to remove the structure directing agent from the pore voids. MSNs were loaded with rhodamine B or with QM-378 and the external surface of the nanoparticles functionalised with (3-isocyanatopropyl)triethoxysilane (solids **NCO-RhB-MSNs** and **NCO-QM-MSNs**). Finally, pores were capped upon addition of TNFR1 peptide, which was linked onto the external surface through the formation of urea bonds. This synthetic procedure yielded the final nanoparticles **TNFR-RhB-MSNs** and **TNFR-QM-MSNs**

(Figure 1A). In both solids, the bulky anchored peptide plays a dual role as capping ensemble and as targeting ligand.

The structural and textural properties of **TNFR-RhB-MSNs**, **TNFR-QM-MSNs** and the intermediary solids, obtained during the different synthesis steps, were characterized by power X-ray diffraction (PXRD), TEM and N_2 adsorption-desorption isotherms. The presence of ordered mesoporous scaffold in all the prepared nanoparticles was confirmed by PXRD measurements which showed the (100) reflexion typical of mesoporous materials (Supporting Information). TEM images showed the spherical morphology of the prepared nanoparticles in which the pores were observed as alternate black and white stripes (Figure 1B). The textural properties were determined for calcined MSNs and **TNFR-RhB-MSNs** by N_2 adsorption-desorption isotherms (see supporting information). MSNs presented a surface area of 954.88 m_2/g, pore volume of 0.71 cm^3/g and pore size of 2.7 nm, compared to **TNFR-RhB-MSNs** with 436.39 m^2/g and 0.33 cm^3/g of surface area and pore volume respectively.

Dynamic light scattering measurements of the prepared nanoparticles showed a marked increase in its hydrodynamic diameter after each of the functionalization steps (see Figure 1C). At this respect, calcined MSNs presented a hydrodynamic diameter of 125 ± 33 nm which was enhanced to 184 ± 9 nm and to 267 ± 27 for **NCO-QM-MSNs** and **TNFR-QM-MSNs** respectively. The hydrodynamic diameter enhancement was ascribed to the grating of isocyanato propyl moieties and TNFR peptide. On the other hand, zeta potential of the calcined MSNs was -31 ± 2 due to the presence of silanolate moieties onto the surface of the nanoparticles. For **NCO-QM-MSNs** solid the zeta potential increased to 15 ± 1 due to QM-378 loading and functionalization of the external surface with isocyanatpropyl moieties. For the final **TNFR-QM-MSNs** nanoparticles the measured zeta potential was 16 ± 2. The small increase, when compared with

NCO-QM-MSNs solid, was ascribed to the proper grafting of TNFR peptide onto the external surface of the nanoparticles.

The amounts of cargo and gating peptide in **TNFR-RhB-MSNs** and **TNFR-QM-MSNs** were determined using thermogravimetric analysis and HPLC measurements. At this respect, **TNFR-RhB-MSNs** nanoparticles contained 0.18 mmol/g SiO_2 of rhodamine B and 0.03 mmol/g SiO_2 of TNFR peptide. Finally, amounts of 72.5 μg/mg SiO_2 of QM-378 and 0.03 mmol/g SiO_2 of peptide were measured for **TNFR-QM-MSNs** nanoparticles.

The controlled cargo release from **TNFR-RhB-MSNs** was evaluated in PBS at pH 7.4 (mimicking physiological conditions) or in lysosomal extract at pH 5 (to mimic endocytic cellular compartments). Rhodamine B delivery profiles in both conditions are depicted in Figure 1C. At pH 7.4 negligible rhodamine B release was observed (ca. 10% of the maximum release after 180 min) which contrast with the marked dye release found in the presence of the lysosomal extract. Poor delivery in the nanoparticles is ascribed to the presence of the bulky peptide anchored onto the external surface of the nanoparticles, whereas rhodamine B delivery is due to hydrolysis of the capping peptide by protease enzymes in the lysosomal extract. In the case of TNFR-QM-MSNs, attending to the poor solubility of the entrapped drug, it was not possible to monitor by HPLC the drug delivery profile. Nevertheless, similar controlled release profile is expected due to TNFR1 peptide acted as gatekeeper in the same way to TNFR-RhB-MSNs.

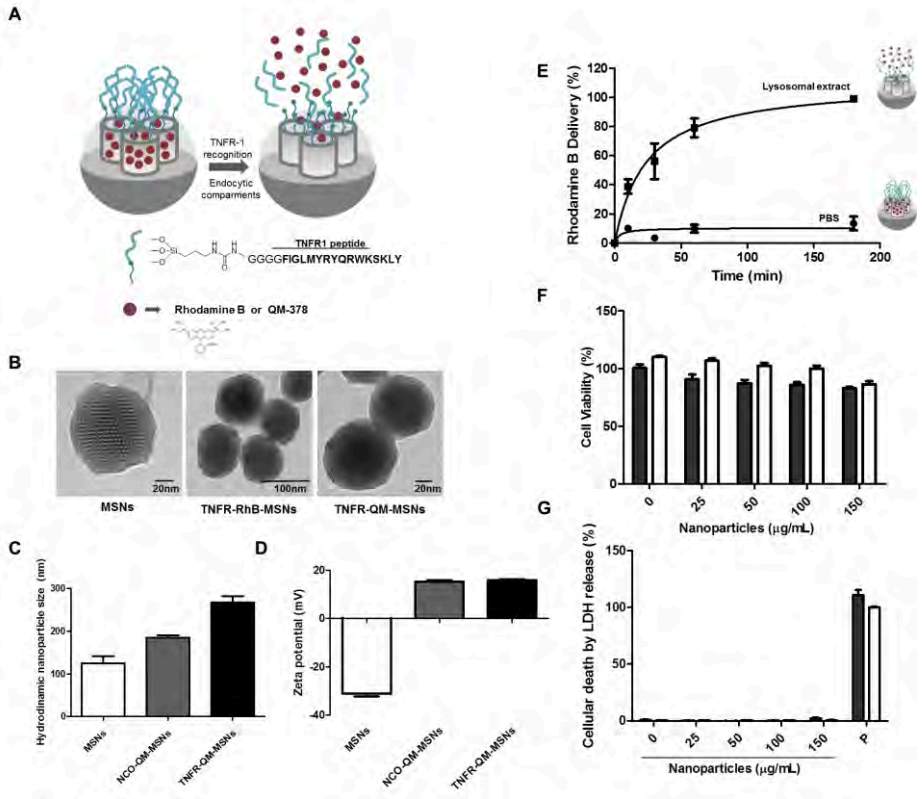

Figure 1. Synthesis and characterization of TNFR-RhB-MSNs and TNFR-QM-MSNs. (A) Representation of **TNFR-RhB-MSNs** and **TNFR-QM-MSNs** solids. (B) TEM images of MSNs, **TNFR-RhB-MSNs** and **TNFR-QM378-MSNs**. (C) Nanoparticle size of MSNs, **NCO-QM-MSNs** and **TNFR-QM-MSNs** determined by dynamic light scattering. (D) Zeta potential of MSNs, **NCO-QM-MSNs** and **TNFR-QM-MSNs**. (E) Rhodamine B release profiles from **TNFR-RhB-MSNs** in PBS at pH 7.4 and in the presence of lysosomal extract at pH 5-6. (F) Cell viability assays using **TNFR-RhB-MSNs** in THP-1 cells (dark bars) and A549 lung cells (white bars) by WST-1 and (G) cellular death using LDH release assay in the presence of **TNFR-RhB-MSNs**. P represents the positive control of lysate cells which is correlated with the high inflammatory cell death.

Biocompatibility of the nanoparticles in THP-1 monocytes and in the epithelial lung adenocarcinoma cell line A549 was evaluated in the presence of different

concentrations of **TNFR-RhB-MSNs** at 24 h by the cell proliferation WST-1 assay (see Figure 1D). As could be seen in Figure 1D, nanoparticles were well-tolerated by THP-1 and A549 cells at concentrations up to 150 μg/mL with viabilities in the 80-100% range. On the other hand, the ability of **TNFR-RhB-MSNs** to activate the immune system (and therefore an inflammatory response) was assessed by measuring the inflammatory cell death pyroptosis by LDH activity assay in THP-1 and A549 cells. **TNFR-RhB-MSNs** were unable to activate the immune system in both cell lines and a non-significant LDH release was observed in all cases indicating the absence of cellular death by necrosis or pyroptosis (Figure 1E). These results evidenced the biocompatibility of the capped mesoporous scaffold.

5.4.2. Cellular uptake studies in pro-inflammatory M1 macrophages

As explained above, the pro-inflammatory cytokine TNF-α has a relevant role in the outcome of pulmonary diseases and in particular in ALI.[58] The responsiveness of macrophages to the pro-inflammatory cytokine TNF-α depends on presence of the TNFR-1 and TNFR-2 receptors on the cellular surface. Binding of TNF-α to the TNFR-1 produces the activation of cell death signalling and contributes to inflammation. For these reasons, in a first step, we evaluated the presence of TNFR-1 receptor on the surface of THP-1 cells, M0 macrophages and pro-inflammatory M1 macrophages by western blot analysis. As could be seen in Figure 2A, pro-inflammatory M1 macrophages overexpress TNFR-1, making this cell surface receptor an appropriate candidate to target selectively those populations of macrophages. In fact, recent reports demonstrated that an anti-TNFR-1 antibody prevents pulmonary inflammation in ALI, reinforcing the relevance of the TNFR-1 receptor in this lung disease model.[52,59] In this scenario, the aim in the use of **TNFR-QM-MSNs** is the specific targeting to those activated macrophages that overexpress TNFR-1 and the intracellular release of the

inflammasome inhibitor QM-378 to eliminate their pro-inflammatory activity. To accomplish this objective, nanoparticles must be preferentially internalized by macrophages in a TNFR-1 dependent manner (see Figure 2B). In order to study the selectivity of **TNFR-RhB-MSNs** nanoparticles (*vide infra*) a similar solid containing the same cargo but capped with a scrambled peptide (KKRSLFGSLLVVGAVTMGTLFWRKK) was prepared (**Rd-RhB-MSNs**). Cellular uptake and cargo release of both solids were tested by confocal microscopy and by flow cytometry. As could be seen in confocal images in Figure 2C, the intensity of the rhodamine B fluorescence signal inside the inflammatory cells was significantly higher when using **TNFR-RhB-MSNs** than that observed in cells treated with **Rd-RhB-MSNs**, indicating a preferential internalization of **TNFR-RhB-MSNs** by M1 macrophages. Moreover, quantification of rhodamine B intensity of M1 macrophages treated with the nanopartilcles using flow cytometry showed also the preferential internalization of **TNFR-RhB-MSNs** (Figure 2D). These results indicate that TNFR-1 peptide, anchored onto the external surface of **TNFR-RhB-MSNs**, selectively recognized the TNFR-1 receptor present in the surface of M1 macrophages.

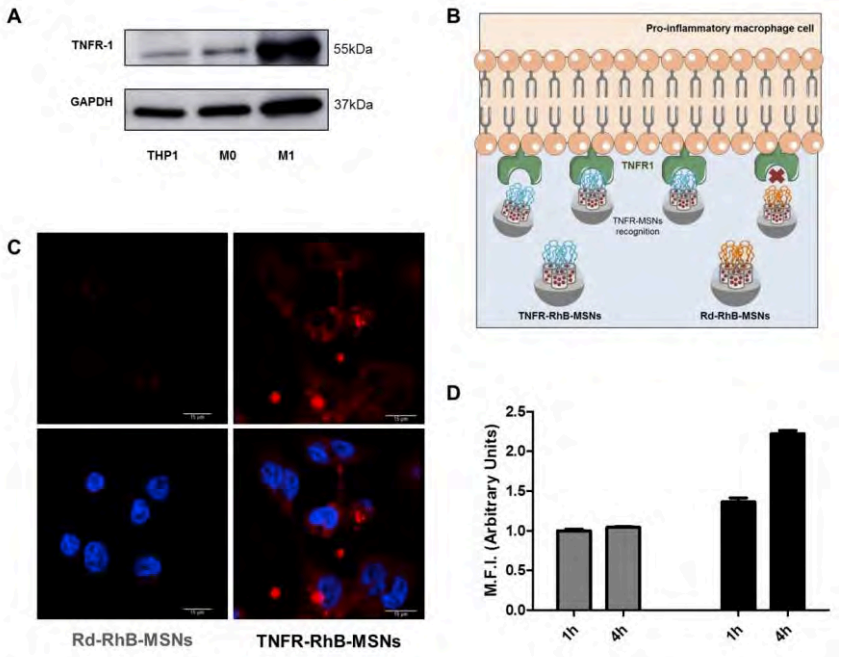

Figure 2. Targeting of TNFR-1 capped nanoaprticles to M1 Macrophages. (A) TNFR-1 expression profile in THP-1 monocytes, M0 macrophages and pro-inflammatory M1 macrophages. (B) Schematic representation of TNFR-1 recognition of **TNFR-RhB-MSNs** by pro-inflammatory macrophages compared to **Rd-RhB-MSNs**. (C) Confocal images of pro-inflammatory M1 macrophages after treatment with **Rd-RhB-MSNs** (left) or **TNFR-RhB-MSNs** (right) for 4 h. Rhodamine B is represented in red and DNA marker Hoechst 33342 in blue. (D) Rhodamine B intensity from pro-inflammatory M1 macrophages quantified by flow cytometry in the presence of **Rd-RhB-MSNs** (grey bars) or **TNFR-RhB-MSNs** (black bars) for 1 and 4 h. The data represent the means ± SEM of at least two independent experiments.

5.4.3. Cellular studies of the anti-inflammatory activity of TNFR-QM-MSNs

In order to test the ability of **TNFR-QM-MSNs** to attenuate the inflammatory response in cellular models, the NLPR3 inflammasome was stimulated in THP-1

monocytes and in pro-inflammatory M1 macrophages by activation with LPS and Nigericin. Under these conditions the activation of the inflammasome produces the cleavage of procaspase-1 to the active form caspase-1 that is secreted by the cell. As a consequence, the processing of pro-IL-1β induced the subsequent release of IL1-β and an increment in the pyroptotic cell death that is reflected in an increased lactate dehydrogenase (LDH) activity, a typically intracellular enzyme, in the extracellular milieu. In a first step, the expression, processing and secretion of the different components from the inflammasome activation cascade were analysed (Figure 3E and 3F). NLPR3 and caspase-1 protein expression in cell lysates was confirmed both in THP-1 monocytes and in M1 pro-inflammatory macrophages. The appearance of active capase-1 in cell supernatants after LPS/Nigericin treatment supports inflammasome activation. Interestingly, caspase-1 is reduced in the supernatants of cells treated with **TNFR-QM-MSNs** and with free QM-378, indicating that an inhibition of the inflammasome is taking place upon treatment. Finally, we also analysed full-length gasdermin D (GSDMD) and the appearance of N-ter GSDMD fragment cleaved by caspase-1 that is responsible of pyroptosis. Upon inflammasome activation the levels of full-length GSDMD decreased and the N-ter GSDMD fragment significantly increased. In contrast, **TNFR-QM-MSNs** and free QM-378 treatments induced a reduction of the N-ter GSDMD levels accompanied by a restoration of full length GSDMD, as expected by inflammasome inhibition.

In a second step, IL-1β levels and LDH activity in THP-1 cells (Figures 3A and 3C) and M1 macrophages (Figures 3B and 3D) was evaluated after treatment with **TNFR-RhB-MSNs**, **TNFR-QM-MSNs** and QM-378. As could be seen, both THP-1 monocytes and M1 pro-inflammatory macrophages showed high levels of IL-1β and increased extracellular LDH activity after LPS/Nigericin treatment. In the presence of **TNFR-RhB-MSNs** negligible changes in the IL-1β and LDH levels were

observed. However, treatment with **TNFR-QM-MSNs** or free QM-378 reduced drastically the levels of IL-1β and the LDH activity. Both facts indicated the reduction of the pyroptotic pro-inflammatory cell death induced by **TNFR-QM-MSNs** or free QM-378 that contributes to inflammation spreading.

The obtained results indicate that QM-378 encapsulated in **TNFR-QM-MSNs** preserves its activity as inflammasome modulator. One of the principal advantages of the use of QM-378 in the nanoformulation form is the improvement in its solubility. QM-378 is scarcely solubilised in water and DMSO should be used instead for cells treatment, whereas **TNFR-QM-MSNs** are suspended in PBS for its administration. On the other hand, in our experiments a similar reduction in IL-1β and LDH levels was observed when using **TNFR-QM-MSNs** and free QM-378 but the amount of the drug administered with the nanoformulation (6 μM) was 3.5-fold lower than that used with free QM-378 (20 μM). Additional advantages of the use of **TNFR-QM-MNSs** are the recognition of alveolar pro-inflammatory macrophages mediated by the TNFR-1 targeting peptide and the potential passive targeting (ELVIS effect) that should be verified in *in viv*o settings (*vide infra*).

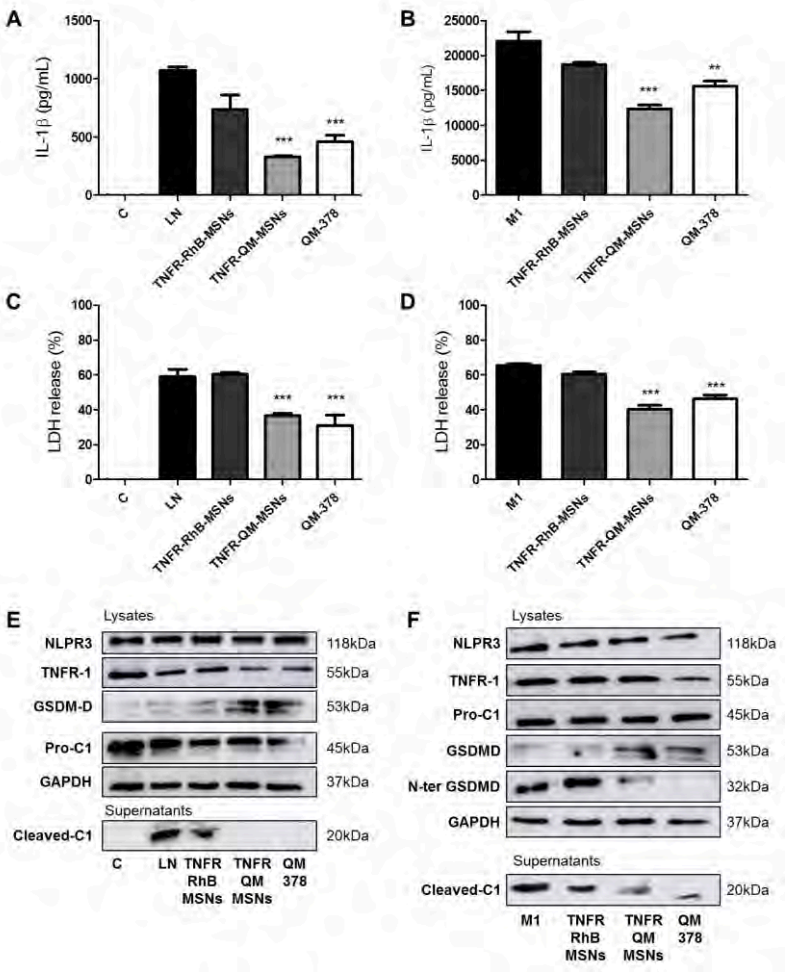

Figure 3. TNFR-QM-MSNs inhibition of inflammasome in human monocytes and macrophages. Inflammatory studies with **TNFR-RhB-MSNs** and **TNFR-QM-MSNs** in THP-1 cells (left) and pro-inflammatory M1 macrophages (right). (A and B) Quantification of IL-1β pro-inflammatory cytokine from cell supernatants by ELISA. (C and D) LDH release measured in cell supernatants as inflammatory cell death marker of pyroptosis. (E and F) Western blot analysis of different proteins involved in the inflammatory response. Levels of cleaved capase-1 were detected in cell supernatants and NLPR3, TNFR1, pro-Caspase 1, GSDMD and N-ter GSDMD detected in cell lysates. GAPDH was used as reference protein. Data represent the means ± SEM of at least three independent experiments.

5.4.4. *In vivo* targeting of inflamed lungs by TNFR-RhB-MSNs

To investigate the targeting of **TNFR-RhB-MSNs** to inflamed lungs we used an *in vivo* ALI mice model. In this model the inflammation was induced by intra-tracheal instillation of LPS. We monitored the presence of **TNFR-RhB-MSNs** in the lungs of animals either treated or not with LPS. 24 h after intravenous injection of nanoparticles, animals were sacrificed and rhodamine B accumulation in lungs was analysed quantifying fluorescence in an IVIS Spectrum (Figure 4A). A significant increase of fluorescence (quantification shown in Figure 4B) was observed in lungs of animals co-treated with **TNFR-RhB-MSNs** and LPS when compared with control animals in which inflammation was not induced. The targeting ability of **TNFR-RhB-MSNs** to inflamed lungs was also studied by the determination of silicon levels, associated to the presence of nanoparticles, in selected organs. The higher silicon content was identified in lungs of individuals treated with LPS and **TNFR-RhB-MSNs** when compared to mice treated with the nanomaterials in the absence of inflammation (Figure 4C). These results confirmed the preferential targeting of **TNFR-RhB-MSNs** in the inflamed lungs in an ALI model.

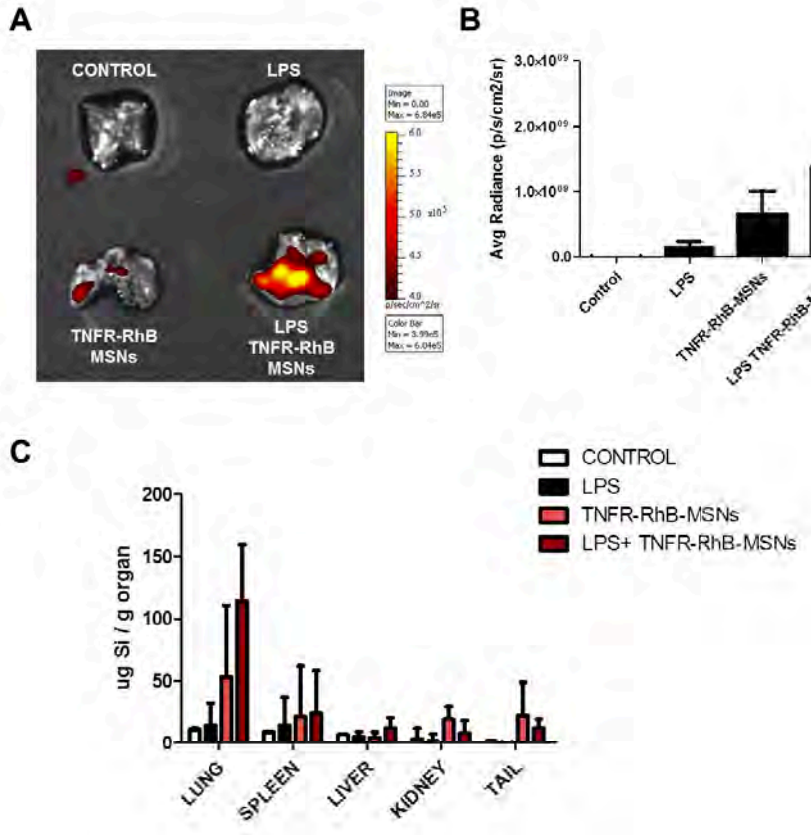

Figure 4. Targeting studies with TNFR-RhB-MSNs to inflamed lungs in an ALI mice model. (A) Representative lung images obtained using IVIS. (B) Quantification of rhodamine B associated fluorescence. (C) Bidiostribution pattern of silicon the in lung, liver, spleen, kidney and tail. The graph showed the µg of silicon per g of organ, measured by Inductively Coupled Plasma Mass Spectroscopy (ICP-MS). The data represent the mean ± SEM and statistical significance was determined using a one-way ANOVA (n = 4).

5.4.5. Anti-inflammatory activity of TNFR-QM-MSNs in ALI model

To study the therapeutic activity of **TNFR-QM-MSNs** in ALI, we analysed different inflammatory parameters upon treatment of mice with the nanoparticles. In our experiments, animals were treated with 10 mg/kg of QM-

378 as reference or **TNFR-QM-MSNs** at 50 mg/kg (equivalent to 3.6 mg/kg of QM-378) for 24 h and then animals were instilled intra-tracheally with LPS. The inflammatory profile and the effect of the treatments were evaluated after 24 h of LPS administration. The inflammatory response was analysed measuring the levels of pro-inflammatory cytokines and the total amount of leukocytes in bronchoalveolar fluid (BALF). The levels of the pro-inflammatory factors, TNF-α, IL-6 and IL-1β increased in BALF of animals treated with LPS (Figure 5B for IL-1β and Supporting Information for other pro-inflammatory factors). Animals treated with QM-378 or **TNFR-QM-MSNs** showed significant reduced levels of TNF-α, IL-6 and IL-1β (Figure 5A and Supporting Information). Moreover, after LPS treatment an increase of leukocytes was observed in BALF associated to the influx of inflammatory cells to injured lungs (Figure 5B). In comparison, in animals treated with QM-378 and **TNFR-QM-MSNs**, the leukocyte counts notably diminished (4.9- and 9.3-fold respectively). The reduction was more evident in animals treated with **TNFR-QM-MSNs**. In accordance with these results, evaluation of the systemic inflammatory parameters showed a reduced neutrophils/lymphocyte ratio in the case of animals treated with **TNFR-QM-MSNs** when compared to free QM-378 (Figures 5C and 5D). This reduced ratio is indicative of a better recovery from the inflammatory insult.[60] We also found that equivalent results in terms of inflammatory signalling were obtained between the groups treated with only LPS or LPS + **TNFR-RhB-MSNs**, indicating that the nanoparticles did not induce any inflammatory response in lungs.

Lung injury and recovery was also assessed by histological analysis, studying the alterations in alveolar tissue. Lung histology in ALI is mainly characterized by the alveolar damage accompanied by interstitial thickening, neutrophil accumulation, formation of hyaline membranes and other proteinaceous debris. In our experimental setting, lung sections for healthy animals show thin alveolar

walls, whereas clear disrupted lung architecture was observed in lungs from LPS treated mice (Figure 5E). Lung architecture was clearly restored in animals treated with **TNFR-QM-MSNs** and QM-378 (Figure 5E). Calculation of an ALI score following standard methods[61] showed the highest punctuation for the LPS groups in which the strongest injury was produced, while the score significantly diminished in the animal groups treated with **TNFR-QM-MSNs** and QM-378 (Figure 5F).

Overall our work demonstrates that **TNFR-QM-MSNs** inhibits the inflammatory response and lung injury in a LPS-mouse model of ALI. Moreover, encapsulation allowed improving the therapeutic effect of the free drug. This improvement was attributed to the encapsulation of the low soluble QM-378 as well as the preferential targeting of **TNFR-QM-MSNs** to inflamed lungs.

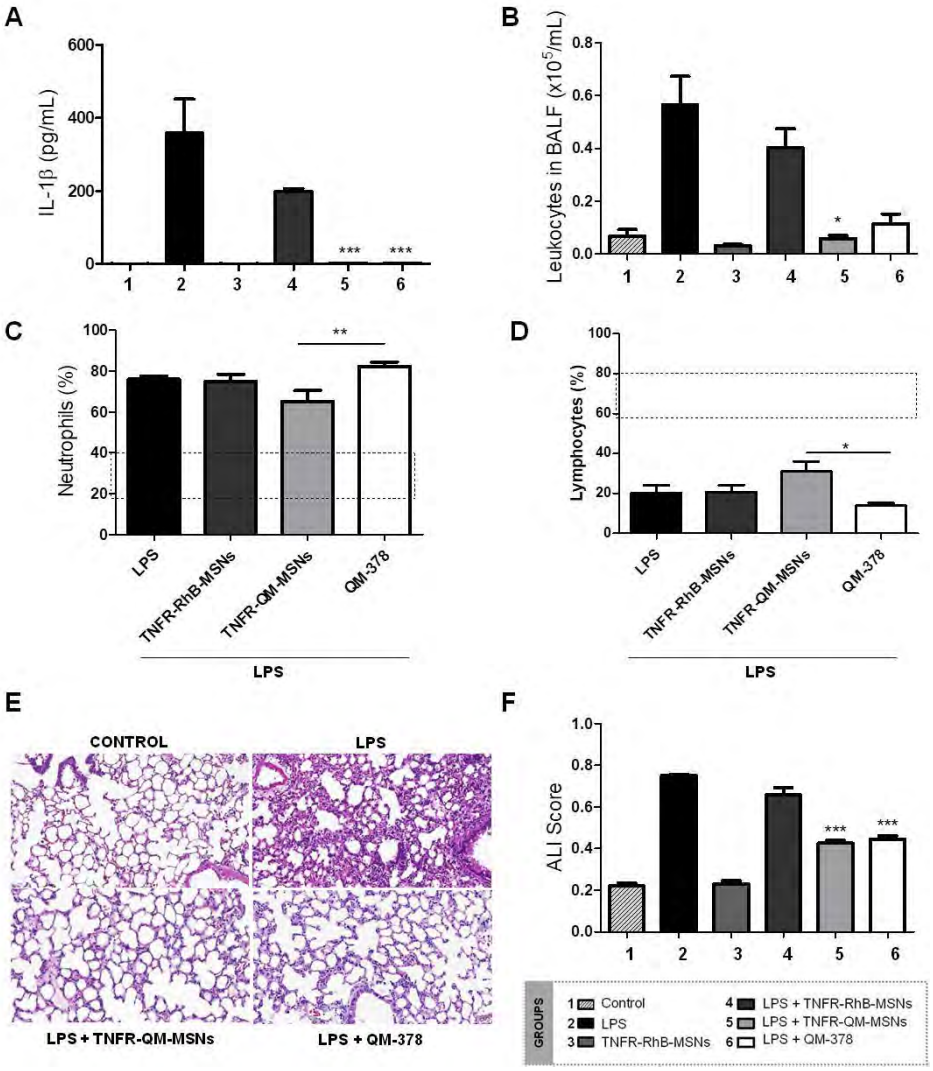

Figure 5. Anti-inflammatory activity of TNFR-QM-MSNs in ALI in vivo model. Evaluation of inflammation in BALF obtained from LPS-acute lung injury mice. (A) Levels of IL-1β pro-inflammatory cytokine quantified by ELISA. (B) Leukocytes account obtained from BALF by flow cytometry analysis, as indicator of inflammation focus. (C) Percentage of neutrophils and (D) lymphocytes quantified from blood by flow cytometry analysis, as systemic inflammation indicators. The data represent the mean ± SD (n = 6-8). (E) Histopathological analysis of images H&E stain of lungs sections and (F) evaluation of the acute lung injury determined by ALI score. The data represent the mean ± SD (n = 4-6).

5.5 Conclusions

The complexity of the ALI pathogenesis accompanied by the scarcity of useful treatments converts the study of new therapeutic alternatives in a medical need. In this work we successfully demonstrate, for the first time, the effectivity of the inflammasome inhibitor QM-378 in the resolution of uncontrolled inflammation and lung injury in ALI. Moreover, two nanomaterials were prepared, based on mesoporous silica nanoparticles, loaded with rhodamine B (**TNFR-RhB-MSNs**) or with the QM-378 drug (**TNFR-QM-MSNs**) capped with the TNFR peptide. This work also described, for the first time, the encapsulation of the poor soluble drug QM-378 as well as their proper activity after encapsulation into MSNs scaffold both *in vitro* and *in vivo* models. Moreover, in concordance with previous reports that also support the use of targeted nanomedicines as promising approach for efficient drug delivery to inflamed lungs,[33,34,62–65] we demonstrated the targeting effect to inflamed lungs of TNFR-MSNs by IVIS and silicon biodistribution analysis using **TNFR-RhB-MSNs** in ALI mice model. Targeted-delivery of QM-378 using **TNFR-QM-MSNs** enhanced the therapeutic effect of the entrapped drug, confirming that nanoencapsulation represents a promising opportunity to overcome the limitations of current treatments in ALI. These nanomedicines are potential tools to efficiently administer anti-inflammatory drugs to solve inflammatory disorders, including from ALI to Chronic Pulmonary Obstructive Disease (COPD), asthma and pulmonary fibrosis which are also major health concerns in the clinics.

5.6 References

[1] G. R. Bernard, A. Artigas, K. L. Brigham, J. Carlet, K. Falke, L. Hudson, M. Lamy, J. R. Legall, A. Morris, R. Spragg, *Am. J. Respir. Crit. Care Med.* **1994**, *149*, 818.

[2] M. A. Matthay, R. L. Zemans, G. A. Zimmerman, Y. M. Arabi, J. R. Beitler, A. Mercat, M.

Herridge, A. G. Randolph, C. S. Calfee, *Nat. Rev. Dis. Prim.* **2019**, *5*, 18.
[3] W.-J. Gu, Y.-D. Wan, H.-T. Tie, Q.-C. Kan, T.-W. Sun, *PLoS One* **2014**, *9*, e90426.
[4] J. F. Avecillas, A. X. Freire, A. C. Arroliga, *Clin. Chest Med.* **2006**, *27*, 549.
[5] M. Cepkova, M. A. Matthay, *J. Intensive Care Med.* **2006**, *21*, 119.
[6] E. R. Johnson, M. A. Matthay, *J. Aerosol Med. Pulm. Drug Deliv.* **2010**, *23*, 243.
[7] G. A. Schmidt, *Clin. Chest Med.* **2016**, *37*, 647.
[8] Y. Butt, A. Kurdowska, T. C. Allen, *Arch. Pathol. Lab. Med.* **2016**, *140*, 345.
[9] P. A. Ward, *Eur. Respir. J.* **2003**, *22*, 22s LP.
[10] M. A. Matthay, R. L. Zemans, *Annu. Rev. Pathol. Mech. Dis.* **2011**, *6*, 147.
[11] G. M. T., R. Jérémie, M. Byron, H. Marybeth, F. J. A., S. George, S. Dean, V. S. M., W. P. H., H. G. S., M. M. A., P. Jean-François, *Circ. Res.* **2008**, *102*, 804.
[12] X. He, Y. Qian, Z. Li, E. K. Fan, Y. Li, L. Wu, T. R. Billiar, M. A. Wilson, X. Shi, J. Fan, *Sci. Rep.* **2016**, *6*, 31663.
[13] J. J. Grailer, B. A. Canning, M. Kalbitz, M. D. Haggadone, R. M. Dhond, A. V Andjelkovic, F. S. Zetoune, P. A. Ward, *J. Immunol.* **2014**, *192*, 5974 LP.
[14] D. Jiang, J. Liang, J. Fan, S. Yu, S. Chen, Y. Luo, G. D. Prestwich, M. M. Mascarenhas, H. G. Garg, D. A. Quinn, R. J. Homer, D. R. Goldstein, R. Bucala, P. J. Lee, R. Medzhitov, P. W. Noble, *Nat. Med.* **2005**, *11*, 1173.
[15] M. Leissinger, R. Kulkarni, R. L. Zemans, G. P. Downey, S. Jeyaseelan, *Am. J. Respir. Crit. Care Med.* **2014**, *189*, 1461.
[16] K. Schroder, J. Tschopp, *Cell* **2010**, *140*, 821.
[17] L. Franchi, T. Eigenbrod, R. Muñoz-Planillo, G. Nuñez, *Nat. Immunol.* **2009**, *10*, 241.
[18] X. Liu, Z. Zhang, J. Ruan, Y. Pan, V. G. Magupalli, H. Wu, J. Lieberman, *Nature* **2016**, *535*, 153.
[19] J. Shi, Y. Zhao, K. Wang, X. Shi, Y. Wang, H. Huang, Y. Zhuang, T. Cai, F. Wang, F. Shao, *Nature* **2015**, *526*, 660.
[20] D. Lin, W. Ren, Z. Jiang, L. Zhu, *Mol. Med. Rep.* **2018**, *18*, 4399.
[21] N. R. Aggarwal, L. S. King, F. R. D'Alessio, *Am. J. Physiol. Cell. Mol. Physiol.* **2014**, *306*, L709.
[22] G. Mathiak, G. Grass, T. Herzmann, T. Luebke, C. C. Zetina, S. A. Boehm, H. Bohlen, L. F. Neville, A. H. Hoelscher, *Br. J. Pharmacol.* **2000**, *131*, 383.
[23] D.-D. Wu, P.-H. Pan, B. Liu, X.-L. Su, L.-M. Zhang, H.-Y. Tan, Z. Cao, Z.-R. Zhou, H.-T. Li, H.-S. Li, L. Huang, Y.-Y. Li, *Chin. Med. J. (Engl).* **2015**, *128*.
[24] P. Gasse, C. Mary, I. Guenon, N. Noulin, S. Charron, S. Schnyder-Candrian, B. Schnyder, S. Akira, V. F. J. Quesniaux, V. Lagente, B. Ryffel, I. Couillin, *J. Clin. Invest.* **2007**, *117*, 3786.
[25] D. Impellizzeri, G. Bruschetta, E. Esposito, S. Cuzzocrea, *Expert Opin. Emerg. Drugs* **2015**, *20*, 75.
[26] V. J. Patel, S. B. Raoy, H. J. Metha, M. Joo, R. T. Sadikot, *Biomed Res. Int.* **2018**, *2018*, 2476824.
[27] M. Shyamsundar, S. T. W. McKeown, C. M. O'Kane, T. R. Craig, V. Brown, D. R. Thickett, M. A. Matthay, C. C. Taggart, J. T. Backman, J. S. Elborn, D. F. McAuley, *Am. J. Respir. Crit. Care Med.* **2009**, *179*, 1107.
[28] H. J. Lago, C. A. Toledo-Arruda, M. Mernak, H. K. Barrosa, A. M. Martins, F. I. Tibério, M. C. Prado, Structure-Activity Association of Flavonoids in Lung Diseases. *Mol.* **2014**, *19*.

[29] S. P. Newman, *Ther. Deliv.* **2017**, *8*, 647.
[30] R.T. Sadikot, A.V. Kolanjiyil, C. Kleinstreuer, I. Rubinstein, *BiomedHub*, **2017**, *2*, *477086*.
[31] R. Iyer, C. C. W. H. and K. T. Nguyen, *Curr. Pharm. Des.,* **2015**, *21*, 5233–5244.
[32] M. M. Bailey, C. J. Berkland, *Med. Res. Rev.* **2009**, *29*, 196.
[33] A. Bohr, N. Tsapis, I. Andreana, A. Chamarat, C. Foged, C. Delomenie, M. Noiray, N. El Brahmi, J. Majoral, S. Mignani, E. Fattal, *Biomacromolecules*, **2017**, *18*, 2379.
[34] C. Y. Zhang, W. Lin, J. Gao, X. Shi, M. Davaritouchaee, A. E. Nielsen, R. J. Mancini, Z. Wang, *ACS Appl. Mater. Interfaces* **2019**, *11*, 16380.
[35] S. Jiang, S. Li, J. Hu, X. Xu, X. Wang, X. Kang, J. Qi, X. Lu, J. Wu, Y. Du, Y. Xiao, *Nanomedicine Nanotechnology, Biol. Med.* **2019**, *15*, 25.
[36] S.-J. Li, X.-J. Wang, J.-B. Hu, X.-Q. Kang, L. Chen, X.-L. Xu, X.-Y. Ying, S.-P. Jiang, Y.-Z. Du, *Drug Deliv.* **2017**, *24*, 402.
[37] Y. Xiong, W. Gao, F. Xia, Y. Sun, L. Sun, L. Wang, S. Ben, S. E. Turvey, H. Yang, Q. Li, *Adv. Healthc. Mater.* **2018**, *7*, 1800510.
[38] F. Tang, L. Li, D. Chen, *Adv. Mater.* **2012**, *24*, 1504.
[39] A. Watermann, J. Brieger, *Nanomaterials* **2017**, *7*, 189/1.
[40] S. T. Haque, E. H. Chowdhury, *Curr. Drug Deliv.* **2018**, *15*, 485.
[41] C. Coll, A. Bernardos, R. Martínez-Máñez, F. Sancenón, *Acc. Chem. Res.* **2013**, *46*, 339.
[42] E. Aznar, M. Oroval, L. Pascual, J. R. Murguía, R. Martínez-Máñez, F. Sancenón, *Chem. Rev.* **2016**, *116*, 561.
[43] X. Pu, J. Li, P. Qiao, M. Li, H. Wang, L. Zong, Q. Yuan, S. Duan, *Curr. Cancer Drug Targets* **2019**, *19*, 285.
[44] A. García-Fernández, G. García-Laínez, M. L. Ferrándiz, E. Aznar, F. Sancenón, M. J. Alcaraz, J. R. Murguía, M. D. Marcos, R. Martínez-Máñez, A. M. Costero, M. Orzáez, *J. Control. Release* **2017**, *248*, 60.
[45] E. Koziolová, K. Venclíková, T. Etrych, *Physiol. Rev.* **2018**, *67*, S281.
[46] C. A. Fromen, W. J. Kelley, M. B. Fish, R. Adili, M. J. Hoenerho, M. Holinstat, O. Eniola-adefeso, *ACS Nano*, **2017**, *11,* 10797.
[47] F. Yuan, L. Quan, L. Cui, S. R. Goldring, D. Wang, *Adv. Drug Deliv. Rev.* **2012**, *64*, 1205.
[48] T. Wu, M. Tang, *J. Appl. Toxicol.* **2018**, *38*, 25.
[49] T. Yu, D. Hubbard, A. Ray, H. Ghandehari, *J. Control. Release* **2012**, *163*, 46.
[50] Y. Chen, H. Chen, J. Shi, *Adv. Mater.* **2013**, *25*, 3144.
[51] D. Hristodorov, R. Mladenov, V. Von Felbert, M. Huhn, R. Fischer, S. Barth, T. Thepen, *MAbs*, **2015**, *7*, 0862.
[52] Y. Weifeng, L. Li, H. Yujie, L. Weifeng, G. Zhenhui, H. Wenjie, *PLoS ONE*, **2016**, *11*, e0151672.
[53] O. A. Akinrinmade, S. Chetty, A. K. Daramola, M. U. Islam, T. Thepen, S. Barth, *Biomedicines*, **2017**, *5*, E56.
[54] M. A. Matthay, D. F. McAuley, L. B. Ware, *Lancet Respir. Med.* **2017**, *5*, 524.
[55] Z. Zhang, L. Chen, H. Ni, *Sci. Rep.,* **2015**, *5*, 17654.
[56] J. V Diaz, R. Brower, C. S. Calfee, M. A. Matthay, *Crit. Care Med,* **2010**, *38,* 1644.
[57] M. S. Kluger, J. H. Li, R. Al-lamki, J. R. Bradley, J. S. Pober, *J. Biol. Chem*., **2010**, *285*, 23868.
[58] S. Mukhopadhyay, J. R. Hoidal, T. K. Mukherjee, *Respir. Res.* **2006**, *7*, 125.

[59] M. R. Wilson, K. Wakabayashi, S. Bertok, C. M. Oakley, R. Lucas, J. Mcguire, *Front. Immunol.,* **2017**, *8*, 1.

[60] Y. A. Sato, K. Gonda, M. Harada, Y. Tanisaka, S. Arai, Y. Mashimo, H. Iwano, H. Sato, S-Ryozawa, T. Takahashi, S. Sakuramoto, M. Shibata, *Biomed. Reports,* **2017**, *7*, 79.

[61] G. Matute-bello, G. Downey, B. B. Moore, S. D. Groshong, M. A. Matthay, *Am J Respir Cell Mol Biol.,* **2011**, *44*, 725.

[62] S. H. van Rijt, D. A. Bölükbas, C. Argyo, K. Wipplinger, M. Naureen, S. Datz, O. Eickelberg, S. Meiners, T. Bein, O. Schmid, T. Stoeger, *Nanoscale,* **2016**, *8*, 8058.

[63] S. Hussain, Z. Ji, A. J. Taylor, L. M. Degra, M. George, C. J. Tucker, C. H. Chang, R. Li, J. C. Bonner, S. Garantziotis, *ACS Nano*, **2016**, *10*, 7675.

[64] M. Bouchoucha, E. Beliveau, F. Kleitz, F. Calon, M.-A. Fortin, *J. Mater. Chem. B Mater. Biol. Med.,* **2017**, *5*, 7721.

[65] M. Santha Moorthy, G. Hoang, B. Subramanian, N. Q. Bui, M. Panchanathan, S. Mondal, V. P. Thi Tuong, H. Kim, J. Oh, *J. Mater. Chem. B Mater. Biol. Med.*, **2018**, *6*, 5220.

Acknowledgements

A. García-Fernández is thankful to the Spanish government for her FPU fellowship. The authors tanks to the Spanish Government (project RTI2018-100910-B-C41 (MCUI/AEI/FEDER, UE) and the Generalitat Valencia (Project PROMETEO/2018/024 and PROMETEOII/2014/061) for support. The authors would like to thank Animal Facilities from Centro de Investigación Principe Felipe for its support in the animal research and procedures and I. Borred and J. Forteza from Instituo Valenciano de Patología for its technical support in the histopathology analysis.

5.7 Supporting Information

Characterization of TNFR-gated nanodevices

In a first step, the presence of an ordered mesoporous scaffold was confirmed using power-X-ray diffraction measurements. As could be seen in Figure S1 A, the typical PXRD pattern associated to a hexagonal-ordered array was observed for the as made nanoparticles. The most characteristic peak indexed as (100) was observed and it was maintained in all the prepared-materials (calcined MSNs, **NCO-RhB-MSNs** and **TNFR-RhB-MSNs)**, after loading and functionalization process (see Figure S1 B, C and D respectively). Finally, the textural properties of the starting MSNs and **TNFR-RhB-MSNs** were characterized by N_2 adsorption–desorption studies. As we expected, the typical IV isotherm for mesoporous solids was observed for calcined MSNs (see Figure S1 E) in which an adsorption step between 0.1 and 0.4 low P/P_0 values is present. The specific area was determined by applying BET model (954.88 m^2/g). In addition, pore diameter and pore volume were analysed with the BJH model on the adoption curve at $P/P_0 < 0.8$. In contrast, the isotherm obtained for **TNFR-RhB-MSNs** (Figure S1 F) was characteristic of systems with filled mesopores and BET surface area and pore volume decreased to 436.39 m^2/g and 0.33 cm^3/g, attributed to the loading and capping processes.

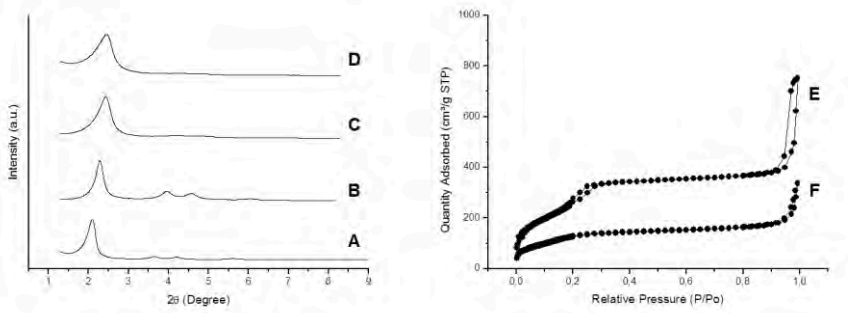

Figure SI. PXRD pattern from (A) as made MSNs (B) calcined MSNs (C) **NCO-RhB-MSNs** and (D) **TNFR-RhB-MSNs**. N_2 adsorption-desorption isotherm of (E) as made MSNs and (F) **TNFR-RhB-MSNs**.

Macrophage phenotype characterization

To characterize the proper macrophage polarization pro-inflammatory (IL-1β) and anti-inflammatory (IL-10) cytokines levels and LDH activity were analysed in cell supernatants by ELISA assay and Lactatase Assay Kit II respectively following the supplier's instructions. Moreover, gene expression of common protein markers of polarized macrophages was studied via QRT-PCR analysis. CCR7 and CXCL10 markers were associated to pro-inflammatory M1 macrophages and mannose receptor CD206 for anti-inflammatory M2 macrophages (Table 1). Total RNA was extracted from THP-1, M0, M1 and M2 cells using the the RNA isolation RNeasy Mini Kit (Qiagen) and then mRNA were obtained by reverse transcription (RT) using super script first strand synthesis system for RT-PCR (Invitrogen). PCR amplification was performed with equal amounts of cDNA from each RT reaction and qPCR using the SYBRGreen Reagent Kit was performed on the Roche Light Cycler 480. The primers for CCR7, CXCL10, CD206 (100 nM) were used and GAPDH was used as the control gene for normalization. In addition, scrambled controls were added for each primer pair to discard contaminants and the specificity of the

PCR products was confirmed by meting-curve analysis. Finally, the mRNA expression was quantified using Roche Applied Science software by the threshold cycle (C_T) method and the abundance was expressed as relative-fold change front GAPDH expression.

Table 1. Macrophage markers used for qPCR

Gene	Primer
CCR7	F 5'-TGGTGGTGGCTCTCCTTGTC-3' R 5'-TGTGGTGTTGTCTCCGATGTAATC-3'
CXCL10	F 5'-GAAAGCAGTTAGCAAGGAAAGGTC-3' R 5'-ATGTAGGGAAGTGATGGGAGAGG-3'
CD206	F 5'-ACCTCACAAGTATCCACACCATC-3' R 5'-CTTTCATCACCACACAATCCTC-3'

A model of macrophage polarization was firstly established in order to study the activity of **TNFR-QM-MSNs** in pro-inflammatory macrophages. For this purpose, THP-1 monocytes, M0 macrophages, pro-inflammatory M1 macrophages and anti-inflammatory M2 macrophages were derived as we described above and characterized comparing different inflammatory markers. In the case of pro-inflammatory M1 macrophages, the presence of cytokine IL-1β and protein markers such as CCR7 and CXCL10 were attributed to a pro-inflammatory expression profile, as we observed in Figure S2. In contrast, no expression of anti-inflammatory markers was determined for M1 polarized macrophages. The anti-inflammatory M2 profile was identified by the high expression of the mannose receptor CD206 and the cytokine IL-10. As we expected, the anti-inflammatory pattern was confirmed to M2 derived macrophages, whereas any signal of pro-inflammatory profile was evidenced. Finally, the inflammatory cell death pyroptosis was studied in the different inflammatory cells by measuring the LDH activity. The highest level of LDH activity was attributed to pro-inflammatory M1

macrophages due to the IFN-γ and LPS activation, compared to no activated THP-1, M0 and M2 macrophages in which less amount of LDH activity was observed. These results confirmed the accurate differentiation to pro-inflammatory M1 macrophages from of THP-1 monocytes using PMA for 24 h, IFN-ϒ for another 24h and finally LPS during 3 h.

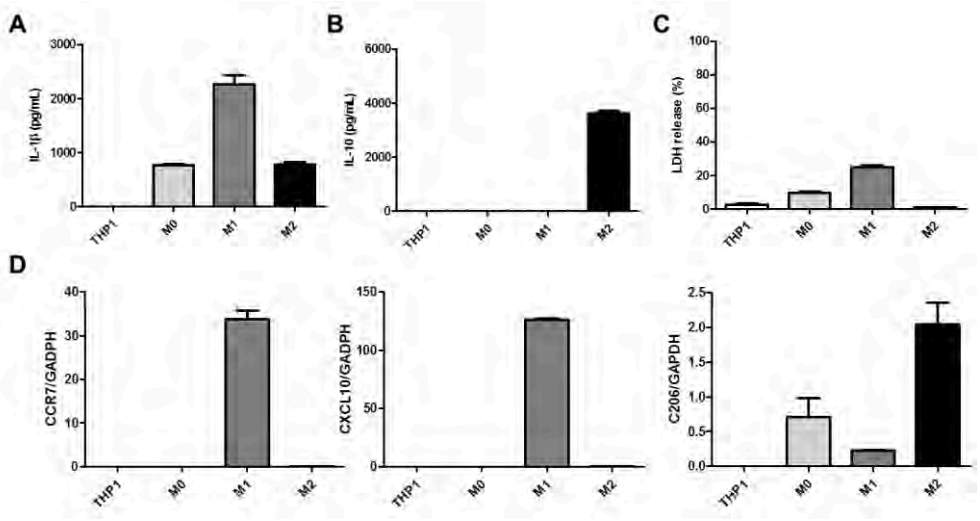

Figure S2. Characterization of derived macrophages from THP-1 monocyte cells. (A) Quantification of pro-inflammatory IL-1β levels and (B) anti-inflammatory cytokine levels of IL-10. (C) Quantification of LDH release associated to inflammatory cell death called pyroptosis in the different cell populations. (D) Analysis of gene expression of CCR7, CXCL10 and CD206 markers (from left to right) in inflammatory cells.

Anti-inflammatory activity of TNFR-QM-MSNs in inflammatory cells by western blot analysis

Table 2. Primary antibody used in western blot

Protein	Antibody	Molecular Weight (kDa)
NLPR3	NLRP3 (D4D8T) Rabbit mAb #15101	118
TNFR1	TNF-R1 (C25C1) Rabbit mAb #3736S from Cell Signaling	55
Pro-Caspase 1	Caspase-1 antibody, Rabbit, #2225 from Cell Signaling	45
GAPDH	Anti-GAPDH antibody, Mouse monoclonal, G8795 from Sigma Aldrich	37
Cleaved Caspase 1	Cleaved Caspase-1 (Asp297) (D57A2) Rabbit mAb, #4199 from Cell Signaling	20
Gasdermin D	Anti-GSDMDC1 antibody (SAB1411444) in rabbit from Sigma Aldrich	53
N-ter Gasdermin D	Anti-GSDMDC1 antibody (SAB1411444) in rabbit from Sigma Aldrich	32

Evaluation of anti-inflammatory activity of TNFR-QM-MSNs in inflammatory cells

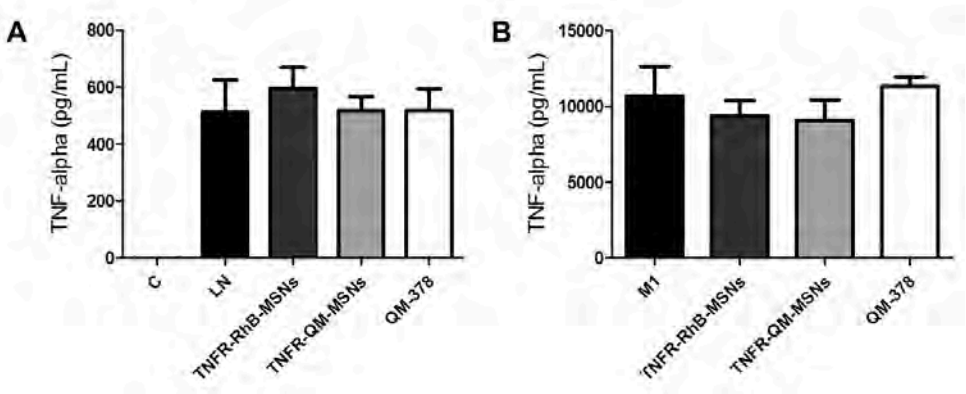

Figure S3. Inflammatory studies with **TNFR-QM-MSNs** in THP-1 cells (left) and pro-inflammatory M1 macrophages (right). (A and B) Quantification of TNF-α pro-inflammatory cytokine from cell supernatants by ELISA

Anti-inflammatory activity of TNFR-QM-MSNs in acute lung injury model

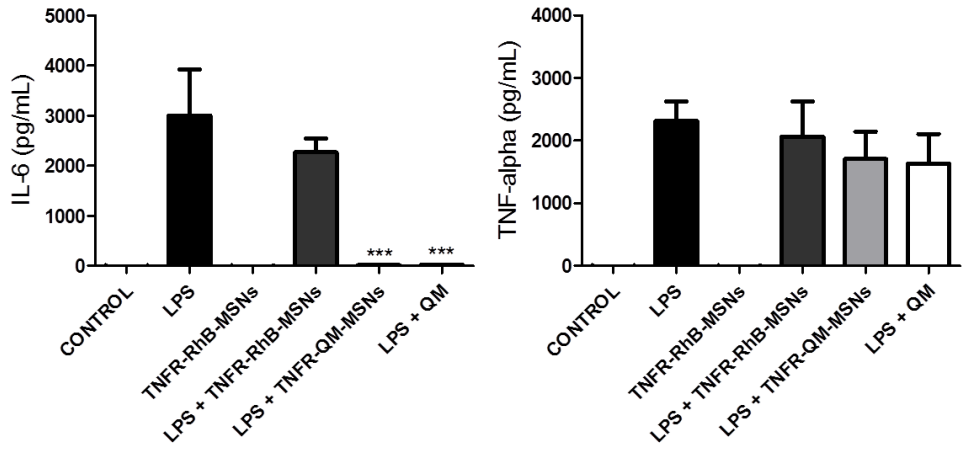

Figure S4. Inflammatory studies with **TNFR-QM-MSNs** in acute lung injury model. (A) Levels of IL-6 and (B) TNF-α pro-inflammatory cytokines analysed in BALF from acute lung injury mice.

Histopathology analysis of lungs sections from ALI mice

Lung sections were prepared in a DAKO PT link with the Dako 3-in-1 AR buffer EDTA pH 9.0 after a rehydration and antigen retrieval procedure. The endogenous peroxidase activity was blocked for 5 min and finally the sections were processed using the Envision Flexþ kit (DAKO) for incubate with the correspondent primary antibody. The primary antibodies used were anti-myeloperoxidase (Dako, IR511 for 20 minutes), anti-Von Willebrand Factor (Dako, IR527 for 20 minutes), and Masson's trichrome (Dako, AR173) and Periodic Acid Schiff (PAS) (Dako AR165) were added using the Artisan LinkPro de Dako. Envision Flexþ horseradish peroxidase diaminobenzidine were added for 20 minutes and for 10 minutes respectively to determine the associated signal in each case. Sections were counterstained with Mayer's hematoxylin (DAKO, S3309, ready-to-use) for 5 minutes. Finally, the slides were processed by Leica ASP300 tissue equipment and analysed with the CaseViewer program.

In the case of myeloperoxidase, the accumulation of inflammatory cells is stained in brown or dark yellow, compared to healthy conditions in a light blue colour. As observe in Figure S5, the most significant accumulation of inflammatory cells was observed in the LPS groups, in which myeloperoxidase activity was positive. In contrast, in the LPS+**TNFR-QM-MSNs** and LPS+QM conditions the melyoperoxidase activity decreased associated to a reduced inflammation.

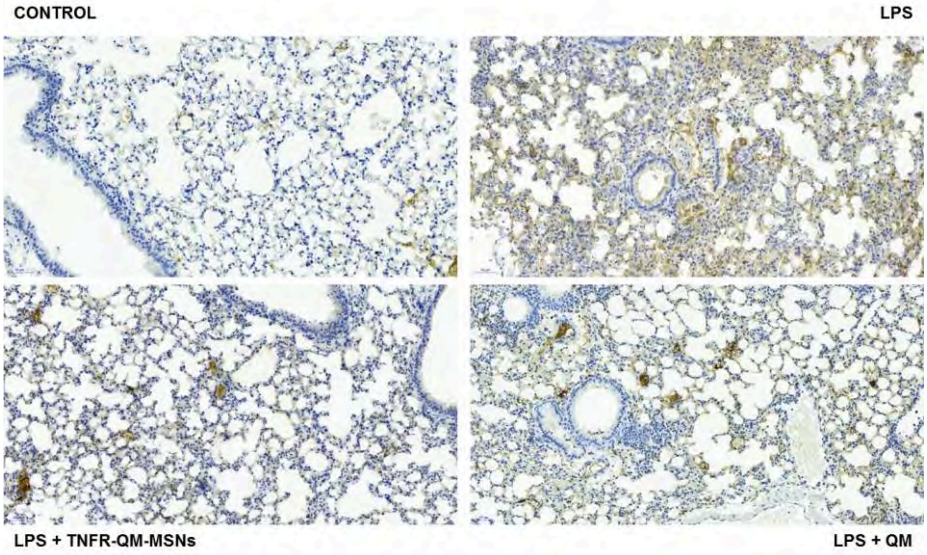

Figure S5. Representative images of myeloperoxidase stain of lung tissue from mice (n = 4-6).

To discard the fibrotic stage in the ALI model, which is composed by an early exudative phase followed by a late fibrotic phase, Masson's staining was carried out. The fibrotic associated fibres appeared in marked bright dark blue. As could observe in Figure S6, all the groups showed a predominantly dark red colour stain thus discarding the fibrosis phase. Although, in some cases slightly blue fibres were stained, these little findings were considered non-significant and could be associated to the intraalveolar edema with variable amounts of haemorrhage and fibrin deposition in the early stage of ALI.

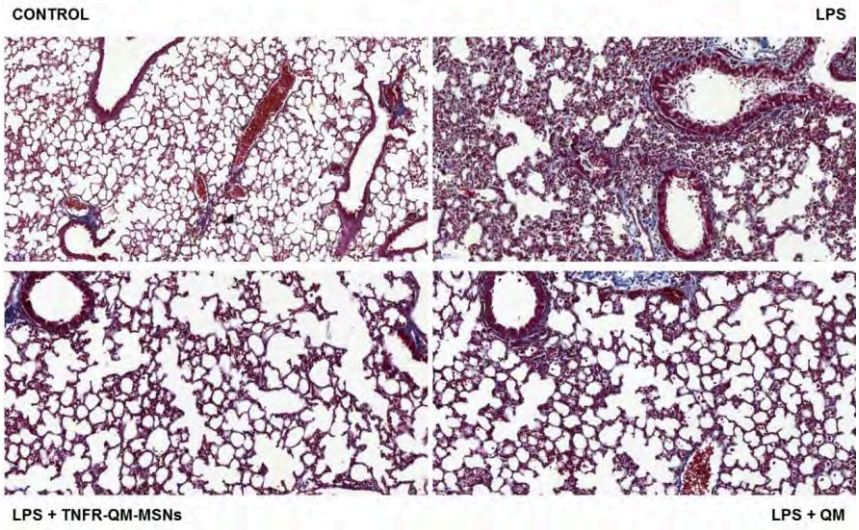

Figure S6. Representative images of Masson's marker of lung tissue from mice (n = 4-6).

In addition, the factor VIII/Von Willebrand factor was used to evaluate the platelet aggression and adhesion (Figure S7). Attending to the acute inflammatory processes could be related with a local vascular inflammation, we analyzed the increase of factor VIII in blood vessels and in the alveolar septum and bronchoalveolar epithelium. The bloods vessels from the endothelium were marked in dark yellow or brown as an internal control. The images from LPS exhibited the development of an acute inflammation with some microtrhombosis complication, marked in dark yellow or brown, whereas in the case of LPS+**TNFR-QM-MSNs** and LPS+QM treatment the presence of the factor is more similar to healthy conditions. It should be noted that in the case of LPS+QM the presence of the factor VIII was slightly major compared to LPS+**TNFR-QM-MSNs** treatment.

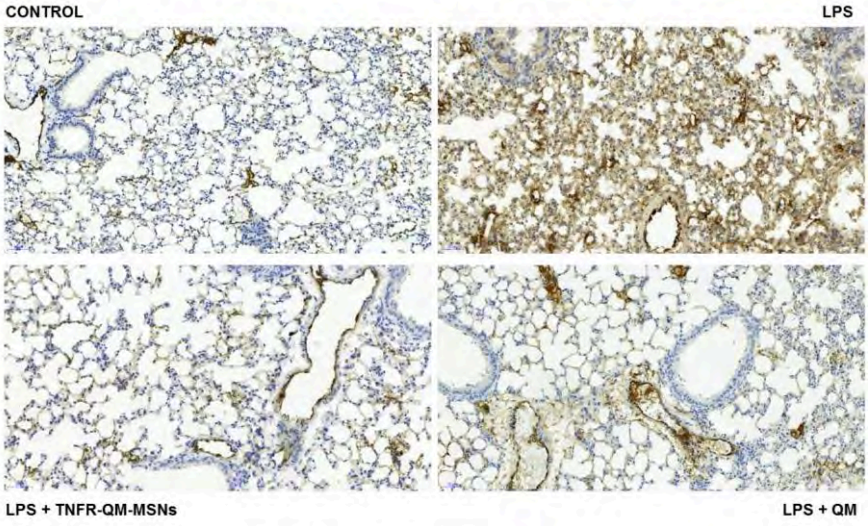

Figure S7. Representative images of factor VIII/von Willebrand factor staining of lung tissue from mice (n = 4-6).

Finally, the alveolar proteinuria characteristic from the exudative phase of ALI was evaluated using the PAS marker, which stain the proteinuria in pink or fuchsia. In this case, we only observed a pink stain associated to the LPS group, in which high inflammation is developed with the accumulation of cellular debris (see Figure S8).

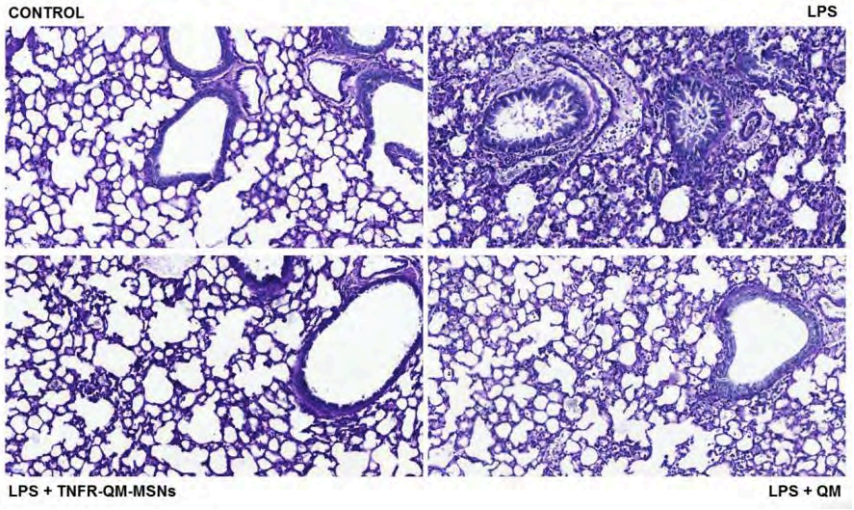

Figure S8. Representative images of PAS staining of lung tissues from mice (n = 4-6).

Chapter 6 | Conclusions and Perspectives

In the last decades, nanomedicine and nanotherapy are gaining an increasing attention as alternative to conventional treatments in pathologies that requires a selective and controlled drug administration. At this respect nanotechnology has became a potential tool to overcome many of the current limitations of conventional therapy, attending to the capability of nanomedicines to specific drug delivery to molecular targets in the diseased cells and tissues while minimizing undesired side effects.

In this context, MSNs may play a crucial role due to their unique features (such as large surface area, high drug-loading capacity, nontoxicity and easy functionalization) which make them ideal candidates for the preparation of gated stimuli-responsive nanomaterials able to release an entrapped cargo on-demand. In fact, MSNs has emerged as a promising tool to improve the solubility and bioavailability of drugs as well as the delivery of an accurate amount of drug specifically to the diseased cells, thus reducing the impact on healthy cells and in the organism.

In the last years, the use of gated nanomaterials based on mesoporous silica nanoparticles has remarkably increased in the biomedicine field. Despite the advances made in drug delivery applications, the design of gated nanomaterials as drug delivery platforms to manage inflammatory disorders is a less explored field compared to other types of biomedical applications such as cancer nanotherapy. In this context, this PhD thesis has attempeted to contribute to this field by designing new stimuli-responsive nanodevices based on gated mesoporous silica nanoparticles to targeted drug delivery for inflammatory disorders. For this purpose, three different nanomaterials, for controlled drug release in inflammatory conditions, and designed to respond to current biomedical needs, are reported.

In the third chapter, a nanocarrier consisting of ε-poly-L-lysine-gated mesoporous silica nanoparticles loaded with the inflammasome inhibitor VX-765 has been developed. The proper gating mechanism of the ε-poly-L-lysine gatekeeper was corroborated, being the drug released only in the presence of proteases able to degrade the ε-poly-L-lysine cap. Besides, despite the controversy of the possible immunogenicity associated to MSNs, it was confirmed that the use of MSNs in non-toxic doses does not trigger an inflammatory response. As far as we know, for the first time the delivery of anti-inflammatory drugs using gated mesoporus silica nanoparticles at the inflammatory focus in an inflammatory animal model has been described. The therapeutic effect of VX-765 is enhanced with a significant reduction in the inflammatory response, compared with the free drug in an air pouch mouse model. The designed nanoparticles take adavantge of the preferential accumulation of nanoparticles to macrophages (and thus inflamed tissues) that resulted in drug delivery of modulators of inflammasome in the inflamed focus. Besides, it was demonstrated that delivery of anti-inflammatory drugs using gated mesoporous silica nanoparticles is a potential aproach for the development of new therapeutic strategies to treat inflammatory diseases.

In the fourth chapter, a targeted-lung delivery nanosystem for the treatment of acute lung injury (ALI) has been reported. The designed nanodevice is based on mesoporous silica nanoparticles loaded with the glucocorticoid dexamethasone and functionalized with a peptidic cap that target the TNFR1 receptor expressed in pro-inflammatory macrophages. The prepared nanoparticles take adavantge of the intrinsic passive targeting effect from MSNs to inflamed areas and lungs, as well as the active targeting effect through TNFR1 recognition. The proper working of the caping ensemble was tested and the cargo was only released in the presence of lysosomal extract upon the enzymatic hydrolysis of the capping

peptide. Additionally, it was demonstrated the specific uptake of the nanoparticles for the pro-inflammatory macrophages as well as the ability to reduce the cytokines levels *in vitro* in pro-inflammatory macrophages. Besides, the nanodevice based on mesoporous silica nanoparticles was tested *in vivo* in an acute lung injury mouse model for the first time. The nanoparticles showed greater therapeutic effect in the reduction of inflammatory response and lung injury while minimizing undesried side effects compared to free dexamethasone. Finally, the targeting effect to inflamed lungs was confirmed in the *in vivo* model upon biodistribucion assays with the nanoparticles. All these effects finally demonstrated that targeted-lung gated-mesoporous silica nanoparticles are a potential tool for direct lung drug release. This or similar nanocarriers are promising systems to overcome the limitations of current treatments in ALI.

In the fifth chapter, a drug delivery system for ALI is also presented. In this case the effectivity of the novel inflammasome inhibitor QM-378 to manage inflammation in acute lung injury was successfully demonstrated. Additionally, MSNs were used to improve the solubility of QM-378 and, therefore, enhance its bioavility and therapeutic effect. The prepared nanodevice is based on MSNs loaded with QM-378 and capped with a peptide targetting TNFR1. The gating properties of the nanosystem were demonstrated as well as the preferential targeting for pro-inflammatory macrophages, which express TNFR1. The ability to reduce inflammatory response using QM-378 loaded gated-mesoporous silica nanoparticles was demonstrated *in vitro* in activated monocytes and pro-inflammatory macrophages. Finally, the potential use of the targeted-lung delivery of the QM-378 for acute lung injury using gated mesoporous silica nanoaprticles has been demonstrated in *in vivo* assays thus achieving greater therapeutic effect in the resolution of inflammation and lung injury. Moreover, the preferential accumulation of the nanoparticles in the inflamed lungs was

confirmed in the ALI mouse model by IVIS and silicon biodistribution analysis. The obtained results indicated that QM-378 could be an alternative candidate for the acute lung injury therapy and its encapsulation using targeted-lung mesoporous silica nanoparticles constitute a promising opportunity to overcome the limitations of current treatments in acute lung injury.

A general conclusion that can be extracted from this PhD thesis is that gated mesoporous silica nanoparticles can be used for the development of new nanodevices to solve inflammatory disorders. Moreover, the incorporation of the nanotechnology allows performing new functions, such as the controlled drug release on demand and the functionalization with targeting agents to specifically reach the diassed organ, that with conventional therapy would be very difficult or impossible to achieve.

However, taking into the account that gated nanomaterials are still in the initial stages of biomedicine applications, some drawbacks still need to be overcome and the effects in the organism of these new nanodevices have to be completely analyzed. The benefit-to-risk ratio has to be study and more research efforts are needed to finally regulate these nanomedicines for clinical applications. Several new advances in the field of gated nanomaterials are expected in the near future and smart nano-drug delivery technology development for more precise medicines looks promising. It is our hope that the results achieved in this PhD thesis open new research opportunities and inspire the development of new smart nanomaterials for their application in the inflammatory field, as well as in other biomedical unresolved needs.